2

AIR DATA MEASUREMENT SYSTEM FOR SPACE SHUTTLE

Interim Report

CR-123812

By

J. C. deJesus
Delroy J. Sowada
Fred A. Moynihan

Prepared under Contract No. NAS 8-26326

by

Honeywell Inc.
Government and Aeronautical Products Division
Minneapolis, Minnesota 55413

for

NATIONAL AERONAUTICS AND SPACE ADMINISTRATION

AIR DATA MEASUREMENT SYSTEM FOR SPACE SHUTTLE

Interim Report

By

J. C. deJesus
Delroy J. Sowada
Fred A. Moynihan

Prepared under Contract No. NAS 8-26326

by

Honeywell Inc.
Government and Aeronautical Products Division
Minneapolis, Minnesota 55413

for

NATIONAL AERONAUTICS AND SPACE ADMINISTRATION

CONTENTS

	Page
AIR DATA MEASUREMENT SYSTEM FOR SPACE SHUTTLE	1
SUMMARY	1
1.0 SCOPE AND ACCOMPLISHMENTS	3
2.0 CONCLUSIONS AND RECOMMENDATIONS	6
3.0 TECHNICAL DISCUSSION	8
3.1 Background and Summary	8
3.2 Air Data Measurement (ADM) System Configuration Tradeoffs	14
3.3 Sphere-Nose Sensor Design	41
3.4 Conventional Pitot-Static Probe	81
3.5 Detailed Description and Analysis of Specific Sphere-Nose Configuration	84
APPENDIX A - SENSITIVITY OF AN ANGLE-OF-ATTACK SENSOR COMPARISON OF THEORY AND EXPERIMENT	115
APPENDIX B - SHUTTLE VEHICLE FLIGHT PROFILES	117
APPENDIX C - DENSITY ALTITUDE FROM INERTIAL SYSTEM MEASUREMENTS	138
APPENDIX D - HEMISPHERE SURFACE PRESSURE DISTRIBUTION	144
REFERENCES	173
BIBLIOGRAPHY	175

ILLUSTRATIONS

Figure		Page
1	Space Shuttle Air Data Measurement Sensors	8
2	Air Data: Atmospheric Flight Parameters from Flow or Reaction Measurements	15
3	ADM Hardware	15
4	Nominal Profile Mission	17
5	Altitude/Velocity Trajectories (Re-Entry)	22
6	Flow Pattern IF Boom Acts as a Skip Spike	33
7	Air Data Sensors Measurement Concepts Summary	36
8	Swallowed Shock Probe	37
9	Boom with a Spherical Tip for Measuring α, β, P_T, P_S, q, hp	37
10	Proposed Orbiter Nose Configuration	43
11	Proposed Booster Nose Configuration	44
12	Hemisphere Pressure Distribution	46
13	Pressure Coefficient Factor "B" versus Mach Number for Hemisphere Pressure Distribution Formula I	48
14	Conventions Used to Define Angle of Attack and Sideslip	53
15	Angle-of-Attack Values for Various Flight Phases	62
16	Angle-of-Attack Error Sensitivity Variation for Several ±45° and ±30° Port Sets and Transducer Hookups	66
17	60° Nose (Booster)	68
18	40° Nose (Booster)	69
19	60° Nose (Orbiter)	69
20	Subsonic Pitot/Static System Elements	72
21	Sphere Nose Sensor System Elements	72

ILLUSTRATIONS (Continued)

Figure		Page
22	Pressure (PSF)	78
23	Sensor Pressure Difference versus Altitude During Δ Wing Orbiter Entry Trajectory	80
24	Orbiter Air Data Measurement System Sensor - LRU Interconnection	85
25	Booster 40° Nose Air Data Measurement Sensor - LRU Interconnection	86
26	Booster 60° Nose Air Data Measurement Sensor - LRU Interconnection	87
27	Shuttle Air Data Measurement Electronics	88
28	Orbiter Altitude and Relative Velocity versus Time	96
29	Orbiter Entry Trajectory 603	96
30	Pressure Differential versus Time	98
31	RSS α Error for 1 psf Pressure Differential Error versus QB for Unit 1	99
32	RSS α Error for 1 psf Pressure Differential Error versus QB for Unit 2	99
33	RSS α Error for 1 psf Pressure Differential Error versus QB for Unit 3	100
34	RSS α Error versus Time	101
35	β Error versus QB - Unit 1	101
36	β Error versus QB - Unit 2	102
37	β Error versus QB - Unit 3	102
38	Orbiter β Error versus Time	103
39	RSS Error in P_{T2} Due to 1 psf Error in Differential Pressure Transducers versus Alpha	103
40	Booster Alpha and QB versus Time (B-9U Baseline) (B-9U Alternate QB in Dashes)	105

ILLUSTRATIONS (Concluded)

Figure		Page
41	Booster Altitude and Relative Velocity versus Time (B-9U Baseline)	105
42	Differential Pressure versus Time, 40° Nose	106
43	Differential Pressure versus Time, 60° Nose	106
44	40° Nose RSS α Error versus QB [Equation (8)]	107
45	40° Nose RSS α Error versus QB [Equation (9)]	107
46	60° Nose RSS α Error versus QB [Equation (1)]	108
47	60° Nose Rss α Error versus QB [Equation (9)]	108
48	RSS α Error from 1 psf Pressure Differential versus Time, 40° Nose	109
49	RSS A Error versus Time, 60° Nose	110
50	β Error 40° Nose versus QB for 1 psf Error in (Port 5 - Port 3) [Equation (8)]	110
51	β Error 40° Nose versus QB for 1 psf Error in (Port 5 - Port 3) [Equation (9)]	111
52	Booster 60° Nose β Error versus QB [Equation (8)]	111
53	Booster 60° Nose β Error versus QB [Equation (9)]	112
54	Booster β Error versus Time	112
55	RSS P_{T2} Error from 1 psf Error in Differential Pressure versus Alpha, (40° Nose)	114
56	RSS P_{T2} Variation for 1 psf Variation versus Alpha (60° Nose)	114

TABLES

Table		Page
I	Winds	21
II	Needed Air Data Parameters	25
III	Corrected Pressure Word Derivation Approaches	40
IV	Backup Possibilities for Particular Sources of Failure	73
V	Summary of Needed Transducer Characteristics	76

AIR DATA MEASUREMENT SYSTEM FOR SPACE SHUTTLE

By J.C. deJesus, Delroy J. Sowada, and Fred A. Moynihan

SUMMARY

This interim report describes the work accomplished by Honeywell Inc. for NASA Marshall Space Flight Center (MSFC), Huntsville, Alabama, in accordance with the requirements defined by Contract NAS 8-26326, "Space Shuttle Air Data Measuring System Definition Study and Design." This report has been prepared to fulfill the requirements of Item 2 of the Data Requirements List of the subject contract.

Some of the information presented herein is now out of date due to changes in the Shuttle vehicle configuration since initial writing of this report. An updated version will be provided in the final report, which will be issued when all tasks associated with this study contract are completed.

From November 1969 to January 1970 NASA Manned Spacecraft Center's Information System Division (ISD) was active in defining what air data would be required to support the Space Shuttle program and identifying the present state of the art in air data sensor technology.

Inputs as to air data requirements of the Space Shuttle Vehicles (SSV) were obtained from NASA Manned Spacecraft Center (MSC) Guidance and Control Division and Flight Research Center's (FRC) Data Systems and Research Projects Directorates. State-of-the-art information was obtained through an MSC library search, documents from industrial corporations, and from personal contacts with FRC and Ames Research Center (ARC) personnel. The main results of ISD's study are documented in a memorandum EB85-1/70-032 dated 28 January 1970, to the Chairman, Space Shuttle Integrated Electronics Technology Committee.

A summary of NASA's position as outlined in the memorandum is as follows:

a. Some air data will be required as a backup during the re-entry through landing phases for both the booster and orbiter vehicles. A system that will allow the pilot to make a successful re-entry and landing despite a total failure of the inertial guidance system is most desirable.

b. The present state of the art appears to be such that an air data system satisfactory for all phases is attainable.

c. A more in-depth study of research work completed and now being done by ARC, FRC, and MSFC is indicated before a new development project is initiated. (After subject contract initiation, Honeywell contacted all concerned NASA Centers to inquire about Shuttle air data requirement and any change in NASA's position.)

In January 1970 the air data sensor development portion of Space Shuttle Vehicle Air Data Sensor Study (RTOP-125-64-13-00) was transferred to MSFC where this contract was monitored beginning 14 August 1970.

It is concluded from this study that air data measurements of angle of attack and sideslip are needed to control the SSV. The basis for this conclusion, along with recommended sensor design and implementation, are described in this report.

The authors wish to acknowledge the guidance provided by Mr. Alex Hafner, who monitored this work, Mr. John Hamlet and Mr. Thomas Marshall, all of whom participated in the contract design reviews at NASA/MSFC.

Acknowledgment is also given for numerous helpful contacts with personnel at NASA-FRC including Mr. Donald Veatch and Mr. Rodney Bogue; at NASA-MSFC with Mr. Raymond Holder; at NASA-MSC; North American Rockwell Space Division; General Dynamics - Convair; and McDonnell-Douglas.

This contract program was conducted concurrently with the Shuttle Phase B studies where Honeywell Inc. was teamed with North American Rockwell Space Division and General Dynamics - Convair for definition of orbiter and booster Guidance, Navigation and Control. Shuttle air data requirements and data base were established through the help of many Honeywell engineers/scientists associated with the Phase B studies and other Shuttle control technology contracts.

1.0 SCOPE AND ACCOMPLISHMENTS

The program objective was to perform a study of the requirements for air data measurements on the Space Shuttle,[1] define and design an air data measurement (ADM) system, and prove feasibility of the design approach.[2] To accomplish this objective, the following key tasks were defined and accomplished.

1) Perform a preliminary requirements study of an ADM system for the Space Shuttle orbiter and booster vehicles
2) Select a measurement method for each required air data quantity
3) Define a tentative ADM system and describe its characteristics. This included completion of a preliminary contract End Item Part I specification.
4) Design the flow direction probe and conventional pitot-static probe for the Shuttle vehicles. This included:
   - Mathematical representation, development, and pressure port location optimization
   - Simulation of the flow direction probe performance over applicable Shuttle trajectories
   - Adaptation of the flow direction probe to the Shuttle vehicles.
5) Define the transducer performance characteristics necessary for the ADM system and assess the performance of transducers under test at NASA against the requirements.
6) Consign to NASA, for approximately 30 days, the Honeywell digital air data computer to allow evaluation of its performance over its normal operating range.
7) Conduct a trade study between a dedicated air data computer and utilization of the GN&C computer for air data computations and recommend the optimum approach.

---

[1] Original scope only included the hypersonic re-entry to landing portion of the mission profile; however, per mutual agreement the ascent portion of the mission profile was also included.

[2] Original scope included fabrication and test of the critical sensor to prove feasibility; however, it was subsequently established that existing wind tunnel and flight test data on the critical sensor (flow direction sensor) was sufficient to prove feasibility and, in addition, provide the data base for development of system mechanization equations.

8) Define the computation requirements including switching logic sizing, computational equation sizing, monitoring and self-check sizing, and word length/computation rate requirements.

9) Analyze the ADM system performance for a typical booster and orbiter trajectory. This task included design of the system electronics such that a comprehensive performance analysis could be properly executed.

10) Develop the mechanization equations for converting the flow direction probe pressures to the related output parameters and generate a FORTRAN computer program containing the equations so that it can be utilized by NASA to assess the effect of the transducer performance (item 5 above) on ADM output parameter performance.

11) Provide the required data and reporting.

All of the above tasks have been completed. In addition, although they were not specifically requested in the work statement, the following tasks were accomplished in the course of the program:

- Redundancy analysis - the eventual choice of redundancy concepts among the detailed approaches has significant impact on the system design. Therefore, inclusion of an analysis was deemed necessary to reflect properties of various alternatives.
- Skin temperature measurement analysis - although not typically an air data function per se, the potential of such measurement for at least a backup control approach for sideslip and angle of attack was judged to be significant enough to warrant an application analysis.
- An analysis of drag measurement stabilization for the GN&C system - this approach to stabilization of the GN&C system was defined and analyzed bdcause it is somewhat related to the subject of air data measurement (using internal force sensors) and it was judged to be a feasible solution to the classic problem of inertial system divergence when "sensible" atmosphere is encountered during re-entry.

The Technical Discussion section of this report, in conjunction with the appendices, presents the detailed definition, design, development, and analysis information that was generated during the performance of the above tasks. The report also includes conclusions and recommendations relative to integration of the air data measurement system into the Shuttle vehicles and avionics system during Phases C and D of the Shuttle design and development program.

A corollary objective of this Shuttle technology support contract was to define those feasible and useful air data sensing technologies for use by the mainstream Shuttle program. The ultimate selection of air data sensors depends on vehicle configuration, mission profile, and the particular redundancy and avionics integration philosophies chosen by the Shuttle designers. This work, providing the air data alternatives available to these designers, is summarized in this report.

Progress reports were sent to mainstream Shuttle design teams during the course of this study.

2.0 CONCLUSIONS AND RECOMMENDATIONS

The Space Shuttle air data function consists of the sensing and transducing of local flow pressures plus computations in the integrated avionics computer to derive flight parameters used to complete the Shuttle mission. Considerations for air data measurement (ADM) configurations apply equally to the booster and orbiter.

It is concluded from the study that air data information is needed for Space Shuttle. The Space Shuttle vehicle cannot be controlled during re-entry without a knowledge of angle of attack and sideslip angle. Although these parameters may be determined inertially at the higher re-entry altitudes, the velocity errors at lower altitudes caused by wind result in errors in α and β of 1 degree and higher. Also, the inertial system error can conservatively reach 1 degree because of the long entry time. Therefore, because the vehicle must be controlled to within less than 1 degree of β to prevent an unstable moment about the yaw axis, a flow direction sensor must be used. Also, α and β are necessary for effective piloting or the equivalent automatic modes during subsonic flight including descent, cruise, and landing.

The flow direction sensor recommended for Space Shuttle is a spherical shaped body with flush ports for measuring and transducing pressure which can be used to calculate α and β independent of Mach number and altitude. The sensor has no moving parts and, therefore, has relatively high reliability and low maintenance. These factors reflect a more cost-effective instrument compared to movable flow direction sensors such as vanes, Q-ball, and rotating arms. The recommended configuration is the result of a concept literature search, evaluation, selection, and preliminary design.

The flow direction sensor must be located in an undisturbed flow field on the Space Shuttle vehicle. The best location is at the leading edge of the vehicle as an integral portion of the vehicle nose section.

When the sensor is "right on the nose", it strongly influences vehicle design. The nose shape affects the Space Shuttle vehicle aerodynamic coefficients which in turn dictate trajectory and aerodynamic heating. With such strong vehicle design influence, the sensor nose must be integrated into the vehicle early in the vehicle development program.

An important step in sensor/vehicle integration is wind tunnel tests of the sensor/vehicle. These tests are needed to confirm predicted sensor performance prior to Shuttle flight tests. Predicted performance is largely based on wind tunnel pressure data correlated on the current phase of the program. This data base provides high confidence in the sensing concept. Also, flight tests of similar configurations on the X-15 aircraft and a USAF advanced lifting re-entry vehicle show good agreement with other on-board measurements, i.e., the Q-ball on the X-15 and inertial gyro on the re-entry vehicle.

The flow direction sensor and design presented in this technology report will meet Shuttle flight requirements and can be integrated into the SSV nose. Although the fixed-sphere α - β sensor configuration is an advancement, it can be developed within the Space Shuttle time frame.

In addition to providing flow direction, the sphere-shaped nose sensor provides total (stagnation) pressure measurements during entry following the point where dynamic pressure, q = 15 psf. Because total pressure for M > 2 is nearly a constant times q, total pressure is useful for scheduling. Knowledge of q, along with inertial velocity, provides a means of arriving at density altitude.

It is concluded that for subsonic flight, a conventional subsonic pitot-static probe is needed. It provides total pressure and static pressure measurements for calculation of pressure altitude which is mandatory for inertial system clamping. This probe also provides airspeed and Mach number where winds are a significant fraction of speed, thus ruling out inertial measurement. It is recommended that the pitot-static probe be mounted on the fuselage where the flow is attached, and aligning it with the local flow direction as determined by wind tunnel tests. Deployment or cooling is necessary to avoid excessive entry heating damage.

Sideslip measurement to $\pm 1/2°$ overall and angle of attack measurement to $\pm 1°$ overall is possible with differential transducers having ± 1 psf error over a ± 500 psf range. These errors are reduced for flight conditions with increased dynamic pressure.

These flow angle measurements require a transducer accuracy of ± 1 psf or 0.5 percent of value. Calibration of null offsets prior to entry and arrangements with improved performance at specific attitudes can be employed to reduce flow direction measurement errors. Maximum differential transducer exposure range is $\pm$ 1100 psf with a maximum measurement range of ± 600 psf. This accuracy requirement is no more stringent than that which is required for current air data system applications. However, some development may be required to achieve differential (as opposed to absolute) pressure measurement to this accuracy; for example, potential candidate transducers under test at NASA/MSFC to date exhibit accuracy characteristics only marginally compatible with Shuttle ADM accuracy requirements.

Shuttle air data system hardware provides raw measurements which are converted to air data by added software in the central computer, rather than signals representing air data.

On the basis of analysis summarized above, utilization of the Shuttle central computer for air data computations is judged to be acceptable and more cost effective than utilization of a dedicated computer.

Because there were no baseline requirements for redundancy in the ADM system, no conclusions or recommendations concerning redundancy will be presented here, except to state that redundancy was considered in the study, and results are presented.

3.0 TECHNICAL DISCUSSION

This section provides the detailed technical information which establishes the ADM configuration needed for the Shuttle booster and orbiter vehicles, describes the design, and assesses capability and impact for typical installations. The discussion has the following major sections:

- Background
- Air data measurement system tradeoffs
- Fixed-sphere nose sensor design
- Conventional pitot-static probe design
- Detailed description and analysis of specific configurations

3.1 BACKGROUND AND SUMMARY

The combination of spherical nose flow direction, sensor and deployed subsonic pitot-static probe depicted in Figure 1 meets Shuttle guidance, control and piloting needs with minimum installation impact, development risk and measurement hardware complexity. These ADM sensors are essential and complement the basic redundant inertial guidance approach defined as baseline for Shuttle.

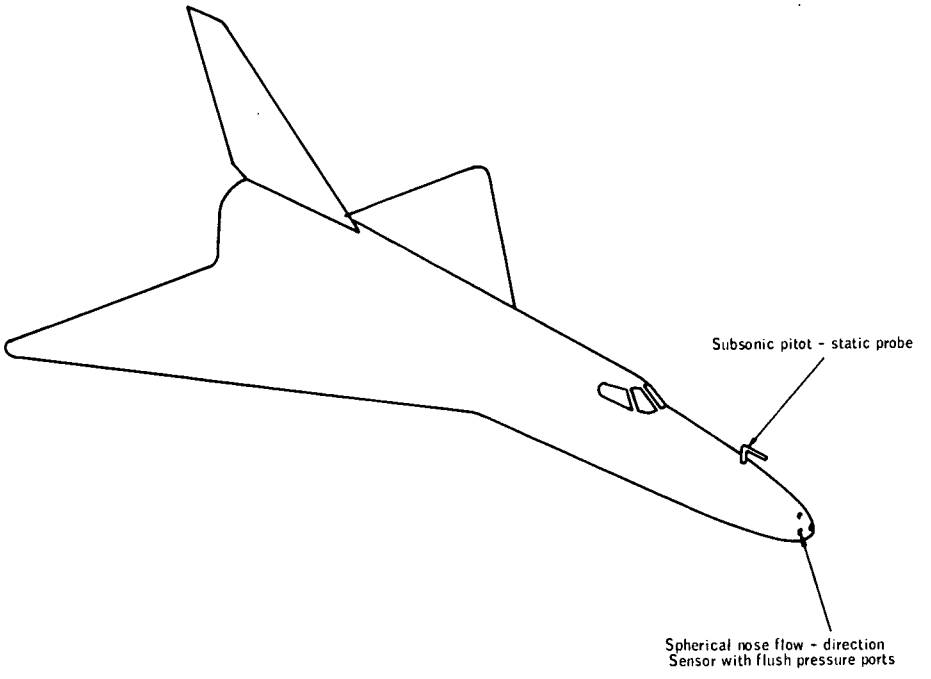

Figure 1. Space Shuttle Air Data Measurement Sensors

The considerations leading to the selection of these ADM sensors follows.

3.1.1 General Shuttle Requirements

The air data sensor and added avionics must be consistent with the general Shuttle mission, vehicle, and avionics requirements. A brief statement of these is presented below. These have been drawn from ref. 1 and 2 and data bases.

- Equipment Use - Nominal mission and trajectories, up to 7 days mission time; 2 weeks turnaround over 100 missions lifetime. No special provisions for flight test or off-nominal missions.
- Selection Criteria - Man-rated equipment with 1972 technology base, maximizing payload weight with minimum cost per launch. Support costs minimized with autonomous GN&C (and abort), redundancy of similar backup units, and on-board isolation to faulty units that are replaced.
- Configuration and Integration Constraints - Air data measurement is part of the GN&C subsystem containing redundant inertial sensors; interfaces are via redundant digital busses and standardized interface modules; computation integrated with GN&C and data management subsystems; units accept self-test commands and provide test points for failure monitoring; display functions integrated with data management system's multi-format displays.
- Other - Redundancy of flight-critical units to avoid single-point failure and provide automatically switched FO/FO/FS control. Airline practices for ferry flight with FAA certification to Category II (with III C goal). Consistency with environments of boost and entry and the vehicle's thermal protection and aerodynamic design.

3.1.2 Needed Air Data Parameters

Actual flow direction angles (angle of attack, α, and sideslip, β) are necessary air data parameters after a point late in entry (through the subsonic and landing phases. When atmospheric winds become 10 percent of the vehicle velocity, the inertial system's earth-relative velocity and attitude determinations can be 6 deg away from actual flow direction. The X-15 pilots (ref. 3) felt α and β were primary control parameters; α and β installations appear on high-performance aircraft because of necessary sacrifices in aerodynamic characteristic over the subsonic speed range. Since flow direction angles are necessary for Shuttle vehicles and the inertial determination has serious error at lower velocities., flow direction must be sensed with air data sensors.

Airspeed or Mach number during all subsonic phases must be air data sensor outputs because wind is a significant difference between actual and inertially derived velocity.

Pressure altitude is necessary for observing altimetry corridors when flying through commercial flight lanes. Otherwise the air data source of altitude is one of several available means to clamp the vertical channel divergence characteristics of the inertial system. Rate of climb is better provided from the inertial system's clamped-vertical channel than as pressure-altitude rate.

Various control scheduling parameters (like q or Mach) could be used from air data sensors; in all cases an adequate equivalent can be derived from inertial measurements.

The need for $q\alpha$ and $q\beta$ during combined boost could be provided by air data means. Avoiding the orbiter-to-booster interface for booster control in "orbiter-nose-ahead" configurations, the equivalent compensated-lateral-accelerometer approach is preferred (see paragraph 3.2.2.1).

Multiple redundancy of inertial measurement units, interfaces, and computers is the baseline Shuttle avionics approach precluding need for back-up entry guidance using air data. Skin temperature sensing during entry is desirable to indicate override of primary control mode in event actual skin temperature is dangerously higher than anticipated in simulations. Such sensing is part of the thermal protection subsystem, not air data sideslip sensing, such skin temperature sensors are also part of the thermal protection subsystem, not air data (see ref. 1 and 2). With extension of skin temperature sensing sensitivity, sideslip is derivable from differential wing-skin temperatures (see paragraph 3.2.3.3). Though an alternate or backup to air data sideslip sensing, such skin temperature sensors are also part of the thermal protection subsystem.

The continued availability of inertial sensors on Shuttle vehicles leads to air data sensing needs that complement rather than backup the inertial approach. Many of the entry guidance studies in the literature call for various air data parameters. Such needs evaporate once inertial guidance is viewed as always available for the entry guidance task.

This study of requirements and air data parameter parameter usage is discussed in more detail in subsections 3.2.1 and 3.2.2.

3.1.3 Candidate ADM Configuration

The fixed-sphere nose sensor on the orbiter and booster vehicles provides angle of attack, sideslip, and stagnation (total) pressure measurements (following the point where q = 15 psf during entry). The fact that stagnation pressure for $M > 2$ is nearly a constant times dynamic pressure q, is useful for scheduling. With use of inertial velocity, knowledge of q provides a means to estimate density altitude for divergence clamping of the inertial system.

For subsonic flight phases, a conventional subsonic pitot-static probe is deployed. It provides total pressure and static pressure measurements enabling computation of pressure altitude, airspeed, and Mach. Deployment is necessary to avoid entry heating effects. This combination of sensors is the recommended approach, meeting all accuracy and functional needs while providing redundancy during subsonic flight.

Use of the fixed-sphere nose sensor alone provides all needed functions (including subsonic P_T and P_S) with reduced subsonic accuracy; a gimbaled Q-ball sphere may survive booster entry (not orbiter entry) providing more accuracy over a reduced angle-of-attack range. Deployed α, β, P_T, and P_S probes either have undesirable length-of-boom for use during supersonic flight, or do not meet supersonic needs when deployed subsonically. The summary of studies relating these and other alternatives considered are discussed in subsection 3.2.3 and the overall recommendation is given in subsection 3.2.5.

3.1.4 Spherical Sensor Pressure Distribution and Measurement Relationships

Significant advancement was achieved in the derivation of mechanization, sensitivity, and error equations for the spherical sensor (flow direction, stagnation and subsonic static pressure). The distribution model was compared with test data available from the literature to another serious effort to make entry measurements. Theoretical backup for most all of the Space Shuttle speed range was obtained (see Appendix A).

The chosen model allows use of differential transducers, whose dynamic measurement range is much smaller than equivalent absolute pressure transducers, thus easing mechanization for flow direction angle determination.

These design data are summarized in subsection 3.3, including interpretation of Shuttle vehicle and trajectory constraints regarding installation, pressure port locations, redundancy considerations and transducer requirements. Equations for specific configurations (subsection 3.5) were verified using a FORTRAN program delivered to NASA MSFC.

3.1.5 Error Analysis

Using the relationships presented in subsection 3.3, the spherical sensor errors were evaluated for typical port configurations over typical entry and subsonic flight conditions. For the fixed-sphere sensor primary error sources are:

a) Misalignments of ports relative to vehicle axes.

b) Deviations of actual pressures (or at least the test data used) from the spherical distribution model.

c) Pressure measurement errors in converting physically sensed pressure to digital word representation.

Error source (a) is repeatable and can be calibrated out to less than 1/4 deg using misalignment coefficients in the computation of outputs. Flow direction angles are affected directly by error source (a).

Error source (b) has little effect when one of the difference pressures used to measure flow directions is near zero; over the angle of attack range, this error source can be as large as 1 deg one-sigma for 45 deg or larger port pairs and 1.7 deg for 30 deg port pairs; small local perturbations due to surface imperfections should be less than 1/4 deg per X-15 Q-ball experience.

Error source (c) varies primarily with size of transducer errors and the port location choices, becoming small with increased level of dynamic pressure, q.

The sideslip measurement to ±1/2 deg overall and angle of attack measurement to ±1 deg overall is possible with differential transducers having ±1 psf error over a ±500 psf range. These errors are reduced for flight conditions with increased dynamic pressure. Calibration of null offsets prior to entry and arrangements with improved performance at specific attitudes can be employed to reduce flow direction measurement errors.

If the vehicle has low-q during entry (like the straight-wing orbiter considered early in study) the transducer errors would have to be reduced (factor of 2.5) to achieve these overall accuracies. The detailed discussion of the error analysis and assumed trajectories is given in subsection 3.5.

The error in absolute pressure measurement is the primary source for stagnation pressure measurement and one of the primary sources for subsonic static pressure measurement from the sphere nose. The other subsonic static pressure (P_S) uncertainty is the 0.7 percent P_S per degree uncertainty in location of point where surface pressure equals ambient static pressure. Absolute transducer accuracies of 0.1 percent to 0.3 percent of full scale (3000 psf or 42 in. Hg) are achievable and compatible with needs for stagnation pressure when M >2. For 3 and 9 psf transducer errors and 0.7 percent P_S static port uncertainty the RSS subsonic output errors at 0.5 Mach and 20 000-ft altitude are:

	P_T & P_S ± 3 psf	P_T & P_S ± 9 psf	P_S ± 9 psf Q_c ± 2 psf
Altitude error	±181 ft	±277 ft	±277 ft
Airspeed error	± 4.9 kt	± 8.8 kt	± 4.3 kt
Mach error	±0.0011 Mach	±0.0019 Mach	±0.001 Mach

The last column assumes use of ± 2 psf differential transducer to measure the uncorrected $Q_C = P_T - P_S$ (the static port location uncertainty remains).

Better subsonic measurement accuracies are possible using a pitot-static probe oriented within ± 10 deg of flow direction in a region of minimized static pressure defect.

Such a pitot-static probe provides the subsonic outputs in the simplest manner possible, from two pressure measurements: P_T and P_S. Measurement of these on the sphere nose is a good degraded backup, but requires correct flow direction sensing for valid compensation. The preference is for the less complex process yielding better accuracy (in spite of additional sensor hardware) for the primary source(s) of subsonic outputs, with the sphere nose subsonic output used as backup in place of redundant pitot-static probes.

3.1.6 Mechanization Analyses

The standard Shuttle equipment bay environmental requirements on the installed transducer/electronics unit were included in the CEI specification for the ADM system delivered to NASA MSFC. In subsection 3.5 typical hardware content of these units is described relative to example orbiter and booster mechanizations. The pitot-static probe installation design is discussed in subsection 3.4.1 while the fixed sphere nose installation is discussed in subsection 3.3.1.

Final pressure transducer selection was not made. Candidates in response to Honeywell procurement request and under test at NASA MSFC exhibit performance characteristics marginally compatible with transducer requirements detailed in subsection 3.3.6; however, the accuracy requirements are no more stringent than current typical air data computer applications. (The increased dynamic pressure in recent Shuttle trajectories has relaxed the accuracy requirements from that needed for the now-discarded straight-wing orbiter.) Therefore, the requirements are considered achievable

3.1.7 Remaining Areas of Uncertainty

The sphere nose sensor plus subsonic pitot-static probe system is beneficial, necessary and feasible for Shuttle vehicle installations; thus, its implementation is strongly recommended. There remain several unresolved questions which need to be considered. Among these are:

a) Validity of model and actual pressure distribution behavior when sphere nose is attached to actual vehicle afterbodies. The concern is most critical at subsonic speeds where flow circulation around the sensor/vehicle may exist, and at near sonic speeds where there is a lack of theoretical prediction. Wind tunnel tests on realistic vehicle front sections are being planned.

b) System configuration as regards sphere nose ports, transducer connections, and redundancy throughout the configuration is not finalized. Such decision depends on vehicle,

trajectory, outputs needed, other avionics, integration philosophy, and a degree of arbitrariness. This study provides a wealth of possibilities from which the system designer can choose.

c) Certain practicalities of installations need more design and development on specific vehicles to resolve. Among these are:

- Means to protect prior to launch
- Need for de-icing heaters
- Design of plumbing connectors and traps
- Separate location of pitot-static measurement electronics
- Pitot-static probe deployment mechanism.

3.2 AIR DATA MEASUREMENT (ADM) SYSTEM CONFIGURATION TRADEOFFS

As depicted in Figures 2 and 3, the air data measuring system for Space Shuttle is not the independent system with probes, transducers, computer, displays and special flight control interfaces typical aboard conventional aircraft. The Shuttle integrated avionics are interconnected with standardized digital data busses; all computations are integrated into one or more computation centers; and the display and data management functions are integrated into multipurpose/multiformat displays.

The Shuttle air data function is thus primarily the sensing, transducer and converting (to digital) of local flow parameters (pressures) plus added computations in the integrated avionics computer to derive parameters of flight relative to the surrounding air mass.

The need for Shuttle air data measurement is a tradeoff result compared against the alternative of no air data sensing and against sensing air data-like parameters by other means, rather than an accepted apriori need true of conventional aircraft. The redundant inertial guidance aboard Shuttle is the primary source of guidance, control, and piloting data during all aerodynamic flight phases. Air data measurement is a necessary addition to the GN&C system for successful guidance, control and piloting during normal atmospheric flight phases.

This subsection summarizes results concerned with establishing the necessity, the degree of performance, and the feasible configurations of air data sensors augmenting the baseline GN&C system. In the course of investigations, alternatives for deriving parameters by non-air data sensing means were posed, evaluated, and compared to the air data method.

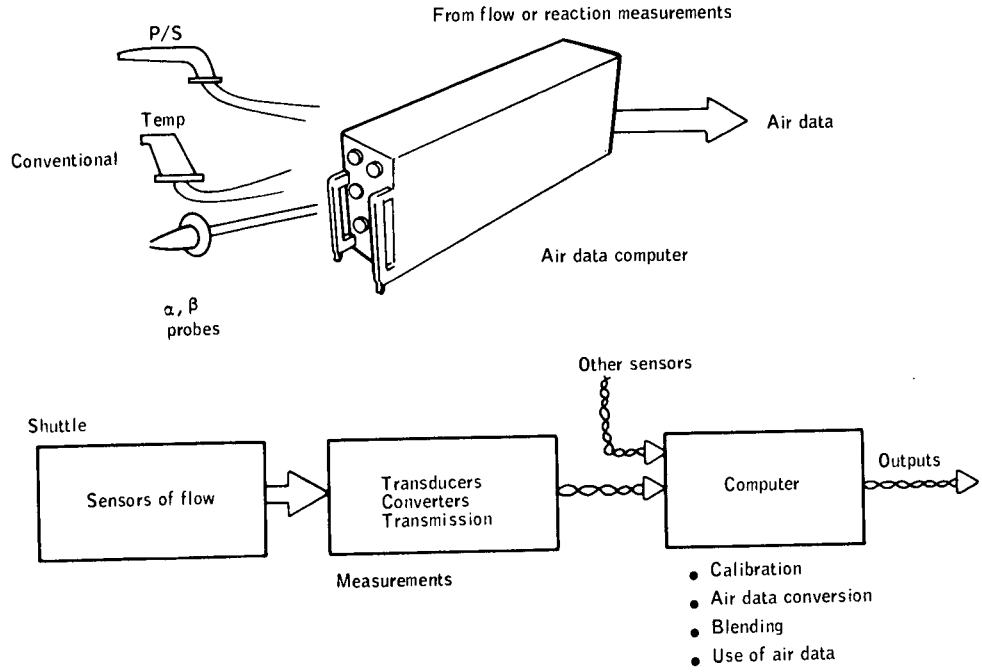

Figure 2. Air Data: Atmospheric Flight Parameters from Flow or Reaction Measurements

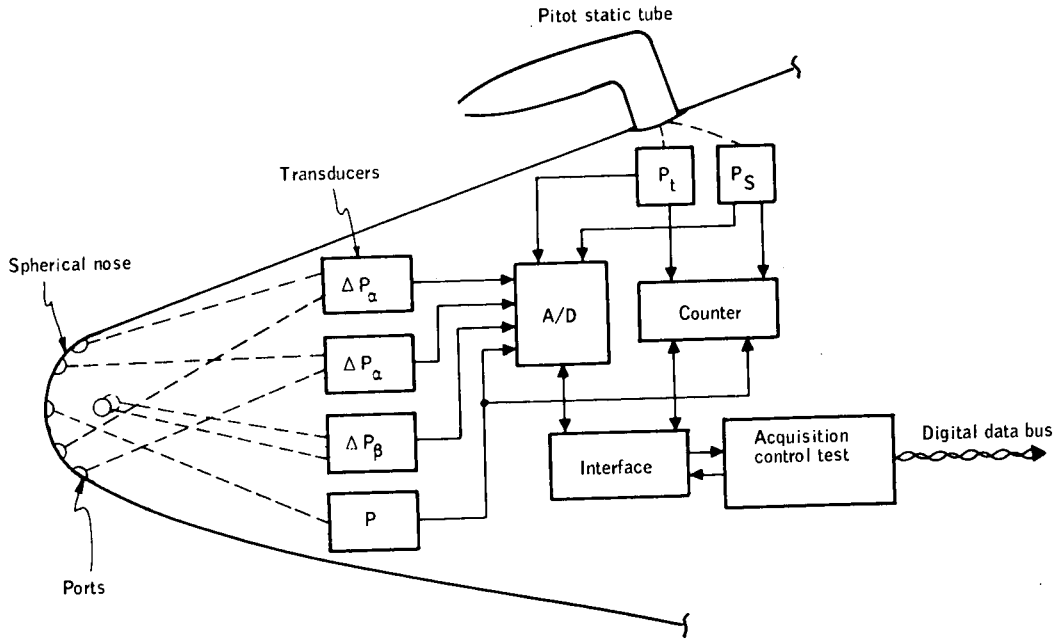

Figure 3. ADM Hardware

3.2.1 Baseline Vehicle and Avionics Data and Sources

The Phase B and other Shuttle technology study effort concurrent with this study were a primary source of vehicle, trajectory, and integrated avionics baseline data. By coordination with personnel on these contracts, primarily at Honeywell, needs were identified and alternate means of providing for them were assessed.

The scope of concern was bounded by considering only that sensing of atmospheric flight parameters needed for normal-mission guidance, control, and piloting displays. Special flight test instrumentation and air data sensing associated with payload experiments were thus not considered. Flight aborts, constrained by need to use on-board propellants, are accomplished with re-entry very similar to that of normal flight.

Reference 1 provided definition of subsonic altitude and airspeed requirements; Ref. 2 confirms the avionics organization and digital buss interfaces.

3.2.1.1 Basic considerations. - The Shuttle baseline avionics contains a redundant inertial system; in absence of atmospheric winds, with uniform conformance to the standard atmosphere, and with some means to control the inertial-altitude-divergence characteristic, no air data measurement would be required. Under these conditions, the inertial system could provide all needed parameters of the air data type from its earth-relative-velocity, position, and vehicle-attitude measurements. Since these ideal no-wind conditions are not true of the real atmosphere, this is one point of departure for the air data requirements study.

The second source of requirements are the mechanization assumptions for the guidance, control, and pilot display systems. Survey and follow-up coordination allowed definition of such needs and manner of usage for air data parameters.

The baseline integrated avionics configuration (see refs. 1 and 2) defined the use of digital busses for transmitting of signals within the vehicle and use of the computing capability of the central computing complex for computations associated with a system function (such as air data). Air data was defined as part of the GN&C subsystem of the Shuttle avionics. Contrasting with current aircraft air data systems, the Shuttle air data system hardware provides raw measurements which are converted to air data by added software in the central computer, rather than signals representing air data.

3.2.1.2 Flight phases - typical flight conditions. - The flight phases can be seen in Figure 4. The combined vehicle (orbiter plus booster) lifts off vertically and proceeds through the first stage boost trajectory reaching cutoff in about 210 seconds. This phase will be termed the combined boost phase.

At cutoff the vehicles separate and proceed on separate trajectories. The orbiter continues the ascent under its own rocket engine power reaching orbit-injection cutoff at about 450 sec. The orbiter then proceeds to its orbital operations which are associated with flight objectives. These orbiter flight

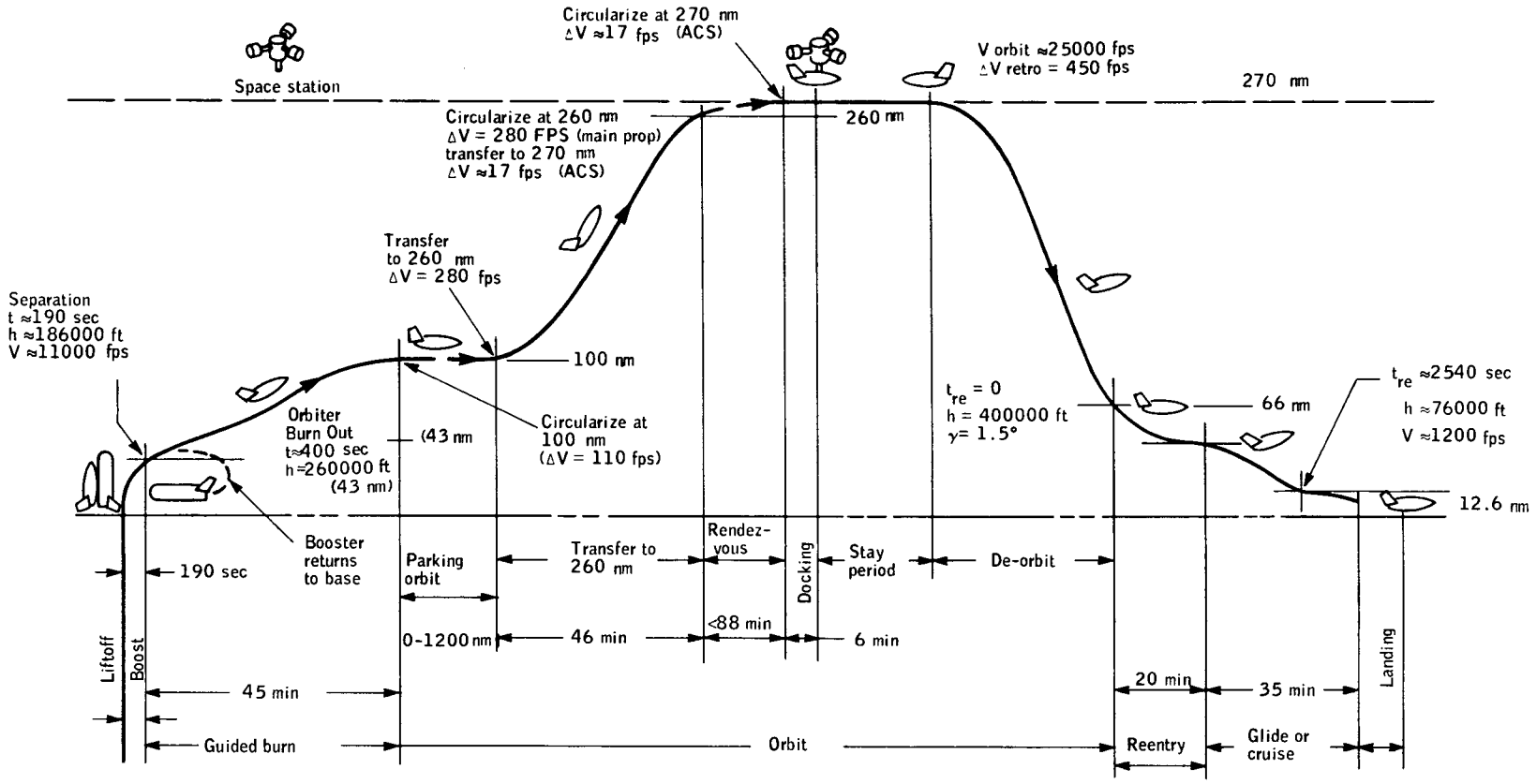

Figure 4. Nominal Profile Mission

phases, following combined boost, have practically zero dynamic pressure, q. With large velocities no air data measurements are meaningful in these exo-atmospheric phases.

After separation, the booster coasts with very small drag through apogee at about 250 sec after lift off and into its aerodynamic braking return. The velocity at separation is about 10 800 fps with an upward flight path angle of 5.6°. Little velocity decrease occurs until 310 seconds after lift off.

The aerodynamic braking force quickly builds up to 4 g at 360 sec and is controlled to below 4 g by reducing angle of attack from its initial 60°. Booster entry continues with modulation of angle of attack and bank angle to reduce and turn the velocity toward the launch site. At 680 sec a 400 n. mi. subsonic flyback under jet-engine power is started; at this point velocity is 600 fps and altitude is 20 000 ft. In less than 12 minutes the booster has gone through combined boost, coast, reentry, and transition to powered subsonic flight. Flyback has about 1-1/2 hours duration.

The orbiter's return from orbit starts with a de-orbit thrusting maneuver to reduce velocity below circular, followed by coast down to the denser atmosphere. The atmospheric braking entry is controlled with angle of attack and bank angle modulation according to guidance laws that: 1) minimize aerodynamic heating, 2) assure reaching of landing field, and 3) reduce the velocity from about 25 000 fps at start of entry to 2000 fps at about 85 000 ft.

The transition phase continues this targeting and velocity-and-altitude reduction while stablizing flight to a near 1-g vertical component of aerodynamic lift at subsonic velocities. Subsonic glide then manages the remaining velocity and altitude energy in a manner assuring landing on the target runway at safe landing speeds. An alternate subsonic configuration using deployed air-breathing engines has been abandoned in recent orbiter baselines. In this alternate case, subsonic flight would be similar to booster flyback.

The remaining flight phase is ferry flight. Both the booster and orbiter (with strapped on engines) ferry to the launch site at subsonic speed of 0.4 to 0.6 Mach at a cruise altitude near 20 000 ft.

Broadly the Shuttle vehicle flight phases can be grouped for air data sensing purposes as:

- Combined boost
- Supersonic entry and transition
- Subsonic glide, powered cruise, landing and take-off.

For the booster, the phases during the short 12-minute period from lift-off to start of powered flyback can be grouped into one boost-and-entry phase since equipment used in any part of this flight period must be checked out and operating at time of lift off.

More detailed data on Shuttle vehicle flight conditions is contained in Appendix B.

3.2.1.3 Summary of basic considerations. - Among the most consequential baseline definitions are:

a) Guidance and control is based on redundant inertial navigation systems and supporting sensors.

b) Interfaces between equipment are via digital busses.

c) A very powerful digital computing complex provides for the bulk of computations associated with navigation, guidance, control and display.

The need for sensor additions of the air data type is determined by the inadequacies of the baseline inertial system approach without air data sensing. These inadequacies are:

a) Wind Error of INS - In the presence of atmospheric winds, the inertial system's determination of vehicle velocity magnitude and direction relative to the surrounding air mass has percentage-of-magnitude and direction errors inversely proportional to velocity.

b) Altitude Error of INS - Without another means to determine altitude, the inertial system's vertical channel diverges with doubling of error in times like 5 minutes at subsonic speed and longer times at higher speeds.

c) Possible Modeling Inadequacies of Guidance - Orbiter entry guidance controls skin temperature within limits by implicit means proven by simulated flight through model atmospheres that include expected deviations from standard. For those flights requiring near-limit temperatures, explicit skin temperature measurements may be necessary to signal override or modulate the primary guidance law. Such measurement is defined as part of the thermal protection system not air data.

d) Control Mode Defined as Explicit Air Data Parameter - Maintaining a specific pressure altitude, Mach, or other air data parameter as a mode of flight, rather than the form available from inertial system and its navigational aids requires air data measurement of that parameter.

3.2.2 Candidate Uses of Air Data Parameters

By considering the operation of guidance and control systems used during atmospheric mission phases, possible uses of air data are identified and described.

3.2.2.1 Air data needs during combined boost. - Boost flight guidance and control is primarily inertial guidance with inner-loop attitude and rate stabilization controlling the direction of thrust relative to the vehicle and the earth. The velocity, position, and attitude measurements in earth-relative coordinates are very accurate during the short period of flight following very accurate initialization on the pad. No air data measurements are needed for the guidance function.

Complications arise from winds in the atmosphere. The high q region occurs when Mach number is between 0.5 and 2.5 (wind velocities are a significant fraction of vehicle velocity). Earth-referenced inertial measurements are not adequate for determination of angle of attack and sideslip; winds can cause a ±5° off-nominal angle of attack and sideslip.

The vehicle wings experience large loads proportional to $q\alpha$ that demand relief to stay within structural design limits. The vehicle has unstable sideslip moment and sideload bending due to sideslip; however, the sideslip (yaw) problem is less severe than the angle of attack (pitch) wind loads. For load alleviation and stability augmentation the following air data measurements of $q\alpha$ and $q\beta$ are desired:

Range	- ±5000 psf-degrees overall ±2500 psf-degrees with 10 percent linearity
Null offset	- ±70 psf-degrees
Hysteresis	- ±30 psf-degrees
Time constant	- Less than 0.1 second.

One alternative to air data sensing is use of accelerometers (compensated for instantaneous engine gimbal angle component of thrust) to sense specific side forces due to the relative wind. Another sensing approach to measure wingloads due to angle of attack is to measure differential pressure between top and bottom of wing. These are considered to be special load relief mechanizations, not air data sensing. To avoid the problems of flow interaction for orbiter ahead of booster, "$q\alpha$" sensing in the orbiter could be transmitted to the booster system. The alternate approaches are preferred to such air data sensing.

Other requirements for air data during boost are q and Mach for control scheduling and potentially $q\alpha$ and $q\beta$ or α and β for monitoring of need to abort (as done on Saturn/Apollo); measurements from the redundant inertial guidance system without accounting for winds are adequate for scheduling. Different criteria will be used for abort monitoring.

In summary, air data measurements during boost are desirable but not mandatory. The air data measurement configuration suitable for entry, transition, and subsonic flight needs has additional merit if, during boost, it provides:

q - dynamic pressure

M - Mach number

$q\alpha$ - for load relief

$q\beta$ - for lateral stabilization

α - switches when greater than +2° or less than -2° to enable pitch slewing control for reducing angle of attack.

3.2.2.2 Air data needs during entry. - Entry guidance and control is based on inertial system measurements. Two sources of error are of concern: 1) difference between earth-relative and atmosphere-relative velocity due to presence of atmospheric winds, and 2) divergence of the inertial system vertical channel. Velocity measurement errors due to other inertial guidance system sources are small relative to these.

Atmospheric winds (see Table I) in the 100 000 to 260 000 altitude region are 240 fps (mean) and 340 fps (max). Use of inertial velocity and attitude yields approximation of angle of attack, α, and sideslip, β, to within ±2° when velocity is greater than 7000 to 10 000 fps (for worst case bank angle and wind perpendicular to the velocity). Averaging overall possible directions of wind in the horizontal plane and over possible bank angles the inertially derived α and β would have an rms error of 2° when velocity reaches 3500 to 5000 fps. In either the worst case or probabilistic sense, direct sensing

TABLE I. WINDS

Altitude (feet)	Altitude (meters)	Mean (fps)	Mean (mps)	Maximum (fps)	Maximum (mps)
20 000	6000	80	24	125	38
30 000 to 45 000	9000 to 14 000	300	90	420	128
100 000 to 260 000	30 000 to 79 000	240	73	340	104

Reference: Handbook of Geophysics, Revised Edition - 1960
United States Air Force
Air Research & Development Command
Air Force Research Division
Geophysics Research Directorate

of α and β is necessary when velocity has been reduced to approximately Mach 4 and desirable below Mach 10. Figure 5 presents entry altitude velocity trajectories where this range of conditions can be viewed.

Sideslip measurements are used to stabilize to the $\beta = 0$ attitude within a tolerance that assures β never exceeding the sideslip angle where the unstable aerodynamic moment exceeds restoring torque available. Normal flight control is accomplished by modulating angle of attack and bank angle; release of bank angle provides backup means to achieve attitude stability at expense of targeting accuracy. Angle of attack measurement is used as a reference with respect to which angle of attack command from guidance law produces an error signal for angle of attack (pitch axis) control.

Inertial system altitude divergence in altitude and vertical velocity increases with initial condition errors and time of flight with a doubling of errors in a time period that decreases with decreased velocity. In orbit, the vertical channel exhibits oscillatory errors; at subsonic speeds vertical channel errors double in less than 7 minutes. For the orbiter entry from orbit, vertical channel errors have magnitude of autonomous position determination while in orbit and oscillatory behavior until drag forces start reducing velocity; during the braking portion of entry, errors increase with ever-increasing rate. At 2000 fps and 85 000 ft this error divergence can have magnitudes of 80 000 ft and 140 fps, unless some external means to clamp the altitude channel is provided. Among the methods possible for external altitude measurement are:

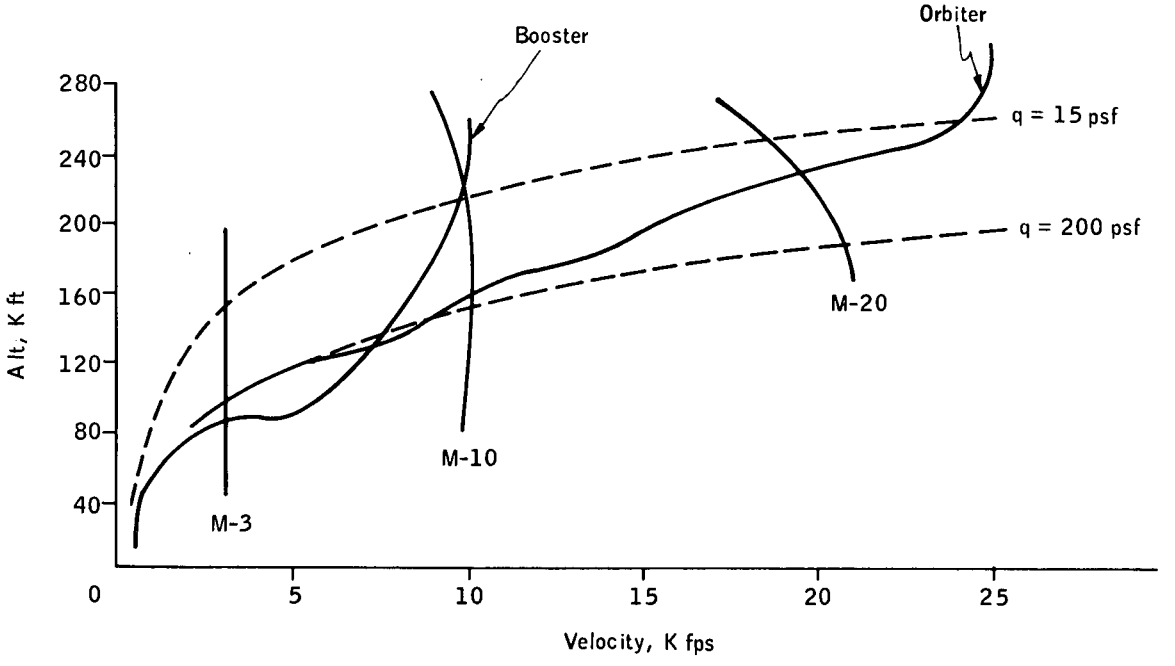

Figure 5. Altitude/Velocity Trajectories (Re-Entry)

a) A crude altitude versus the time profile for nominal entry trajectory.

b) Measuring specific lift force which can be related through aerodynamic coefficients to dynamic pressure, q, and with knowledge of velocity to ambient density. (Lift is better than drag or total force because of less aerodynamic coefficient uncertainty.) This approach is detailed in Appendix C.

c) Measuring stagnation pressure which is relatable to q at high Mach number ($M > 2$), and with knowledge of inertial velocity derive ambient density.

d) Use of static pressure altimetry at subsonic speeds as in conventional aircraft.

e) Use of returns from known-location transponders to determine position (including altitude).

f) Use of radar altimeter.

Some combination of these is necessary; the recommended air data approach involving (c) and (d) is an attractive candidate but not mandatory when alternatives are provided. Method (b) has the advantage of no sensors in addition to on-board inertial sensors.

For booster reentry, the 700-second period from launch to start of flyback does not provide much time for divergence to take place; thus primary vertical channel errors will occur because of inertial sensor errors (not divergence or initial conditions). These vertical channel errors should be tolerable until subsonic flyback when methods (d), (e), or (f) can be used to clamp the vertical channel. Angle of attack and sideslip sensing are necessary to account for winds in the later portion of booster reentry (for reasons similar to that for orbiter entry).

In summary, the entry and transition requirements for air data sensing include:

- Measurement of sideslip, β, to ensure yaw attitude stability
- Measurement of angle of attack, α, to give more accurate trajectory control and assure keeping α within stability limits at the lower Mach numbers
- Measurement of stagnation pressure as a possible means to obtain dynamic pressure, q, and altitude for $M > 2$.

The use of skin temperature measurements provides an alternate approach to inertial guidance for entry guidance and control. Such skin temperature measurements will probably be made on Shuttle vehicles as part of the thermal protection system (not air data) for monitoring of structure temperature with respect to its safe limits (and indicating need for override) and possibly as a backup sideslip sensing method in event of air data sensor failure. The need for this latter form of backup sideslip sensing is reduced when choosing a vehicle design that has better inherent sideslip stability than vehicles considered in the course of this study.

3.2.2.3 Air data needs during subsonic glide, powered cruise, take-off, and landing. - During these subsonic flight phases a means to derive altitude for inertial system clamping is mandatory. Pressure altimetry is a very good choice but mandatory only if the powered cruise must be flown through airways at an assigned pressure altitude.

With winds that are a significant fraction of speed, the use of airspeed hold and Mach hold modes during cruise dictates the conventional pitot-static system. In the conventional subsonic pitot-static system, 1) static pressure is calibrated to represent pressure altitude according to the standard atmosphere, 2) Q-sub-c, the difference between pitot and static pressure (or impact pressure) is calibrated to represent indicated, calibrated, or computed airspeed, and 3) the ratio of Q-sub-c and static pressure enables computation of Mach number according to Bernoulli's formula.

Vertical speed or altitude rate is also a conventional pitot-static system parameter; on Shuttle, the clamped vertical channel is a better source of this parameter because of better dynamic characteristics of the vertical accelerometer. At lower subsonic Mach numbers, Q-sub-c is a good approximation of q-dynamic pressure needed for control scheduling ($Q_c/q = 1.01$ at $M = 0.3$ and 1.09 $M = 0.6$).

In addition to these outputs available from a conventional pitot-static system, actual angle of attack and sideslip are necessary for effective piloting or the equivalent automatic modes of subsonic flight. Pilots view α/β sensing as a necessary measurement on X-15 (see Ref. 3); the Shuttle vehicle's subsonic flight characteristics have many contrary demands necessitating compromises that cause α/β sensing to be extremely desirable if not mandatory.

3.2.2.4 Summary of parameters needed for shuttle vehicles. - In summary form, Table II shows air data parameters needed during the indicated flight phases.

TABLE II. - NEEDED AIR DATA PARAMETERS

Parameter	Flight Phase	Use	Alternates
Airspeed, Mach, Qc	Subsonic	Cruise, glide, landing & take-off control	None
Pressure altitude	Subsonic	Cruise altitude assignment	None
		INS divergence control	Radar altimeter, multiple transponder
Density altitude	Later entry M > 2	INS divergence control	Radar altimeter, multiple transponder or drag (lift) measurement
Angle of attack and sideslip	Subsonic	Descent, landing, take-off, climb-out, & glide control	None
	Later entry & transition	Control sideslip to zero & control actual angle of attack (instead of INS)	None for selected inertial guidance; alternate skin temperature methods are possible
Flight intensity (a or P_T2)	Entry	Scheduling of control	Can be derived approximately from inertial system
$q\alpha$, $q\beta$, α, b	Boost	Load relief and stabilization	Accelerometers, rate sensors
q and Mach	Boost	Scheduling	Inertial system gives adequate approximate values

3.2.2.5 Summary of performance characteristics for needed parameters -- These performance values were obtained from Shuttle control studies on Phase B and technology contracts:

a) Subsonic Phases

Pressure altitude	- ±50 ft or ± 1% for 0 to 25 000 ft with 2-second time constant
	- ±3% for 25-40K ft
	- ±5& for 40-85 K ft
Airspeed	- ±4 kt or ±2% for 120 to 500 kt with 2-second time constant.
Mach	- ±0.01 M or 1.5% for 0.25 to 1.0 Mach range with 2-second time constant.
q	- 30 psf or 10% over 0 to 500 psf range.
α and β	- ±0.5° or 10% for $\lvert\beta\rvert < 15°$ and α between 0° and 30° (assuming compensation of installation misalignments at α = 15°, β = 0° nominal attitude).

b) Re-entry and Transition (M < 9)

α	- ±2° over 0 to 30° or 0 to 60° range
β	- ±1° over ± 10° range
q	- ±10% over 50-500 psf range
Altitude	- ±5% 70 K to 100 K ft
	- ±10% over 100 K ft

c) Boost Load Relief

q α, qβ	- ±30 psf-degree (0.1° α and β) hysteresis, ±70 psf-degree (0.3° α and β) null offset, 10% linearity out to ±2500 psf-degree (±5° α and β) with ±5000 psf-degree (±15 α and β) range. With less than 0.1-second time constant.

If air data outputs are provided for these functions, they represent the approximate level of performance desired to be useful. Better performance of actual sensors can have merit; larger errors in some cases may be acceptable.

3.2.3 Assessment of Potential Air Data Configurations

3.2.3.1 General Discussion. - Having chosen the properties to be measured the question is how to measure them. Ideally the air data parameters would be measured directly and not by inference, but such is not the case. For example, atmospheric conditions of pressure and temperature cannot be directly sampled from a moving vehicle because compressibility, heating, and shock waves all cause local conditions to be very different from ambient. Likewise, air data parameters associated with movement through the air such as air flow direction, magnitude and intensity relative to vehicle (e.g., angle of attack, airspeed and dynamic pressure) cannot be sampled directly but rely on measurement by inference.

A constraint of inference measuring is knowing the laws relating the sample to the desired parameter. For example, one must know the flow relations to relate the pressure sample of a pitot/static tube to measure airspeed or similarly the thermodynamic laws to relate a heating measurement to airspeed. Flow relations are developed for particular flight speed ranges as well as air density regimes. Speed is related to sonic velocity and is divided into the familiar subsonic, transonic, supersonic and hypersonic ranges. Air density regimes are related to the molecular mean-free-path-length between collisions compared to a body dimension of interest.

Space Shuttle covers all speed ranges and densities low enough so this also is a consideration for ADM. Hence, when considering ADM configurations one must be aware of these regimes and where on the entry trajectory of speed and density (Mach number versus altitude) the various laws apply.

Using 0.2 in. as a dimension (which is a reasonable pressure tap size) the altitude where the mean-free-path-length is also 0.2 in. is approximately 260 000 ft. This altitude then is approximately the maximum where measured pressures can be interpreted by conventional laws and above this altitude rarefied gas relations need to be considered.

Typical entry trajectories show the speeds to be hypersonic ($M > 4$) down, to about 100 000 ft, then supersonic ($1.5 < M < 4$) down to 60 000 ft, then transonic ($0.8 < M < 1.5$) down to 20 000 ft, and subsonic at lower altitudes.

These range limits are intended to scope the areas of interest and are not precise boundaries and apply to both the booster and orbiter.

Considerations for ADM configurations apply equally to the booster and orbiter. An exception is during ascent when the vehicles are mated. Then, if the nose of the orbiter is ahead of the booster, sensors in the booster nose will not provide accurate measurement because they are influenced by the orbiter flow field. Under this condition sensing would be done on the orbiter and a data link to the booster is required.

3.2.3.2 Inertial methods of ADM. - A complete reliance on inertial methods for providing air data measurement is a logical first consideration because it is already on-board. This implies that there is a separate measurement of altitude to prevent the vertical channel divergence which is characteristic of inertial sensing.

On conventional aircraft inertial systems the separate altitude measurement is a baro-altimeter. Problems with this are discussed below. A second scheme for a reference altitude which relies on knowing the aerodynamic coefficients is also discussed. Other types of altitude reference such as radar (ground and/or airborne) are possible. Problems of radio-type altitude measurement are not discussed separately but assessment of this and all such schemes is included under Inertial Scheme Assessment.

The inertial system with some non-air data-sensed altitude reference for divergence control can provide approximations of sideslip, angle of attack, flight intensity, etc. As velocity decreases the uncertainties of atmospheric winds and inertial system errors become a significant fraction of vehicle velocity. For example, at 2 000 fps, a 200-fps wind can cause an intolerable 0.1 rad (6 deg) uncertainty in angle of attack or sideslip; however, at 10 000 fps or greater the uncertainty is 1 deg or less; thus, now inertial air data sensing is necessary.

Following this line of reasoning the possibility exists for using the inertial system alone above velocities of 4000 fps. For lower speeds, a pressure sensor such as fixed sphere nose on the aircraft can measure static and total pressures and angles of attack and sideslip.

3.2.3.2.1 Inertial with baro-altitude reference: Usual aircraft practice for curbing vertical-channel-divergence is to slave the vertical channel to the baro-altimeter as an external altitude reference. Transducers do exist for measuring the very small ambient static pressures at 250 000 ft if a sample of the ambient could be obtained. Unfortunately there is no simple way to capture a sample of the ambient atmosphere and place it within such a transducer aboard the high-velocity Shuttle vehicle. The severe shock wave between the ambient and the vehicle causes compression, heating, and ionization of the potential sample that cannot be undone adequately in any probe concept.

The swallowed-shock static pressure probe concept comes closest capturing an ambient sample using a probe by attempting to sample the ambient ahead of the shock wave. This concept had to be abandoned because the probe lip design necessary to survive the heating environment and to provide flow for reducing molecular composition sensitivity of the low-pressure transducer invalidated the shock-swallowing characteristics of this probe.

Another method to sample the ambient is to use a flush port which is at ambient pressure. For a given flight condition there is some point on the vehicle where the local pressure equals the ambient static pressure. Since this point moves drastically and at times unpredictably with velocity and attitude changes, direct sensing attempts are very difficult. For a known simple shape like a sphere, this location and its movement is more predictable, given location of the stagnation point, attitude, and Mach number. This implies an

implicit solution for angle of attack, sideslip and altitude. Of course, putational iteration schemes are possible which improve on assumed values of α, β and altitude. This scheme is possible but with limitations. At high altitude and velocity ($M > 5$) the limitation is an accurate interpretation of the pressure seen by the transducer because the air sample has been subjected to high temperatures, which results in alteration of the molecular constitution. These could be corrected for, providing the sought for parameter of Mach number and ambient conditions were already known. The baro-altitude method is not hopeless, and offers a possible altitude reference particularly at lower altitudes and lower speed if it is the only way.

3.2.3.2.2 Inertial with altitude reference by calculation using aerodynamic coefficients: The inertial system sensors provide another possible altitude sensing approach. In addition to the usual double integration of specific force plus computed gravity, the specific force can be related to dynamic pressure, given mass of the vehicle and aerodynamic coefficients. Since dynamic pressure is $q = \rho V^2/2$, inertially determined velocity relative to the air mass, V, can be used to solve for ambient air density, ρ. Using a fit of ρ versus H_D the density altitude is determined according to the standard atmosphere. This approach is attractive since the only aid data addition to the Shuttle vehicle is additional software in the central computer. How well does this approach measure altitude?

Appendix C presents a more detailed discussion from which the following observations are made.

The gradient of air density versus altitude over the region of interest (below 80 km) is between 4 percent and 6 percent per thousand feet. Density variations of ±25percent from standard atmosphere due to location, season, and weather cause an uncertainty of about 5000 ft. Mechanization errors due to a) knowledge of vehicle mass, b) measurement of specific force, c) resolving to lift force, d) knowledge of aerodynamic lift coefficient versus angle of attack, and e) difference between inertial velocity and relative wind could be held within ±15 to ±25 percent after reaching sensible levels of aerodynamic force (0.05 g or more).

Early in entry flight, the largest mechanization error is characterization of the aerodynamic coefficient. The lift coefficient is distributed less by aeroelastic bending than drag or total force. Lift coefficient versus angle of attack and determination of angle of attack inertially early in entry flight is possible to the order of ±10 percent.

Later in entry flight vehicle velocity is reduced; the difference between relative wind and inertially determined velocity becomes a significant fraction of velocity. All determinations of aerodynamic parameters by the inertial system increase in uncertainty. Larger errors in relative wind, angle of attack, sideslip, lift coefficient, and hence acceleration-sensed density-altitude require turning off this mechanism when vehicle velocity reduces to the order of 2000 fps.

E

The expected density-altitude error during the phase from point of encountering reasonable aerodynamic force to the point where velocity is nearly transonic is less than 10 000 ft overall. Neglecting the deviations from standard day, a determination to ±2500 ft is possible with resolution of the order of 1000 ft with smoothing. Such a measurement should be adequate for vertical loop slaving. The actual altitude is not important to entry guidance. Inertial determination of aerodynamic attitude is enhanced because the vertical velocity determination in the vertical channel mixing loop is improved.

This lift-sensing determination of density altitude improves the inertial guidance of entry and can be considered a feasible and reasonable alternative for the high-velocity portion of return flight.

3.2.3.2.3 Assessment of inertial sensing schemes: The discussion has been aimed at using the on-board inertial system measurements and curbing the vertical-channel-divergence using sensing or assumed lift coefficients to determine an independent measure of altitude. Is this approach adequate?

Closer study of the means for controlling entry using the inertial system alone raises some questions. First, the vehicle must be stabilized about particular aerodynamic attitude (bank angle, angle of attack, sideslip equals zero) determined by the guidance law. The restoring moments in sideslip are such that actual sideslip must be kept small at all times. At high velocities the inertial determination is entirely adequate; however, as velocity is decreased the inertial sideslip determination degrades to point of being questionable.

Vehicle stability in angle of attack is adequate over a wide range of actual angles of attack; the primary concern of degraded inertial angle-of-attack determination with decreasing velocity is deviation from the nominal guided trajectory. Following transition to low-speed flight, angle of attack and sideslip in the presence of significant atmospheric winds are needed for piloting. Thus, an air data sensor measuring actual angle of attack and sideslip in the air throughout the entry and post-entry phases is desirable and perhaps mandatory in view of the sideslip stability question.

Other functions needed during the return flight are means to schedule control as a function of flight intensity (like dynamic pressure), a measure of altitude and airspeed during cruise and landing phases, and an alternate means for determining altitude during the entry phase. These suggest strongly that inertial systems without any external sensing are not possible.

A possible scheme is to use pressure sensors along with inertial sensors. One system is the redundant sphere nose $\alpha/\beta/P_{T2}$ sensor concept, detailed later, augmented by subsonic pitot-static probes, to provide these functions with minimum additions to the vehicle and avionics. Actual sideslip, measured redundantly and blended with inertial measurements early in entry, assures sideslip stability. Angle-of-attack measurement blended with inertial again enhances entry guidance. During high-velocity flight, the stagnation pressure behind the shock, P_{T2}, provides a measure of flight intensity for scheduling and in addition provides a simpler and more accurate approach for determining density altitude for inertial divergence control.

3.2.3.3 Temperature and heating rate methods of ADM. - Air data measurement consists of local on-vehicle measurements that can be converted to measures of vehicle velocity (magnitude and direction) relative to the air mass and properties of the proximate undisturbed air mass (implying altitude relative to a standard atmosphere). Various studies have proposed skim temperature and heating rate measurements to provide entry control and guidance signals. These sources are summarized and interpreted in the following discussion.

3.2.3.3.1 Sphere nose temperatures or heating rates: On a sphere, the temperature distribution and heating flux distribution have functions similar to the pressure distribution used for the recommended sphere-nose sensor (see ref. 4). The stagnation point values are largest with reduced values at points with spherical surface angles, E, away from the stagnation point. Given an array of thermocouples or heating rate transducers, flow direction and stagnation point values can be inferred from a fixed sphere nose.

The variation of temperature with local surface thermal conditions and the reduced response caused by sheathing materials used to protect and insulate the thermocouples cause the spherical temperature sensing approach to have uncertainties larger than ±1° and time constants slower than 1 second. The spherical pressure-sensing is discussed in subsection 3.2.3.4 for air data purposes.

Heating rate can be measured with thermocouple pairs imbedded in known-thermal-conductivity materials. The differential temperature is proportional to heat flow. Another heating-rate measurement approach is to measure the amount of coolant needed to keep a sensor tip at constant temperature. Such sensors would be much larger than the pressure ports used in the sphere/nose pressure sensor. Response to attitude changes would also be far slower than the pressure approach and flow direction accuracy of ±1° would be difficult to achieve.

The possibility of integrating a single temperature or heating rate sensor with pressure measurements of flow direction and stagnation pressure offers some advantage. Flow direction could be used to convert temperature or heating rate at a fixed point to stagnation values (using spherical distribution functions). The knowledge of two stagnation parameters - pressure and temperature or heating rate - enables determination of free-stream density and velocity.

If the Shuttle inertial measurements are always available there is no reason to have such determination of velocity in the air data system. Stagnation temperature, if necessary, can be provided by a high-total temperature sensing probe such as the one developed by Honeywell and tested on the X-15 (see ref. 5). This sensor would have less development risk than some yet-to-be-developed sensors mounted within the sphere nose.

3.2.3.3.2 Skin temperature sensing methods: The thermal protection surfaces on the Space Shuttle vehicles will have temperature sensors for monitoring of surface structure temperatures. The inertial-entry-guidance-

law simulations assure flight temperatures that are a design margin below maximum allowable temperatures. Skin temperature measurement could be used in the guidance law to further reduce the risk of exceeding allowable skin temperatures.

A non-inertial entry guidance and control system based on only skin temperature methods has been analyzed and verified in flight test of the ASSET AEV-2 vehicle (see ref. 6 and 7). The specific temperature sensor used in this flight test would not survive multiple Shuttle missions; reportedly, development on improved sensors is being pursued by the Air Force Flight Dynamics Laboratory.

Differential wing temperature is used for sideslip control in this temperature-rate flight control system (TRFCS); the survivability, accuracy, and response required of temperature sensors on the skin surfaces for sideslip is near state of the art. The critical need for sideslip backup on Shuttle could make use of this principle in conjunction with the less critical skin temperature-monitoring function now determining the skin temperature-sensing designs.

The remaining entry guidance aspect of the TRFCS is simply a different means than primary inertial of the Shuttle baselines. Unless backup guidance is necessary the TRFCS concept is inconsistent with present guidance and control approaches.

Other entry guidance methods using temperature measurements and other forms of air data parameters are presented in ref. 8 and 9. These are useful only as independent backup systems, being inconsistent and unnecessary when postulating the baseline inertial guidance approach. Of special note is the use of wing leading edge and wing bottom temperatures in the Bell System reviewed in ref. 9. Since these thermal protective structures have temperature sensors in any event, the empirical relationships between such temperatures and the velocity, density, and angle of attack could provide additional sensing backup capability.

3.2.3.3.3 Conclusion: The use of temperature measurement in addition to the sphere nose pressure sensor is not necessary except as potential back-up approaches. More development is necessary to achieve the necessary multi-mission surface temperature sensors with adequate accuracy and response. Since thermal protective structures have integral temperature sensors for monitoring reason, extension to guidance and control function backup use may be achievable with small additional costs.

3.2.3.4 Pressure sensing methods of air data measurement.-

3.2.3.4.1 General: Pressure sensing can perform air data measurements of angle of attack, angle of sideslip, pressure altitude, density altitude, and dynamic pressure. Location of the pressure taps in the flow field determines the correlation law between the pressure and the ADM parameter which implies that the flow field is the known. Hence, the advantage of locating pressure taps on simple shapes located away from other disturbances. This is the reason for locating pressure sensors on a boom away from the aircraft, particularly

at supersonic speeds where the boom penetrates the vehicle shock and forms its own flow field.

3.2.3.4.2 Nose boom consideration: Use of a nose boom on the Space Shuttle at supersonic speeds involves more problems than conventional aircraft. First, to survive the heating during entry requires cooling the tip whose shape must be preserved for accurate pressure readings. A thermal protection system such as for the rest of the Shuttle is not possible because the smaller diameter (6 in.) both elevates the temperature and reduces the space for it. Length of the nose boom (about 5 ft for the orbiter and 10 ft for the booster to avoid aircraft shock interference) requires additional nose structure to carry the loads. Also, a boom can alter the aerodynamics of the aircraft, particularly at supersonic speeds (M = 1.5 to 4) for the blunt booster nose where it may act as a skip spike (Figure 6). This can be an unstable flow in that it alternately separates from the tip of the spike and then the base of the spike causing large, dangerous changes of forces. At subsonic speeds the nose boom is not as necessary as at supersonic speeds.

A boom retracted during the high heating of entry and deployed at supersonic speeds, $M < 4$, is a possibility. This speed corresponds with the lower limit of the all inertial system for providing ADM types information and is attractive. The obvious disadvantage is the size and complexity of the retracting mechanism.

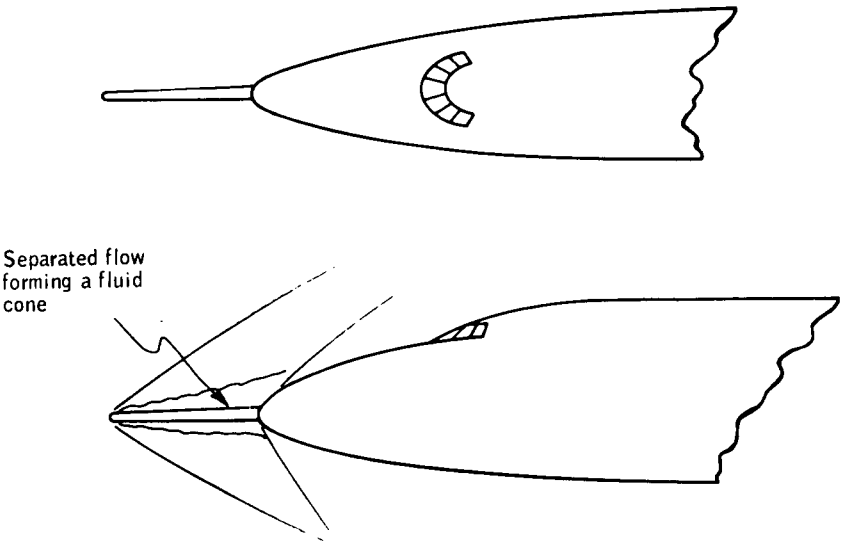

Figure 6. Flow Pattern IF Boom Acts as a Skip Spike

3.2.3.4.3 Sphere nose: An alternative to a boom is to simply use the nose of the aircraft itself as a spherical sensing surface. The radius is large enough to bring heating within capabilities of the existing thermal protection system and the need for structural alterations required by large fixed or deployed booms at high speeds is eliminated. The spherical portion of the nose need not be a complete hemisphere but cover only an arc from the axis equal or a little larger than the expected angle of attack or sideslip. Thus, the concept needs early incorporation into the airframe design.

Angle of attack, α, and sideslip, β, sensed by pressure measurement is best done on a spherical surface compared to other asymmetric shapes for obvious simplicity. The question then is whether the spheres is movable or fixed.

A movable sphere pivots abouts its center to null the pressure difference between symmetrically located pressure taps. The center of the tap pattern (usually four holes) is the direction of the on-coming air and the angle to the aircraft axis is resolved into α and β. With a fixed sphere, the pressure differences between pairs of taps are measured and the flow direction is calculated from them using a known pressure distribution.

The first advantages of a movable sphere is that it can read α, and β, directly without computation and knowledge of the pressure distribution and read total (P_T) and static pressure (P_∞). A disadvantage of the movable sphere is mechanization problems which would be particularly severe for the high temperatures on the Shuttle nose during entry. Another problem is the flow separation on the sphere surface caused by lips that house the nose, as shown below.

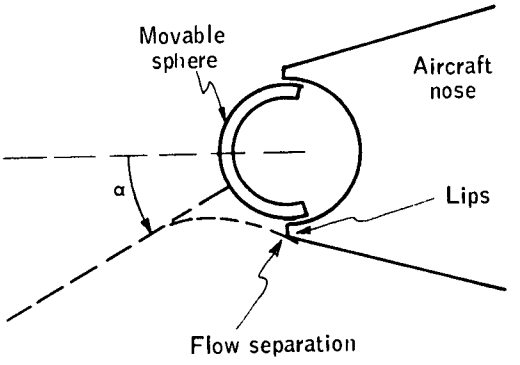

The flow separation problem which can affect accuracy was noted on the X-15 Q-ball and would be more severe on Shuttle because not only are thicker lips needed but a greater α range is also required. Temperature problems of mechanization show up in maintaining clearance between the sphere and the lips as well as high temperatures for the mechanism that moves the sphere typically hydraulic.

An advantage of a fixed sphere is no-moving parts or flow disturbances and a disadvantage is the need for computation facility and knowledge of the sphere pressure distribution. Computational capability is already onboard the Shuttle and knowledge of sphere pressure distribution is essentially state of the art (Appendix D). The conclusion then is that a fixed sphere nose sensor is better than a movable sphere, "Q-ball", for the Space Shuttle vehicles.

3.2.3.4.4 Pitot-static tubes: Considering that a fixed-nose sphere is chosen over a boom, then it is theoretically possible to calculate both pitot and static pressure from pressure measurements on the nose taps. This would, at first thought, negate the need for a conventional pitot-static tube

which is commonly used to measure airspeed and pressure altitude. However, considering the need for redundancy, especially for piloted cruise and landing, a completely self-contained passive system familiar to a pilot, is attractive. Consequently, it seems logical to include it in the ADM system for subsonic operation. A disadvantage is that it would need to be retracted or protected during high heating re-entry. However, being of relatively small size and because of the wide latitude of location possibilities (for subsonic use) this disadvantage is not insurmountable. Details of this are discussed in subsection 3.4.1.

3.2.3.4.5 Summary of pressure sensor ADM concepts: A summary of pressure sensing approaches which were considered for the ADM system along with sketches (Figures 7 through 9) are presented below. The optimum approach is No. 7, the sphere cone nose ports.

1) Deployed subsonic conventional pitot-static probe - Can be mounted most anywhere away from the body skin. Must be deployed and operating below 25 000 ft. Outputs are P_S and P_T for accurate airspeed data during landing maneuvers. Not good at high speed or angles of attack because of location in body flow field.

2) Deployed supersonic conventional pitot-static probe - Must be mounted ahead of nose to be applicable up to Mach 4 and 150 000 ft. Outputs are P_S and P_T. Could also be adapted for use at subsonic speeds.

3) Deployed supersonic conventional pitot-static probe with α and β Augmentation - Same as No. 2 with additional outputs of α and β. This α, β sensing could be accomplished with either a special head (like the SR-71) or vanes (like the early X-15).

4) Permanent boom with sphere cone probe face plus (No. 1) deployed body mounted pitot-static probe - Must be mounted ahead of nose. The boom may be about 6 feet long and 6 inches in diameter with cooling provisions. The sphere ports yield pressures that can be interpreted as α and β for boost and entry, and enable computation of static and stagnation pressures.

5) Permanent boom with swallowed shock probe plus (No. 1) deployed body-mounted pitot-static probe - Must be gimbaled or redundant to assure less than 10 degrees to relative wind. The lip shape must be broadened to survive entry environment at the expense of accurately measuring static pressure. Since this concept has these problems, it does not appear beneficial to Shuttle application.

6) Nose pressure ports plus (No. 1) deployed body-mounted pitot-static probe - This probe could simply use ports in the nose of the vehicle to measure flow direction and stagnation pressure.

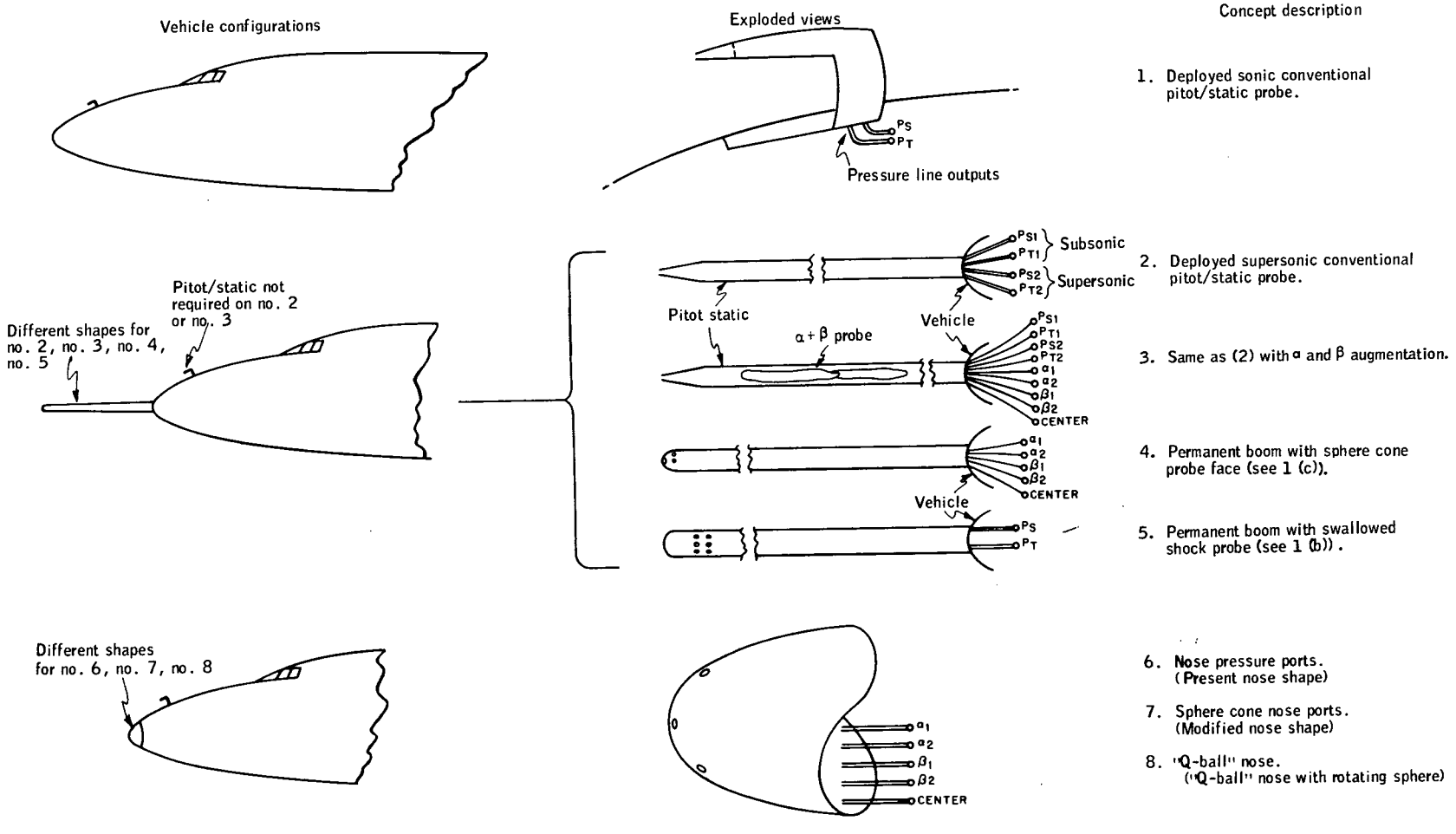

Figure 7. Air Data Sensors Measurement Concepts Summary

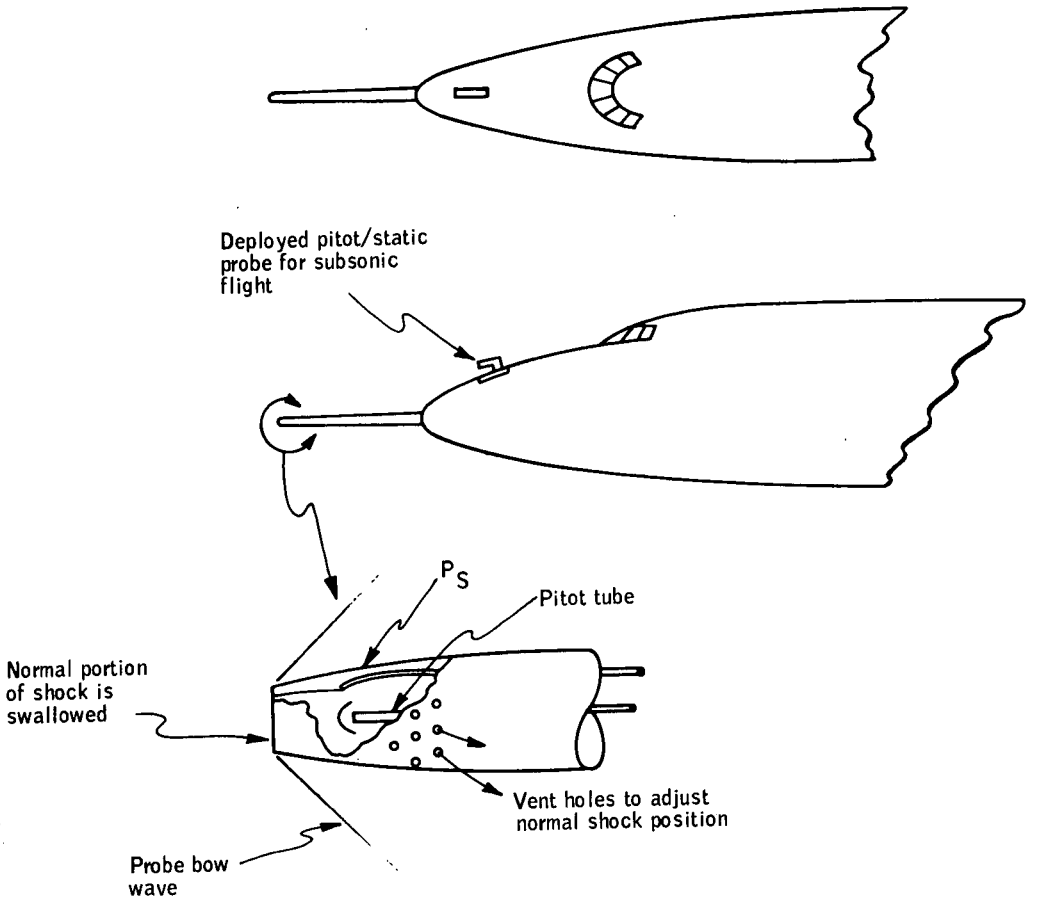

Figure 8. Swallowed Shock Probe

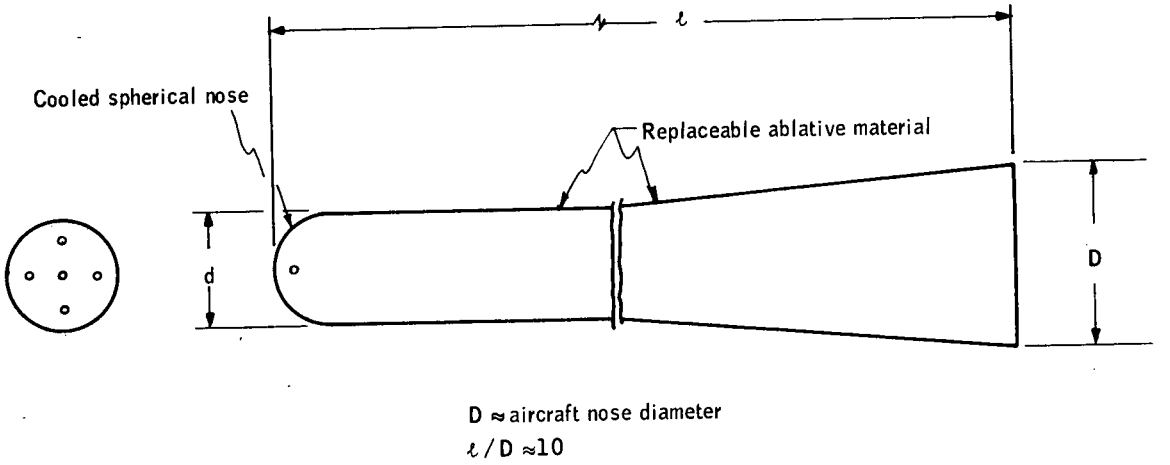

D ≈ aircraft nose diameter

$\ell / D \approx 10$

Figure 9. Boom with a Spherical Tip for Measuring α, β, P_T, P_S, q, hp

The present nose shape and body shock effects may cause such measurements to be uncorrectable to air data.

7) Sphere cone nose ports plus (No. 1) deployed body-mounted pitot-static probe - Same as No. 6 above except requires a sphere shape of the nose section configuration to make measurements more correlatable. Nose section would have a stationary sphere.

8) "Q-ball" nose plus (No. 1) deployed body mounted pitot-static probe - Requires special design of the nose section to incorporate a servoed sphere with α and β pickoffs. The "Q-ball has been used on the X-15 hypersonic vehicle and the Saturn launch vehicles to measure flow direction. The ball is servoed until a null is reached between a set of pressure ports within the ball.

3.2.4 Central Versus Dedicated ADM Computation

The air data measurement (ADM) system design, computation requirements definition coupled with information available from the Phase B Shuttle program provides the basis for the ADM computation interface point finalization. The trade is between using a dedicated computer versus the Shuttle vehicle central computer to perform air data computations:

Given the fact that the current Shuttle-integrated avionics approach is to use a central computer capability unless there is an overriding need for a dedicated computer, the following criteria were analyzed from that standpoint:

1) Digital word length requirements

2) Memory capacity requirements (instructions, constants, and scratchpad)

3) Computation rate requirements

4) Signal transmission quality (potential signal degradation as a function of signal format and transmission line lengths)

5) LRU checkout capability

6) Reliability

7) Weight

8) Cost

The word size for the computation is limited at 16 or more bits accuracy because of the transducer calibration computation. However, both the central and dedicated machines satisfy this requirement.

The sizing of the computational requirements per air data system channel for the pressure α, β, and P_{T2} computations yielded the following data.

	Instructions	Constants	Total
Pressure computations (output from 3 transducers)	305	60	365
α, β, and P_{T2} computations	85	15	100
Altitude and CAS computation	205	40	245
Service and Library functions			215
	Total locations		925

The triple-redundancy requirement would increase the size requirements to about 2700 locations, though the elimination of duplication for general-purpose routines could reduce this figure slightly.

An estimate of the computational speed required to execute the programs was also made. The computations were reduced to equivalent adds (EA) for a computer like the Honeywell digital air data computer (DADC). Assumptions were that a multiply is 10 EA and a divide is 20 EA. The resulting figures per air data system channel are given below.

	EA
Pressure computation	640
α, β, and P_{T2} computation	240
Altitude and CAS computation	250
Service and library calls	635
Total	1765

This is a worst-case condition where all functions of the software are used. Thus for the triple-redundant system the total EA would be 5300. Again, for a small machine computer like the DADC where an add is 10 microseconds the figures would be approximately 18 milliseconds per channel. With a system using dedicated ADM computer each channel would be doing its computations separately so the 18 milliseconds is the appropriate time for completion. However, the central computer, with its faster speed, would probably reduce the 53 milliseconds (associated with 5300 EA) for the total computation resulting from the basic assumption of a 10-microsecond add time. Both dedicated and central computers have the size and speed necessary for the computations.

Either analog or digital signals can be transmitted from the air data measurement system to the central computer, within the context of the accuracies required, without significant degradation if normal design practices for precision signal transmission are utilized.

A significant difference between the use of the dedicated or the use of central computer for the computation is the amount of data which must be transmitted between the ADM and the central computer. For the dedicated system there would be the transmissions to the central of the computed α, β, and P_{T2}, the altitude and CAS when appropriate, and the six computed pressures if necessary for failure determination computations. For each air data system this would be 11 words of data. If the central is used for computation, then for each system the two outputs from the six transducers and the associated fifteen calibration constants would have to be transmitted for each measurement cycle, about 102 words of data.

There is an advantage for a dedicated computer in the area of checkout capability as follows (it does not constitute an overriding need but is discussed below):

The signal interface between the present transducers and the computer will probably consist of:

a) Pressure output signals that will require additional processing in the computer to linearize the signal and provide temperature compensation.

b) A temperature output signal that is a function of the transducer ambient temperature.

The corrected pressure word that is used for subsequent air data parameter calculations is produced in the computer by a polynomial modeling equation that utilizes the above signals (a) and (b). Thus, the desirable point to assess transducer accuracy is after the modeling computation and, therefore, an LRU that includes a computer provides optimum checkout capability. The situation can be handled, without a computer in the LRU, in three ways as summarized in Table III.

TABLE III. CORRECTED PRESSURE WORD DERIVATION APPROACHES

Approach	Advantage	Disadvantage
1. Incorporate small computer in test equipment.	Provides desired checkout speed and confidence.	Cost
2. Incorporate tape printer in test equipment, feed raw data on tape to nearest general-purpose computer facility.	Cost	Final results not available in real time.
3. Specify individual transducer temperature and pressure outputs independently.	Cost	Reduced confidence in checkout validity.

Analysis to date shows that utilization of approach 3 with backup capability for approach 2 is the most cost-effective approach. There will be a slight advantage in cost, size, and weight utilizing the central computer.

On the basis of analysis summarized above, utilization of the Shuttle central computer for air data computations is judged to be acceptable and more cost effective than utilization of a dedicated computer.

3.3 SPHERE-NOSE SENSOR DESIGN

The nose is the front-most part of the vehicle projecting into the incoming airflow. Pressure ports in the nose can be made flush ports on the vehicle, thus having minimum flow disturbance. Also, choice of the spherical nose shape provides increased sensitivity of pressure change per unit flow direction change; the means to correlate pressure measurements with flow direction and stagnation point values is readily derived for the symmetrical spherical shape.

This subsection presents the sphere-nose sensor design factors under the following topic headings:

- Sphere nose installation factors
- Hemisphere pressure distribution
- Measurement and correlation equations for sphere nose sensor
  - pressure at a port
  - use of differences to determine flow direction
  - stagnation and static measurements

3.3.1 Nose Sensor Installation

The fixed sphere-nose sensor combines instrumentation tradeoffs with both the airframe and flight trajectory. Shape of the nose must be spherical and fabricated to allow mounting of surface pressure ports. The trajectory maximum angle of attack affects the arc size of the spherical surface because the stagnation point should be on the sphere and the arc should also allow sufficient angular spacing of pressure tap pairs for increased sensitivity.

Conferences with North American Rockwell (NAR) and McDonnell-Douglas Corporation resulted in agreement on the beneficial aspects of integrating the spherical-nose sensor into the nose section of the orbiter vehicle.

The NAR orbiter nose section, showing location and fastening of the air data pressure signal lines, is shown in Figure 10. The orbiter nose includes a 120° hemisphere with a 12-1/2-in. radius. These dimensions are compatible with the 13-pressure tap pattern proposed and analyzed (later in report) for the orbiter. Namely, α sensing taps analyzed are located on the $\beta = 0$ great circle (see subsection 3.3.4) at angles of -45, -15, 0, 15, 30, 45, and 60°. This tap pattern provides good sensitivity for the proposed orbiter with a maximum angle of attack of 30°.

While experimental evidence (ref. 10) shows that a tap at the tangent point of a sphere cone is unaffected, the extreme tap is conservatively located at 55° on the drawing instead of 60°. Moving the tap from 60° to 55° causes a small signal strength loss. The question of locating a pressure tap on the tangency point should be resolved by integrated sensor/vehicle. wind tunnel testing, particularly at high subsonic and transonic speeds.

Ribs are located in the nose behind the 3/16-inch diameter pressure taps. Tantalum tubing is inserted into the pressure taps, and sealed with a silica gasket. A pair of clevises grip the nose rib and hold the tube in place as shown in Figure 10. The tantalum tubing from each pressure tap is terminated at a bulkhead fitting located in the nose cap. Thus, the nose cap can be removed as an integral unit. Tubing from the bulkhead to the transducers in the instrumentation bay should be compatible with their elevated, but less severe, temperature environment.

A review of the General Dynamics (GD) booster information initially showed that the nose shape was not spherical, and the entry trajectory (Baseline B-9U) maximum angle of attack was 60°. Through discussions with GD, the booster nose was modified to a spherical shape, with an unspecified arc.

There are two primary alternatives in establishing the booster nose arc size to be compatible with trajectory and vehicle nose change. The first alternative is a spherical surface extending 40° below the aircraft axis and use of the air data sensing at and below the altitude where $\alpha = 40°$ (i.e., below 140 000 feet). The 40° spherical surface represents a relatively small modification of the external nose shape, Figure 11. The upper spherical arc is shown as 50°.

A second alternative is to alter the nose by increasing the sphere to 60° from the axis to the point of tangency on the underside of the nose. This would mean a significant change in body shape for several stations behind the nose. The nose radius of this booster configuration is about 32 inches, which is ample space for mounting the internal hardware, similar to that described for the orbiter. The B-9U alternate trajectory (see Appendix D) has α less than 30° after initial entry. The 40° nose for booster may be acceptable provided that trajectories are so constrained. Hence, air data measurement may not be required at $\alpha > 40°$

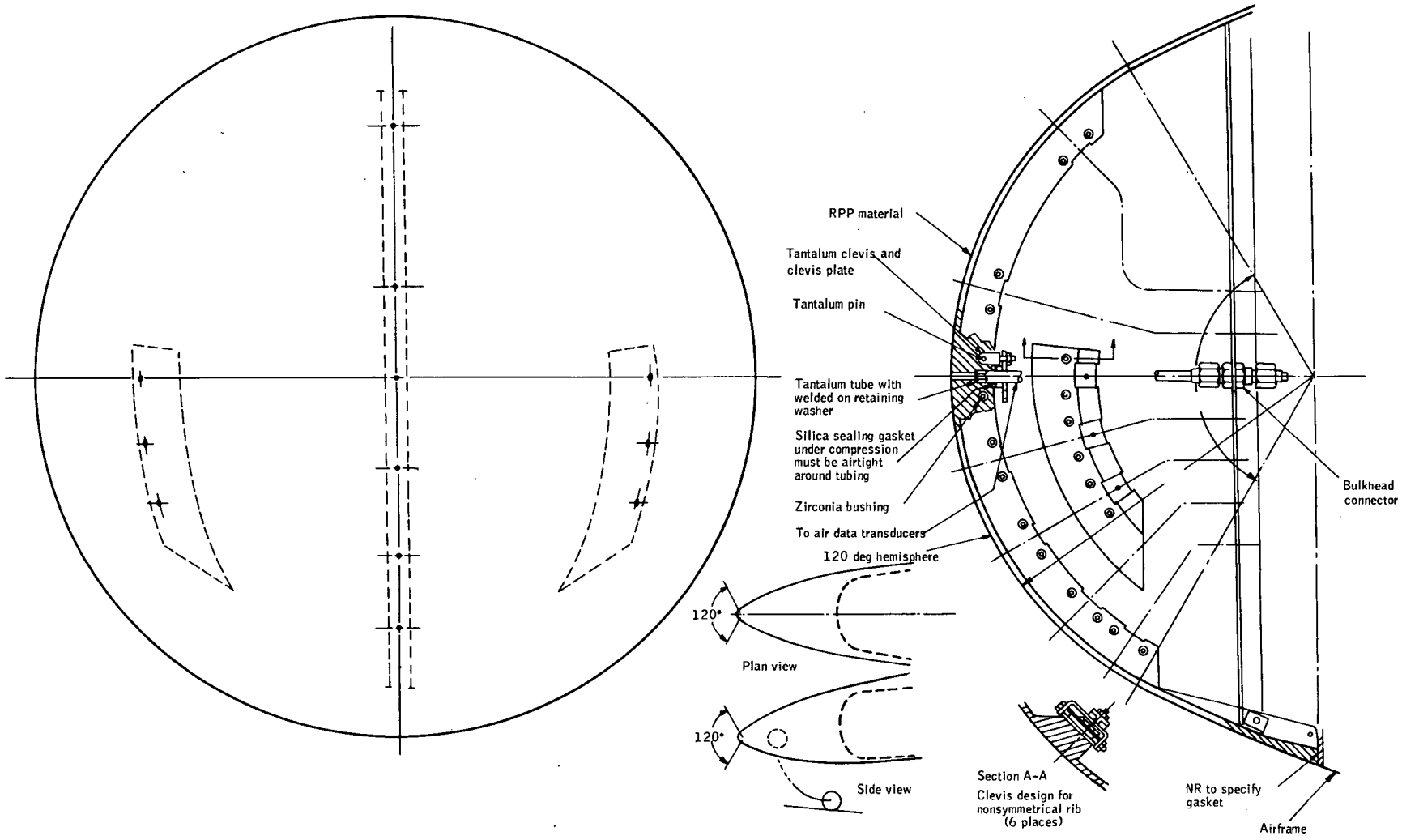

Figure 10. Proposed Orbiter Nose Configuration

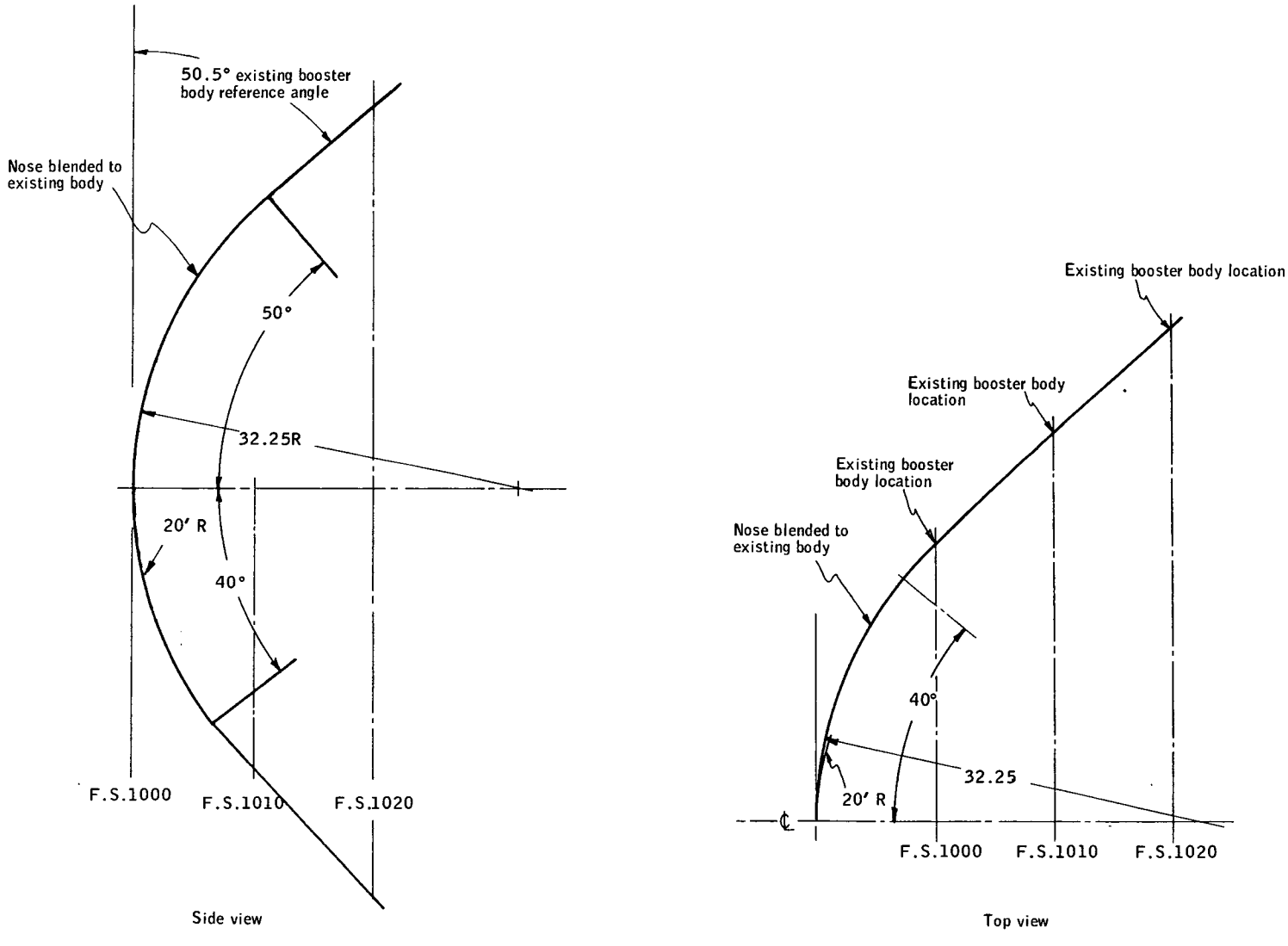

Figure 11. Proposed Booster Nose Configuration

3.3.2 Hemisphere Surface Pressure Distribution

The interest in pressure distribution functions is two-fold:

- Provide a simple relationship that closely represents actual distribution at various flight conditions and points on the sphere.
- Provide a means to derive mechanizations for determining flow direction and pressures at particular points (like the stagnation point) from pressure measurements at particular fixed points on the sphere.

An acceptable distribution function must have both properties, the first with its degree of "closeness of fit" becomes a premise for the second. A third factor is that of having parallelism with flow theory enhancing credibility of the fitting and derivation process. In any event the process is empirical, rather than analytical; deviations between test data and empirical model cannot be separated into measurement and modeling approximation errors.

A wealth of past work relates the nature of airflow around spheres and spheres with afterbodies. The Shuttle vehicle sphere nose is a sphere with nearly conical afterbody. The spherical pressure distribution is valid to the point where the afterbody begins (see ref. 11). Non-spherical nose shapes do not have this historical data base and could not be used for air data sensing until very extensive tests with actual nose sections were performed and associated measurement equations were derived.

The work summarized in Appendix D establishes that the function: $C_p = C_{po} - B \sin^2 E$ (for pressure coefficient C_p at a point and angle E from stagnation point in terms of stagnation point pressure coefficient C_{po} and an empirical function of the Mach number, B) (see Figure 12), closely fits all data for $E < 70°$ at all Mach numbers. Another result was that during a typical trajectory the angle-of-attack error due to formulation error (formula disagreement with hemisphere experimental data) was ±1 or 2 degrees. This is within scatter of comparable data from several experimental sources. Of course, the scatter for a single set of experimental data is much less, usually parts of a degree.

In the following subsections the pressure distribution is used to derive design equations for use in measurement computations, error analysis, and port placement. This result is shown to have parallelism with classical relationships with exception of an arbitrary fit of B versus Mach number in the 0.57 to 1.8 M range. For Shuttle flight profiles, this Mach range is traversed in about 40 seconds during boost and 180 seconds during the transition phase following re-entry of booster and orbiter; otherwise flight is outside this range.

The pressure model appears adequate in this transonic range only if local shockwaves are not attached to the sphere nose. The pressure discontinuities and asymmetric disturbances due to these local shock waves precludes use over part of this Mach range. This small invalid range and insight into nature of flow instabilities vary with afterbody effects and constitute part of the objective for wind tunnel tests of vehicle sphere nose with actual afterbody.

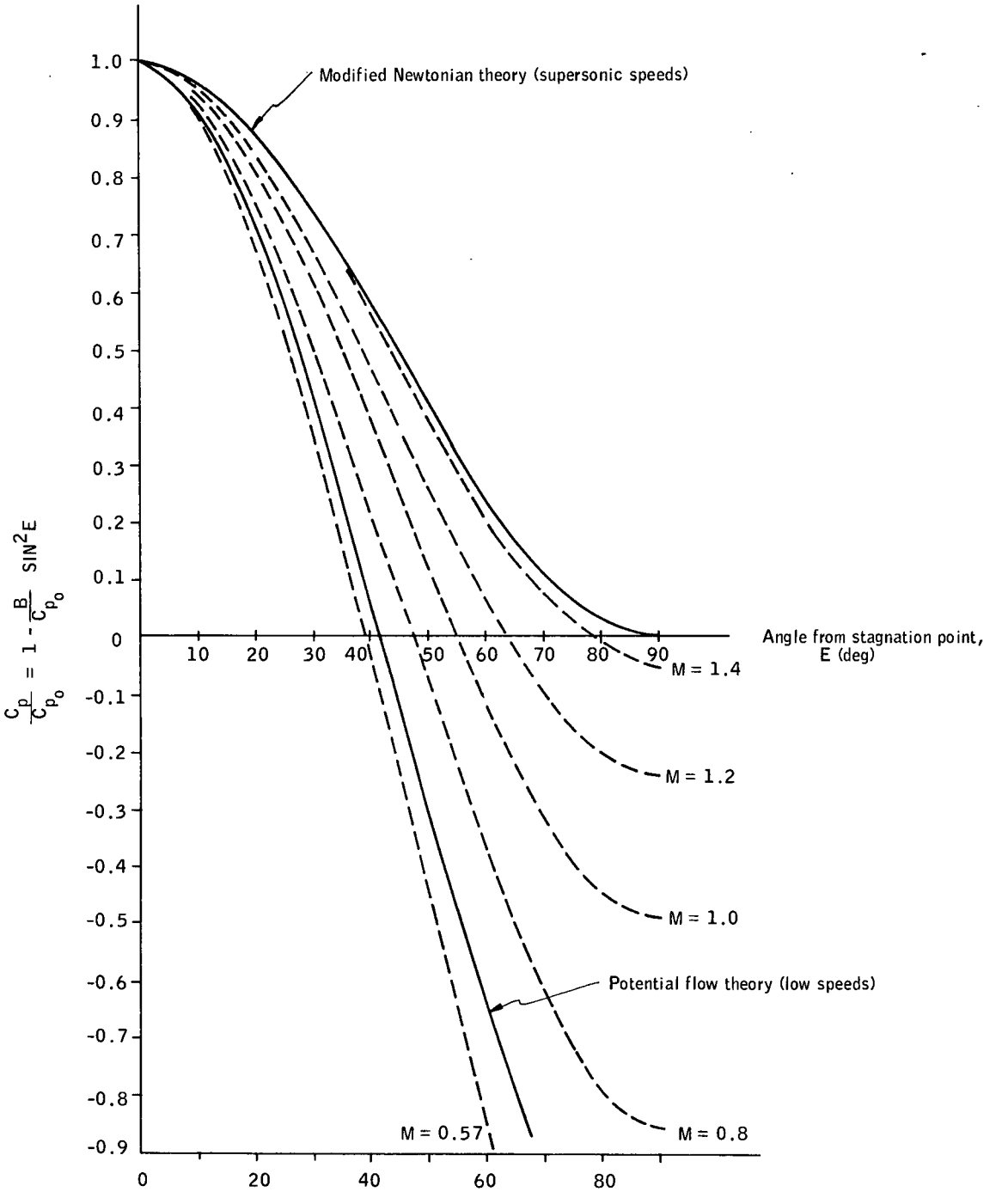

Figure 12. Hemisphere Pressure Distribution

Means to detect this range and size of perturbations will determine mechanizations which circumvent this effect.

Fortunately Shuttle flight profiles are outside this range for most of the atmospheric flight time. On the other hand this invalid operating condition coincides with maximum q during boost and with engine deploy and start following entry which are especially critical. More detail on this phenomenon is obviously warranted.

3.3.3 Measurements and Correlation Equations for Sphere Nose Air Data Sensor

This subsection details the generalized relationships between pressures at points on a sphere and means to convert pressure measurements to air data parameters including angle of attack (α), sideslip (β), stagnation point pressure (P_T), and subsonic static pressure (P_S). In later subsections, these equations are used to derive mechanization equations associated with the sphere nose air data sensor. As far as can be determined, the spherical distribution and associated sensing relationships have not previously appeared in the literature.

3.3.3.1 Spherical pressure distribution - pressure at a port. - The pressure at the stagnation point (total pressure) for a given atmospheric flight condition is a function of Mach number and static pressure according to the Rayleigh pitot formula (in the presence of normal shock) and Bernoulli's equation (subsonic flow). These well-known relationships (see NACA Report 1135) apply to conditions of perfect gas (air) and continum flow (dimensions of sensor ports larger than mean free-path between molecular collisions within flow). For Shuttle flight conditions below Mach 10, these assumptions are valid.

The stagnation point pressure is the highest pressure on the sphere with reduced pressure at points on circles with fixed surface angle from the stagnation point. The variation with flight condition (Mach number) and surface angle from stagnation point is termed the spherical pressure distribution, Figure 13.

Appendix D compares two empirical distributions to an abundance of test data available in the literature concluding that the function of paragraph 3.3.3.1.1 adequately describes the distribution over angles $0° \leq E \leq 65°$ and all Mach numbers (data available to M = 15). Note that the maximum sensitivity pressure change per unit angle occurs at E = 45° and varies with qB, as can be seen in:

$$\frac{dP}{dE} = qB \sin 2\ E$$

Comparison of the sensitivity of an aircraft angle of attack sensor, predicted by this distribution formula, with wind tunnel data is presented in Appendix A.

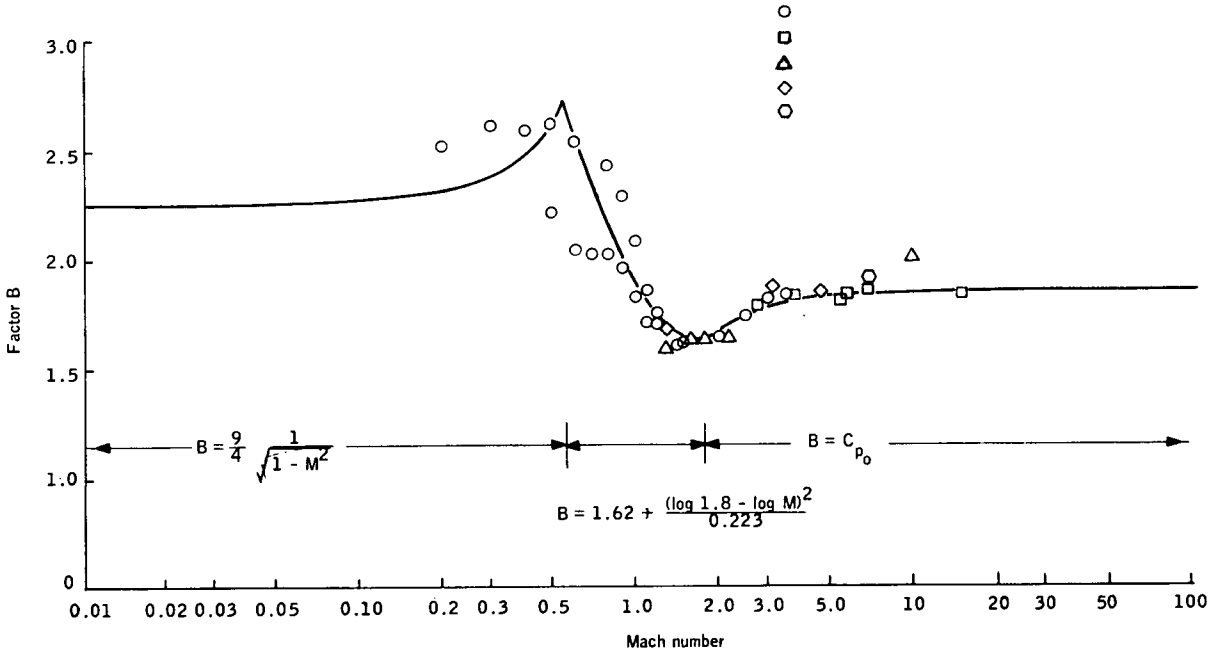

Figure 13. Pressure Coefficient Factor "B" versus Mach Number for Hemisphere Pressure Distribution Formula I

3.3.3.1.1 Basic pressure distribution equation summary:

$$C_p = C_{po} - B \sin^2 E \qquad (1)$$

where

$C_{po} = \frac{P_T - P_S}{q}$, the pressure coefficient at stagnation point

$C_p = \frac{P - P_S}{q}$, the pressure coefficient at point of interest

E = the spherical surface angle from stagnation point to point of interest

P = pressure at point of interest

P_T = =stagnation point pressure

P_S = ambient atmosphere static pressure

q = free stream dynamic pressure expressible as $q = \frac{1}{2} \rho V^2 = 0.7 M^2 P_S$

ρ = ambient air density

V = velocity relative to air mass

M = Mach number = V/a

a = speed of sound in ambient atmosphere

and $$B = \begin{cases} \dfrac{9}{4\sqrt{1 - M^2}} & \text{for } M \leq 0.57 \\ 1.62 + \dfrac{(\log 1.8 - \log M)^2}{0.223} & \text{for } 0.57 \leq M \leq 1.8 \\ C_{po} & \text{for } M > 1.8 \end{cases}$$

3.3.3.1.2 Alternate forms of distribution equations:

$$P = P_T - qB \sin^2 E;\ P_T = P + qB \sin^2 E \tag{2}$$

$$\frac{C_p}{C_{po}} = 1 - \frac{B}{C_{po}} \sin^2 E \tag{3}$$

$$\frac{C_p}{C_{po}} = \cos^2 E \text{ for } M > 1.8 \tag{4}$$

$$\frac{C_p}{C_{po}} = 0 \text{ when } E = \sin^{-1} \left[\frac{C_{po}}{B}\right]^{1/2} \tag{5}$$

(i.e., where $P = P_S$)

$$\frac{P}{P_T} = 1 - \frac{qB}{P_T} \sin^2 E \tag{6}$$

$$= \cos^2 E + \frac{P_S}{P_T} \sin^2 E \text{ for } M > 1.8 \tag{7}$$

Given two of the parameters M, P_S, q (or ρ, V, and q) to define flight condition, the various parameters are determinable from equations or tables like those of NACA Report 1135. The factor B is the only new parameter introduced.

3.3.3.2 Use of pressure differences to determine flow direction angles α and β. - The following subsections provide general computation and error as sensitivity equations for various configurations allowing determination of flow direction.

3.3.3.2.1 Expression for pressure difference between pressures at two points: Introducing two angles γ and δ defining the location of the stagnation point relative to the great circle between the two points of interest a and b, the pressure difference, ΔP can be expressed as:

$$\Delta P = Pa - Pb = qB \cos^2 \delta \sin \Delta\theta \sin 2\gamma$$

The derivation follows from Equation (2) using trigonometric identities and relationships of spherical trigonometry. The angular relationships are depicted by:

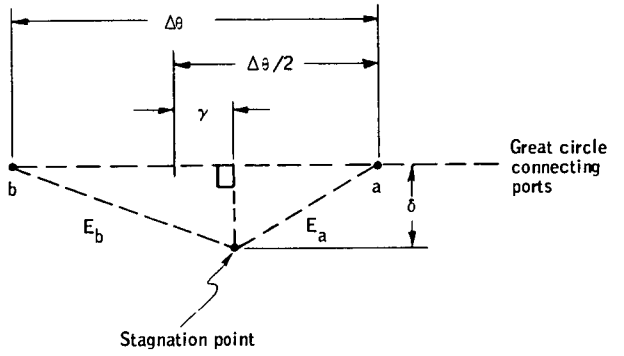

Note that the difference is independent of P_T, having a maximum magnitude qB when $\Delta\theta = 2\gamma = 90$ deg and $\delta = 0$. With $qB < P_T$ and choices having small angle γ, differential transducers need less dynamic range than absolute transducers for forming the difference to a given accuracy.

For cases of interest (points less than 65 deg from stagnation point) the pressure difference is sensitive to changes in γ, and relatively insensitive to changes in δ, with maximum sensitivity to changes in γ at $\gamma = \delta = 0$ and $\Delta\theta = 90$ deg as can be seen from the sensitivity equation:

$$d(\Delta P) = qB \sin \Delta\theta \left[2 \cos^2 \delta \cos 2\gamma d\gamma - \sin 2\delta \sin 2\gamma d\delta \right]$$

This explains the past use of ±45 deg positions of sensitivie ports on the X-15 Q-ball nose and various commercial probes for measurement of angle of attack and sideslip. The sensitivity of ΔP per degree change in γ is maximized at $\frac{qB}{57.3 \text{ deg/radian}}$ when the stagnation point is near the midpoint of the ±45 deg port pairs.

For the fixed sphere nose with wide excursions of angle of attack, single angle of attack and sideslip sensitive differences require measurement of the parameter "qB" to determine the angles when not near zero. The ratio

function of two pressure differences for ports on the same great circle was found which allows determination of the angle independent of qB and δ.

The ratio function can be used to determine angle of attack and sideslip from four pressure differences, two for angle of attack and two for sideslip. Alternatively, both flow direction angles can be determined from three pressure differences. The following details these possibilities.

3.3.3.2.2 Ratio function of two differences for determining flow direction angle: For two pressure differences between points on the same great circle:

$$\Delta Pn = Pa - Pb = qB \cos^2\delta \sin \Delta\theta n \sin 2\gamma n$$

$$\Delta Pd = Pc - Pd = qB \cos^2\delta \sin \Delta\theta d \sin 2\gamma d$$

The ratio function:

$$\tan 2\gamma' = \frac{\left[\frac{\Delta P_D}{\sin \Delta\theta_D} + \frac{\Delta P_N}{\sin \Delta\theta_N}\right]}{\left[\frac{\Delta P_D}{\sin \Delta\theta_D} - \frac{\Delta P_N}{\sin \Delta\theta_N}\right]} \tan \Delta\phi$$

allows determination of the angle γ', while effectively cancelling out the term $qB \cos^2\delta$. The angles are defined by:

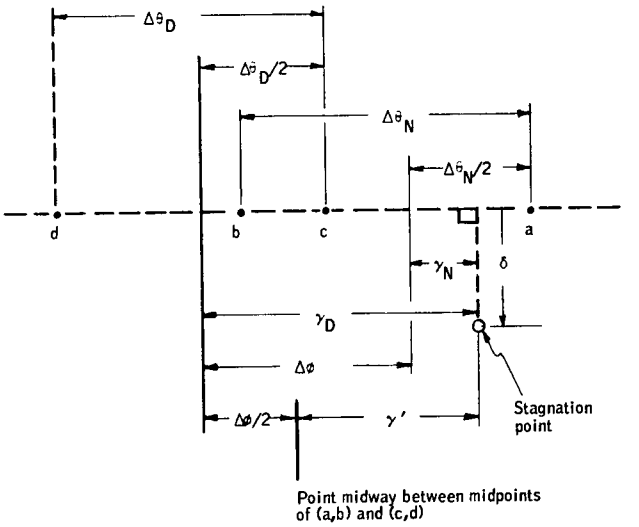

The proof of this equation involves substitutions of trigonometric identities. By use of the identity for tangent of sums or differences of two angles, equivalent equations referencing γ' to points other than the midpoint between midpoints can be derived. The result yields flow direction angle as a function of two pressure measurements; no other parameter is required since coefficients are constants determined by choice of pressure port locations.

3.3.3.2.3 Angle-of-attack measurement using ratio function: Choosing points on the zero sideslip great circle (see Figure 14), the ratio function can be used to measure angle of attack using pressure differences ΔP_N and ΔP_D from port pairs centered at α_N and α_D with spans of $\Delta\theta_N$ and $\Delta\theta_D$ the ratio function becomes:

$$\tan 2(\alpha - \alpha_c) = \frac{\left[\frac{\Delta P_D}{\sin \Delta\theta_D} + \frac{\Delta P_N}{\sin \Delta\theta_N}\right]}{\left[\frac{\Delta P_D}{\sin \Delta\theta_D} - \frac{\Delta P_N}{\sin \Delta\theta_N}\right]} \tan(\alpha_N - \alpha_D)$$

where

$\alpha_c = \frac{\alpha_N + \alpha_D}{2}$; $\alpha_N > \alpha_D$ by choice of notation and α_n, α_D, α_C and α are referenced to the point on the zero sideslip circle where vehicle angle of attack is zero.

The result provides angle-of-attack measurement that is independent of sideslip and flight parameters. Only two pressure differences measurements and four constants depending on chosen pressure port configuration are needed to compute angle of attack.

The sensitivity equation or error equation relating uncertainties in pressure measurement to small changes in α can be derived by partial differentiation (or by using the tangent of sums identity to obtain $\tan 2(\alpha - \alpha_j)$ which equals $2\,d\alpha$ at $\alpha = \alpha_j$) as:

$$d(\alpha) = \frac{57.3\,\text{deg/rad}}{2qB\cos^2\beta}\left[\frac{1}{\sin 2(\alpha_N - \alpha_D)}\right]$$
$$\left[\frac{\sin 2(\alpha_j - \alpha_D}{\sin \Delta\theta_N}\, d(\Delta P_N) - \frac{\sin 2(\alpha_j - \alpha_N)}{\sin \Delta\theta_D}\, d(\Delta P_D)\right]$$

where $d(\alpha)$ is the uncertainty in degrees due to $d(\Delta P_N)$ and $d(\Delta P_D)$, the uncertainties in the two pressure measurements when $\alpha = \alpha_j$ and α_N, α_D, $\Delta\theta_N$ and $\Delta\theta_D$ are determined when choosing the locations of pressure ports.

The best choices for pressure ports are discussed in subsection 3.3.4 using this equation. The error is seen to be smallest when qB is large, $\beta = 0$, $2(\alpha_N - \alpha_D) = \pm 90$ deg and $\Delta\theta_N = \Delta\theta_D = 90$ deg; unfortunately, the end ports are more than 65 deg from the center of such a set, violating the restriction of keeping sensitive ports with 65 deg of the stagnation point.

Definition of α and β

The angles of attack (α) and sideslip (β) are defined in terms of vehicle-axis components of the vehicle velocity relative to the airmass (u, v, and w) along the body axes of roll, pitch and yaw with positive directions of forward, right, and down, respectively as:

$$\alpha = \tan^{-1} \left\{ \frac{w}{u} \right\}$$

$$\beta = \tan^{-1} \left\{ \frac{-v}{(u^2 + w^2)} \right\} \frac{1}{2}$$

The minus sign in β equation defines β as a positive yaw angle in the right handed sense. Looking from the front of vehicle, the stagnation point is located at spherical angles (α, β) on the sphere nose as can be seen in:

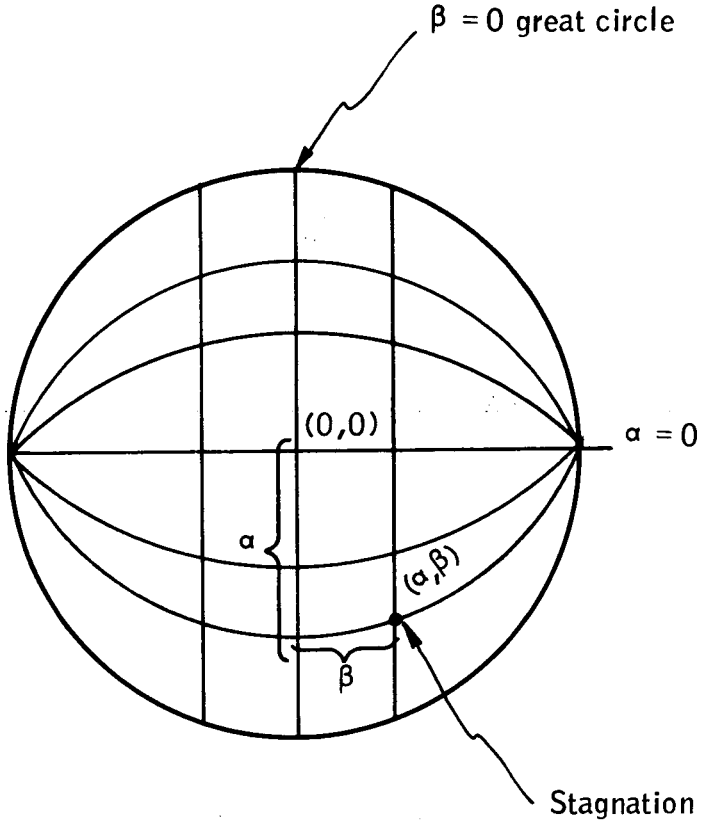

Figure 14. Conventions Used to Define Angle of Attack and Sideslip

β

At the points where one of the pressure differences is zero (i.e., $\alpha_j = \alpha_N$ or $\alpha_j = \alpha_D$), the error $d\alpha$ becomes

$$d\alpha = \frac{57.3 \text{ deg/rad}}{2 \text{ qB } \cos^2} \frac{d(\Delta P_N) \text{ or } d(\Delta P_D)}{\sin (\Delta\theta_N \text{ or } \Delta\theta_D)}$$

a function only of null offset in the measurement having zero value.

3.3.3.2.4 Sideslip measurement using the ratio function: Choosing a pair of differences on an α = constant great circle yields sideslip measurement and error equations identical in form to those for angle of attack. Due to definition of α and β as ordered angles, the equations are in terms of α' and β' rather than β and $\alpha - \alpha\beta$ as indicated in the spherical triangle:

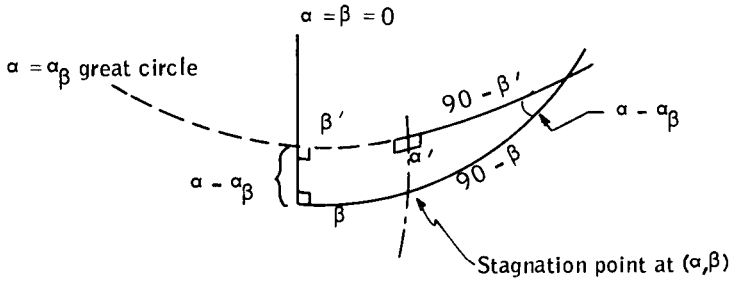

The pair of sideslip-sensitive differences determines β' independent of qB and α' and requires knowledge of $(\alpha - \alpha_\beta)$ to determine the desired angle of sideslip β (according to spherical triangle relationships like $\sin \beta = \sin \beta' \cos (\alpha - \alpha_\beta)$. The pair of differences method determines projected location of stagnation point on great circle of sensitive ports independent of angular distance from stagnation point to this great circle. The angles (α, β) are ordered spherical angles ordered opposite to (β', α').

3.3.3.2.5 Sideslip from one sideslip-sensitive difference and two angle-of-attack-sensitive differences: Choosing the pair of sideslip-sensitive ports on the $\alpha = \alpha\beta$ great circle with spacing $\Delta\theta_\beta$ and centers at $\beta = 0 = \beta'$, the equation for the β-sensitive pressure difference is given by:

$$\Delta P_\beta = \text{qB } \cos^2 \alpha' \sin \Delta\theta_\beta \sin 2\beta'$$

For the two α-sensitive differences ΔP_N and ΔP_D it can be shown that for $\alpha_N > \alpha_D$ and $\alpha_C = \frac{\alpha_N + \alpha_D}{2}$:

$$M = \frac{\frac{\Delta P_D}{\sin \Delta\theta_D} + \frac{\Delta P_N}{\sin \Delta\theta_N}}{\cos (\alpha_N - \alpha_D)} = 2\, qB \cos^2\beta \sin 2(\alpha - \alpha_c)$$

$$N = \frac{\frac{\Delta P_D}{\sin \Delta\theta_D} - \frac{\Delta P_N}{\sin \Delta\theta_N}}{\sin (\alpha_N - \alpha_D)} 2\, qB \cos^2\beta \cos 2 (\alpha - \alpha_c)$$

While the ratio of these two functions is $\tan 2(\alpha - \alpha_c)$, the square root of the sum of squares of the two functions is:

$$F = 2\, qB \cos^2\beta = (M^2 + N^2)^{1/2}$$

From spherical triangle relationships for $(\alpha - \alpha_\beta)$ and β in terms of α' and β', it can be shown:

$$\tan \beta = \frac{\Delta P_\beta}{F \cos (\alpha - \alpha_\beta)}$$

Enabling computation of β from one β-sensitive difference ΔP_β, the two α-sensitive differences involved in F, and the solution for α from the $\tan 2(\alpha - \alpha_c)$ equation.

A similar solution for the case where ΔP_β ports are not centered on the $\beta = 0 = \beta'$ great circle was not found. Such a case would be less optimum for sideslip sensing; however, it restricts the corollary problem using two β-sensitive differences and one α-sensitive difference for determining α and β to the special case where the α-sensitive difference is zero when the stagnation point lies on the great circle connecting the β-sensitive ports. This special case is used in redundant equation solutions for the 40 deg nose and 60 deg nose booster configurations analyzed and described later in this report.

3.3.3.2.6 β-error equation for three-pressure difference case: By differentiation and substitutions the error in β can be expressed as:

$$d\beta = \frac{d(\Delta P_\beta)}{2\, qB \cos(\alpha - \alpha_\beta)} - \frac{\tan \beta\, dF}{2qB} + \frac{\sin 2\beta \tan(\alpha - \alpha_\beta)\, d\alpha}{2}$$

where

$$dF = \frac{2}{\sin 2(\alpha_N - \alpha_D)} \left[\frac{d(\Delta P_D)}{\sin \Delta\theta_D} \cos 2(\alpha - \alpha_N) - \frac{d(\Delta P_N)}{\sin \Delta\theta_N} \cos 2(\alpha - \alpha_D) \right]$$

$$d\alpha = \frac{1}{2\ qB\ \cos^2\beta}\left[\frac{1}{\sin 2(\alpha_N - \alpha_D)}\right]$$

$$\left[\frac{d(\Delta P_N)}{\sin \Delta\theta_N}\sin 2(\alpha - \alpha_D) - \frac{d(\Delta P_D)}{\sin\Delta\theta_D}\sin 2(\alpha - \alpha_N)\right]$$

which allows $d\beta$ to be expressed in terms of three pressure measurement errors as:

$$d\beta = \frac{d(\Delta P_\beta)}{2\ qB\ \cos(\alpha - \alpha_\beta)} + \frac{\tan\beta}{2\ qB\ \sin 2(\alpha_N - \alpha_D)} \times$$

$$\left\{\frac{d(\Delta P_N)}{\sin\Delta\theta_N}\left[2\cos(\alpha - \alpha_D) + \sin 2(\alpha - \alpha_D)\tan(\alpha - \alpha_\beta)\right]\right.$$

$$\left. - \frac{d(\Delta P_D)}{\sin\Delta P_D}\left[2\cos(\alpha - \alpha_N) + \sin 2(\alpha - \alpha_N)\tan(\alpha - \alpha_\beta)\right]\right\}$$

The angular error here is in units of radians; multiply by 57.3 deg/rad to get error in degrees.

Note that only the $d(\Delta P_\beta)$ error term is present when $\beta = 0$; the error decreases with higher qB and is minimized when the stagnation point lies on the great circle of β-sensitive ports (i.e., $\alpha = \alpha_\beta$), the α-sensitive pressure measurement errors $d(\Delta P_N)$ and $d(\Delta P_D)$ are seen to produce a gain error (an error proportional to β).

3.3.3.3 Stagnation and static pressure measurements on the sphere nose. -In addition to flow direction angles measurable with configurations of port pressure differences, there is the desire to determine the stagnation pressure and static pressure from measurements on the sphere. The basic relationships to be used are from the distribution model (Figure 12):

1) For $M > 1.8$, $B = C_{po} = \dfrac{P_T - P_S}{q}$

$$qB = P_T - P_S \cong P_T \text{ when } P_S << P_T$$

allowing qB from difference measurements to approximate P_T.

2) $P_T = P + qB \sin^2 E$

allowing stagnation pressure measurement by measuring P and determining $qB \sin^2 E$ from port pressure differences.

3) For $M < 0.6$, the pressure at a port that is an angle $E = \sin^{-1}\left[\frac{C_{po}}{B}\right]^{1/2} \cong 41.9$ deg from the stagnation point approximates ambient static pressure. Since the stagnation point moves relative to a port on the fixed-sphere nose, Compensation for attitude changes is necessary.

3.3.3.3.1 Total or stagnation pressure approximation by use of difference measurements: For $M > 1.8$, $B = Cpo$ and thus $P_T \cong P_T - P_S = qB$ to the extent that $P_S << P_T$.

From the relationship $F = 2\,qB \cos^2\beta = (M^2 + N^2)^{1/2}$, qB could be derived from

$$qB = \frac{F}{2 \cos^2\beta}$$

Since β is near zero, the error in qB is given by

$$d(qB) = \frac{dF}{2} + 2\,qB \tan\beta d\beta$$

for $|\beta| < 6$ deg and $|d\beta| < 1$ deg the second term becomes a scale factor (< 0.35 percent qB).

As given previously:

$$\frac{dF}{2} = \frac{1}{\sin 2(\alpha_N - \alpha_D)}\left[\frac{d(\Delta P_N)}{\sin\Delta\theta_N}\cos 2(\alpha - \alpha_D) - \frac{d(\Delta P_D)}{\sin\Delta\theta_D}\cos 2(\alpha - \alpha_N)\right]$$

$$\cong d(\Delta P)\ [1 \text{ to } 3]$$

Thus the measurement error in qB is less 3X (differential transducer error) plus 0.35 percent qB which is small compared to the basic approximation that $P_T \cong P_T - P_S$ which has errors of 1-2 percent at 140 000 ft, 2.5-6 percent at 100 000 ft, and 20 percent at 80 000 ft for new delta wing orbiter and booster trajectories (and much worse for old SWO). This approach should be used only as a monitoring function to detect failures.

3.3.3.3.2 Total or stagnation pressure measurements by correcting absolute pressure at a port near the stagnation point: If P is measured at the port located at $\beta = 0$ and $\alpha = \alpha_j$, then the stagnation or total pressure P_T is given by:

$$P_T = P + qB \sin^2 E$$

where $qB = \frac{F}{2\cos^2\beta}$ and F is determined from the two α-sensitive differences (as above) and

$$\sin^2 E = 1 - \cos^2 E = 1 - \cos^2\beta \cos^2(\alpha - \alpha_j)$$

allows computation of P_T according to:

$$P_T = P + \frac{F}{2}\left\{\frac{1}{\cos^2\beta} - \cos^2(\alpha - \alpha_j)\right\}$$

The error in P_T is primarily due to the error in measuring P at a port near the stagnation point as can be seen from the error equation:

$$d(P_T) = d(P) + \frac{d(F)}{2}\sin^2(\alpha - \alpha_j) + \frac{F}{2}\sin 2(\alpha - \alpha_j)\, d(\alpha)$$

$$= d(P) + \frac{\sin(\alpha - \alpha_j)}{2}\left[d(F)\sin(\alpha - \alpha_j) + F d(\alpha)\cos(\alpha - \alpha_j)\right]$$

For the cases of interest $Fd(\alpha) = S\, d(\Delta P)$ where S is the α-error normalized sensitivity (having value 1 to 1.6) and $d(\Delta P)$ is the error in difference pressure measurements used to determine α and F.

3.3.3.3.3 Subsonic static pressure measurement on the sphere nose: Strictly-speaking, static pressure is the ambient pressure of the atmosphere being disturbed by the vehicle as it passes through and can't be measured directly. However, the pressure distribution functions:

$$\frac{P - P_S}{q} = Cpo - \beta \sin^2 E$$

is zero when the pressure P is equal to P_S at locations at angle E_S from the stagnation point where:

$$E_S = \sin^{-1}\left\{\frac{Cpo}{B}\right\}^{1/2}$$

varies with Mach number. For low Mach (< 0.6), E_S is about 41.9 deg. For Mach greater than 1.8, B = Cpo and E_S = 90 deg. Between 0.55 and 1.8 Mach, E_S changes rapidly with Mach number between 41 deg and 90 deg ($E_S \cong 52$ deg at M = 1). Because the model is valid for $E \leq 65$ deg and the midrange is both transitory in Shuttle vehicle trajectories and difficult to correlate accurately, only the low Mach range is of interest for purposes of static pressure measurement.

The gimballed nose-sphere Q-ball (as on X-15) is servoed so that its $\Delta\alpha$ and $\Delta\beta$ deviations from flow direction are small. For this gimballed case, the center port yields total pressure while an additional port on the circle 41.9 deg from center measures static pressure for $M < 0.6$ or so. The measurement process is more involved for our case where the stagnation point moves relative to the fixed sphere-nose pressure ports.

The amount of pressure change due to a change in E is obtained by differentiating the pressure distribution function as:

$$\frac{dP}{dE} = - qB \sin 2E = - qB (\sin 2 (41.9 \text{ deg})) = -0.994 qB$$

which for 0.4 to 0.6 M has value, dP, about 4 percent q per degree dE. Since $q = 0.7 M^2 P_S = 0.175 P_S$ at M = 0.5, the port pressure varies 0.7 percent of P_S from the desired value of P_S per degree E at 0.5 M. This result is both a correction factor for known port location deviation from the ideal 41.9 deg and an uncertainty sensitivity due to errors in determining flow direction angles α and β.

One way to arrange the subsonic P_S measurement on the fixed sphere nose is to locate the β-sensitive ports at ±41 deg (instead of ±45 deg) on the $\alpha = \alpha_\beta$ great circle. When α is near α_β, these ports are nearly 41.9 deg from the stagnation point with primary variation due to β changes. By averaging the pressures appearing at the two β-sensitive ports, this variation due to β is removed, leaving an α-variation, needing correction. Static pressure is computed from

$$P_S = P_{\beta 1} - \frac{\Delta P_\beta}{2} + \frac{0.994F}{2\cos^2\beta} \frac{\left[\cos^{-1}\{\cos(\alpha - \alpha_\beta)\cos 41 \text{ deg}\} - 41.9 \text{ deg}\right]}{57.3 \text{ deg/rad}}$$

where

$P_{\beta 1}$ is an absolute pressure measurement at one of the β-sensitive ports

ΔP_β is the β-sensitive difference measurement phased so that

$$P_{\beta 1} - \frac{\Delta P_\beta}{2} = 1\beta 3 (P_{\beta 1} + P_{\beta 2}) \text{ and}$$

F = $2 qB \cos^2\beta$, α, and B are determined from the sphere nose computations discussed above.

The primary errors in measuring static pressure by this method are:

a) $d(P_{\beta 1})$ - the absolute transducer error

b) $\frac{d(\Delta P_{\beta})}{2}$ one half the difference transducer error

c) The error due to mislocating ports at ±41 deg

d) The deviation of actual distribution from P_S at 41.9 deg from the stagnation point

The overall error is thus a combination of two transducer errors and an attitude uncertainty of the order of 0.7 percent of P_S magnitude per degree.

For 1-degree attitude uncertainty, 0.3 percent of full scale absolute pressure measurement and ±2 psf differential measurement, the static pressure measurement error is equivalent to ±250 ft altitude error at subsonic altitudes less than 25 000 ft. This error is larger than the desired ±50 ft but may be acceptable.

The separate pitot-static probe is made part of the air data measurement system because it has been flight-proven, simple, accurate and desirable as a primary subsonic flight sensor.

With a fixed sphere nose (rather than gimballed) no port directly senses stagnation pressure or static pressure making P_T/P_S snesing from the nose dependent on α-sensing. To avoid these complications, the best approach is a permanently mounted subconic pitot-static tube mounted to minimize static source error, heating and effects of booster vibration.

For redundancy respons, subsonic static pressure from the sphere nose as a degraded backup may be more desirable than additional pitot-static probes.

3 3.4 Port Locations on the Spherical Nose

Several considerations determine the most suitable locations of pressure ports and the associated hookup of differential and absolute transducers. Among these are:

a) Vehicle angle-of-attack range during period of use.

b) Angular size of the spherical nose cap which smoothly transitions to the afterbody.

c) Minimization of angle-of-attack and sideslip errors due to transducer errors and asymmetric deviations of true pressure from the pressure distribution model.

d) Minimum errors and/or increased sensitivity at those attitudes which are nominal for the mission phase (like 5 deg to 15 deg alpha for subsonic flight, 0 deg beta throughout flight, and zero $q\alpha$ during boost).

e) Redundancy needs

f) Allowability of unused ports during high-angle of attack flight.

3.3.4.1 General restrictions on port placement. -As a design rule the maximum angle from stagnation point to pressure ports should always be below 75 deg and preferably below 65 deg to avoid effects of flow separation and deviation from the pressure distribution model.

When α equals 60 deg, this 65-deg restriction permits locating the α-sensitive ports between -5 deg and the lowest edge of the spherical nose cap. When α equals 30 deg the highest port could be placed at -35 deg. For ±45 deg β-sensitive port pairs and ±5 deg β, the 65-deg restriction limits α-range to ±45 deg about the angle of attack for which the stagnation point falls on the great circle connecting the β-sensitive ports.

For valid operation of the spherical nose sensor, the stagnation point must lie on the spherical surface. For angles of attack larger than the bottom-most transition from spherical nose cap to afterbody, flow from the afterbody to the nose cap destroys the spherical symmetry of pressure distribution. In this situation the ±45 deg β ports continue to sense sideslip deviation but with a different gain (sensitivity); the angle of attack and total pressure measurement formulae are completely invalid.

For smooth transitions from spherical nose cap to the afterbody, the pressure port within a degree or two of this transition satisfies the spherical pressure distribution model. Thus pressure ports can be located on the spherical nose cap so that the port is within 65 deg of all possible locations of the stagnation point and at least 2 deg away from transition to afterbody. For the Shuttle vehicle atmospheric flight phases sideslip is within ±50 deg and angle of attack has nominal value as indicated on Figure 15.

3.3.4.2 Port locations to minimize α and β errors. -The measurement approach is one of using two α-sensitive and one β-sensitive measurements as the only parameters needed to determine α and β. The α-sensitive ports lie on the $\beta = 0$ great circle with β always near zero; this choice increases α-sensitivity. The β-sensitive ports are chosen to be insensitive to α changes with minimum error at $\beta = 0$; this is arranged by placing the port pair symmetrically on a perpendicular great circle intersecting the $\beta = 0$ great circle at $\alpha = \alpha_\beta$.

Choosing a spherical coordinate system on the spherical nose cap so that $\alpha = 0$, $\beta = 0$ is the forward-most point, α increases downward on the $\beta = 0$

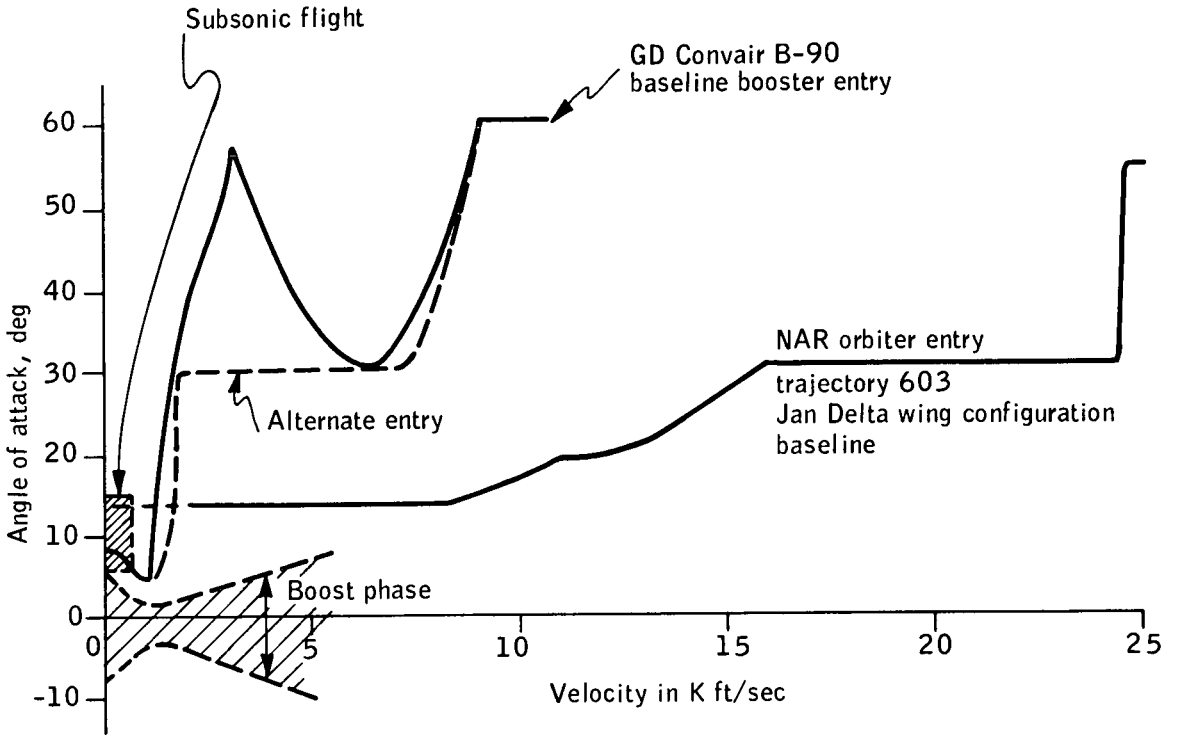

Figure 15. Angle-of-Attack Values for Various Flight Phases

great circle, and β is positive to the right of the $\beta = 0$ great circle as viewed from in front of the vehicle:

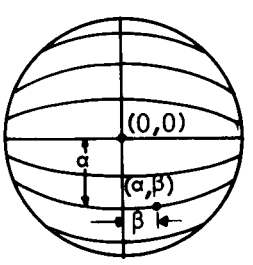

Spherical coordinate system viewed from directly in front of vehicle

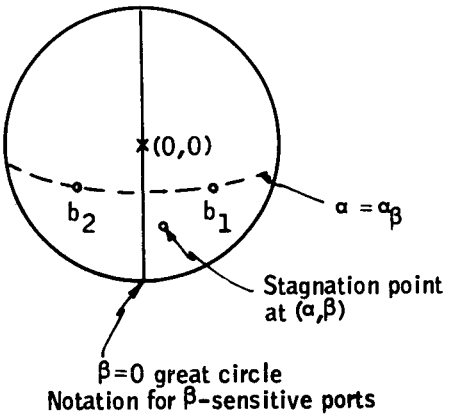

Notation for β-sensitive ports

3.3.4.3 β-sensitive port locations. -For ports located $\pm\theta$ from the $\beta = 0$ great circle on the $\alpha = \alpha_\beta$ great circle, the β-sensitive pressure differences ΔP_β is given by:

$$\Delta P_\beta = P_{b_1} - P_{b_2} = qB \cos(\alpha - \alpha_\beta) \sin 2\theta \sin 2\beta$$

and the sensitivity per unit β-change is given by:

$$\frac{2(\Delta P_\beta}{2\beta} = 2\ qB \cos(\alpha - \alpha_\beta) \sin 2\theta \cos 2\beta$$

where qB is a pressure intensity function varying with flight speed and altitude.

At $\beta = 0$, the differential pressure ΔP_β is zero, and sensitivity is maximized when $\theta = 45$ deg and $\alpha = \alpha_\beta$, that is when the stagnation point lies on the $\alpha = \alpha_\beta$ great circle. The sensitivity is reduced by a factor of 2 if $\theta = 22.5$ deg and $\alpha - \alpha_\beta = \pm 45$ deg.

Thus the criteria for choosing β-sensitive ports are:

a) ± 45 deg spacing best; reduced sensitivity with smaller spacing proportional to the sin of angle between ports.

b) Place the β-sensitive ports on a $\alpha = \alpha_\beta$ great circle for which minimizes angle $\alpha - \alpha_\beta$ that stagnation point is away from great circle connecting these ports.

c) If necessary satisfy the 65 deg maximum port distance restriction when $\alpha - \alpha_\beta$ and β are largest by reducing spacing and locating to minimize $\alpha - \alpha_\beta$ throughout range.

For the orbiter, $-10 < \alpha < 30$ deg for all flight phases below 24 000 fps. A 60 deg nose cap allows β ports to be located at ± 45 deg on an $\alpha = \alpha_\beta$ great circle for $0 < \alpha_\beta < 30$ deg, with $\alpha_\beta = 15$ deg seemingly the best choice. For booster entry with a 60 deg booster nose, the β ports should be at ± 45 deg on the $\alpha = 30$ deg great circle; however, viewing long duration of subsonic flight $\alpha = 15$ deg great circle is better.

The best choice for booster and orbiter β-sensitive ports is ± 45 deg on the $\alpha = 15$ deg great circle. For the booster at $\alpha = 60$ deg sensitivity is 70 percent of ideal; for most of the flight time (of both vehicles) α is within 15 deg of $\alpha = 15$ deg affording very near the ideal sensitivity.

The symmetric choice for β ports causes cancellation of deviations of spherical pressures from the ideal pressure distribution model at $\beta = 0$ (see Appendix A). The error in degrees is given by:

$$d\beta = \frac{d(\Delta P_\beta)}{2\ qB \cos(\alpha - \alpha_\beta)} \times 57.3 \text{ deg/rad}$$

where $d(\Delta P_\beta)$ is the error of the β-sensitive transducer for zero differential input.

Other errors in this β-measurement are:

a) Misalignments of nose to vehicle and of β-sensitive ports on nose.

b) Flow perturbations due to surface irregularities and edges of the ports.

c) A scale factor error for nonzero β because of α-measurement errors.

3.4.4.4 α-sensitive port locations. -Since a pair of α-sensitive pressure differences is used in a ratio function to determine α (without knowledge of any other parameter), the choice of best locations becomes more involved than for β-sensitive ports.

Denoting the two α-sensitive pressure differences as ΔP_N and ΔP_D, the port pairs having spacing θ_N and θ_D are centered at α_N and α_D. Furthermore, the three or four α-sensitive ports all lie on the $\beta = 0$ great circle. The values of these difference pressures are given by:

$$\Delta P_N = qB \cos^2 \beta \sin \theta_N \sin 2(\alpha - \alpha_N)$$

$$\Delta P_D = qB \cos^2 \beta \sin \theta_D \sin 2(\alpha - \alpha_D)$$

The sensitivities of these pressures to α changes are given by:

$$\frac{\partial(\Delta P_N)}{\partial \alpha} = 2\, qB \cos^2 \beta \sin \theta_N \cos 2(\alpha - \alpha_N)$$

$$\frac{\partial(\Delta P_D)}{\partial \alpha} = 2\, qB \cos^2 \beta \sin \theta_D \cos 2(\alpha - \alpha_D)$$

However, the error in computed α ($d\alpha$ in degrees) due to errors in pressure measurements, $d(\Delta P_N)$ and $d(\Delta P_D)$, is given by:

$$d\alpha = \frac{57.3 \text{ deg/rad}}{2\, qB \cos^2 \beta} \left[\frac{1}{\sin 2(\alpha_N - \alpha_D)}\right] \left[\frac{\sin 2(\alpha - \alpha_D)}{\sin \theta_N} d(\Delta P_N) - \frac{\sin 2(\alpha - \alpha_N)}{\sin \theta_D} d(\Delta P_D)\right]$$

As in the case of β-sensitive ports the α error decreases with larger values of pressure intensity "qB". For every possible value of α the right term changes value; two particular values $\alpha = \alpha_N$ and $\alpha = \alpha_D$ have simpler expressions for the last two terms, namely:

$$\frac{d(\Delta P_N)}{\sin \theta_N} \text{ and } \frac{d(\Delta P_D)}{\sin \theta_D}$$

These results indicate that when the stagnation point is at the middle of one α-sensitive port pair (where difference is zero), the angle-of-attack error is not a function of the other measurement; the error is merely a function of the null measurement error divided by the sine of the port spacing angle (similar to the β-sensitive pair at $\beta = 0$).

If one chooses $2(\alpha_N - \alpha_D) = \theta_N = \theta_D = 90$ deg to maximize the denominators of the last two terms of the $d\alpha$ equation, these terms can be expressed as either:

$$- \cos 2(\alpha - \alpha_N)\, d(\Delta P_N) - \sin 2(\alpha - \alpha_N)\, d(\Delta P_D)$$

$$\sin 2(\alpha - \alpha_D)\, d(\Delta P_N) + \cos 2(\alpha - \alpha_D)\, d(\Delta P_D)$$

which root-sum-square to a value dP representing the equal one-sigma value of uncertainties $d(\Delta P_N)$ and $d(\Delta P_D)$. This particular port configuration is unusable. With the extreme ports 135 deg apart, there is no location of the stagnation point for which all ports are less than 65 deg away. To study other configurations and variation of error with α, we define a normalized sensitivity, "S", which is one in value for all α in this "ideal" configuration.

The α-error equation can be rewritten in terms of "S" as:

$$d\alpha = \frac{57.3 \text{ deg/radian (dP)}}{2\, qB \cos^2 \beta} S$$

where

$$S = \frac{1}{\sin 2(\alpha_N - \alpha_D)} \left[\left(\frac{\sin 2(\alpha - \alpha_D)}{\sin \theta_N} \right)^2 + \left(\frac{\sin 2(\alpha - \alpha_N)}{\sin \theta_D} \right)^2 \right]^{1/2}$$

and

dP = the standard deviation of pressure errors $d(\Delta P_N)$ and $d(\Delta P_D)$ which are assumed to be equal.

An assumed -7.5 deg to 32.5 deg angle of attack range for orbiter entry, subsonic flight, and boost requires extreme port locations at $\alpha = -32.5$ deg and 57.5 deg to satisfy the 65 degree constraint, the 2 deg from edge of 60 deg nose constraint, and needs for useful measurement range with one port configuration. The extreme ports must be ±45 deg relative to the center of extremes at $\alpha = 12.5$ deg (which is the center of the assumed range). What is the best location for middle port(s) and the best way to hook up the pairs of transducers while minimizing the value of "S"?

Five possibilities with reasonably small error characteristics over the ±20 deg useful range are indicated as configurations 1 through 5 in Figure 16. Configuration 1 has constant S = 1.41 over ±20 deg range. Configurations 2 and 3 have smaller errors over range with minimum error at center of range (values 0.94 and 0.83). Configurations 4 and 5 or their reflections about the center have minimums of 0.88 and 0.82 at five to ten degrees from center (on side having small span difference) but largest values of S at other end of range (1.91 and 2.17).

Configurations 2 and 3 are best except for requiring four ports instead of three. The choice among the three remaining three-port configurations (1, 2, and 5) depends on desire to have smaller errors at some attitude relative to others within the useful range.

To extend the useful range from ±20 deg to ±35 deg requires reducing the port extremes from ±45 deg to ±30 deg. Configurations 6 through 10 are among the best possibilities. Errors are two to three times larger than for the sets of ±20 deg range configurations. Of these 6 is best overall, 7 has less midrange but more end range error, as is more pronounced for 9. Configurations 8 and 10 have yet more end and less middle error (with minimum skewed from center).

Note that the ±20 deg range for ±45 deg extreme port falls 25 deg short of the end port, while the ±35 deg range for ±30 deg ports extends beyond the extreme port. Thus to measure 57 deg α on a 60 deg nose requires choosing of one of the ±30 deg configurations in spite of the larger error at the edge of the useful range.

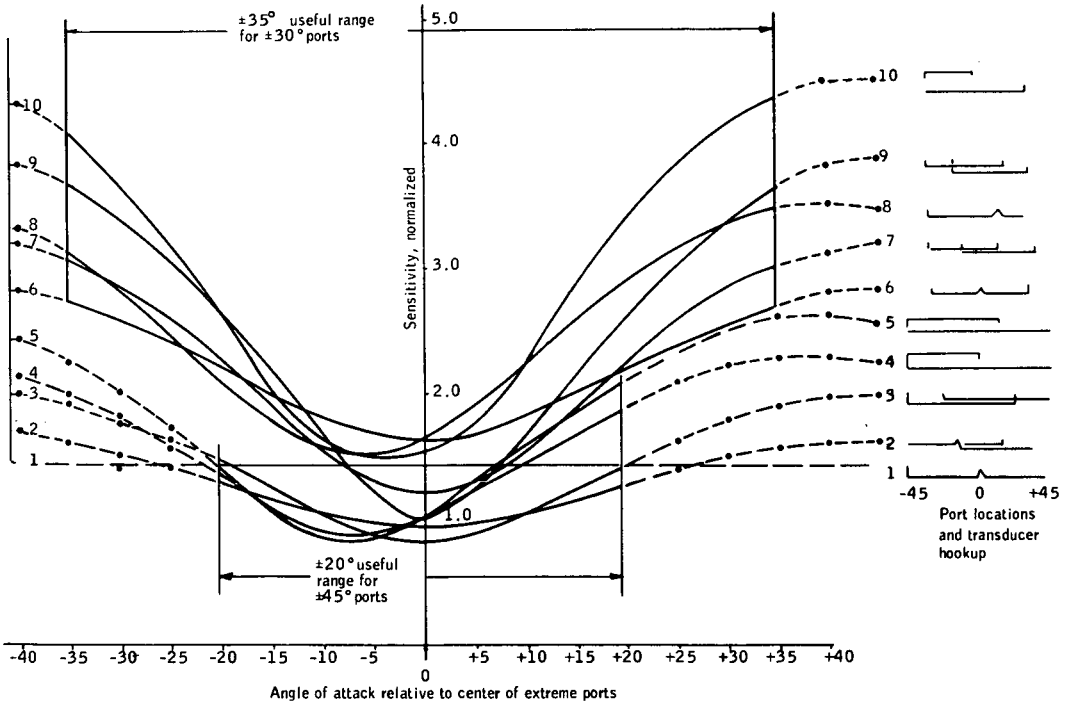

Figure 16. Angle-of-Attack Error Sensitivity Variation for Several ±45° and ±30° Port Sets and Transducer Hookups

For the 60 deg booster nose analyzed in detail elsewhere in this report configuration 6 was used; for the redundant orbiter nose configuration variations of configuration 2 with 45 deg, 60 deg and 75 deg spans were analyzed. For the 40 deg booster nose analysis a shrunk (±22.5 deg) version of configuration 6 was used; since this configuration can't measure beyond 40 deg α in any event, a shifted version of configuration 6 would have yielded smaller error over the valid range.

3.3.4.5 Simplest optimized configurations. - Examining the error characteristics and useful range properties with aim of:

a) Simplest configuration possible (no redundancy).

b) Coverage of -10 to +30 (orbiter) and -10 to +60 (booster) angle of attack ranges.

c) One port pair having center at α = 0 for use as $q\alpha$ sensor during boost.

d) Minimized error for 5 deg to 15 deg subsonic angle of attack.

e) Means to measure absolute pressure about 41.7 deg from stagnation point to approximate the subsonic static pressure.

results in the following candidate configurations in addition to those analyzed. Each of the following figures (Figures 17 through 19) illustrates the port configuration and transducer hookup and presents the value of normalized α-error sensitivity, S, versus actual angle of attack.

3.3.4.6 Additional notes on these selected configurations. - The additional $\Delta P_{q\alpha}$ measurement on the 60 deg booster nose is necessary because at 60 deg = α the ΔP_D port at -2.5 deg is just within the 65 deg constraint. The $\Delta P_{q\alpha}$ difference is not used until α is less than 27.5 deg.

The α-sensitive difference centered at α = 0 for all three cases is used to compute α and is proportional to $q\alpha$ in its value of pressure difference. For various booster/orbiter configurations during combined boost either the booster or orbiter nose is upstream and will interfere with the flow on the other vehicle nose. The undesirable $q\alpha$ interface from orbiter nose to booster control system for "orbiter-ahead" configurations leads to choice of an accelerometer method of sensing $q\alpha$ within the booster. The $q\alpha$ configurations are presented for completeness in event future Shuttle configurations desire $q\alpha$ from an air data source.

The β-sensitive difference similarly yields a measurement proportional to $q\beta$. For β-ports on non-zero α great circles, the slightly reduced scale factor trades well against the desire for better β accuracy at high angles of attack. For the 40 deg booster nose, the β ports are chosen on the α = 0 great

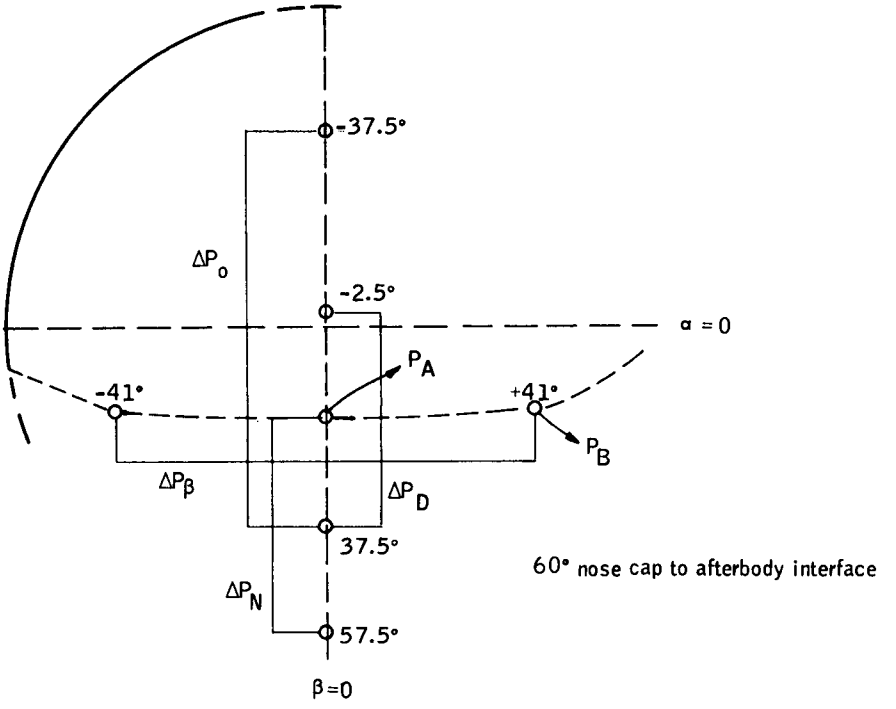

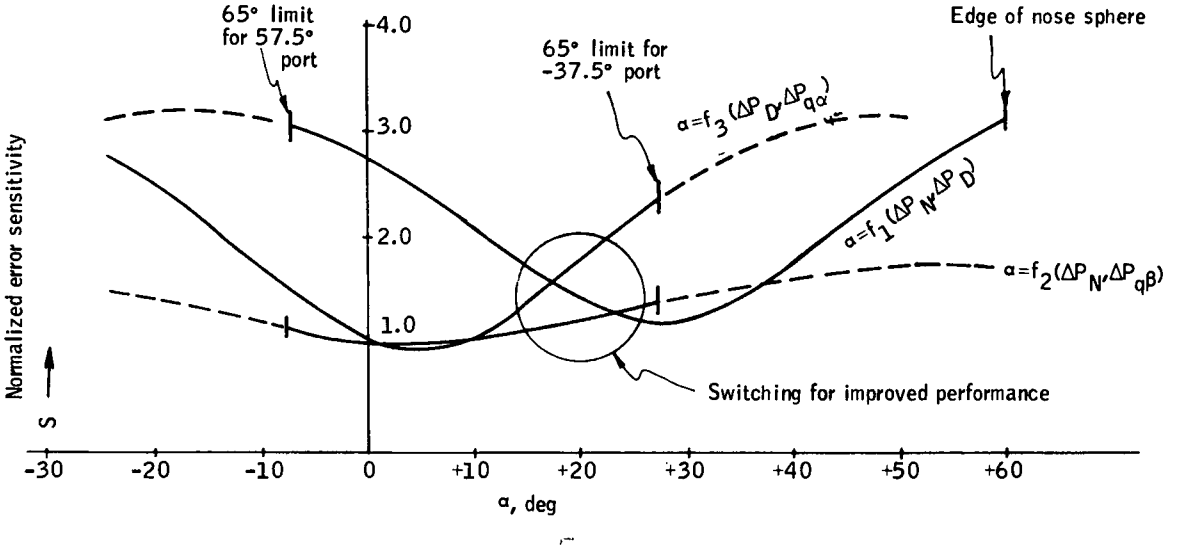

Figure 17. 60° Nose (Booster)

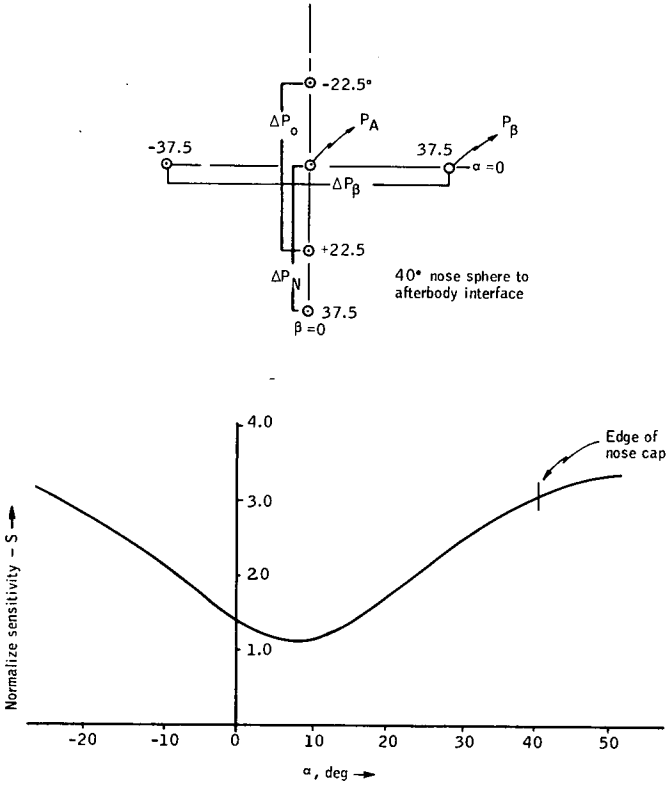

Figure 18. 40° Nose (Booster)

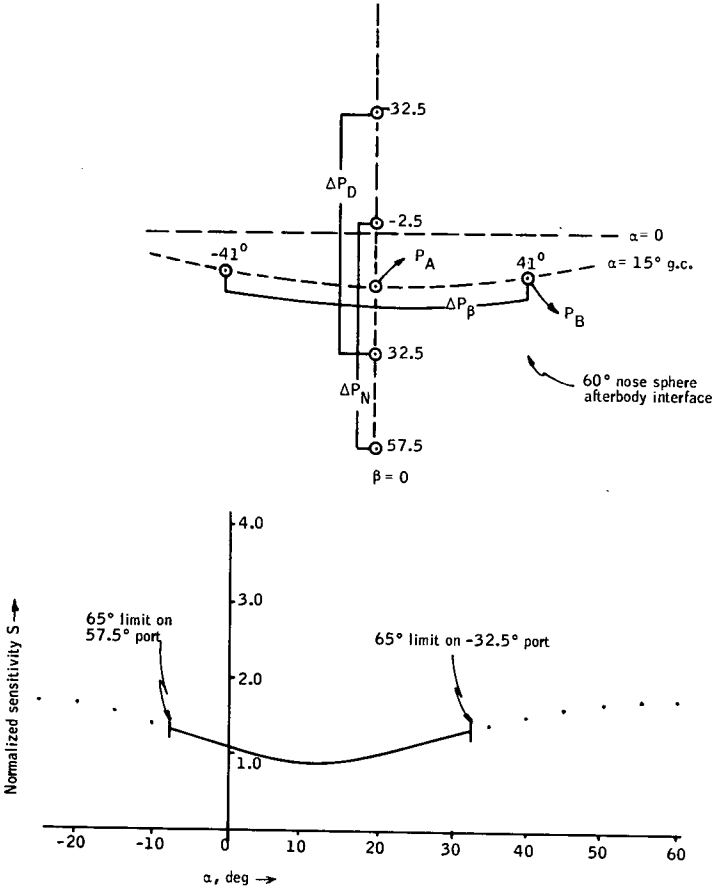

Figure 19. 60° Nose (Orbiter)

circle to maximize the ±37.5 deg spacing and enable nearly 40 deg from stagnation point measurements for use in subsonic static pressure measurement.

The 40 deg nose is a possible candidate because the blunter booster forebody makes 60 deg nose installation difficult. The primary air data sensing penalty is invalid sensing when $\alpha > 40$ deg.

The ±41 deg rather than optimum ±45 deg β-sensitive ports is a compromise trading slightly reduced β-sensitivity for a compensatable absolute pressure measurement at about 41.7 deg from stagnation point. The spherical pressure model indicates that for $M < 0.6$, the pressure at such a port closely approximates the ambient static pressure.

Measuring P_A for purpose of measuring stagnation pressure (after compensating for stagnation point location away from this port) should be accomplished with a port that is near the stagnation point. Since the P_A port is at one end of the ΔP_N pair for the two booster configurations, the combinations of P_A and ΔP_N can be used at high angles of attack (as is shown in booster configurations analyzed in Subsection 3.5). Choosing P_A and P_B on the great circle of β-sensitive ports yields a backup method to compute an approximate β measured along this great circle.

This concludes the considerations related to port locations and transducer hookup configurations for the Shuttle. The redundancy considerations are discussed in the next subsection. The term "qB" appears in sensitivity equations; its effect is discussed in subsections on transducer characteristics and error analysis.

3.3.5 Redundancy Considerations

A singly redundant sensor, electronics, and computing system accomplishes all the operations necessary to produce a system output. There exists a finite probability that the output has:

a) Error larger than needed tolerance nearly continuously.

b) A small percentage of erroneous output samples that are noise-like in nature, however, grossly in error.

c) Become completely erroneous or absent because of a failure in one of the elements of the system.

Backup of these types of failures for system outputs from the singly redundant system constitutes redundancy; the amount of redundancy and the means to back up the primary system depend on consequences after failures, availability of means for backup, ability to recognize failures and switch, compatibility with complete avionics integration, and the assumption of a very small level of risk that the redundant system fails. On the one hand

redundancy is used to decrease output failure rate (increased reliability); on the other hand redundancy is employed to circumvent effects of all possible sources of failure that are of major consequence to vehicle, payload, and crew.

Various redundancy configurations are possible; in general the backup success paths are either similar units or dissimilar units which substitute for the primary path on the basis of decision-criteria-and-switch-over logic. Some of the air data measurement system outputs can be viewed as a dissimilar backup to the inertial system; use of several different measurements and computations to generate an output by different means is another form of dissimilar backup; use of redundant measurements of the same source and identical computations in separate channels constitutes similar backup.

Similar backup redundancy eases the problem of failure detection and switchover because outputs of redundant channels are nominally identical, except in event of failures in one of the channels. Dissimilar backup systems have differing output performance characteristics than the primary to cloud the failure detection process.

Similar backup systems suffer from common mode failures at the source and from identical design defects in the redundant channels but reduce logistics because fewer different devices are needed in the avionics system (same devices are used in parallel channels). To some degree dissimilar backup approaches reduce single-point-source and identical defects; however, more different units are involved.

The avionics organizations for Shuttle use the similar backup concept which is easily applied to the case of three pitot-static probes but not to the sphere nose sensor or fewer pitot-static systems because of the common source of the pressures in redundant channels. The following discussion will describe the possible kinds of redundancy that can be employed in air data measurement system configurations.

3.3.5.1 Redundancy configuration possibilities. - This discussion first defines in Figures 20 and 21 elements of the singly-redundant air data measurement system; then several means toward backing up sources of failure are enumerated in Table IV. Hopefully these will provide alternatives for the eventual integration of the air data measurement system into the Shuttle avionics.

3.3.5.2 Redundancy conclusions. - The critical need for air data measurements dictates redundancy of measurements to the level of three independent channels enabling automatic switching after first failure. The orbiter nose sensor discussed in Subsection 3.5 provides such triple redundancy with identical flight line replaceable units (LRU's). While this approach adequately backs up LRU failures, it does have single-point failures affecting two or three channels in the area of ports and pressure lines. This could be circumvented by adding pressure ports and lines near the indicated ports and routing separately to the three channels, increasing port count from 13 to 21

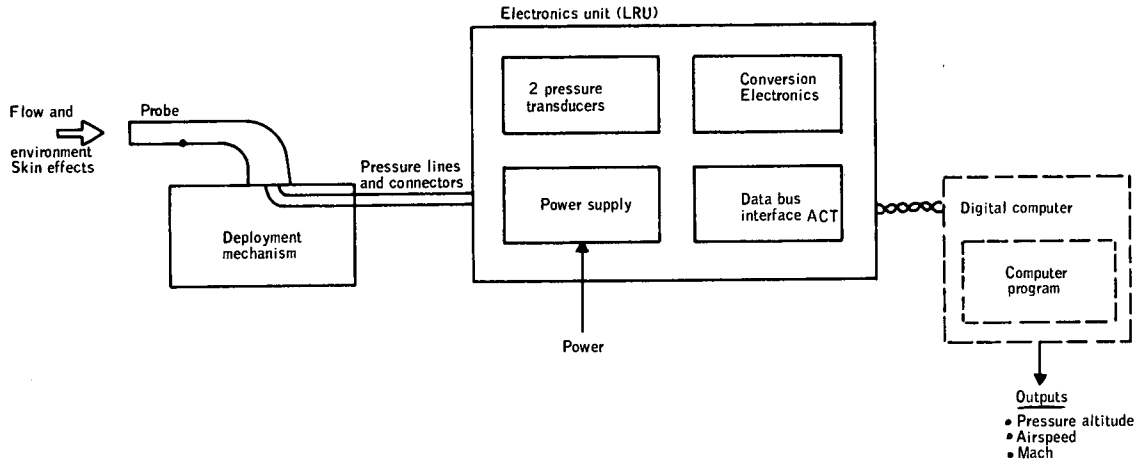

Figure 20. Subsonic Pitot/Static System Elements

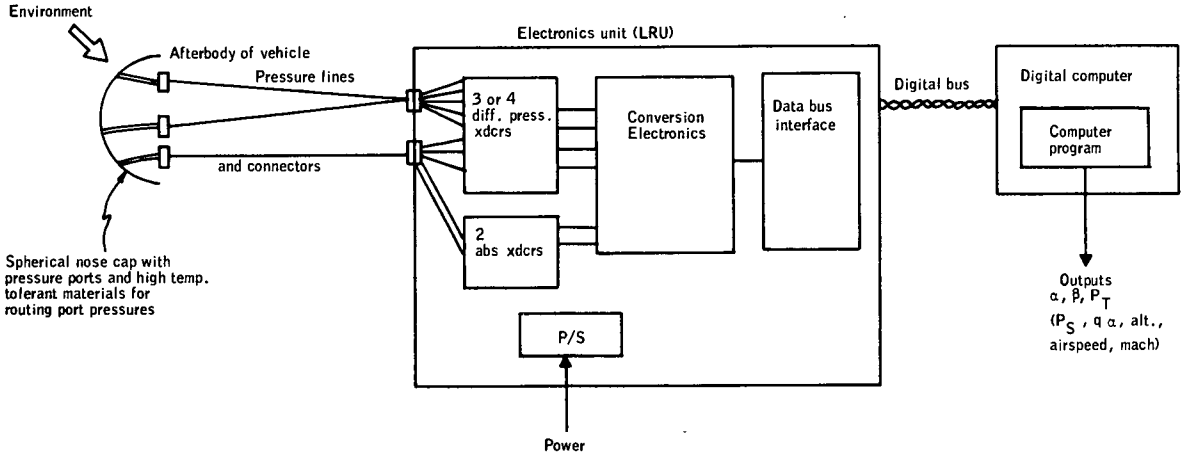

Figure 21. Sphere Nose Sensor System Elements

TABLE IV. BACKUP POSSIBILITIES FOR PARTICULAR SOURCES OF FAILURE

Location of failure	Backup possibility	Comment
1. Pitot-static probe • Deployment • Blockage, icing • Damage • Pressure line leak • Doors not shut in front of probe	PT/PS from sphere nose. 1 or more other pitot/static probes. Pilot and other sensors (radar altimeter, wind data from ground, etc.)	Degraded backup. Prefer separate locations and deployment mechanism. Wind and assigned pressure altitude need on-board sensing backup.
2. Pitot-static transducers and Electronics • Power • Transducers • Electronics • Connector	Same as for 1. Redundant LRU on same pressure lines.	Best. With deployment required LRU and probe have similar failure probabilities.
3. Digital busses and computing (Either air data electronics unit)	Interface with multiple busses; perform computations in redundant computers. Move computing into electronics unit; interface with multiple busses.	This is baseline approach. Reduces traffic on busses and load on central computer with fewer data having form ready for use; simplified monitoring and voting rather than redundant processing of raw data from redundant channels in each channel.
4. Complete sphere nose failure • Crack, dent, etc.	Entry: - Free bank control for stable bank/sideslip response. - More stable β-range on vehicle, use INS. - Use wing skin temp. to derive β. Subsonic: - Deploy pitot-static probe. - Deploy α/β probe. - Use INS data for α/b.	• Increases guidance error. • The sphere nose sensor is merely an INS backup for this case. • Needs special skin temp. sensors. • Necessary. • Additional complexity undesirable. • Degraded but subsonic vehicle tends to self trim.

TABLE IV. BACKUP POSSIBILITIES FOR PARTICULAR SOURCES OF FAILURE (CONCLUDED)

Location of failure	Backup possibility	Comment
5. Localized sphere nose, port, pressure connection, or transducer failure	α-Sensing: 3 or more pairs of α-sensitive ports and transducers with 3 or more equation solutions involving different transducer pairs.	• Different accuracies for each separate determination complicates logic. • Use of different ports, pressure lines, and transducers for each measurement, separates failure modes and increases redundancy while increasing complexity of plumbing and computations.
	β-Sensing: 2 or more pairs of β-sensitive ports having zero difference for β = 0 to yield 2 or more β determinations.	
	β-Sensing: 2 differences along same α = constant great circle by addition differential transducer or subtracting outputs of absolute transducers.	• Computes β' rather than β to give degraded output. • Difference of absolutes less accurate than difference transducer, but costs additional transducer. • Can enable determination of α from one α-difference that is zero on great circle of β ports; with α known β' can be converted to β.
	Redundant measurements of same port pressures.	• Backup for transducers only. • Reduces number of pressure ports and lines. • Ports and pressure lines are single-point failures for redundant channels.
	P_T & P_S Sensing: - Additional absolute transducers at different port locations.	• Differing accuracies.
	- Differential transducer between two absolute sensed ports.	• Measurements valid if 2 out of 3 transducers are good. • Port or line failure invalidates transducers.
	Derive "qB" from pair of α-sensitive differential transducers; use inertial velocity to derive approximate Mach for correction of B factor.	• Enables determination of q as degraded backup for P_T sensing during entry.
	Array of five or more absolute transducers to enable α, β, P_T and P_S measurement.	• Degraded sensor backup. • Should use different ports and lines than for differential sensing.
	Multiple ports at fewer sphere nose locations integrated into a few nose assemblies that keep pressures separate to redundant identical electronic units.	• Redundant channels are separate and identical, with nearly identical measurements. • Simplifies nose design.
6. Global failure in electronics unit • Power • Measurement electronics	• Separate units tied to same pressure lines.	• Does not back up pressure port or line failures. • Simplifies voting and logistics, since redundant units are identical with identical outputs.
• Buss interface	• Separate units tied to different pressure lines and ports that are very near those of redundant channels.	• Backup avoids most single point failure and preserves most of the identical nature of above.
	• 2 or more separate units tied to different pressure ports and lines distributed on spherical nose.	• Nose and pressure lines are more complex. • Noticeable differences between measurements on separate channels.
	Dual electronics units on each dual set of pressure ports and pressure lines.	• 4 units minimum unless 3rd unit can be switched at pressure lines.

to measure α, β, and P_{T2}. An additional three ports would allow three-channel measurement of subsonic static pressure.

These 21 pressure ports and lines could be arranged as seven groups each with three nearby ports for α, β, and P_{T2} measurements to the three redundant electronics units. The seven locations could be chosen at points shown in Figure 19. Since the nose is part of the thermal protection structure, this choice may be simpler to arrange than the 13 or 21 distributed orbiter nose configuration. If port and line failures are to be avoided one of these approaches is required.

Another palatable approach to redundancy is to use the single configuration as shown in Figure 17 as the primary and most accurate measurement of the air data parameters. In the second unit place 5, 6, or 7 absolute transducers measuring pressures at different ports than the primary. Use the measurements from the second unit to monitor the primary unit's performance and to substitute as a degraded backup (since absolute measurements are less accurate) in event of primary unit failures. Such an approach reduces complexity while providing the needed backup. More work is necessary to define the best configuration of such a second unit; it is concluded that primary development emphasis should be placed on developing the optimum single unit as shown in Figures 17 a, b, and c, rather than the configurations analyzed in subsection 3.5.

This degraded backup approach is contrary to the current Shuttle baseline approach of identical backup; in addition the likelihood of port and line failures as compared to transducer/electronics failures is unknown. The nose sensor redundancy problem needs the guidance of vehicle and avionics integration designers. The above discussion provides the possible alternatives available.

3.3.6 Transducer Characteristics

The differential and absolute transducers needed for the Shuttle orbiter and booster nose sensors have two primary parameters: 1) needed performance-pressure input range and 2) pressure conversion accuracy. The following gives the basis for estimates of these parameters given in Table V.

The transducers will be located within a line-replaceable-unit (LRU) that is installed in the nose wheel equipment bay. The environmental requirements are those associated with equipment bays, rather than the most severe temperature environment nearer the nose. The 20-ft (est.) pressure lines are sufficiently leak-free and of small total volume relative to accuracy and time constant (1 to 2 sec) needs. The exceptional case in this regard is the potential need for $q\alpha$ and $q\beta$ during first stage boost where total time constant allowance is 0.1 sec while the 20-ft line causes 20 milliseconds (estimated) of lag for following pressure input changes at the sphere nose.

TABLE V. - SUMMARY OF NEEDED TRANSDUCER CHARACTERISTICS

1) Absolute Transducer - 3 to 9 psf accuracy over a zero to 1.3 atm range with calibratable null offset to improve accuracy when pressure starts from near zero.

2) Differential Transducer -

Maximum exposure range:	±1100 psf (16 in. Hg)
Maximum measurement range:	±600 psf (9 in. Hg)
Desired accuracy:	±1 psf or 0.5% of value with possibility of calibrating zero offsets earlier in flight.

(1 psf ≅ 0.014 in. Hg)

Accuracies are for conversion of physical pressure to digital word representing that pressure. ±1.6 psf or better absolute transducers are needed for altitude measurement from pitot-static probe to within ±50 ft; ±0.7 to ±1.4 psf absolute transducers over 1.3 atm range are needed if used instead of differential transducers to form differences.

3.3.6.1 Absolute transducers. - The absolute transducers are used to measure stagnation and static pressure. The stagnation pressure range is from zero at orbital altitudes to 1.28 times atmospheric (0.6M at sea level). Some arbitrary point (determined by P_T accuracy) during entry (like P_T = 50 psf) will become the starting point for using measurements from the sphere nose. During boost maximum q occurs near M = 1 and H = 25 000 ft where stagnation pressure becomes about 1 atmosphere. Before deorbit, the pressure transducer can be calibrated for its zero offset (for case of orbiter); thus another transducer parameter of interest is the correspondence of null offset with zero pressure input to subsequent errors of pressure measurement when pressures start to build up.

Absolute transducer accuracy at these low level pressures determines when the sensor starts being useful. The orbiter entry starts from zero pressure, the booster entry starts from 6 psf. During entry the stagnation pressure measurement is used to estimate dynamic pressure q which in turn with use of inertial system velocity gives a means to estimate density altitude. The gradient of density to atmospheric altitude is about 5 percent per 1000 ft. The measurement becomes useful when ±2500 ft overall error in an altitude are provided by the combination of deviations from standard day, by wind errors in inertial velocity, and stagnation pressure measurements. Thus a ±5 percent determination of stagnation pressure is needed. For 0.1 percent full scale, the 3 psf error means starting use after stagnation pressure

reaches 60 psf. This level would be required for the old straight-wing orbiter; for the new DWO and booster entry, errors 3 or 4 times this would be acceptable, but not as desirable. The accuracy goal is 0.1 percent to 0.3 percent full scale (3 psf to 9 psf) including conversion of transducer outputs to digital.

The "null-offset-calibratable" characteristics improve usefulness affording a smaller error at low pressure levels, near the beginning of entry.

Use of absolute transducers for subsonic static pressure involves a range up to one atmosphere. The desired altitude accuracy determines its accuracy requirement. Since an attitude uncertainty of 0.7 percent per degree predominates the error for static pressure off the fixed sphere nose, a 0.1 percent to 0.3 percent error allowance is reasonable.

On the other hand, the desire to use pitot-static probe pressure for flight altimetry tightens this allowance toward the equivalent of 50 feet at 25 000 feet which is 0.08 percent of full scale (1 atmosphere) or 1.6 psf.

3.3.6.2 Differential transducers. - The differential pressure measurements can have either plus or minus sign and magnitude that varies from zero to a maximum that the following will estimate. The difference pressure measurements are predicated on the use of the pressure distribution function:

$$\frac{P_j - P_\infty}{q_\infty} = \frac{P_{T2} - P_\infty}{q_\infty} - B \sin^2 E_j$$

where P_j is the pressure at a port j which has

E_j the spherical surface angle from the port to stagnation point having

P_{T2} as the stagnation pressure

P_∞ is the ambient atmospheric static pressure

q_∞ is the dynamic pressure due to flight velocity, expressible as $q_\infty = 1/2\ \rho V^2 = 0.7\ M^2\ P_\infty$

where ρ is atmospheric density, M is Mach number

B is a dimensionless function of Mach number having a value 2.25 at low Mach increasing to a maximum value 2.6 at 0.57 Mach decreasing through near sonic Mach numbers to a minimum value of 1.75, then increasing to 1.85 at high Mach numbers (>3).

The use of differential transducers affords a reduced dynamic range when compared to taking the difference of two absolute pressure measurements. The two absolute pressure measurements being differenced would need to be a factor of 1 to 2 more accurate for pressures that can be as large as the stagnation pressure. The differential pressure is a function:

$$\Delta P = P_a - P_b = qB \cos^2 \delta \sin \Delta\theta \sin 2 (\gamma - \gamma_c)$$

where

q is dynamic pressure

B is the dimensionless function of Mach (as described above).

$\Delta\theta$ is the spherical surface angle between the two ports being differenced

δ is the angle from stagnation point to the great circle connecting the port pair along a perpendicular great circle

$\gamma - \gamma_c$ is the angle relative to the center of the port pair γ_c measured on the great circle connecting the port pair.

3.3.6.2.1 Values of qB: Maximum value and minimum value for desired measurements.

Referring to Figure 22, the maximum values of qB for the given flight regimes are:

New DWO entry - 425 psf
Old SWO entry - 80 psf
Booster entry - 1050 psf
Subsonic flight (below 25 000 ft) - 400 psf to 900 psf (down to 200 psf for SWO)

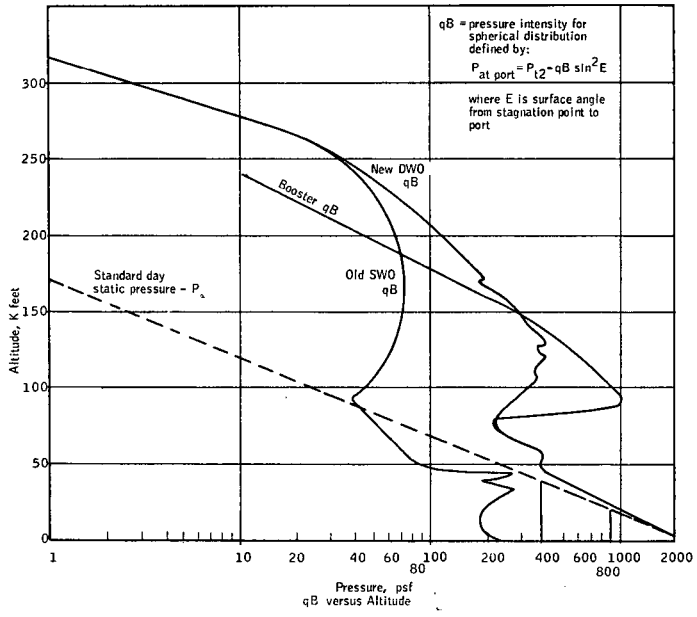

Figure 22. Pressure (PSF)

With additional calculation, the following maximum qB are obtained:

0.6 M cruise or glide - 0.67 X P_∞ = 1000 psf at 10 000 ft

Maximum qB during boost - 1400 psf

Thus, during boost the highest value of qB (1400 psf) is experienced; for booster entry and subsonic flight qB < 1050 psf; the orbiter entry has lower qB. Thus, 1500 psf will be used as maximum exposure range, with 1100 psf used as maximum measurement range values of qB.

Useful measurements are needed after M = 9, H = 130K ft during entry. The value of qB for New DWO and booster entry is about 200 psf. (Note that at M=9 the old SWO has H = 190 000 ft and qB = 80 psf). If capable of achievement, one to two degree α and β accuracy difference measurements are desirable at lower values of qB.

3.3.6.2.2 β-sensitive port pairs: The β-sensitive port pairs with ±45° spacing about $\beta = 0$ on the $\alpha = \alpha_c$ great circle, have $\Delta\theta = 90°$; $\gamma - \gamma_c = \beta$ and $\delta = \alpha - \alpha_c$, thus pressure difference is given by:

$$\Delta P = qB \cos^2 (\alpha - \alpha_c) \sin 2\beta$$

The maximum excursions about $\Delta P = 0$ at $\beta = 0$ would occur at maximum β, with magnitude qB sin 2β maximum with β maximum = 15°, this magnitude is qB/2.

At $\beta = 0$, a 1/2° β error is caused by a ΔP error of

$$\frac{2\ qB \cos^2 (\alpha - \alpha_c) \times 1/2°}{57.3°/\text{radian}}$$

which for $|\alpha - \alpha_c| < 45°$ has a value greater than $\frac{qB}{115}$.

The maximum range is seen to be proportional to to the maximum possible value of the parameter qB and the maximum deviation of stagnation point from center of the port pair. The required error tolerance is proportional to the value of qB above which useful measurements are desired.

Thus, a β-diffference to ±1 psf over a ±500 psf range will yield B measurement error of ±1/2° over ±15° range when qB is greater than 115 psf.

3.3.6.2.3 α-sensitive port pairs: With $\delta = \beta$, $\gamma - \gamma_c = \alpha - \alpha_c$, the α-sensitive port pairs on the $\beta = 0$ great circle with center at α_c and spacing $\Delta\theta$ have a pressure difference:

$$\Delta P = qB \cos^2 \beta \sin \Delta\theta \sin 2 (\alpha - \alpha_c)$$

The ports must lie on the 60. nose. The worst case pressure difference occurs during boost when at $\alpha = -10°$ the difference between ports at 60° and 10° having $2 (\alpha - \alpha_c) = 90°$ and $\Delta\theta = 50°$ yields $\Delta P = 3/4$ qB or about 1100 psf maximum exposure range for this worst case positioning of ports.

During subsonic flight α is between 8° and 15°, while trajectories are available for the entry phases. Calculations of difference pressures (Figure 23) for the new DWO nominal trajectory showed maximum difference

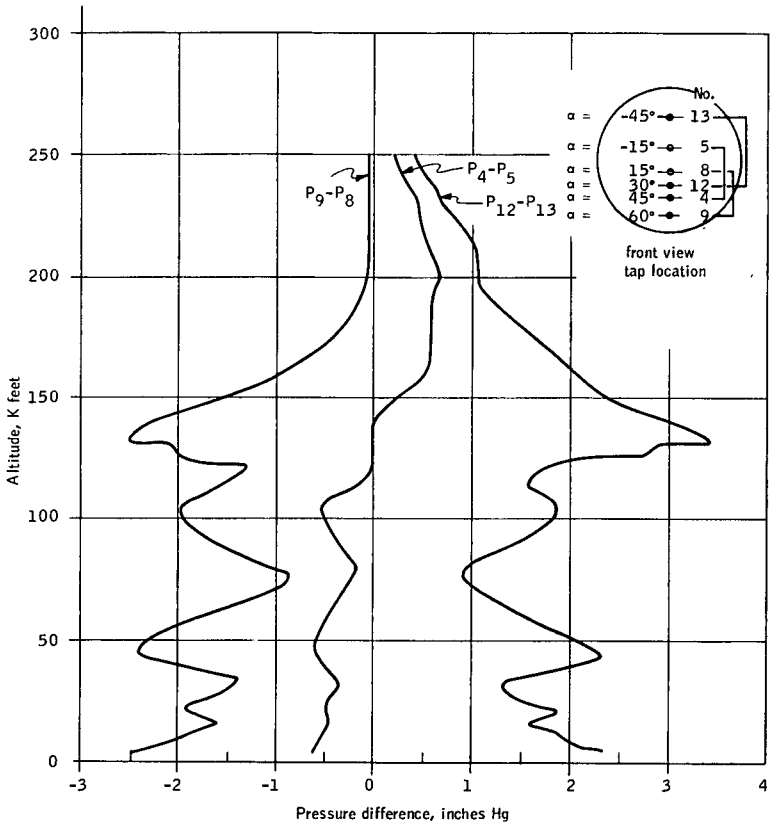

Figure 23. Sensor Pressure Difference versus Altitude During ΔWing Orbiter Entry Trajectory

range for the triple-redundant orbiter nose less than 4 in. Hg (280 psf). Pressure intensity qB is higher for booster entry; however, the smaller port spacings and locations to cover the 0 - 60° or 0 - 40° range for the booster nose configurations resulted in maximum α-sensitive differences of 8.3 inches Hg (660 psf).

The dual set of port differences relates to an α-measurement error primarily dependent on the pair having lower pressure difference (the pair with center nearest stagnation point) and secondarily on the pair having larger pressure. The error function is a complex relationship; however, ±1 psf transducer errors were found to be acceptable for the cases considered in subsection 3.5. For the larger differences used in combination with a smaller difference a somewhat larger error (like 0.5 percent to 1 percent of value) would be tolerable.

The differential transducers could be calibrated for zero offset in orbit and possibly at high altitude of booster coast. Thus, transducers having smaller error for the period following offset calibration are desirable.

With lower values of α during subsonic flight the pairs positioned with center at high angle of attack can experience larger pressure differences than during entry. With qB = 1200 psf, $\Delta\theta$ = 45°, 2 (α - α_c) = -45°, for port pair at 60° and 15°, with α = 12.5°, ΔP could be as large as 600 psf (9 in. Hg). This worst case operating condition defines maximum difference pressure that could be experienced by α-sensitive differential transducers.

3.4 CONVENTIONAL PITOT-STATIC PROBE

3.4.1 Probe Design and Installation

During low-speed flight such as cruise, approach and landing, a conventional pitot-static tube has been shown to be required for the X-15. The reasoning is that it is a standard instrument - familiar, simple and reliable. Applied to Shuttle the above reasoning still holds, with the exception that it must survive boost vibration and re-entry heating before being called upon. On the Shuttle it provides a second airspeed and atmospheric pressure measurement to that possible with a computer output from sphere-nose sensor. The airspeed measurement is particularly attractive to a pilot during landing.

The conventional pitot probe (without static pressure taps) will measure pitot pressure independent of probe angle of attack up to about ±20° without shielding. Further, experience with pitot tubes ahows that it is adequate to fuselage mount them on a strut approximately 5 inches in length. The direction, of course, must be within tolerance to the local flow direction and in a location where the flow is attached (i.e., not in separated flow).

Static pressure taps can be located either in the aircraft skin or on the probe. Static pressure errors of flush fuselage ports may vary between identical airplanes due to fabrication difficulties such as fuselage waviness, edge burrs and other local disturbances. This error source would have to be calibrated out for each individual aircraft.

Nearly all these static pressure problems associated with flush parts installation can be eliminated by using a pitot-static tube. The tolerances associated with repeatability for a pitot-static tube are the simple machine tolerances on the cylindrical portion of a pitot-static tube compared with rigid tolerances on a fuselage section. A tradeoff of static ports on the pitot-static probe is that the probe must be aligned with the local flow on the aircraft to within about ±10°. A pitot-static probe can be strut mounted about 5 inches from the fuselage. Conclusion is that a conventional pitot-static tube be strut mounted on the fuselage of the Shuttle.

Conventional pitot-static probes have been built and operated at supersonic speeds to M = 3.5 by research aircraft, and pitot probes (without static taps) at hypersonic speeds by the X-15. Both cases are well above the subsonic speeds contemplated for Shuttle use.

The design of the pitot-static tube is conventional. Location on the fuselage at low speeds follows established technique of putting it on the fuselage where the flow is attached (usually on the forward portion of the nose), and aligning it with the local flow direction determined either by tunnel tests and/or early flight tests. The unique problem for Shuttle is survival through high heating of entry at high angle of attack. If the orbiter nose is ahead of the booster nose, the pitot-static tube should be so located or protected to avoid heating or flow disturbance by the orbiter bow wave. The logical location for the probe is on the leeside of nose of the aircraft.

The first choice is to mount the probe permanently (as opposed to retracting it). Precise calculations of the probe heating and survival wait specification of vehicle shape and trajectory. However, the present estimates indicate that the probe temperatures for a fixed probe will be marginal, which for currently available probes is 1000°F. Materials similar to that for conventional total temperature probes allow maximum temperature at 2700°F. Cooler alternatives to the fixed pitot-static probe are:

- Retracting the probe within the skin during the flight and deploying only after reaching high subsonic speeds

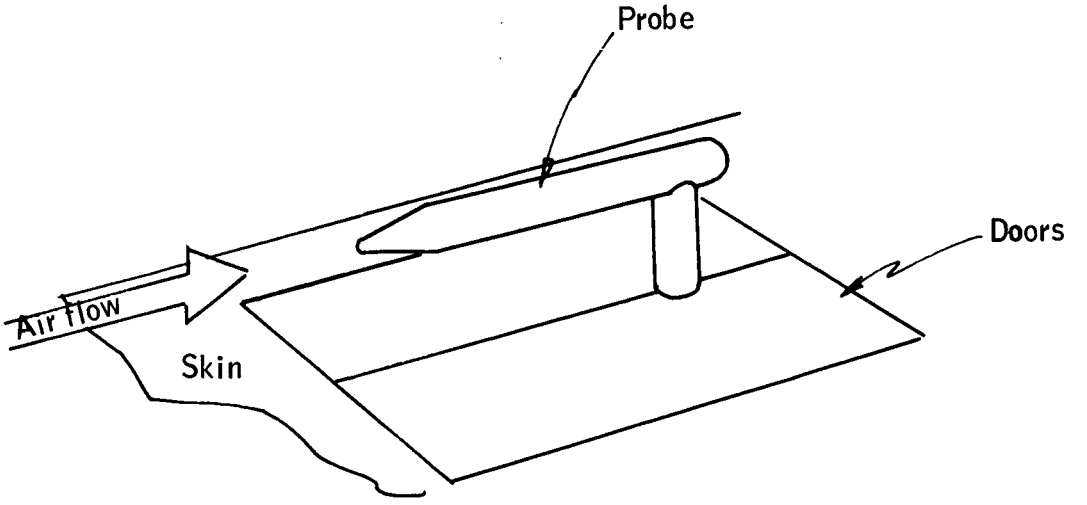

- Rotating the probe during heating so that is faces backwards and the sensitive lips of the pitot tube and static taps are in the cooler region near the trailing edge of the probe. For subsonic flight the probe is rotated to face upstream in the conventional manner. Advantage over retracting is a simpler mechanism but at the expense of some aerodynamic heating.

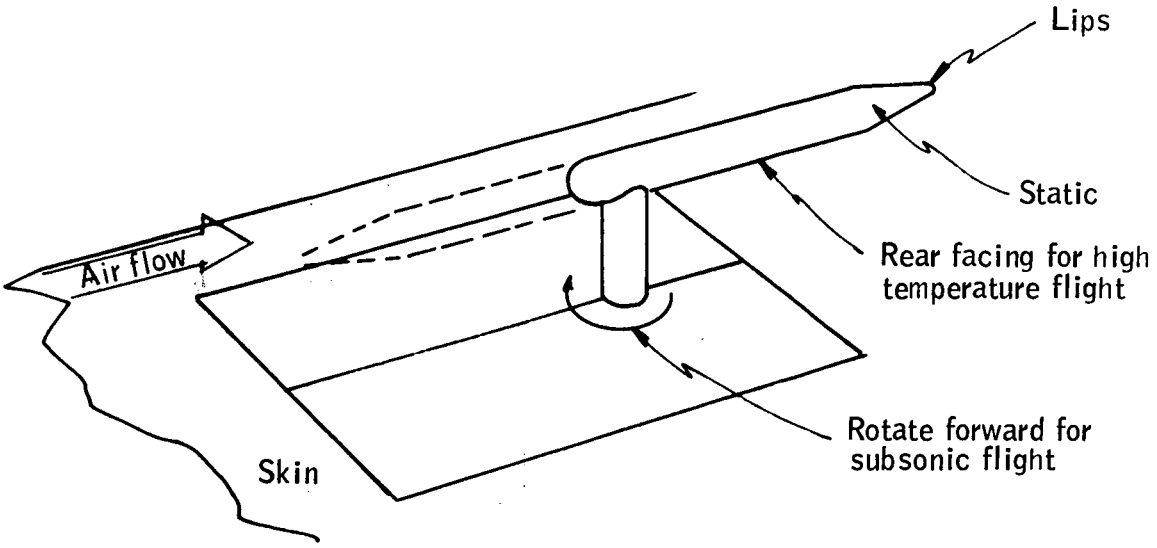

3.4.2 Outputs from Pitot-Static Probe

The two pressures sensed by the pitot-static probe are:

P_{T1} - indicated total pressure

P_{S1} - indicated static pressure

In subsonic aircraft P_{T1} is very close to stagnation pressure P_T and total pressure defect correction is not required. Significant $P_{T1} - P_T$ differences would result when the local flow speed differs from vehicle's air-mass relative speed when the pitot tube is not within ±20° of actual flow direction.

On the other hand correction of static source defects is usually done in subsonic aircraft air data systems. Such correction would be a function of Mach, static pressure, and possible angle of attack. The use of dogleg-mounted pitot-static probe requires less correction than flush ports (typical maximum of ±300 ft). By careful choice of probe location and orientation to inflow at nominal angle of attack, the probe can be shaped to compensate for static defect.

Given correct values of P_T and P_S, the following functions are typically computed:

$$Hp = P_5(P_S) \qquad \text{Pressure altitude}$$

$$CAS = KP_3\left[(P_T - P_S)^{1/2}\right] \qquad \text{Computed airspeed}$$

$$M = P_3\left[\left(\frac{P_T - P_S}{P_S}\right)^{1/2}\right] \qquad \text{Mach number}$$

where the subscript on P indicates the order of polynomial required to fit the compressible flow and standard atmosphere relationships to needed accuracy level (ref. 12 and 13).

The quantities CAS and Mach do not define true airspeed since speed of sound is undetermined (unless a total temperature probe is used). These quantities are those typically used in flight control.

3.5 DETAILED DESCRIPTION AND ANALYSIS OF SPECIFIC SPHERE-NOSE CONFIGURATION

To evaluate the specific mechanization and performance parameters over representative flight configurations the sphere nose sensor was configured for three cases:

a) 60° orbiter nose with triple redundant channels having identical electronics units

b) 40° booster nose with single five-port set

c) 60° booster nose with dual five-port sets, where one of these sets is like case b) with widened β-sensitive ports.

All cases assume separate pitot-static probe(s) for subsonic measurements. The configuration choices reflect different types of redundancy possible. Case a) uses 13 pressure ports cross-fed to three identical channels, while cases b) and c) are single and dual sets with additional transducer allowing different computational equations involving three of four transducers. To allow complete no-single-point-failure measurement of α, β and P_T from the sphere nose requires 21 ports - 7 to each of three redundant identical hardware channels.

Case c) allows a 0 to 60° angle-of-attack range, case b) allows 0 to 40° and case a) allows 0 to 30°. Case b) is included to evaluate a case where a 40° sphere can conveniently be placed on booster.

These configurations (plus the "qα" capable single configurations in subsection 3.3.4) provide examples of port configurations with reasonable performance under different function, range, and redundancy constraints.

3.5.1 Port Location and Hardware Configurations

The assumed port locations for the three cases and their interconnections with electronics units which measure difference and absolute pressures is depicted in Figures 24 through 26. More detail on electronics unit functions is shown in Figure 27.

The installations on eventual Shuttle vehicles could deviate from these for different integration decisions made by the system designer. Variations result from choices like:

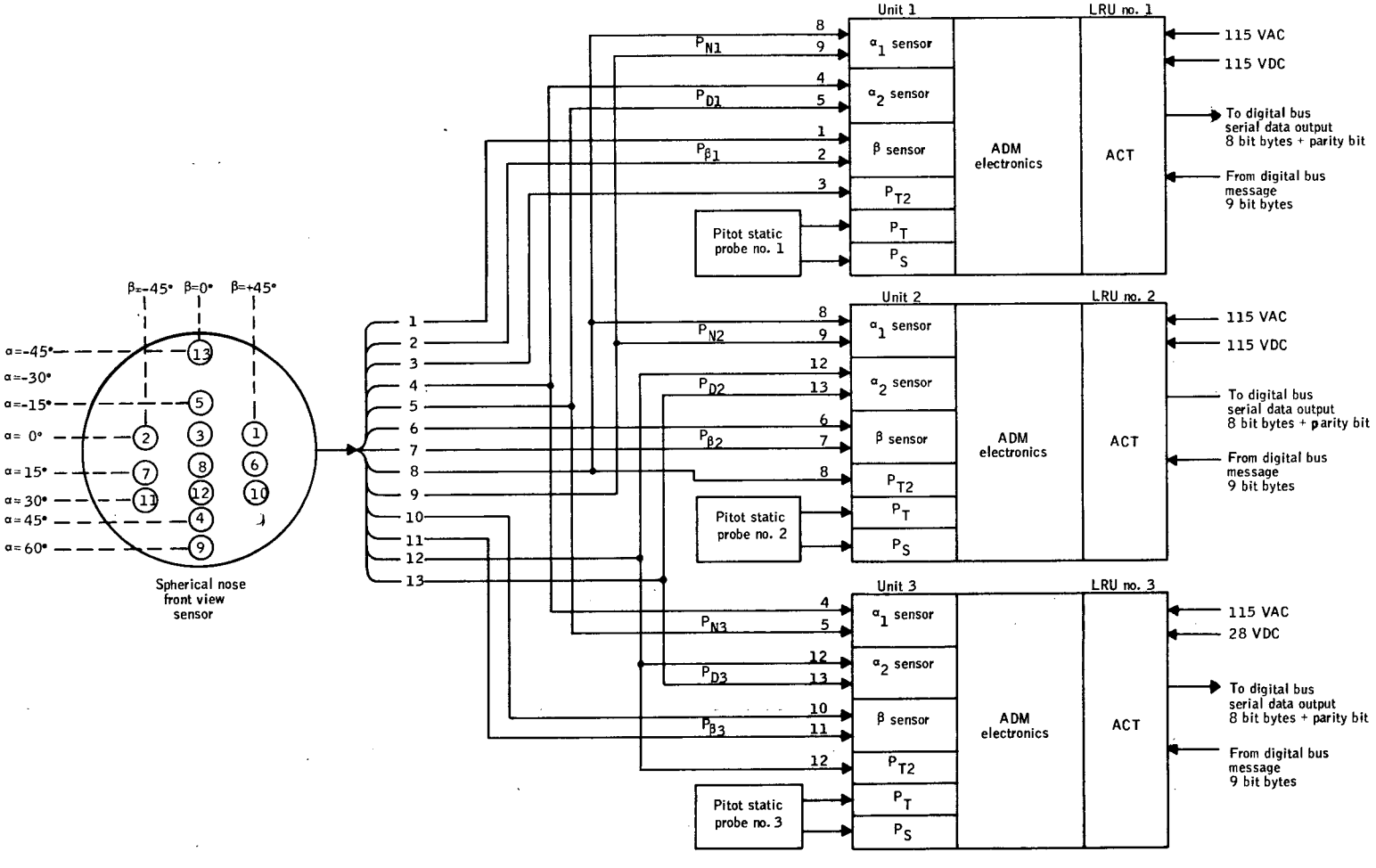

Figure 24. Orbiter Air Data Measurement System Sensor - LRU Interconnection

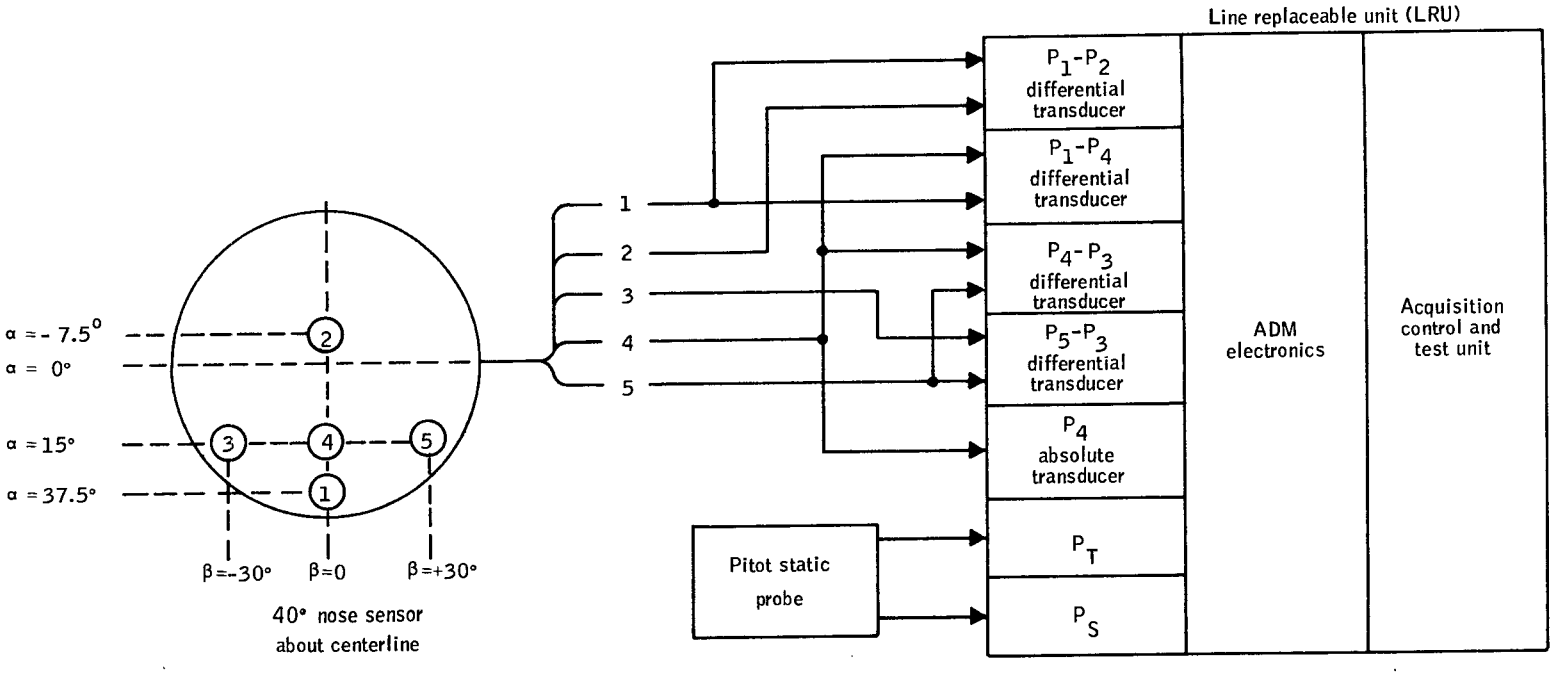

Figure 25. Booster 40° Nose Air Data Measurement Sensor - LRU Interconnection

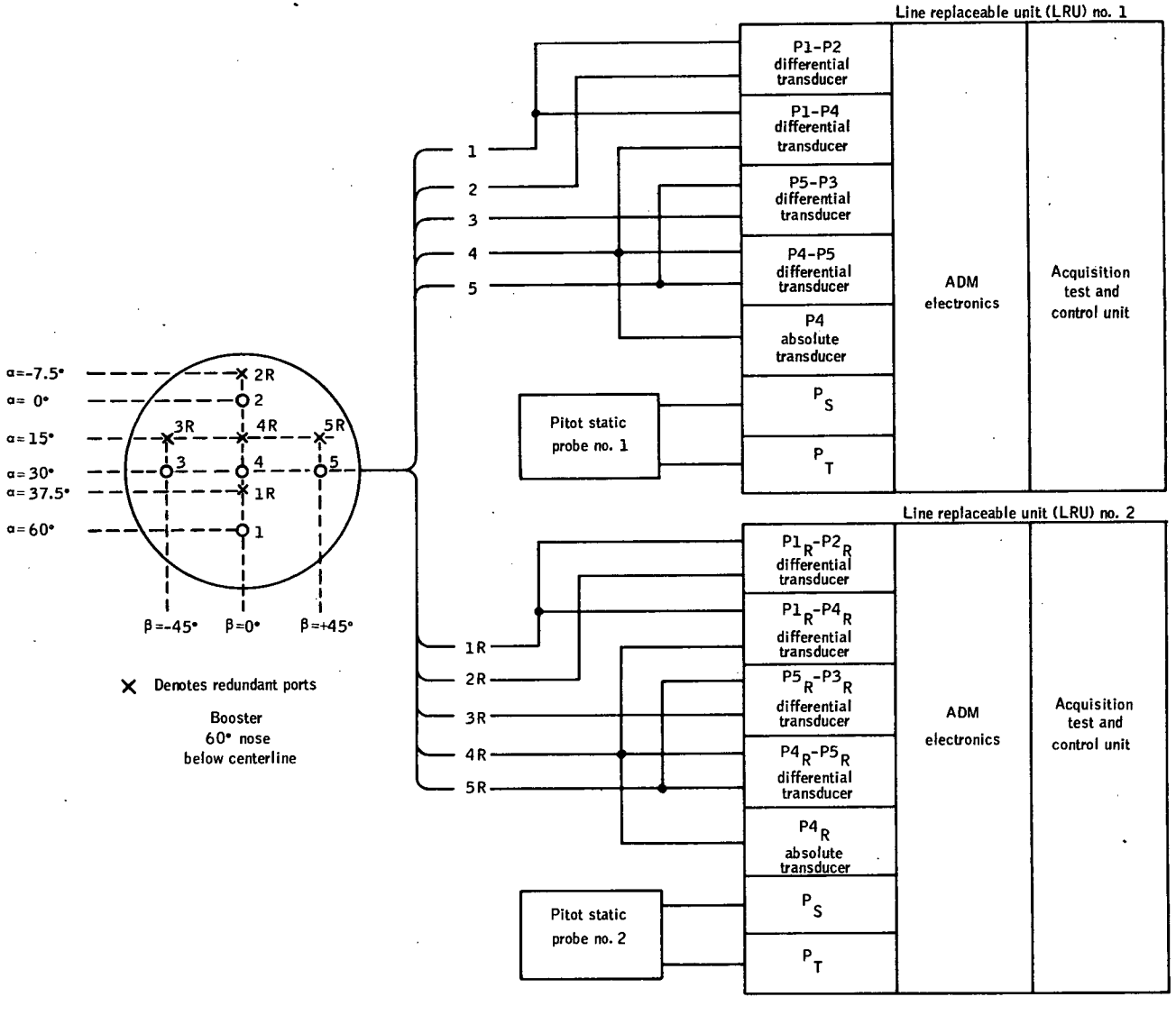

Figure 26. Booster 60° Nose Air Data Measurement Sensor - LRU Interconnection

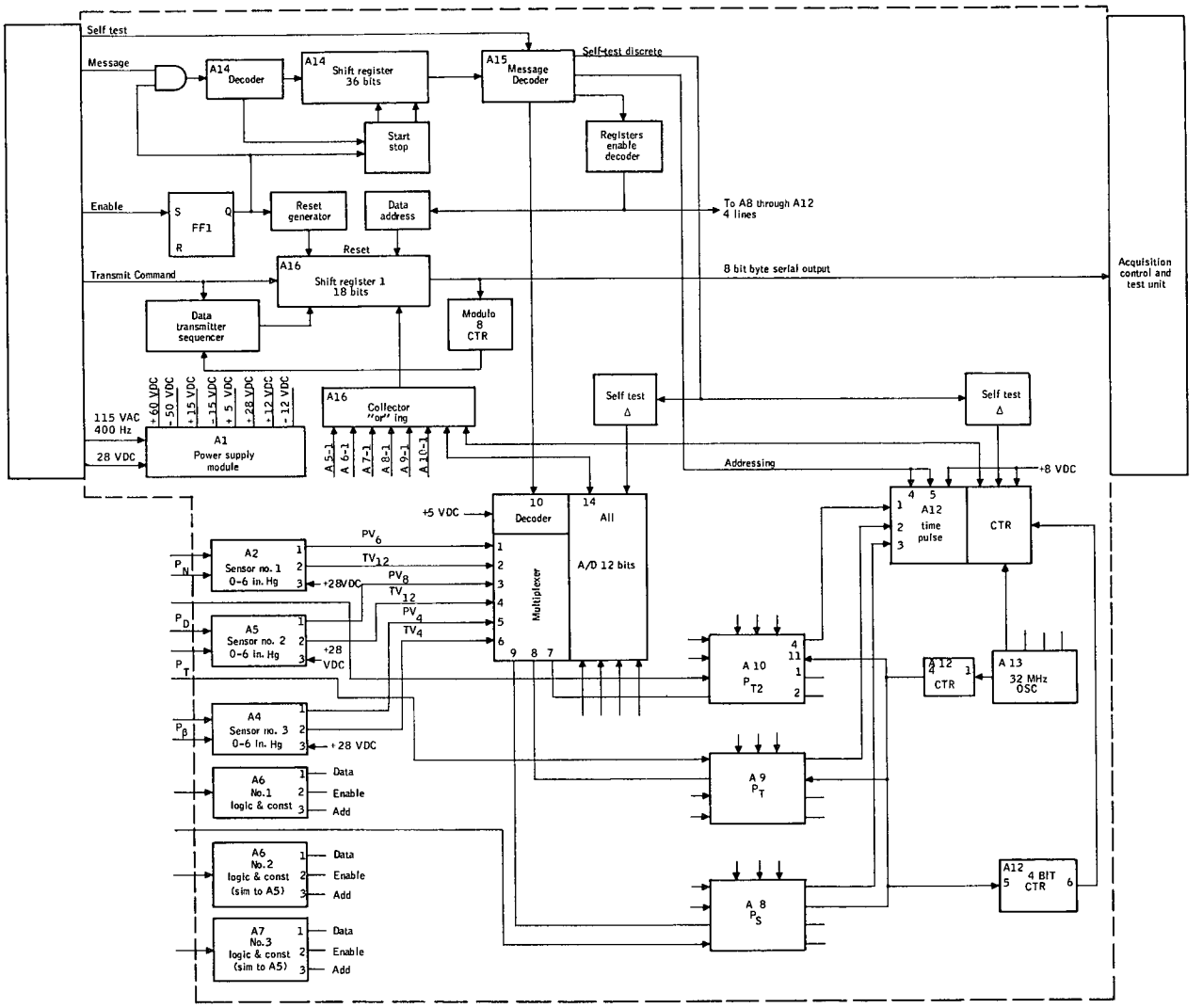

Figure 27. Shuttle Air Data Measurement Electronics

a) Different means to achieve nose port and line redundancy or backup

b) Dedicated computer in ADM electronics

c) Pitot-static transducers located in other units to shorten pressure lines

d) Different redundancy provisions

e) Different angle-of-attack ranges

f) Use of information from two channels to yield an output.

The configurations shown are representative of final configurations.

3.5.2 Computational Equations for Nose Sensor Configurations

The transducers are connected to ports identified on the spherical nose. For each transducer there is a computation resulting in a digital word representing the measured pressure that is a function of several calibration constraints (unique to the particular transducer) and two measurements of transducer outputs (pressure and temperature variables).

Given the pressure words, the air data equations are solved to yield outputs of α, β, and P_T. These equations are based on the generalized equations detailed in subsection 3.3.3.

3.5.2.1 Equations for three units of 60° orbiter nose case. -

a) Pressure Measurements

Unit 1	Unit 2	Unit 3
$P_{\beta 1} = P_1 - P_2$	$P_{\beta 2} = P_6 - P_7$	$P_{\beta 3} = P_{10} - P_{11}$
$P_{A1} = P_3$	$P_{A2} = P_8$	$P_{A3} = P_{12}$
$P_{N1} = P_9 - P_8$	$P_{N2} = P_9 - P_8$	$P_{N3} = P_4 - P_5$
$P_{D1} = P_4 - P_5$	$P_{D2} = P_{12} - P_{13}$	$P_{D3} = P_{12} - P_{13}$

b) Transducer Calibration -- For each measurement, the digital word, P_{jk} is derived from a calibration constants K_{jk} and variables p_{jk} and t_{jk} according to

$$P_{jk} = f(K^i_{jk}, p_{jk}, tjk)$$

where $i = 1, 2, \ldots, n$ 15 and f is a function involving only additions, multiply and divide.

c) Air Data Computations

1) Unit 1:

$$N_1 = \frac{\left(\frac{P_{D1}}{\sin 60°}\right) + \left(\frac{P_{N1}}{\sin 45°}\right)}{\cos 22.5°}$$

$$D_1 = \frac{\left(\frac{P_{D1}}{\sin 60°}\right) - \left(\frac{P_{N1}}{\sin 45°}\right)}{\sin 22.5°}$$

$$\alpha = 1/2 \tan^{-1}\left(\frac{N_1}{D_1}\right) + 26.25°$$

$$F_1 = [N_1^2 + D_1^2]^{1/2}$$

$$\beta = \tan^{-1}\left[\frac{P_{\beta 1}}{F_1 \cos \alpha}\right]$$

$$P_T = P_{A1} + \frac{F_1}{2}\left[\frac{1}{\cos^2 \beta} - \cos^2 \alpha\right]$$

2) Unit 2:

$$N_2 = \frac{\left(\frac{P_{D2}}{\sin 75°}\right) + \left(\frac{P_{N2}}{\sin 45°}\right)}{\cos 45°}$$

$$D_2 = \frac{\left(\frac{P_{D2}}{\sin 75°}\right) - \left(\frac{P_{N2}}{\sin 45°}\right)}{\sin 45°}$$

$$\alpha = 1/2 \tan^{-1}\left(\frac{N_2}{D_2}\right) + 15°$$

$$F_2 = [N_2^2 + D_2^2]^{1/2}$$

$$\beta = \tan^{-1}\left[\frac{P_{\beta 2}}{F_2 \cos (\alpha - 15°)}\right]$$

$$P_T = P_{A2} + \frac{F_2}{2}\left[\frac{1}{\cos^2 \beta} - \cos^2 (\alpha - 15°)\right]$$

3) Unit 3:

$$N_3 = \frac{\left(\frac{P_{D3}}{\sin 75°}\right) + \left(\frac{P_{N3}}{\sin 60°}\right)}{\cos 22.5°}$$

$$D_3 = \frac{\left(\frac{P_{D3}}{\sin 75°}\right) - \left(\frac{P_{N3}}{\sin 60°}\right)}{\sin 22.5°}$$

$$\alpha = 1/2 \tan^{-1} (N_3/D_3) + 3.75°$$

$$F_3 = [N_3^2 + D_3^2]^{1/2}$$

$$\beta = \tan^{-1}\left[\frac{P_{\beta 3}}{F_3 \cos(\alpha - 30°)}\right]$$

$$P_T = P_{A3} + \frac{F_3}{2}\left[\frac{1}{\cos^2\beta} - \cos^2(\alpha - 30°)\right]$$

d) Failure-detection and Redundancy Switching - The three units are seen to generate independent outputs from measurements in separate units; the first stage of comparison and redundancy switching could be a majority vote or middle-picking among the three sources of α, β, and P_T.

In the event one or more of these parameters is different from the other two, failure detection and isolation logic can be based on relationships present such as:

$$F_1 = F_2 = F_3 = F = 2\ qB \cos^2 \beta$$

$$P_{D1} = P_{N2},\ P_{N1} = P_{N3} \text{ and } P_{D2} = P_{D3}$$

$P_{\beta 1}$, $P_{\beta 2}$, and $P_{\beta 3}$ have coinciding zero values, same sign and magnitudes proportional to cos α, cos (α-15°) and cos (α-30°). The three α-sensitive differences and differences formed from the absolute measurements should place the stagnation point at the same point since each

$$\Delta P_j = qB \cos^2 \beta \sin \Delta\theta \sin 2(\alpha - \alpha_j)$$

Upon isolation to the failed port, line, transducer, or electronics unit, this failure isolation logic could proceed to reformulate the remaining measurements from the three channels into more degraded determinations of α, β, and P_T.

For example, P_8 is a single port affecting both units 1 and 2. Its failure can be isolated causing switching to use of unit 3; then by using $P_{A1} - P_{A3}$, degraded backup equations using other measurements of units 1 and 2 can produce substitute units 1 and 2 outputs for the primary voter (perhaps biased to use unit 3).

Thus the triple-redundant system's apparent single-point failure can be backed up for cases of single failure and the more complex 21-port nose is not absolutely necessary. The system designer must settle the redundancy and mechanization questions, realizing this informational redundancy is present. The failure isolation and backup for this case were not detailed beyond this superficial point. In a sense this configuration appears to have too much redundancy.

3.5.2.2 Equations for the 40° booster nose case. -

a) Pressure measurements

$P_{\beta 1} = P_5 - P_3$

$P_A = P_4$

$P_N = P_1 - P_4$

$P_D = P_1 - P_2$

$P_{\beta 2} = P_4 - P_5$

where the ports are located as:

P_1	$\alpha = 37.5°$	$\beta = 0$
P_2	$\alpha = -7.5°$	$\beta = 0°$
P_3	$\alpha = 15°$	$\beta = -30°$
P_4	$\alpha = 15°$	$\beta = 0°$
P_5	$\alpha = 15°$	$\beta = +30°$

Two sets of equations - one set without $P_{\beta 2}$ and the alternate set without P_N - allow separate determinations of α and β.

b) Transducer calibration - Same as subsection 3.5.2.1.

c) Air data equations

1) Without $P_{\beta 2}$

$$\alpha = 1/2 \tan^{-1}\left[\frac{P_D \tan 22.5°}{P_D - 2P_N}\right] + 15°$$

$$F' = \left\{\left[\frac{P_D}{\sin 45°}\right]^2 + \left[\frac{P_D - 2P_N}{1 - \cos 45°}\right]^2\right\}^{1/2}$$

$$\beta = \tan^{-1}\left[\frac{P_{\beta 1}}{2\,F'\sin 60^\circ \cos(\alpha - 15^\circ)}\right]$$

$$P_T = P_4 + F'\left[\frac{1}{\cos^2\beta} - \cos^2(\alpha - 15^\circ)\right]$$

$$= P_4 + P_N + F'\left[\frac{1}{\cos^2\beta} - \cos^2(\alpha - 37.5^\circ)\right] \text{ for } \alpha > 26.25^\circ$$

2) Without P_N

$$\beta' = 1/2\,\tan^{-1}\left[\frac{P_{\beta 1}\tan 30^\circ}{P_{\beta 1} + 2P_{\beta 2}}\right]$$

$$\beta = \tan^{-1}\left[\tan\beta'\cos(\alpha - 15^\circ)\right]$$

$$G = \left\{\left[\frac{P_{\beta 1}}{\sin 60^\circ}\right]^2 + \left[\frac{P_{\beta 1} + 2P_{\beta 2}}{1 - \cos 60^\circ}\right]^2\right\}^{1/2}$$

$$\alpha' = \tan^{-1}\left[\frac{P_D}{2\,G\sin 45^\circ \cos\beta'}\right]$$

$$\alpha = \sin^{-1}\left[\sin\alpha'\sec\beta\right] + 15^\circ$$

$$P_T = P_4 + G\left[\frac{1}{\cos^2\alpha'} - \cos^2\beta'\right]$$

d) Failure detection and redundancy considerations - The means of alternate computations from use of one additional transducer is another possible redundancy option. The reason for consideration here is to compare relative performance of the two methods. For redundancy purposes, the additional transducer and computation merely backing up one transducer is not very effective.

3.5.2.3 Equations for 60° booster nose case. - This case contains two five-port sets which can be described as having ports located at:

Primary: $\alpha = 0^\circ, 30^\circ, 60^\circ$, $\beta = 0^\circ$ and $\alpha = 30^\circ$ $\beta = \pm 45^\circ$

Redundant: $\alpha = -7.5^\circ, 15^\circ, 37.5^\circ$, $\beta = 0^\circ$ and $\alpha = 15^\circ$ $\beta = \pm 45^\circ$

The redundant set is identical to that for the 40° nose(subsection 3.5.3.2) with exception that the β-sensitive ports are at $\pm 45^\circ$ instead of $\pm 30^\circ$. The only changes from equations of subsection 3.5.2.2 for the redundant case

are changing 30° to 45° in the β' equation and 60° to 90° in the G and first-β equations; thus these won't be repeated here.

For the primary five-port set with redundant transducer the dual sets of equations and notation are as follows:

a) Pressure measurements

$P_{\beta 1} = P_5 - P_3$ where P_1 at $\alpha = 60°$ $\beta = 0°$

$P_A = P_4$ P_2 at $\alpha = 0°$ $\beta = 0°$

$P_N = P_1 - P_4$ P_3 at $\alpha = 30°$ $\beta = -45°$

$P_D = P_4 - P_3$ P_4 at $\alpha = 30°$ $\beta = 0°$

$P_{\beta 2} = P_4 - P_5$ P_5 at $\alpha = 30°$ $\beta = -45°$

b) Transducer calibration - Same as subsection 3.5.2.1.

c) Air data equations

1) Without $P_{\beta 2}$

$$\alpha = 1/2 \tan^{-1}\left[\frac{P_D \tan 30°}{P_D - 2P_N}\right] + 30°$$

$$F' = \left\{\left[\frac{P_D}{\sin 60°}\right]^2 + \left[\frac{P_D - 2P_N}{1 - \cos 60°}\right]^2\right\}^{1/2}$$

$$\beta = \tan^{-1}\left[\frac{P_{\beta 1}}{2F' \cos(\alpha - 30°)}\right]$$

$$P_T = P_4 + F'\left[\frac{1}{\cos^2\beta} - \cos^2(\alpha - 30°)\right]$$

$$= P_4 + P_N + F'\left[\frac{1}{\cos^2\beta}\cos^2(\alpha - 60°)\right] \text{ for } \alpha > 45°$$

$$= P_4 + P_N - P_D + F'\left[\frac{1}{\cos^2\beta} - \cos^2\alpha\right] \text{ for } \alpha < 15°$$

2) Without P_N

$$\beta' = 1/2 \tan^{-1}\left[\frac{P_{\beta 1}}{P_{\beta 1} + 2P_{\beta 2}}\right]$$

$$\beta = \tan^{-1} [\tan \beta' \cos (\alpha - 30°)]$$

$$G = \{[P_{\beta 1}]^2 + [P_{\beta 1} + 2 P_{\beta 2}]^2\}^{1/2}$$

$$\alpha' = \tan^{-1}\left[\frac{P_D}{2G \sin 60° \cos \beta'}\right]$$

$$\alpha = \sin^{-1} [\sin \alpha' \sec \beta] + 30°$$

$$P_T = P_4 + G\left[\frac{1}{\cos^2 \alpha'} - \cos^2 \beta'\right]$$

d) Failure detection and redundancy considerations - The five-port set with three transducers sensing $P_1 - P_2$, $P_4 - P_1$, and $P_4 - P_2$ is a redundancy alternative showing computation of the third given the other two. Three more similar β-sensitive transducers (six transducers total) allow triple redundancy of α and β. Such an alternative should be considered strongly compared to the nine transducers required for direct triplication of the primary thread.

The final redundancy mechanization is left to the eventual system designer; these specific cases are analyzed to cover the range of possibilities from the standpoint of relative performance.

3.5.3 Performance and Error Sensitivity Analysis

3.5.3.1 Orbiter. - This subsection of the report discusses the alpha, beta, and P_{T2} measuring sensitivities of the orbiter sensor. The data base used for the study of these sensitivities was the orbiter re-entry trajectory (603). The altitude and relative velocity of the trajectory as a function of time and the alpha and qB of the orbiter in the trajectory as a function of time are shown in Figures 28 and 29. Actual information about the trajectory is given only to 2500 seconds. However, for the purpose of this study, the trajectory was extended beyond 2500 seconds to investigate the sensor sensitivities in this region. These points are shown on some graphs but they do not necessarily represent the actual trajectory.

The orbiter configuration discussed earlier in subsection 3.5.1 is the configuration used in this study. The mathematical model used is discussed in subsection 3.5.2. Theoretically, the modelled system could use the measurements of pressure at a port which is more than 90 spherical degrees from the stagnation point. Practically, however, we have assumed 75° of separation between the stagnation point and the port as a limit for accurate measurement. The alpha operating range of the orbiter is between 0° and 60°. Therefore, port 13 will be out of the 75° limit for an alpha greater than 30°. This means that one of the differential pressures used for alpha measurement on units 2 and 3 will be considered out of range for the portion of the trajectory between 0 and 280 seconds where alpha = 53°. In the graphs

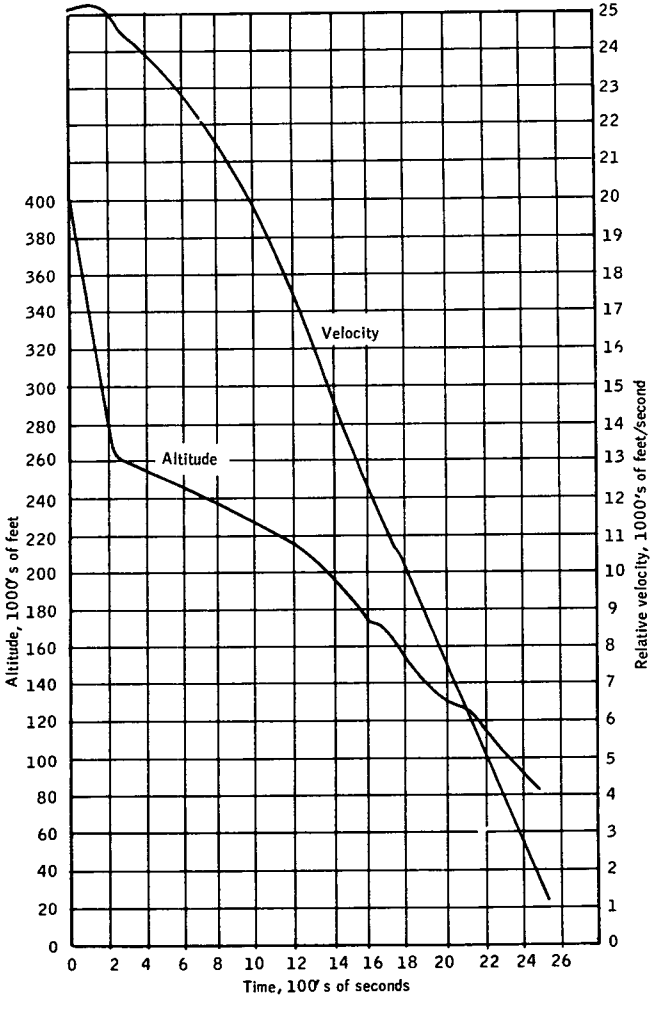

Figure 28. Orbiter Altitude and Relative Velocity versus Time

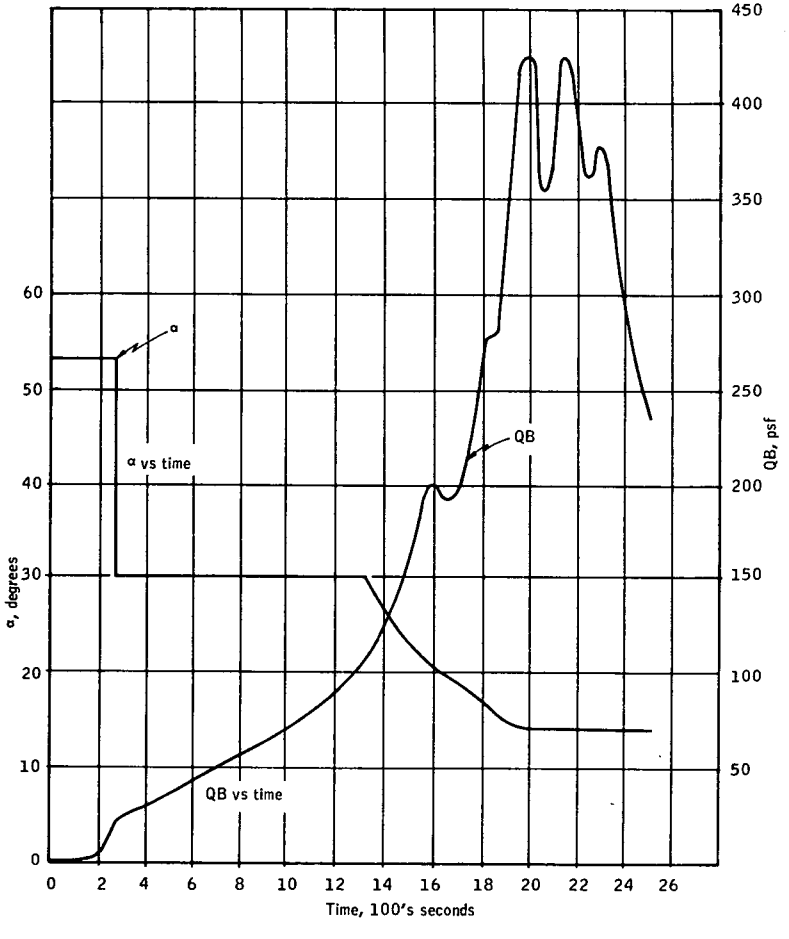

Figure 29. Orbiter Entry Trajectory 603

illustrating the sensitivities of the sensor units in the rest of the discussion, if a unit is operating outside the 75° limit, the lines for that unit will be dashed instead of solid.

The ports in the orbiter nose are combined to form three alpha, beta and P_{T2} measuring units. These pressures and pressure differentials are combined as discussed in subsection 3.5.2 to measure alpha, beta and P_{T2}. There are six pressure differentials and three absolute pressures to be measured. Using the model equations for pressure at a port as a sphere and the input data from the orbiter trajectory the magnitude of the pressures which the transducer will have to measure was computed.

For the absolute pressure transducers the maximum pressures occur below Mach 1 where P_{T2} is maximum. The maximum value was computed as approximately equal to 2250 psf.

The beta-sensitive transducers, which measure pressure differentials, need a very small dynamic range because beta is held to zero. As an example of the absolute maximum pressure which may be expected - if we assume that at the maximum qB, 427 psf (maximum pressure differential occurs at maximum qB), the orbiter would have a 5° beta, the pressure differential is less than 75 psf for the beta-sensitive transducers.

The other three pressure differentials are combined and used for the alpha-sensitive measurements. Let them be called:

$$P_1 = P_9 - P_8$$

$$P_2 = P_4 - P_5$$

$$P_3 = P_{12} - P_{13}$$

As can be derived the equation for differential pressure between ports becomes independent of P_{T2} and if beta is assumed to be held to zero and the ports are on the beta = 0° great circle then the equation reduces to:

$$P_d = P_i - P_j = qB\,(\cos^2(\alpha - \alpha_i) - \cos^2(\alpha - \alpha_j)$$

Thus differential pressure for two ports becomes dependent on qB and alpha. Using qB and alpha inputs from the trajectory, the differential pressures P_1, P_2, and P_3 were computed as a function of trajectory time and the results are shown in Figure 30. P_1 ranges from +10 to -220 psf, P_2 from +40 to -90 psf and P_3 from 0 to 280 psf.

To determine the sensitivity of alpha measurement to errors in the differential pressure transducers the pressure was computed for selected nominal qB points along the trajectories, then computed for an alpha of 0 to 60° at these points. Then the differential pressures were varied by ±1 psf and the measured alpha was recomputed. One psf error was chosen to demonstrate the sensitivities of the alpha, beta and P_{T2} measurements because it

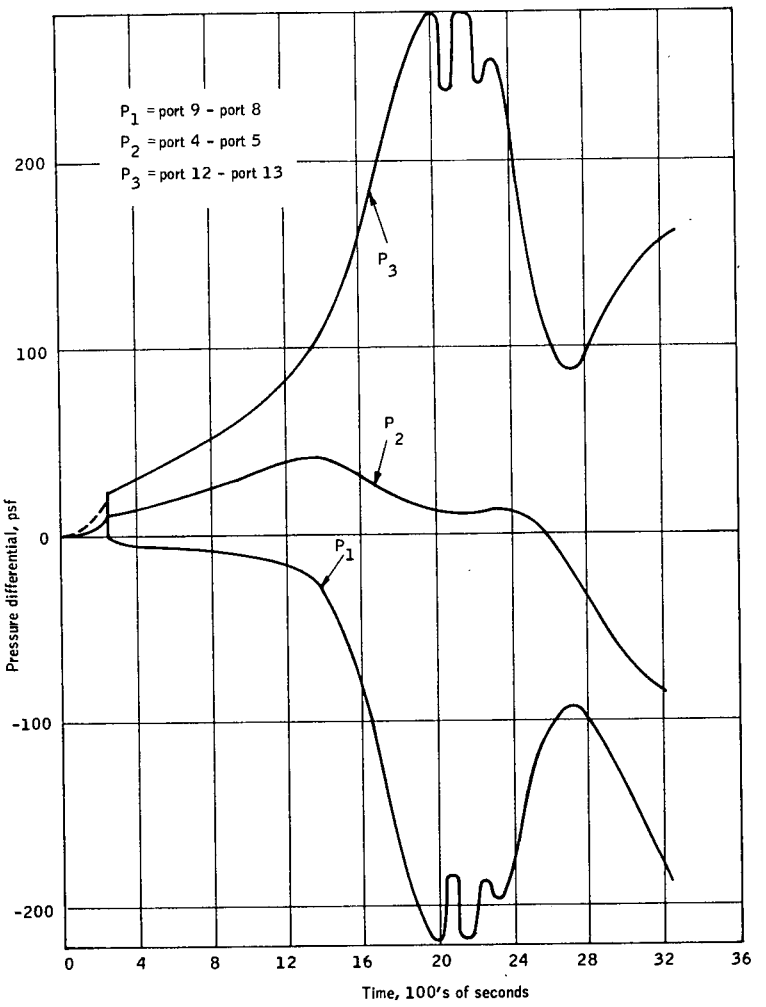

Figure 30. Pressure Differential versus Time

represents a reasonable limit on transducer errors. This error in alpha is the result of errors in two differential pressures, P_1 and P_2 for unit 1, P_1 and P_3 for unit 2, and P_2 and P_3 for unit 3. The errors in alpha resulting from the ±1 psf variation of each differential pressure were then root sum squared to determine an error in alpha. The resulting rss error in alpha is a function of the orbiter alpha and is inversely proportional to qB.

Figures 31 through 33 show the relationship between qB and rss alpha error. To maintain a rss α error of ±1° for a pressure differential error of ±1 psf over the 0° to 60° operating range, qB must be larger than 65 psf for unit 1, 42 psf for unit 2 and 65 psf for unit 3. These qBs correspond to 950, 550, and 920 seconds into the re-entry. However, at an alpha of 30° which is the operating alpha in this region, the qB necessary to satisfy a ±1° alpha error is 40 psf for unit 1, 42 psf for unit 2, and 50 psf for unit 3.

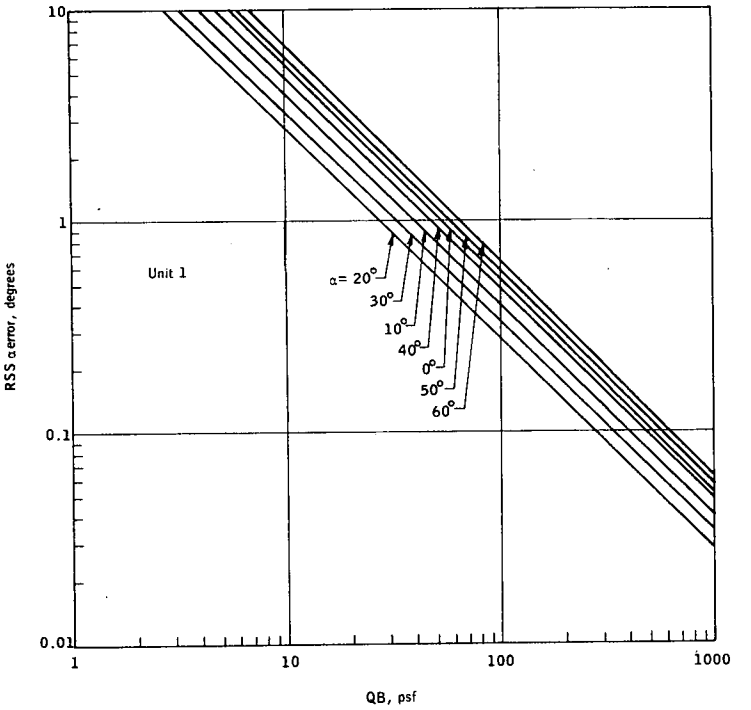

Figure 31. RSS α Error for 1 psf Pressure Differential Error versus QB for Unit 1

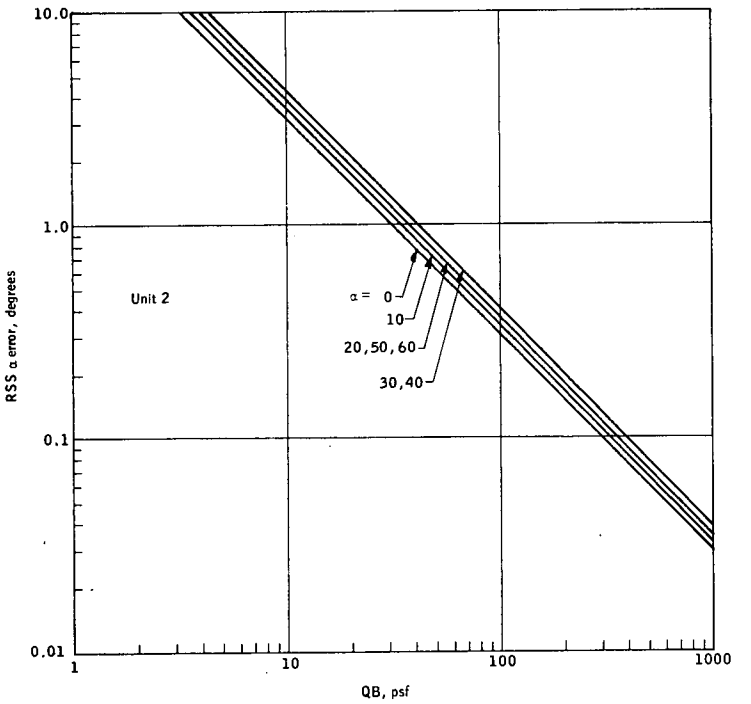

Figure 32. RSS α Error for 1 psf Pressure Differential Error versus QB for Unit 2

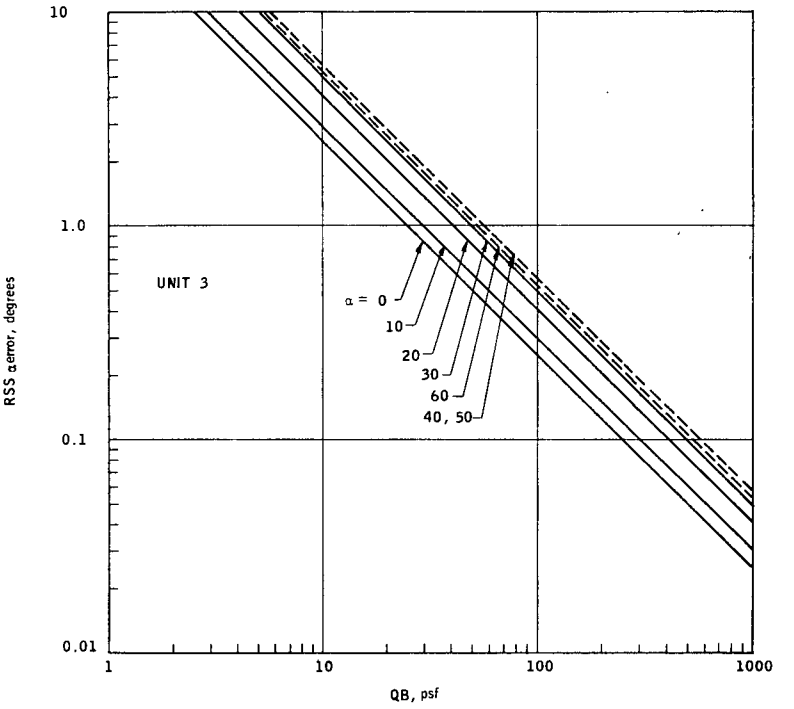

Figure 33. RSS α Error for 1 psf Pressure Differential Error versus QB for Unit 3

So at 540 seconds, unit 1 will be operable and by 700 seconds they will all be operable at ±1° alpha. Figure 34 is a graph of the rss alpha error over the trajectory for the three units. They are all relatively close, unit 1 is more accurate for most of the flight, except at the low angles of attack in the cruise region.

The same method was used to determine the beta error resulting from 1 psf in the beta-sensitive transducers measuring $P_{\beta 1}$, $P_{\beta 2}$, and $P_{\beta 3}$. The results of this computation are shown in Figures 35 through 37 for units 1, 2 and 3, respectively. The smallest qB for a ±1° beta accuracy in the 30° range for all three units is 30 psf which means that all beta sensors will be operating at 420 seconds into the trajectory. The beta error for 1 psf error in the transducers over the trajectory is shown in Figure 38. As can be seen, all three units are essentially the same.

The third quantity to be measured is P_{T2}. P_{T2} is a function of both the differential and absolute pressure transducers as can be seen by the equations in subsection 3.5.2.1. It is directly a function of the absolute transducer error, but there is also an error which is a function of the alpha of the orbiter. The same procedure was used to complete the P_{T2} sensitivities. The pressure transducers were varied by 1 psf and the resulting P_{T2} errors were rss'd to give a total error. The portion of the P_{T2} error due to 1 psf pressure differential measurement errors is dependent on the alpha of the orbiter. Figure 39 shows this error in P_{T2}. This error is small compared to the error in the transducer measurement.

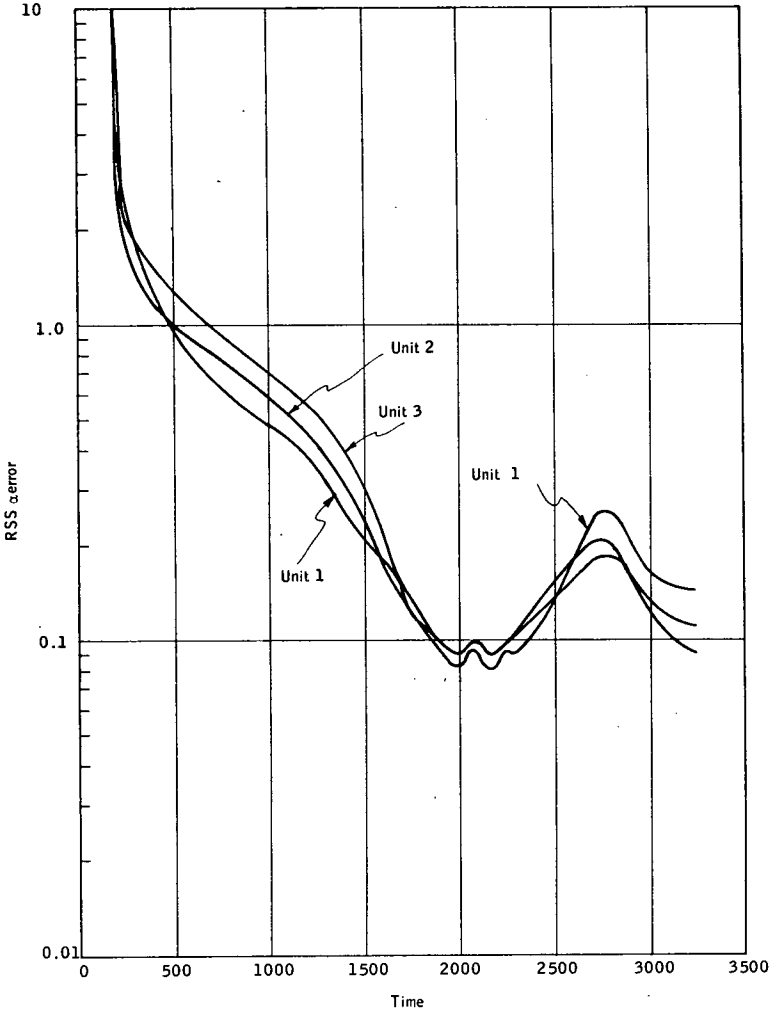

Figure 34. RSS α Error versus Time

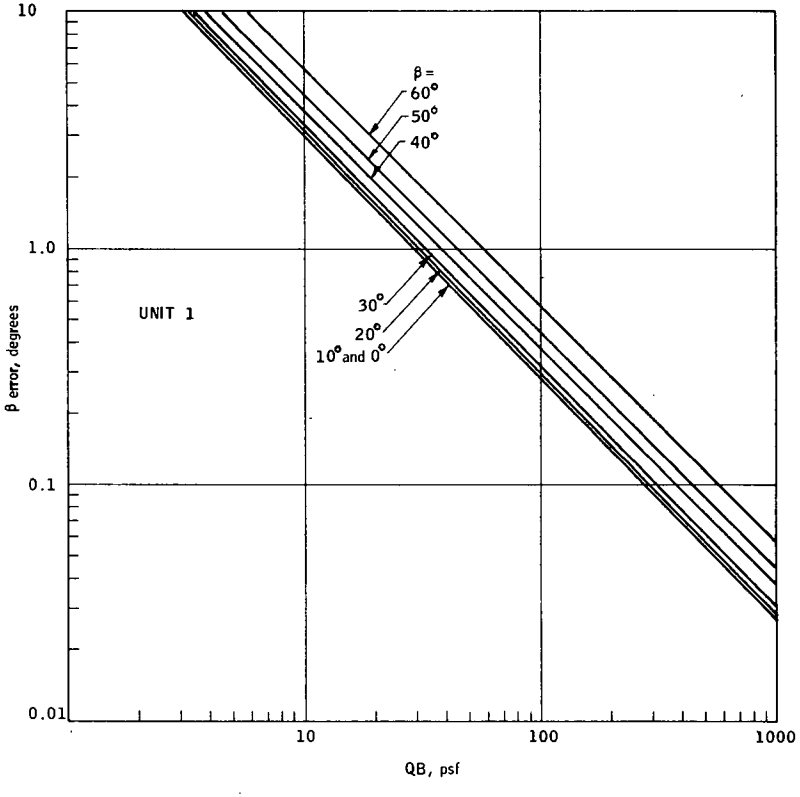

Figure 35. β Error versus QB - Unit 1

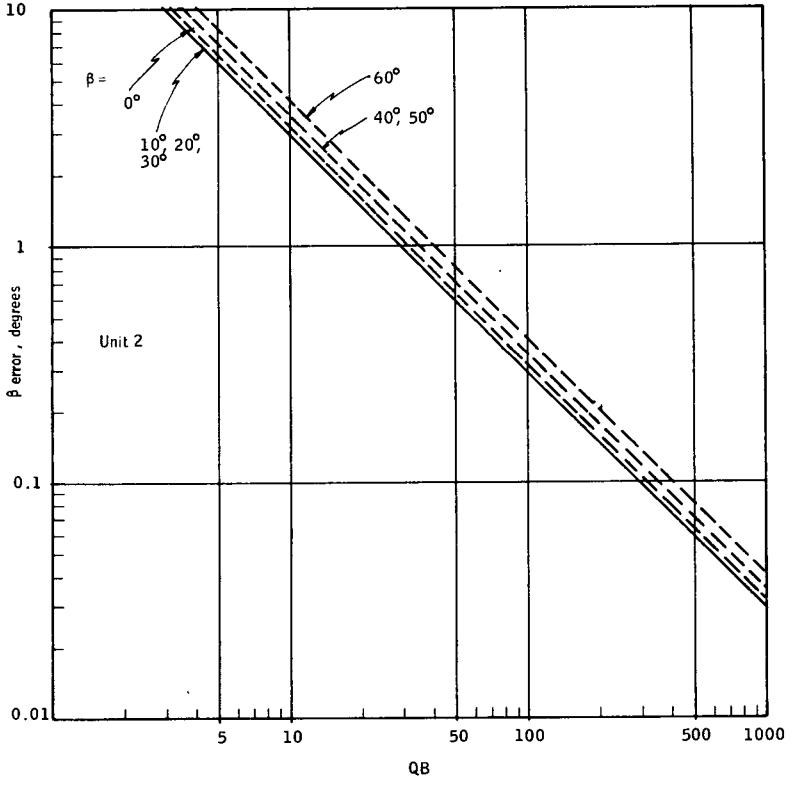

Figure 36. β Error versus QB - Unit 2

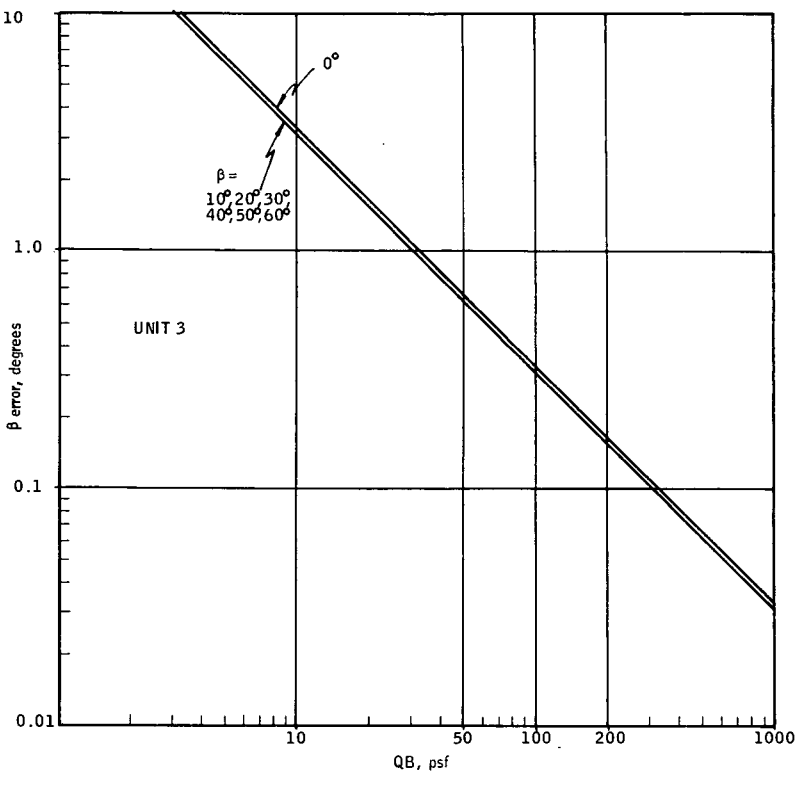

Figure 37. β Error versus QB - Unit 3

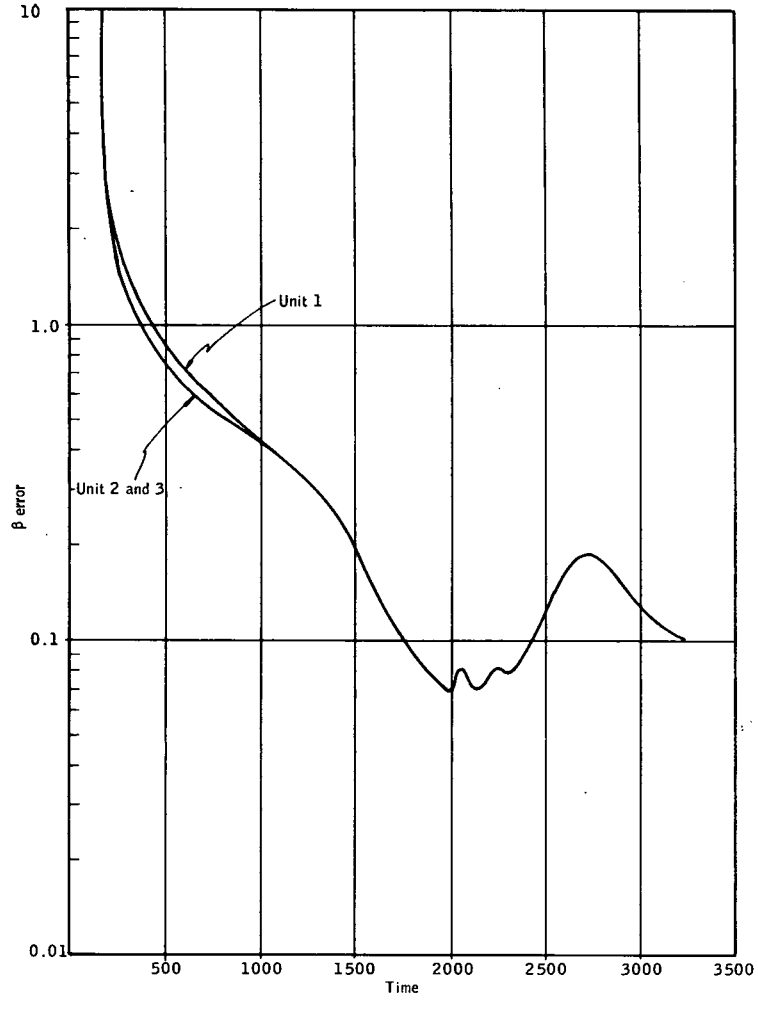

Figure 38. Orbiter β Error versus Time

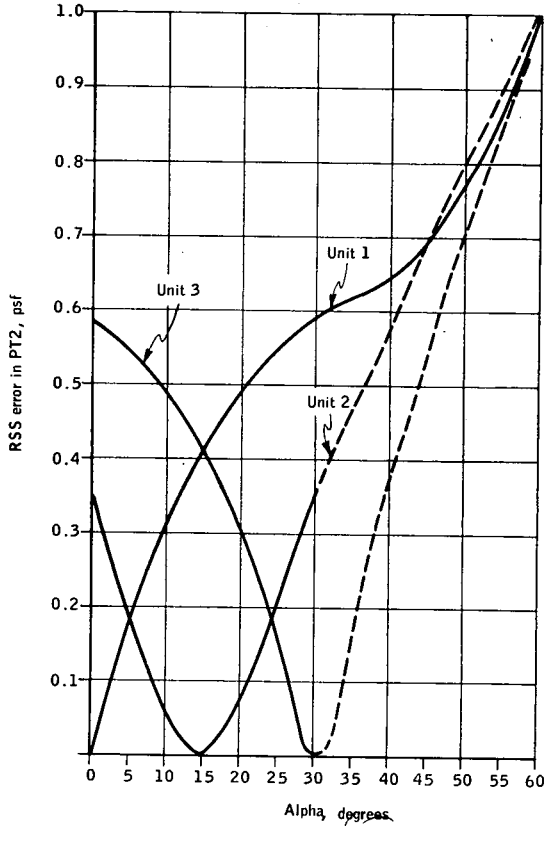

Figure 39. RSS Error in P_{T2} Due to 1 psf Error in Differential Pressure Transducers versus Alpha

3.5.3.2 Booster. - This subsection discusses the alpha, beta and P_{T2} measuring sensitivities of the booster sensor. The data base used for the study of these sensitivities was the baseline booster trajectory B-9U. Attitude, velocity, alpha and qB information about this trajectory is shown in Figures 40 and 41. As in the orbiter, points in the cruise region have been added to the trajectory to allow analysis of the sensitivities in this region..

Two sensor configurations are discussed - the 40° nose and the 60° primary nose. The 60° redundant is assumed to be subset of information on the other two. Both sets of equations were evaluated, those without $P_{\beta 2}$, and those without P_N as discussed in subsections 3.5.2.2 and 3.5.2.3. In the following discussion the equation without $P_{\beta 2}$ will be called Equation (8) and those without P_N will be called Equation (9). The limitation of the 40° nose is that for any alpha greater than 40° the stagnation point is off the sphere and the modelled equations no longer apply. With the 60° nose the entire operating range of the booster (0° to 60°) is within the sensor range. The booster sensors contain five ports. From these five ports four differential pressures are measured along with one absolute pressure. These pressures are used to compute alpha, beta, and P_{T2} as discussed in subsections 3.5.2.2 and 3.5.2.3. To compute the dynamic range of pressures which the transducers must measure, the trajectory data was inputted to the equations for pressure at port or for pressure differential between ports. The absolute pressure transducer must measure a maximum pressure of approximately 2250 psf. This occurs in the cruise region where P_S is maximum. The beta-sensitive pressure differential does not have a large dynamic range because beta is held to 0°. To determine maximum pressure a computation was made at a beta of 5° at the highest qB point in the trajectory. The computer pressure was 115 psf for the 40° nose and 138 psf for the 60° nose. The computed pressure differentials $P_1 - P_2$, $P_1 - P_3$, and $P_4 - P_5$ as a function of time along the trajectory are shown in Figure 42 for the 40° nose and Figure 43 for the 60° nose. For the 40° nose, $P_1 - P_2$ ranges from +295 to -160 psf, $P_1 - P_4$ ranges from +140 to -220 psf, and $P_4 - P_5$ ranges from 0 to 230 psf. For the 60° nose $P_1 - P_2$ ranges from +300 to -570 psf, $P_1 - P_4$ ranges from +100 to -450 psf and $P_4 - P_5$ ranges from 0 to 400 psf.

To determine a sensitivity of alpha measurement to errors in the differential pressures the same procedure was used in the booster cases as was used in the orbiter. The pressure was computed for selected nominal alpha and qB points along the trajectory, then computed for alpha from 0° to 60°. Then the differential pressures were varied by ±1 psf and the measured alphas were recomputed. The errors in alpha resulting from the ±1 psf variation of the pressure differentials were rss'd. The exact relationship between qB and rss'd alpha error resulting from the 1-psf pressure error is shown in Figures 44 through 47. To maintain a ±1° error range on alpha measure for a ±1 psf error is pressure-differential measurement for equap Equation (9) in the 40° nose requires a qB of 240, for Equation (9) of the 40° nose, a qB of 260. For the 60° nose the same condition is met at a qB of 120 and 82, respectively, for Equations (8) and (9). Because alpha is

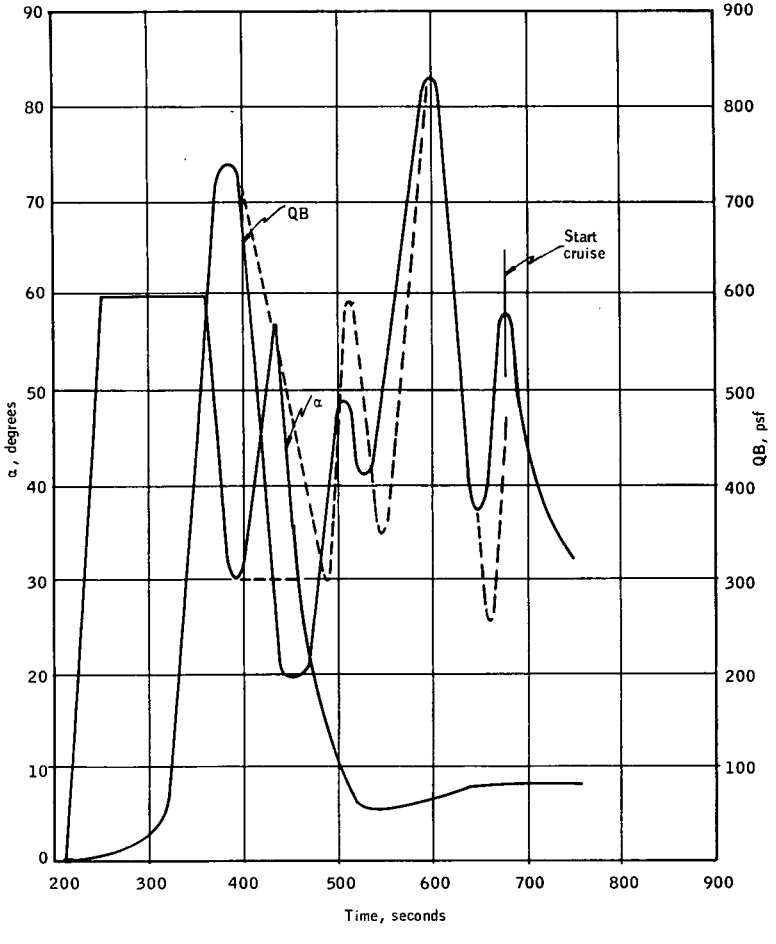

Figure 40. Booster Alpha and QB versus Time
(B-9U Baseline)
(B-9U Alternate QB in Dashes)

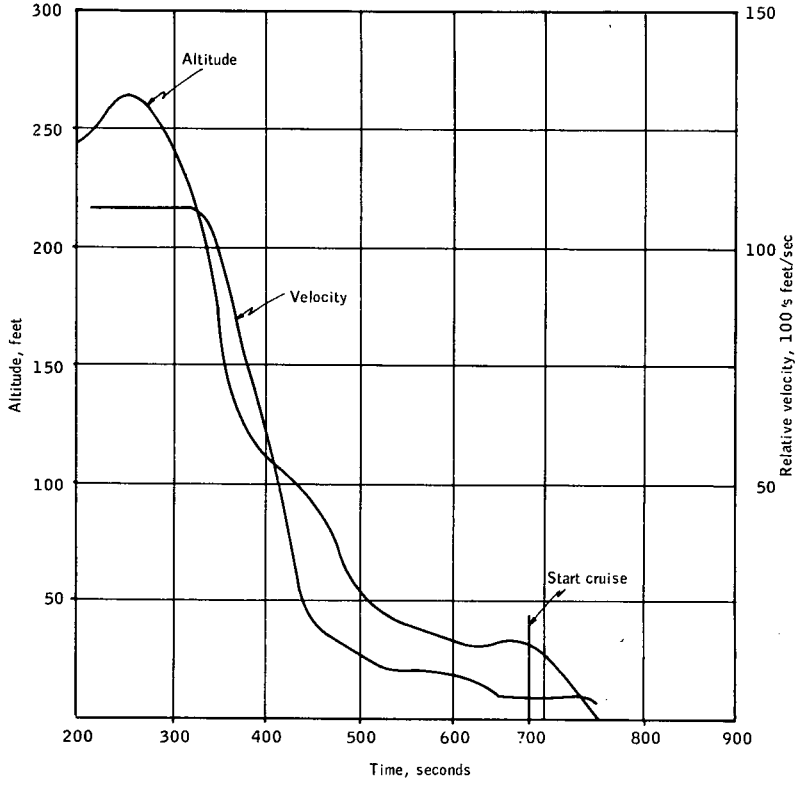

Figure 41. Booster Altitude and Relative Velocity versus Time
(B-9U Baseline)

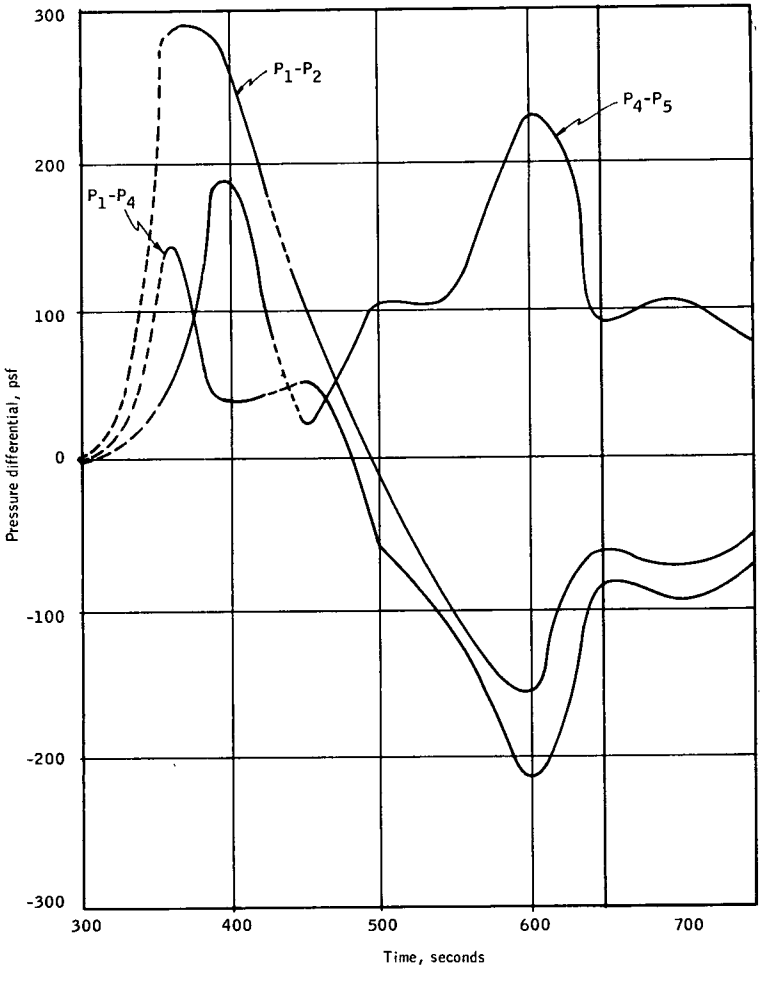

Figure 42. Differential Pressure versus Time, 40° Nose

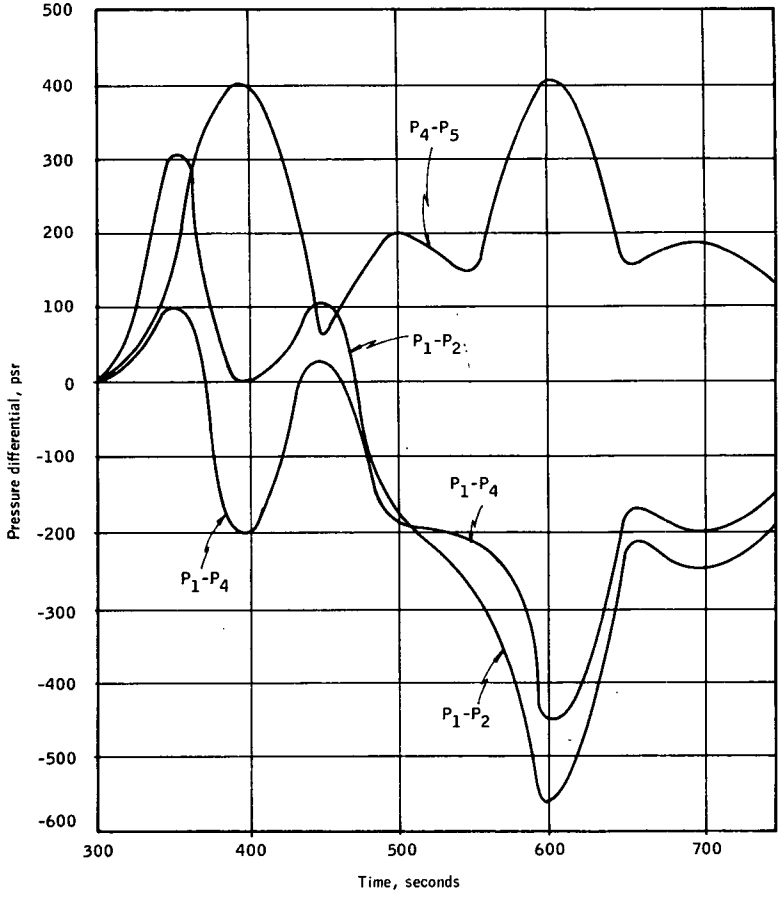

Figure 43. Differential Pressure versus Time, 60° Nose

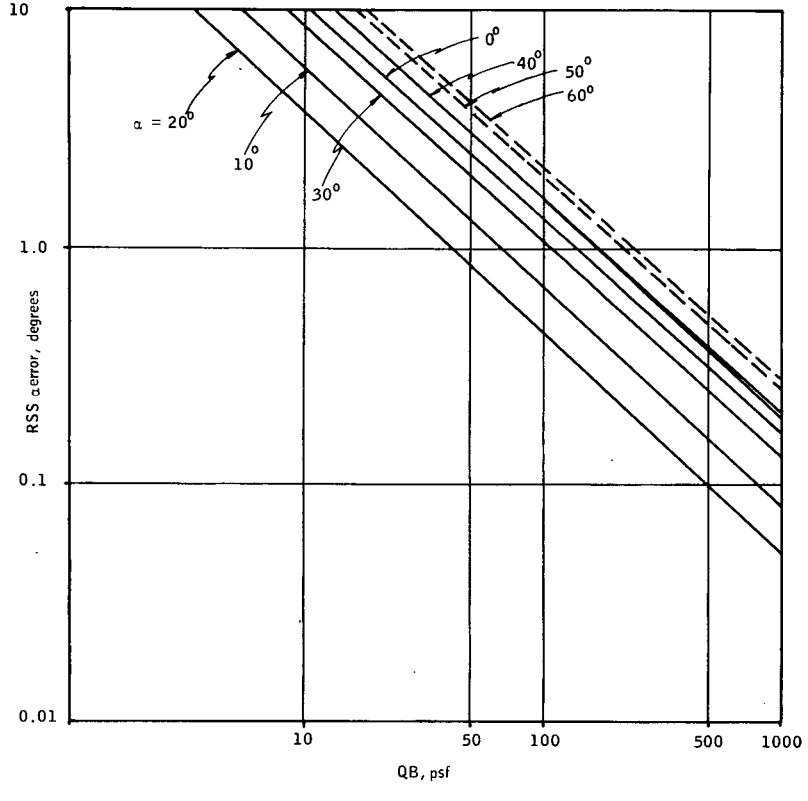

Figure 44. 40° Nose RSS α Error versus QB (Equation (8))

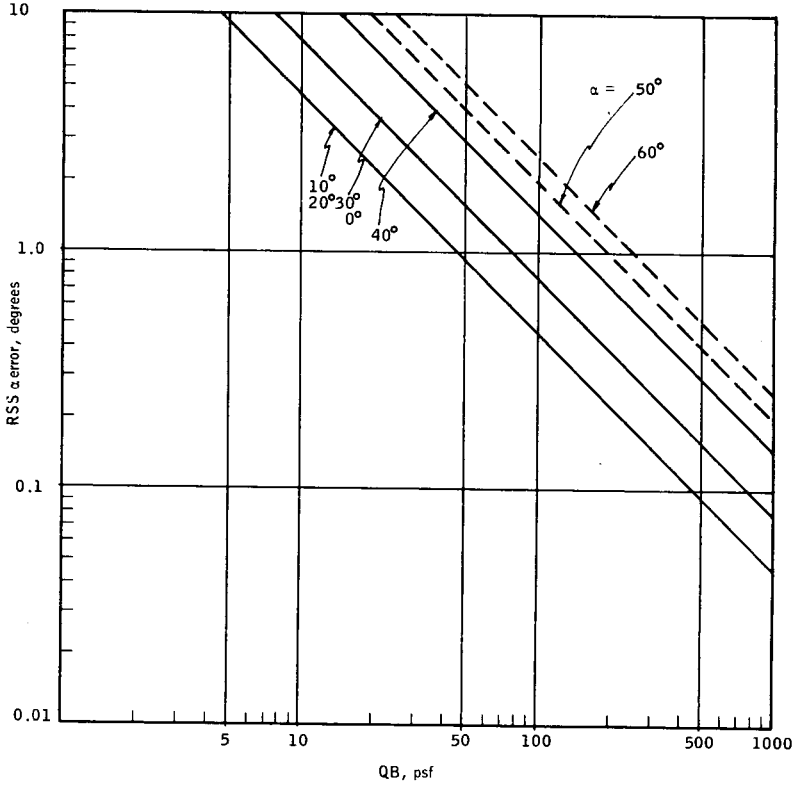

Figure 45. 40° Nose RSS α Error versus QB (Equation (9))

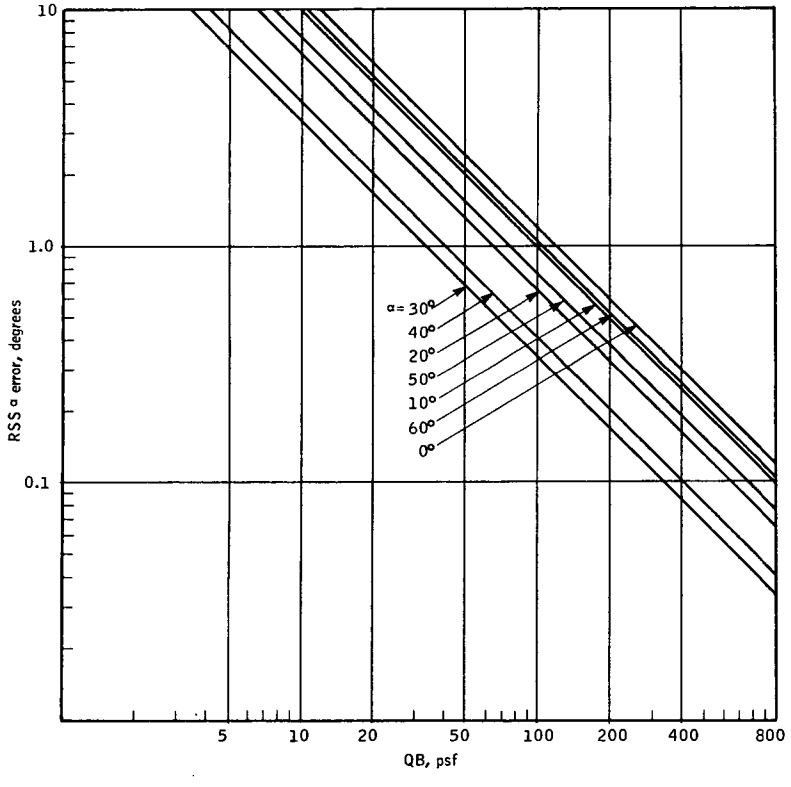

Figure 46. 60° Nose RSS α Error versus QB [Equation (1)]

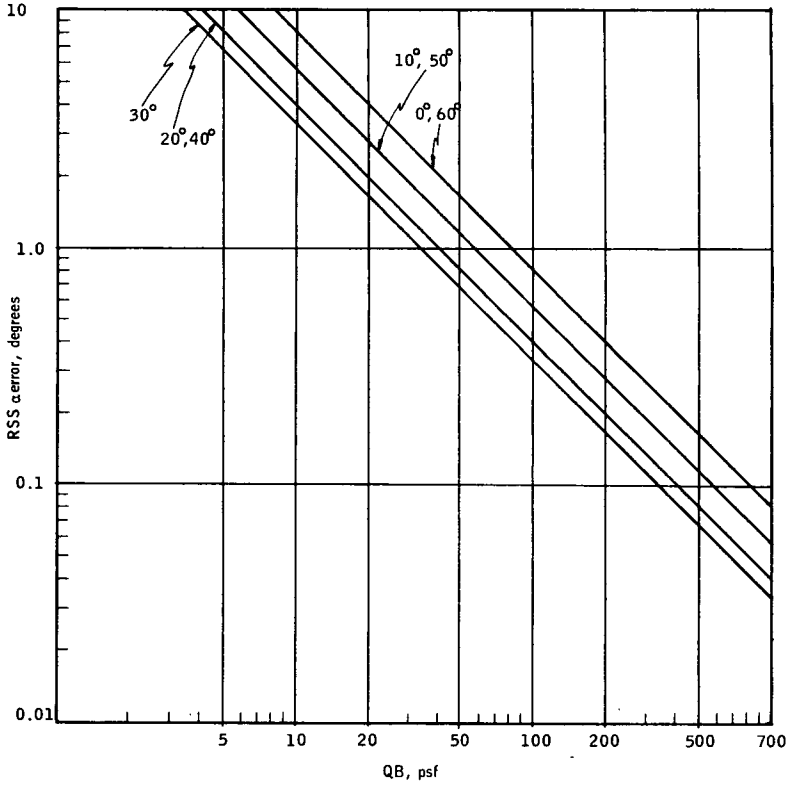

Figure 47. 60° Nose RSS α Error versus QB [Equation (9)]

varying it is necessary to compute the rss'd alpha error as a function of trajectory time to find the time at which rss'd alpha error is below 1°. These plots are shown in Figures 48 and 49 for the 40° and 60° nose. In the 40° nose the error is below 1° from 345 seconds to 430 seconds and then from 450 seconds to landing. However, the stagnation point is off the sphere until 380 seconds and goes off again from 415 seconds to 450 seconds. Because of this the 40° nose is operating in the less than 1° error range from 380 seconds to 415 seconds and then from 450 seconds on to landing. The 60° nose operates at less than 1° error from 320 seconds to landing. In both cases it can be seen that Equation (9) computes an alpha less sensitive to error in pressure differentials than Equation (8). (The alternate trajectory has $\alpha \leq 40°$ for $t > 370°$ sec; allowing increased valid operating time.)

The same method was used to compute beta sensitivities for 1 psf error inthe beta-sensitive pressure transducer. The rss'd beta error resulting from the 1 pst error as a function of qB is shown in Figures 50 through 53. In the computation of rss'd beta error over the trajectory both equations yielded results so close that only one curve representing the rss'd beta error is presented for each nose. This is shown in Figure 54. The 40° nose will be operating with the 1° error and within the 40° alpha limit from 380 seconds to 415 seconds and then from 450 seconds on to landing. The 60° nose will be operating in the 1° beta error limit from 320 seconds on to landing.

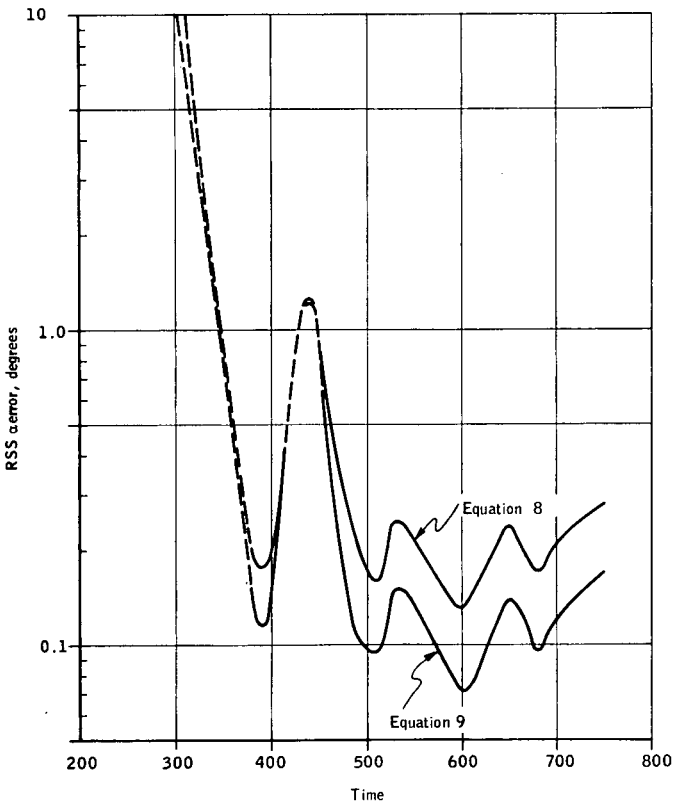

Figure 48. RSS α Error from 1 psf Pressure Differential versus Time, 40° Nose

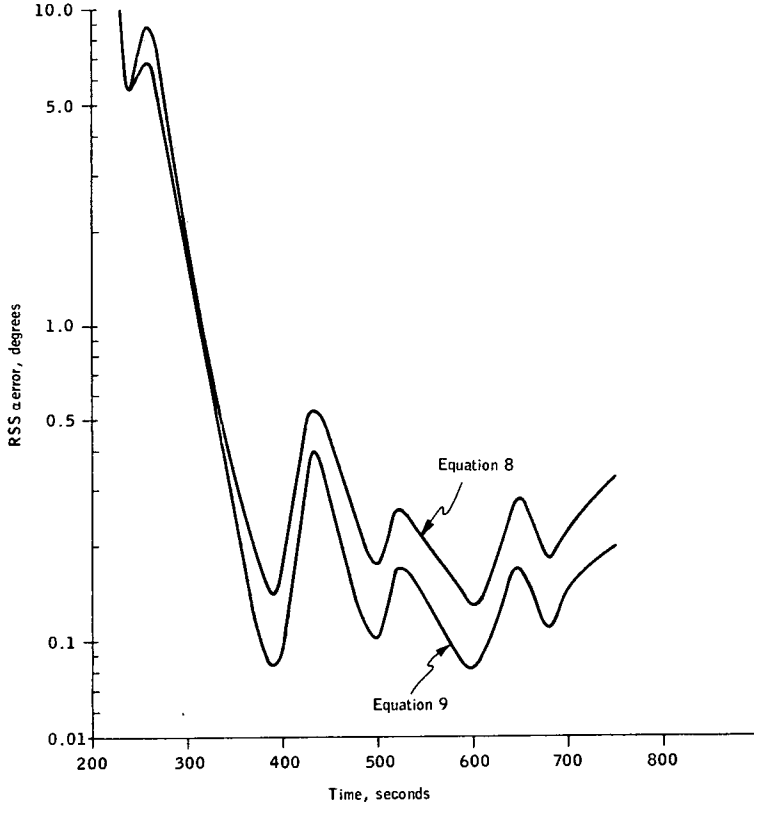

Figure 49. RSS α Error versus Time, 60° Nose

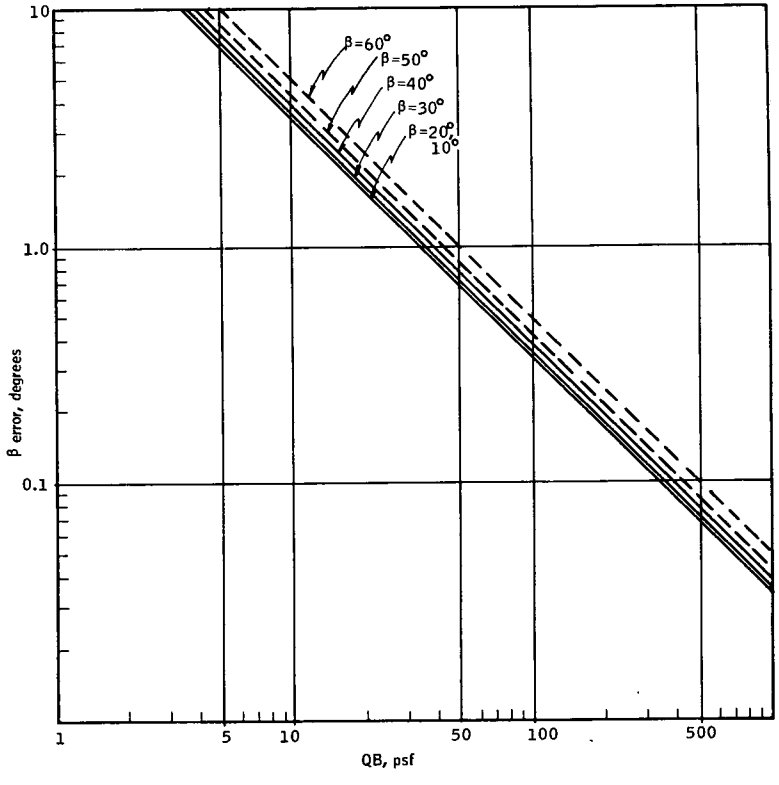

Figure 50. β Error 40° Nose versus QB for 1psf Error in (Port 5 - Port 3) [Equation (8)]

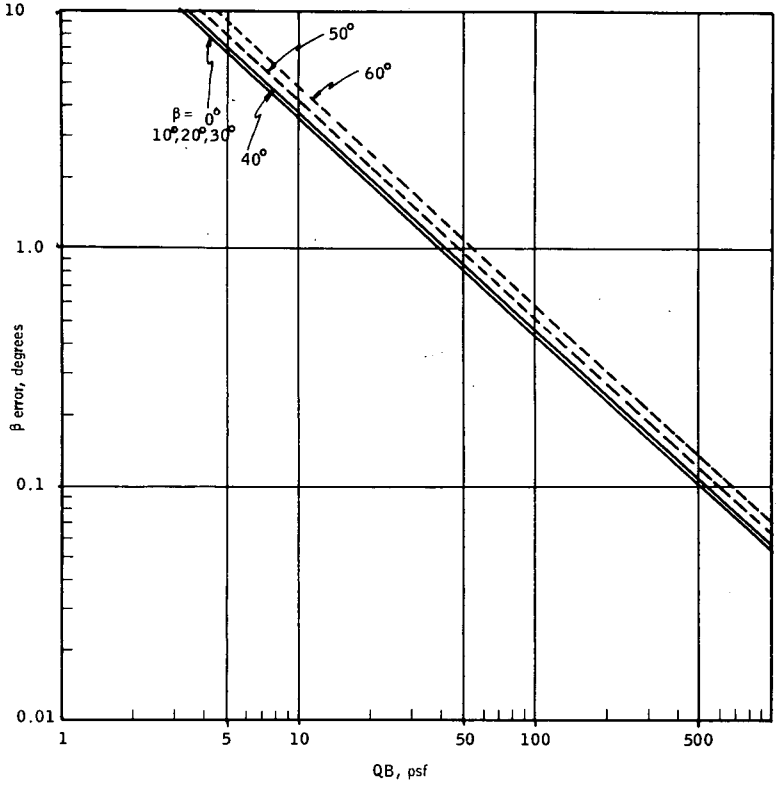

Figure 51. β Error 40° Nose versus QB for 1psf Error in (Port 5 - Port 3) [Equation (9)]

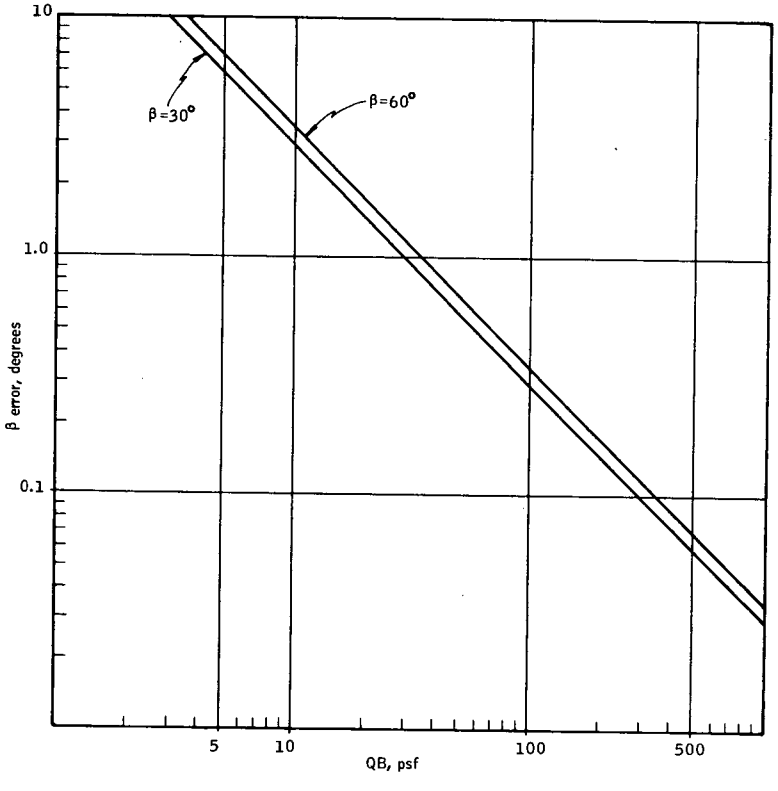

Figure 52. Booster 60° Nose β Error versus QB [Equation (8)]

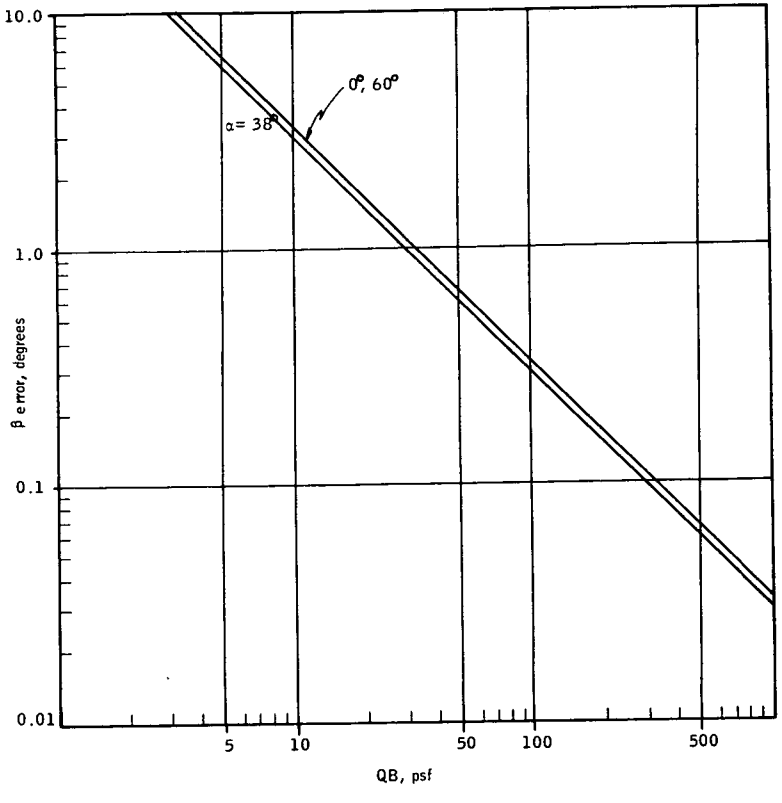

Figure 53. Booster 60° Nose β Error versus QB [Equation (9)]

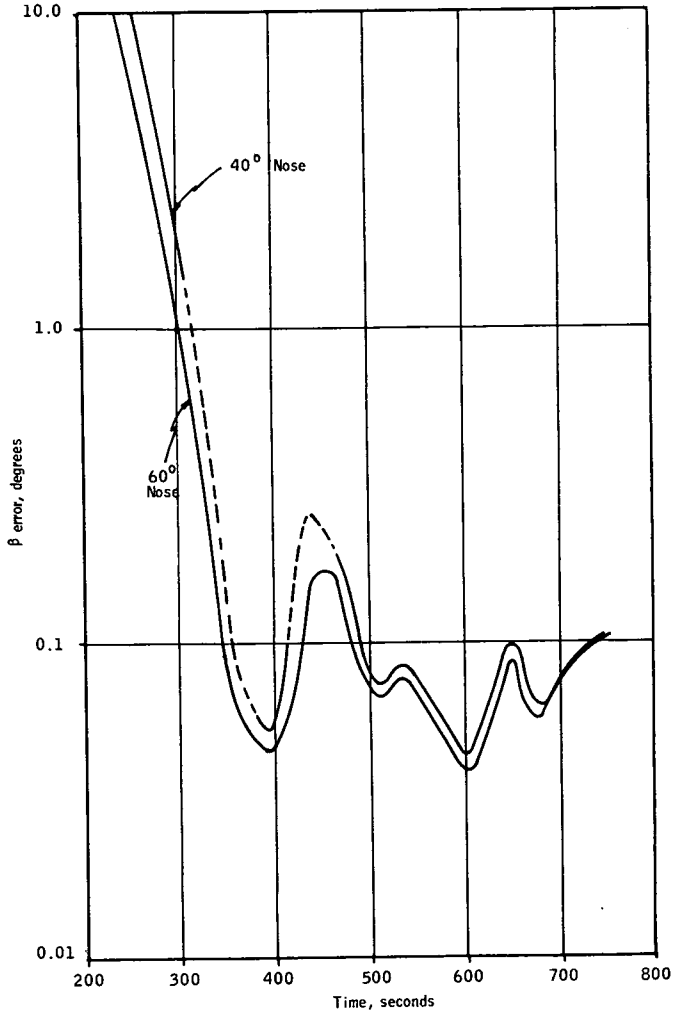

Figure 54. Booster β Error versus Time

P_{T2} measurement is a function of the absolute pressure and the differential pressures. The error in the absolute measurement is added directly into PT2 as can be seen by the the equation in subsections 3.5.2.2 and 3.5.2.3. The sensitivity in P_{T2} due to differential pressure transducer errors was computed in the same manner as the alpha and beta sensitivities. There is a P_{T2} error which is a function of the alpha of the booster. The rss'd error in P_{T2} due to 1 psf error in the differential pressure transducers as a function of alpha is shown in Figures 55 and 56 for the 40° and 60° noses, and is small compared to the tolerances for the absolute transducers.

3.5.4 Overall Performance Expectation Summary

The primary sources of error in the system, as discussed in subsection 3.1.5, are:

a) Calibration misalignments of ports relative to vehicle axes.

b) Deviations of actual pressures (or at least the test data used) from the spherical distribution model.

c) Pressure measurement errors in converting physically sensed pressure to digital word representation.

The effect of error source (a) can be held to less than 1/4°.

The effect of error (b) is minimal for beta measurement because of the symmetry of ports around the stagnation point. For alpha measurement a possible 1° one-sigma error arises for a differential port pair of 45° or larger. This increases to a 1.7° one-sigma for a port pair of 30° separation. In the orbiter all differential port pairs have a separation of at least 45°. In addition, this error can be kept at a minimum by choosing the port pairs which have the lowest differential pressures. In the 40° nose booster the computation system not using P_N provides for a separation of at least 30° while the computations using $P\beta 2$ have a minimum separation of 22.5°. For the 60° primary nose the alpha, beta computation system without P_N has a minimum separation of 45° and computations without $P\beta 2$ provides for a separation of at least 30°.

Error as a result of pressure measurement error is discussed in subsection 3.5.2.1 for the orbiter and subsection 3.5.2.2 for the booster. For pressure measurement error of ±1 psf all measurement units of the orbiter will be operating at less than a ±1° error in both alpha and beta by 700 seconds into re-entry trajectory, ±2° accuracy at 300 seconds. The units are essentially the same in measurement accuracy.

For the 40° booster nose, because of the angle of attack of the booster, the ±1° error for 1 psf error in the transducers will not be satisfied until 450 seconds into the trajectory. The 60° primary nose will satisfy a ±1° for a 1 psf error of the transducer at 315 seconds and a ±20 error at 300 seconds. For the booster configuration, the computation system without P_N (using two beta sensitive differences) has consistently better accuracy.

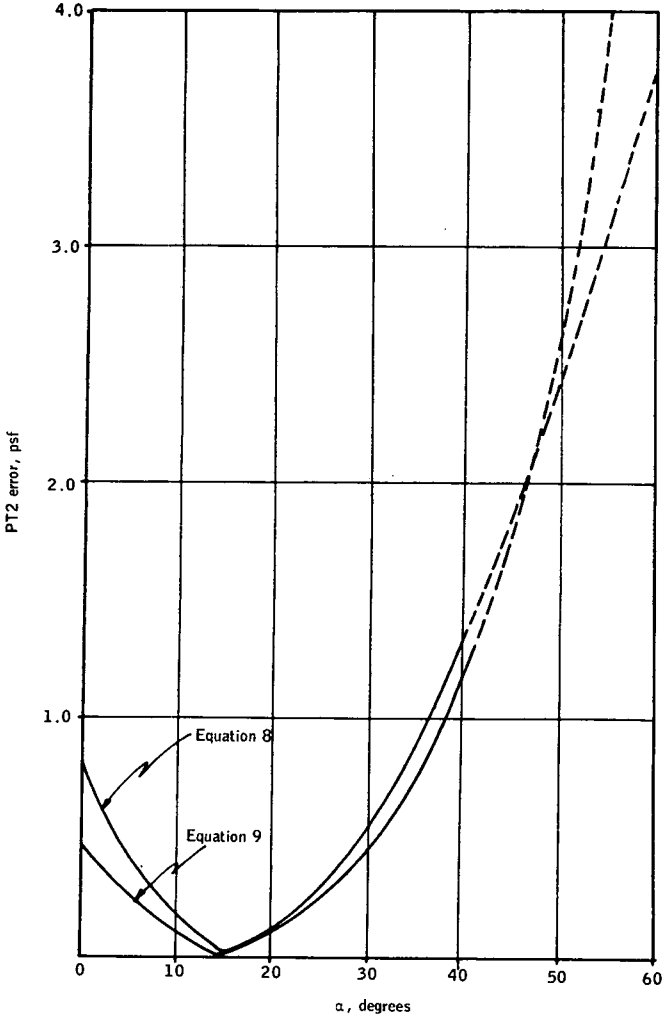

Figure 55. RSS P_{T2} Error from 1psf Error in Differential Pressure versus Alpha, (40° Nose)

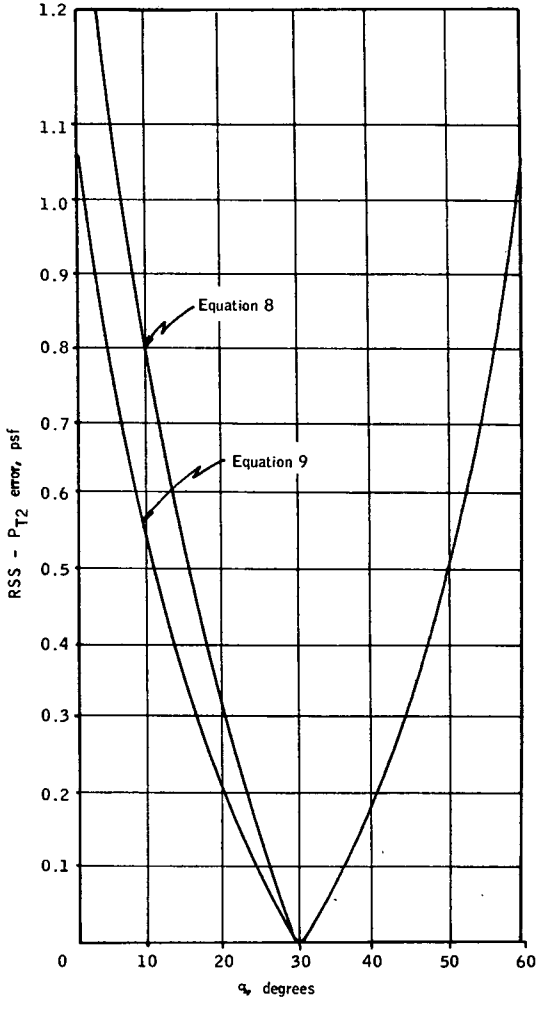

Figure 56. RSS P_{T2} Variation for 1psf Variation versus Alpha (60° Nose)

APPENDIX A

SENSITIVITY OF AN ANGLE-OF-ATTACK SENSOR COMPARISON OF THEORY AND EXPERIMENT

Purpose of this appendix is to compare experimental sensitivity data, measured with hemispherical nose angle-of-attack sensors, with the sensitivity predicted by pressure distribution theories. Result of this comparison affects confidence in the theoretical pressure distribution over a limited arc length on the sphere rather than conclusive proof of the theory over the whole hemisphere at all speeds. The reason is that the sensitivity involves only the slope of the pressure distribution with arc length over a limited region near the pressure tap location rather than the actual pressure over the whole sphere. However, the comparison should be made for completeness of the study.

Sensitivity, as used here, is the amount the pressure difference of two taps changes per degree of angle of attack. Using the flight dynamic pressure as the reference, the sensitivity is written as

$$\frac{d\left(\frac{\Delta P}{q}\right)}{d\,\alpha}$$

Theory refers to the sensitivity derived from the two candidate formulae, considered for the pressure distribution on a hemisphere in Appendix C, namely

$$\text{Formula I} \qquad C_p = C_{p_o} - B \sin^2 E$$

$$\text{Formula II} \qquad C_p = \frac{P_t}{q} \cos^n E \frac{P}{P_t}$$

Experimental sensitivity is that reported by NASA FRC and a probe manufacturer (Rosemount Engineering Co.) each of which tested a similar hemisphere cylinder configuration in wind tunnels at subsonic transonic and supersonic speeds. The probe was a hemisphere cylinder 0.75 in. diameter with pressure taps located $\alpha_t = \pm 45°$ from the axis. ΔP is the pressure difference of these taps. Tap diameter was 0.070 in. which subtends about a 10° angle on the surface of the sphere. Angle-of-attack range of the tests was typically 0 to 12 degrees and the sensitivity was a linear fairing of the ΔP versus α test points. Experimental data from these two sources agree, Figure A1.

At subsonic speeds below the critical Mach number, $M \approx 0.6$, Formula I sensitivity agrees with the experiment within 6 percent while Formula II is unusable because it increases to infinity, Figure A1. Above the critical Mach

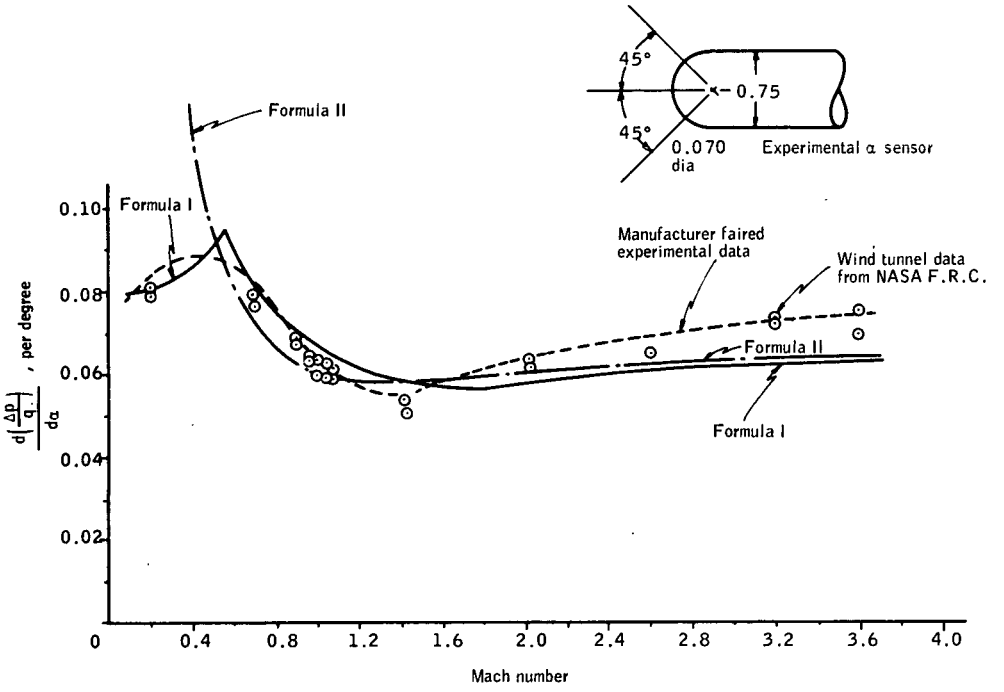

Figure A1. Sensitivity of an α Sensor versus Mach No. Comparison of Experiment and Emperical Formulae

number all the way through the supersonic range both Formulae I and II compare equally with the experimental data. In the transonic speed range (up to M = 1.4) Formula I sensitivity is typically 5 percent higher and Formula II sensitivity is 5 percent lower than experiment. At supersonic speeds sensitivities according to Formulae I and II are 10 to 11 percent lower than experiment.

In the transonic region, the scatter of sensitivities from the Formulae and the experimental data are reasonable. This follows because both of the theories and both of the experiments come from measurements made in a flow regime where complicated asymetrical and random local shock patterns occur from experiment errors in the model surface and other sources such as the wind tunnel mounts.

At supersonic speeds, a cause for the experimental sensitivity being systematically larger than that from the theories is not as readily found.

One possible error source of the experimental sensitivity measurements is the large tap sizes used on the experimental model. These large taps can be considered as flat spots on the sphere surface which alter the local flow pattern and pressure distribution in the vicinity of the tap.

The conclusion is that Formula I is better than Formula II because it predicts the sensitivity over the whole speed range. However, if accuracy of sensitivity better than that discussed above is required, experimental data at sample speeds should be taken to verify the calibration of the particular sensor.

APPENDIX B
SHUTTLE VEHICLE FLIGHT PROFILES

This appendix contains the following Shuttle vehicle flight profiles:

- Nominal profile mission (Figure B1)
- Ascent trajectory profile (Figure B2)
- Glide, powered flight and ferry flight conditions (Figure B3)
- Trajectory #603 January 1971 delta-wing orbiter entry baseline (Figure B4)
- Baseline B-9u booster entry trajectory (Figures B5 through B8)

With regard to Figures B5 through B8 the entry trajectory (T-B9u-26) as of 5 March 1971 of the B-9u booster for the polar launch mission from Western Test Range is discussed below.

The only change in the entry transition from the previous B-9u entry (T-B9u-1, dated 2-10-71) was a new bank angle schedule. Previously, the bank angle was held at a constant value (51°) until the vehicle had turned around. The new entry transition maintains a bank angle of 48° until the minimum angle-of-attack point during the pitch modulation maneuver has been passed. The bank angle is then increased to 75° and is maintained until the turnaround is completed. This alteration in the trajectory reduces the flyback distance to 404 n. mi. (from the previous 418 n. mi.).

The initial staging conditions (end coast) are:

Altitude = 244 784 ft

Velocity (Relative) = 10 824 fps

Gamma (Relative) = 5. 654 deg

Heading Azimuth (Relative) = 182. 495 deg

Latitude = 32, 788 deg

Longitude = 239. 343 deg

Wing Loading (W/S) = 91. 29 psf

Staging Time = 216. 36 sec

(Reference: NR Synthesis Run No. 5 of 2/5/71)

A schematic of important points during the entry is shown in Figure B5. A more detailed analysis of the entry is presented in Figures B6 through B8.

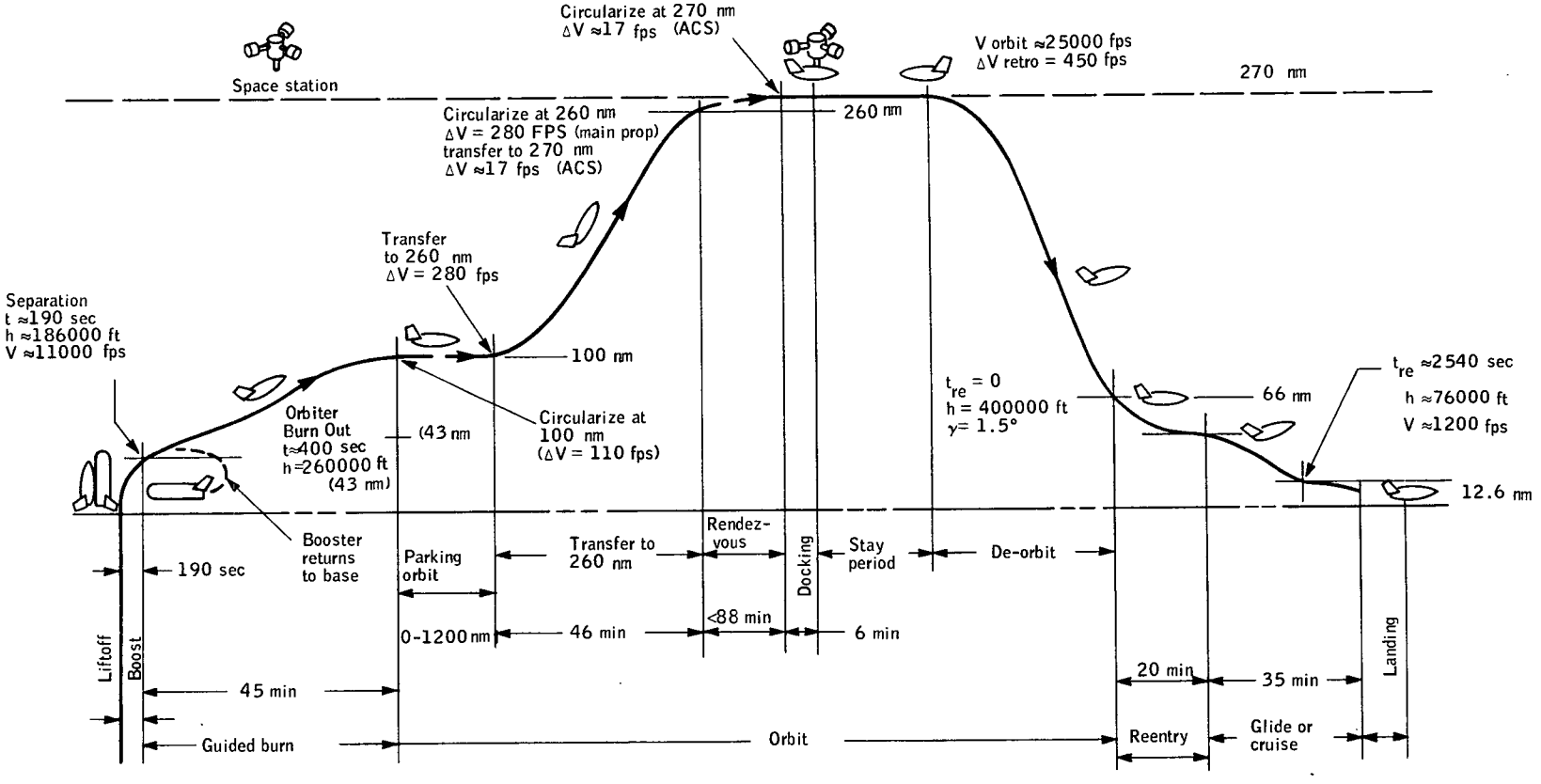

Figure B1. Nominal Profile Mission

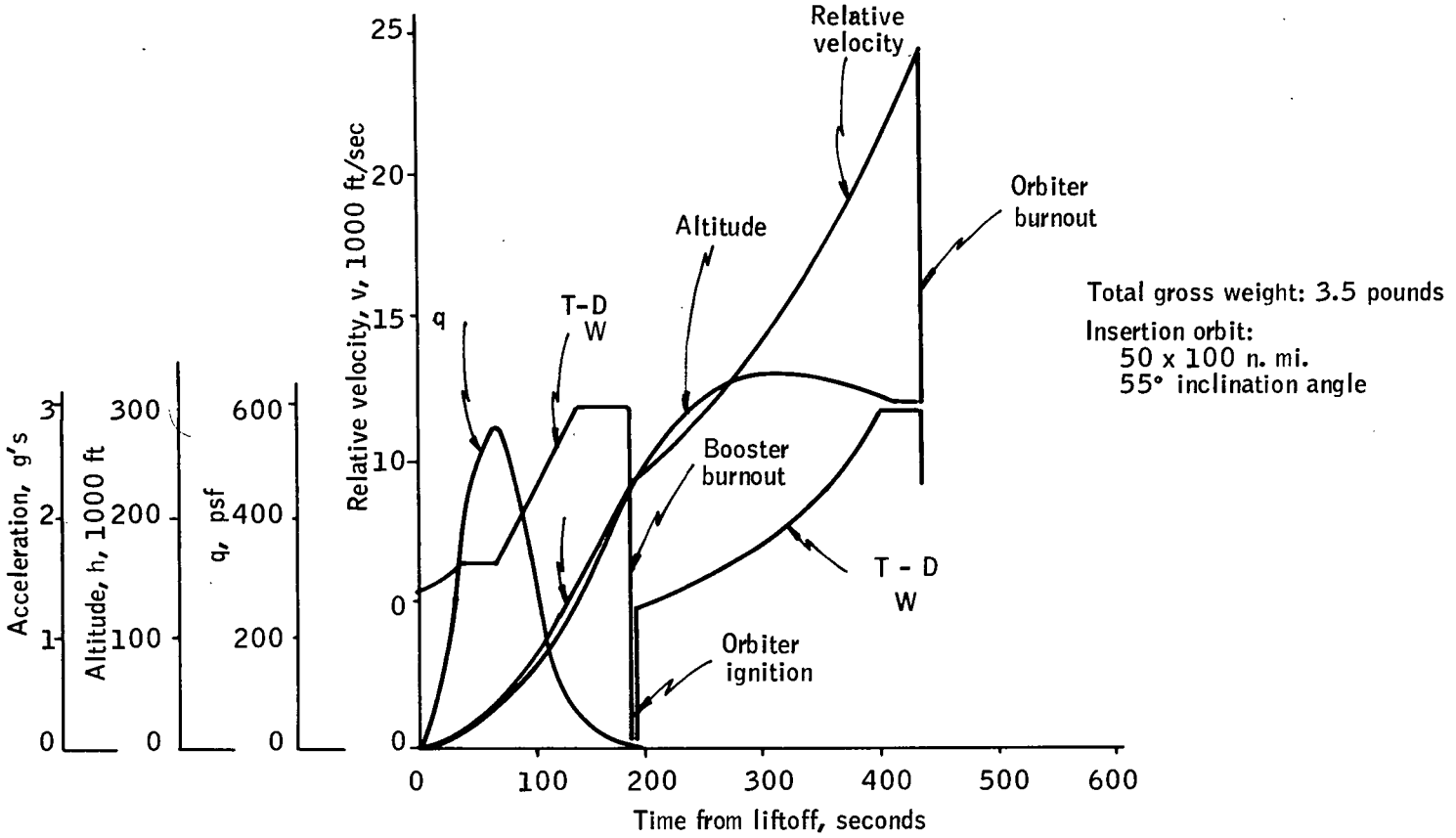

Figure B2. Ascent Trajectory Profile

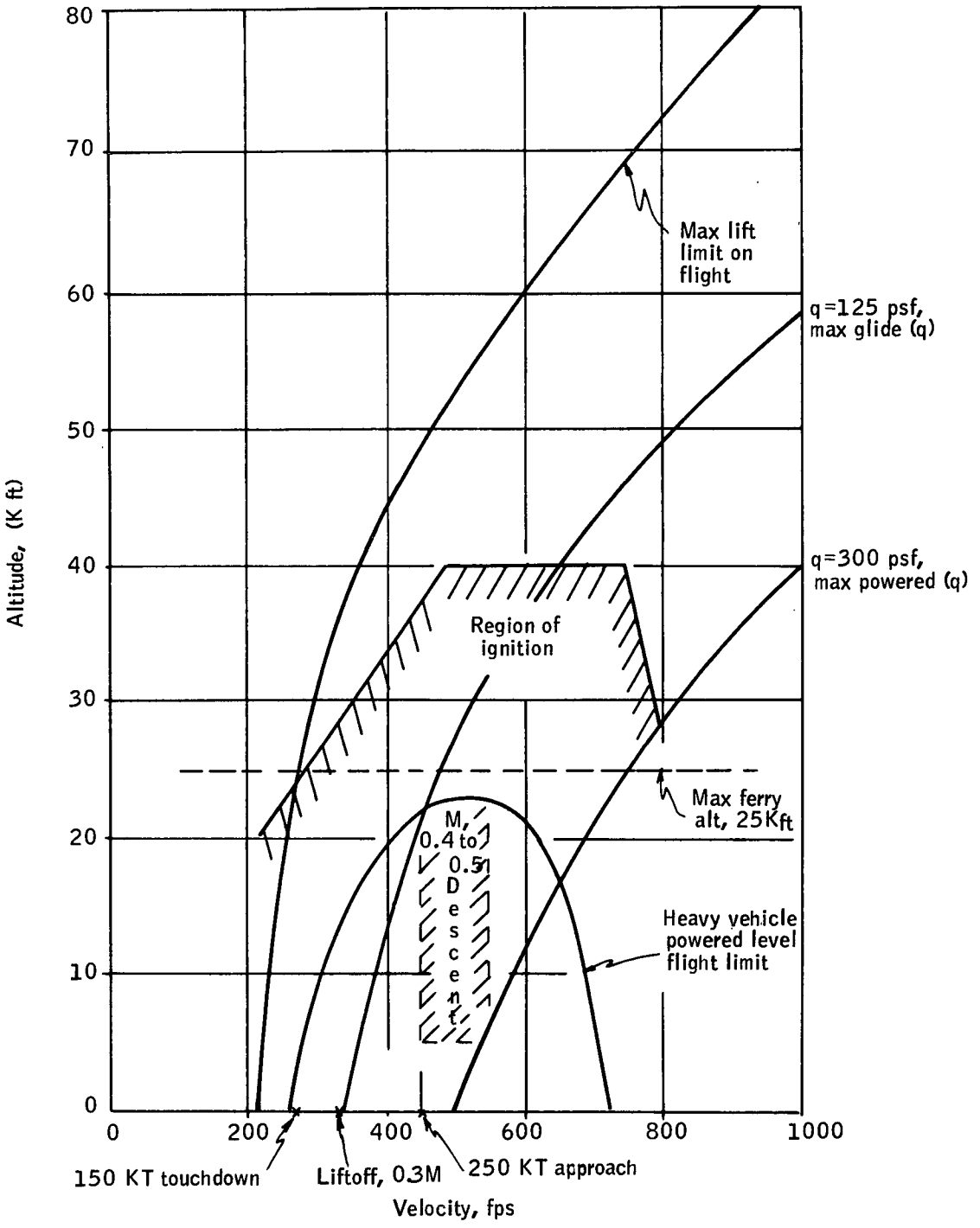

Figure B3. Glide, Powered Flight, and Ferry Flight Conditions

Traj No. 603 Jan delta baseline parametric 235 H-V + delta H

Weight	= 282000	Longitude	= 0.0
Ref area	= 8650	Latitude	= 0.0
Altitude	= 4000000	Inclination	= 55.00
Gamma (R)	= -1.55	Gamma (1)	= -1.50
Azimuth (R)	= 32.10	Azimuth (1)	= 35.00
Velocity (R)	= 25134	Velocity (1)	= 25992

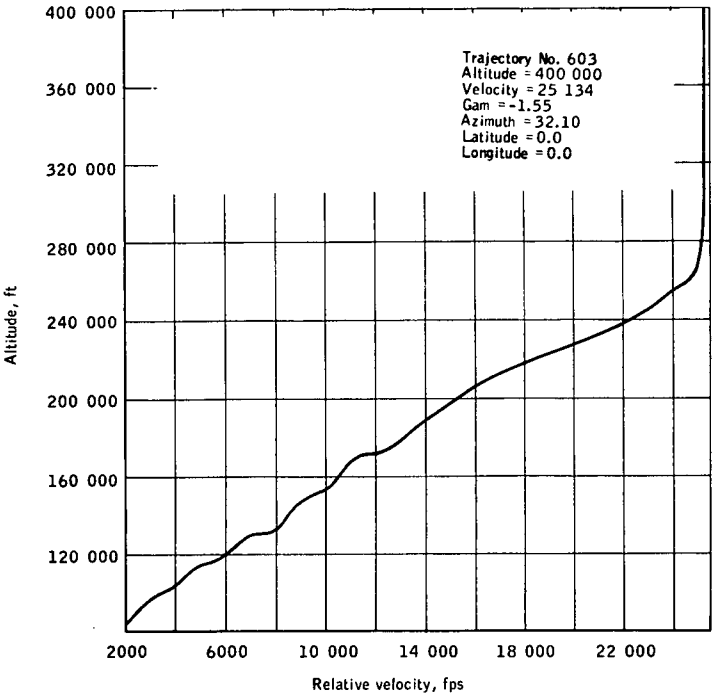

Figure B4a. Altitude versus Relative Velocity

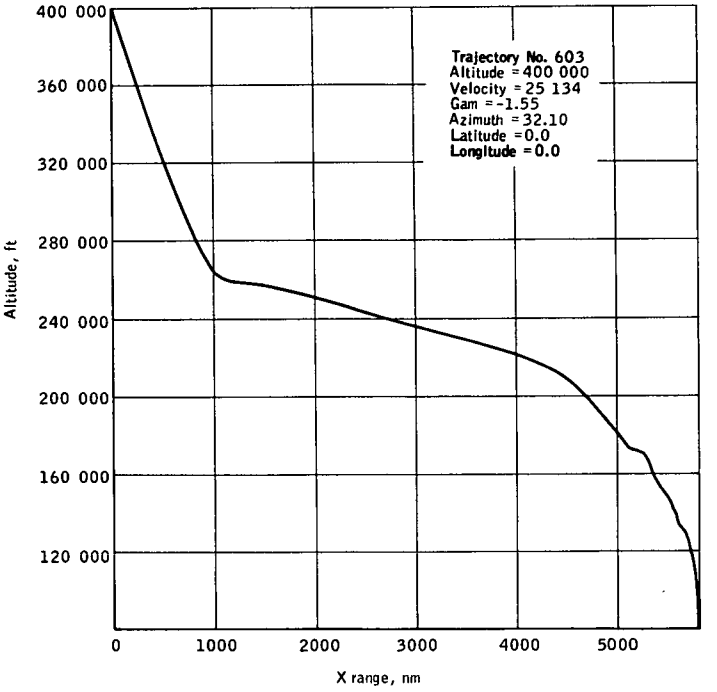

Figure B4b. Altitude versus X-Range

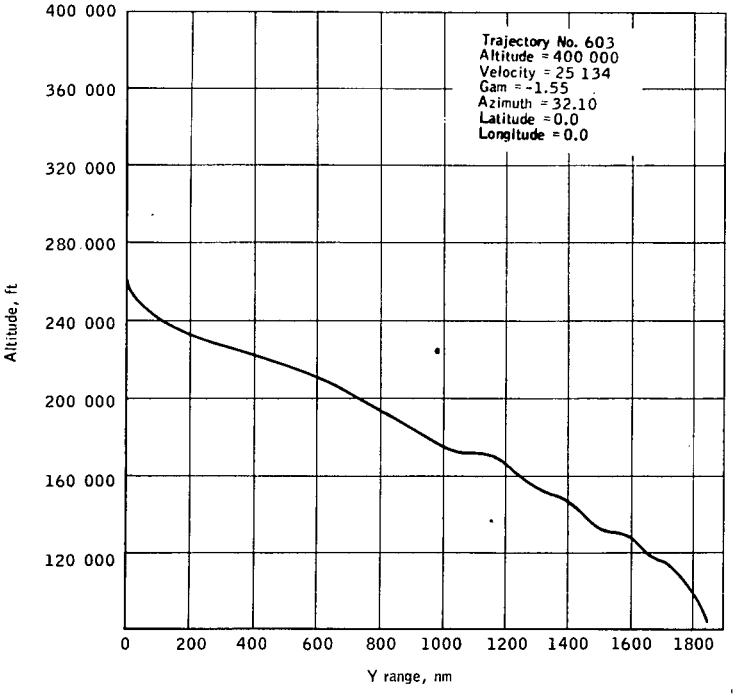

Figure B4c. Altitude versus Y-Range

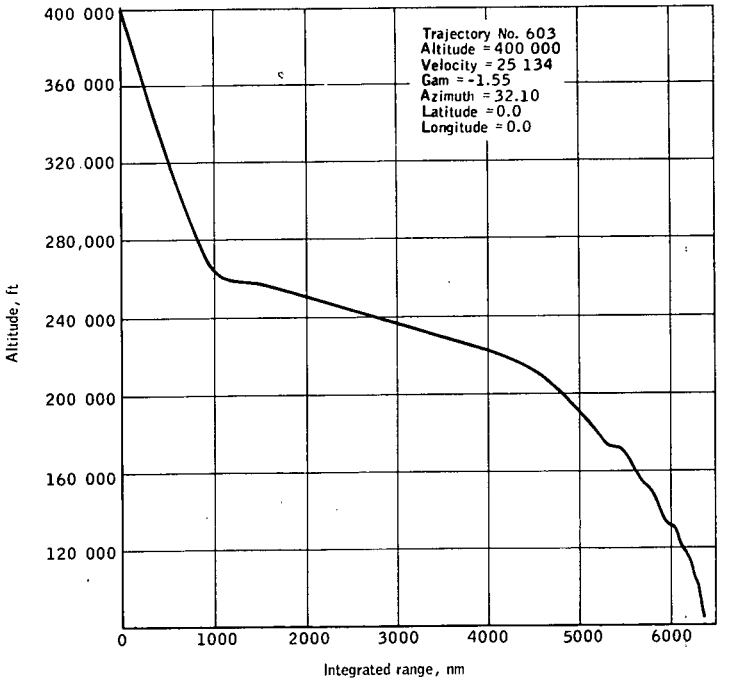

Figure B4d. Altitude versus Integrated Range

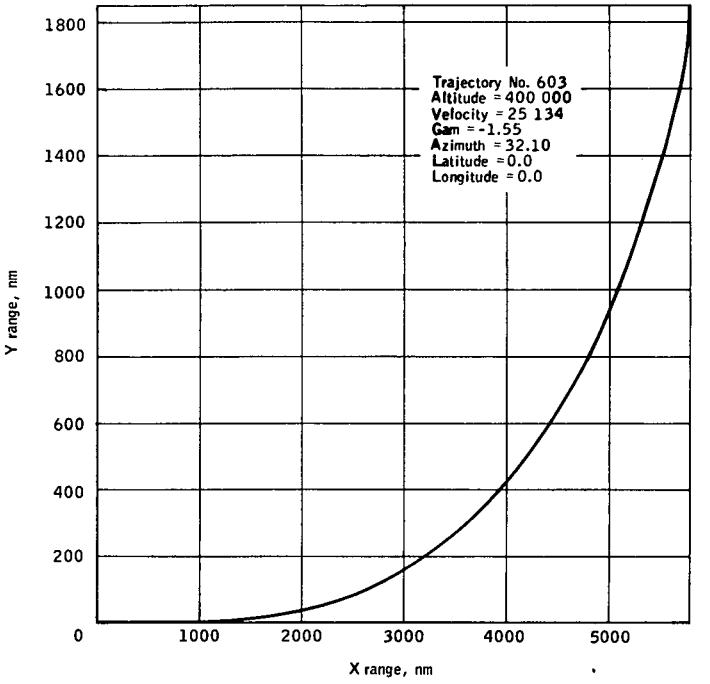

Figure B4e. Y-Range versus X-Range

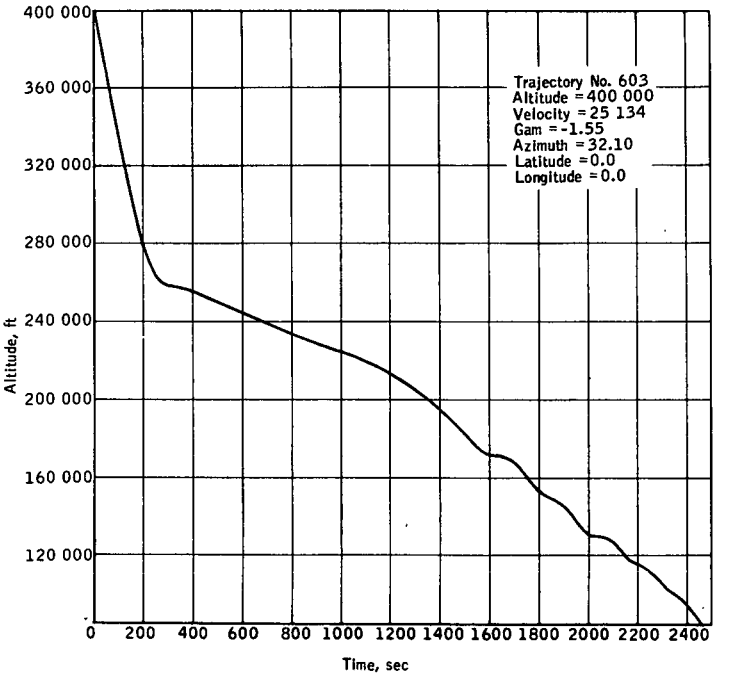

Figure B4f. Altitude versus Time

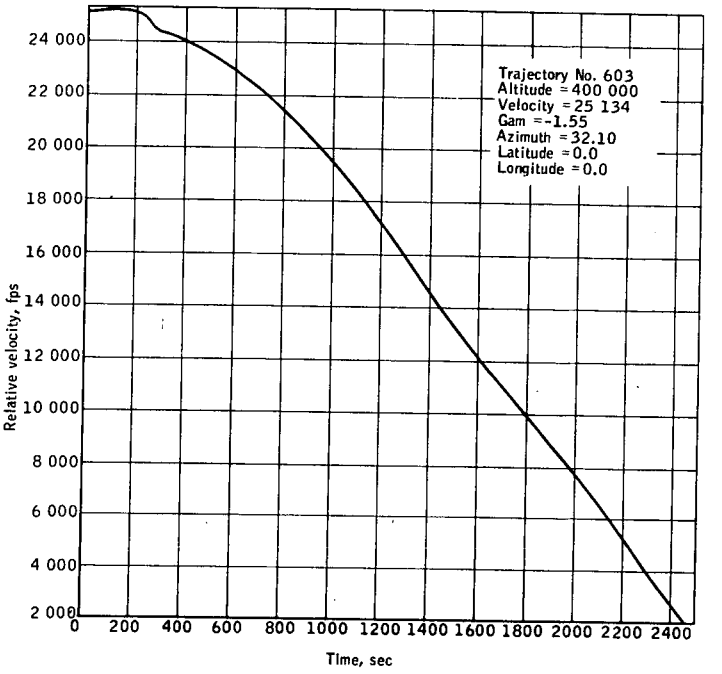

Figure B4g. Relative Velocity versus Time

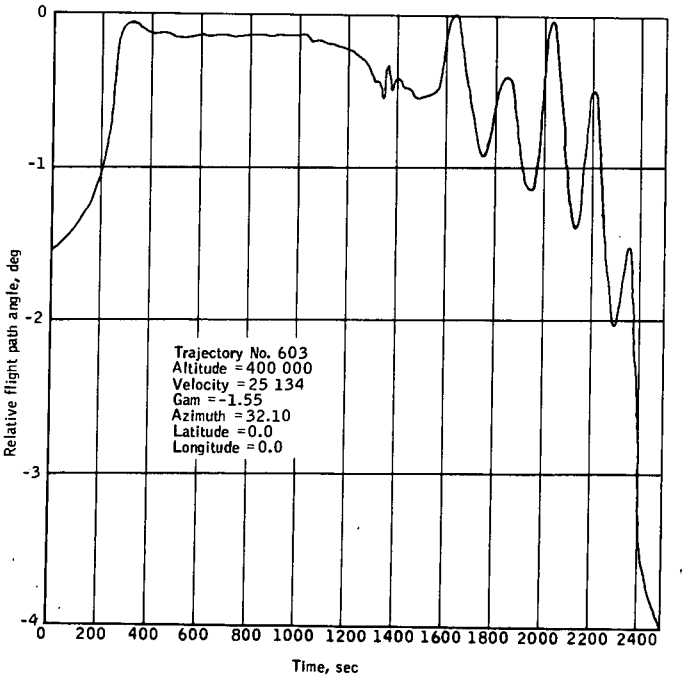

Figure B4h. Relative Flight Path Angle versus Time

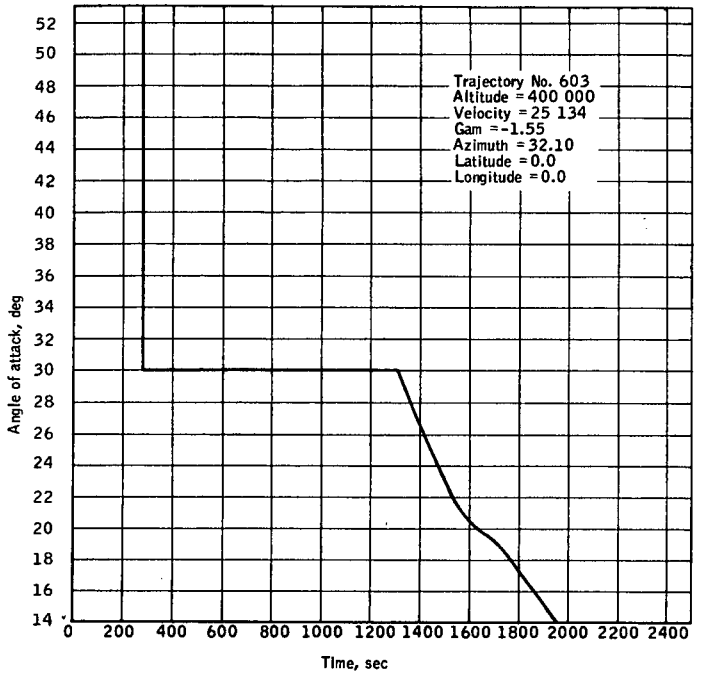

Figure B4i. Angle of Attack versus Time

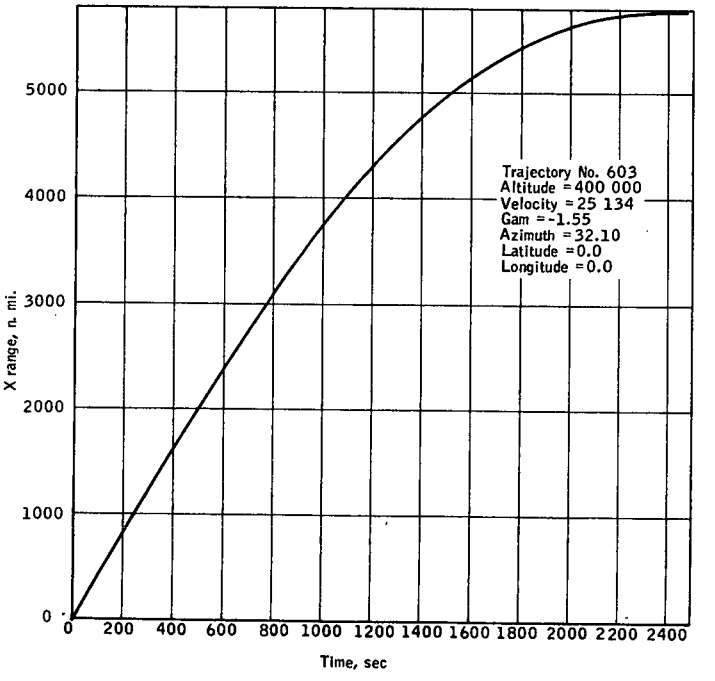

Figure B4j. X-Range versus Time

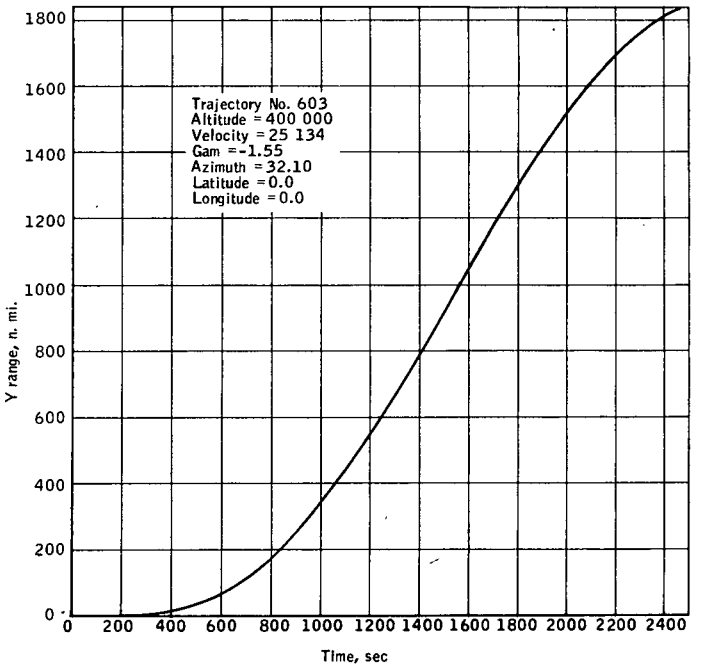

Figure B4k. Y-Range versus Time

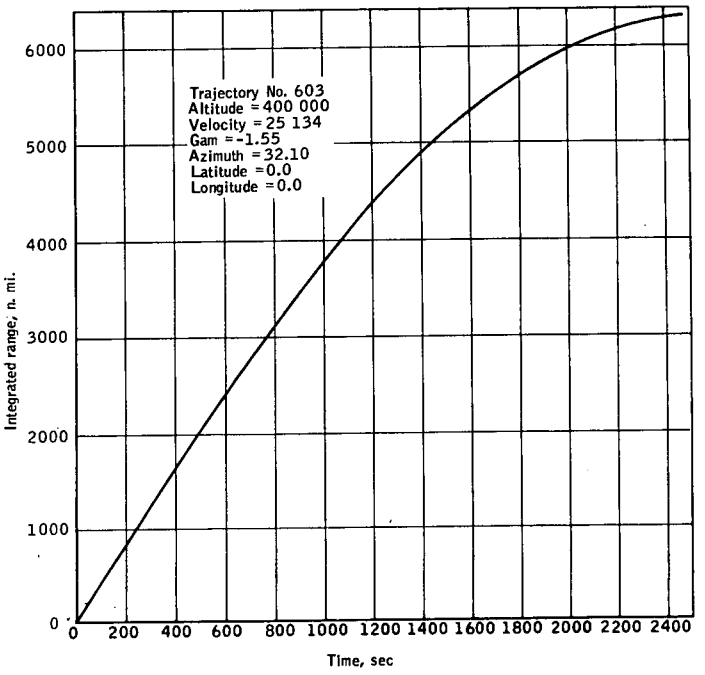

Figure B4l. Integrated Range versus Time

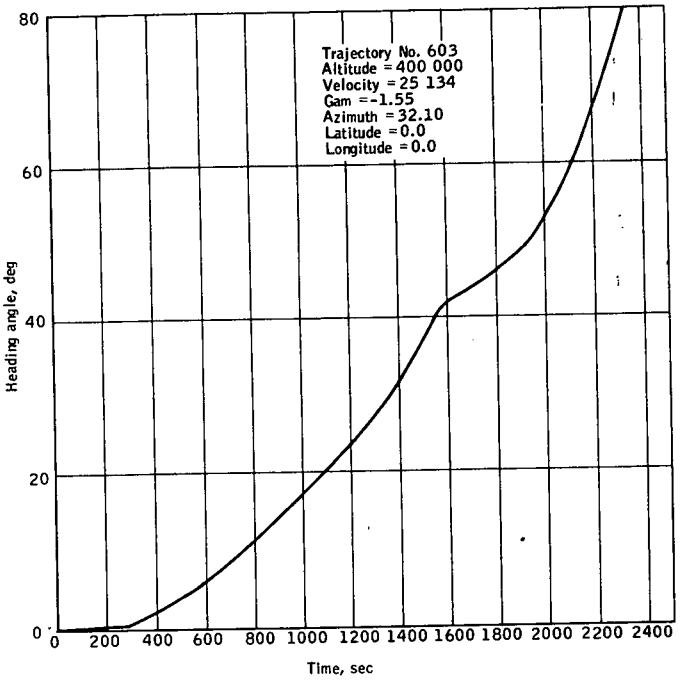

Figure B4m. Heading Angle versus Time

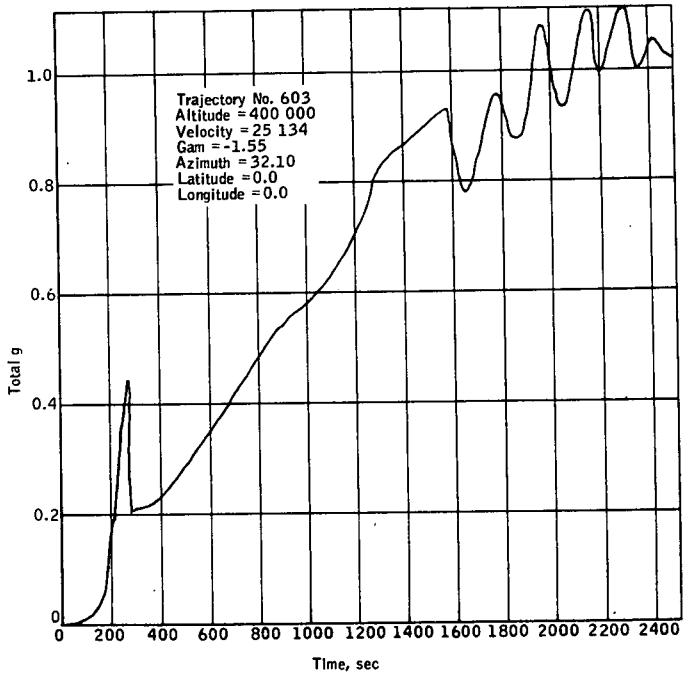

Figure B4n. G-Total versus Time

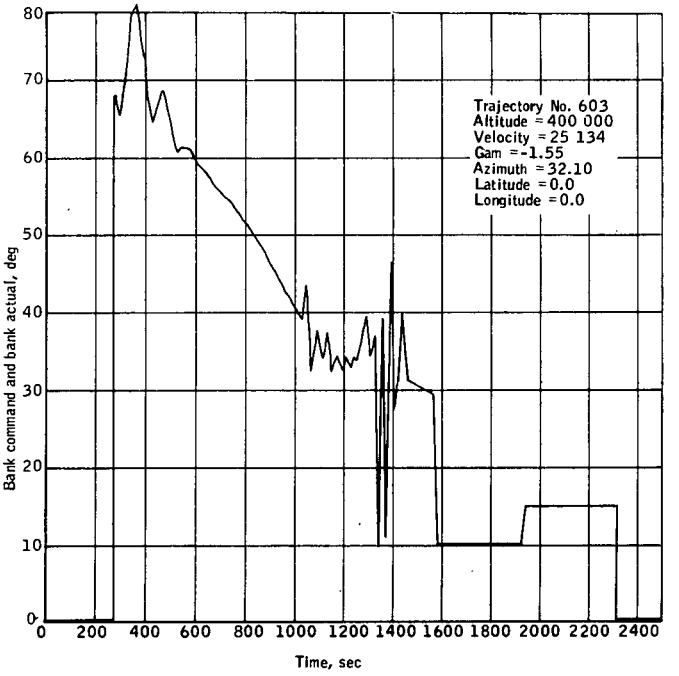

Figure B4o. Bank Command and Bank Actual versus Time

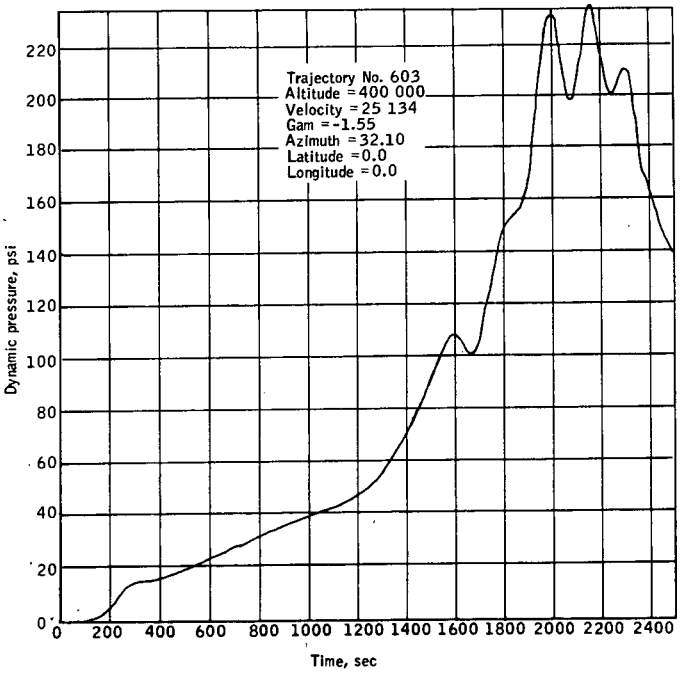

Figure B4p. Dynamic Pressure versus Time

MEMO TO: Distribution

FROM: Nick Ponomareff

SUBJECT: Baseline B-9U Booster Entry Trajectory

The current entry trajectory (T-B9U-26) of the B-9U booster for the polar launch mission from WTR is presented in this memo.

The only change in the entry transition from the previous B-9U entry (T-B9U-1, dated 2-10-71) is a new bank angle schedule. Previously, the bank angle was held at a constant value (51°) until the vehicle had turned around. The new entry transition maintains a bank angle of 48° until the minimum angle of attack point during the pitch modulation maneuver has been passed. The bank angle is then increased to 75° and is maintained until the turnaround is completed. This alteration in the trajectory reduces the flyback distance to 404 n. mi. (from the previous 418 n. mi.).

The initial staging conditions (end coast) are:

Altitude = 244, 784 ft
Velocity (Relative) = 10, 824 fps
Gamma (Relative) = 5. 654 deg
Heading Azimuth (Relative) = 182. 495 deg
Latitude = 32. 788 deg
Longitude = 239. 343 deg
Wing Loading (W/S) = 91. 29 psf
Staging Time = 216. 36 sec

(Reference: NR Synthesis Run No. 5 of 2/5/71)

A schematic sketch of important points during the entry is shown in Figure B5. A more detailed analysis of the entry is presented in Figure B6.

The next revision in the B-9U entry trajectory should occur in early April 1971 when new aerodynamic data from current wind tunnel tests will be used.

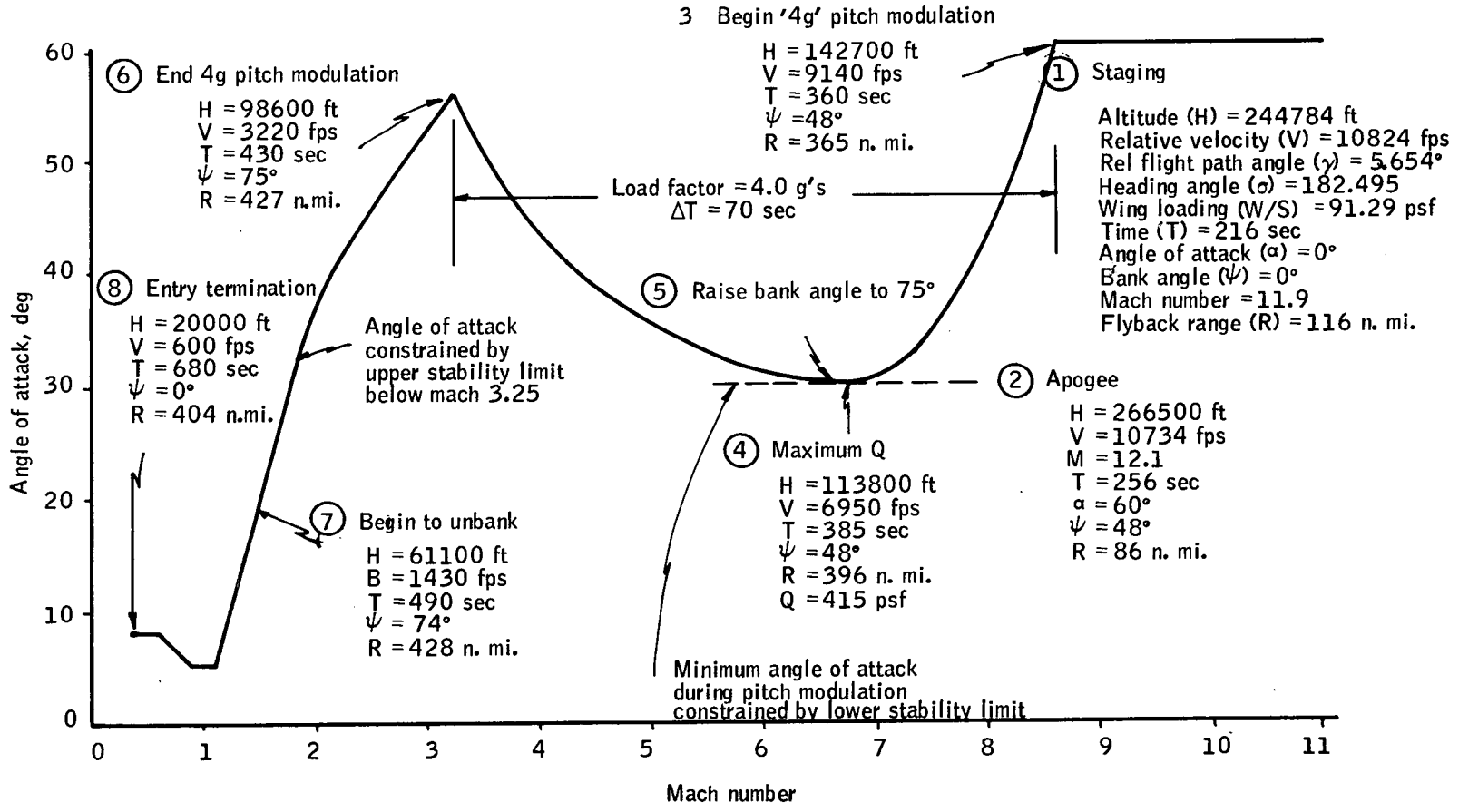

Figure B5. B-9U Booster Entry Trajectory Supersonic Gradual Transition

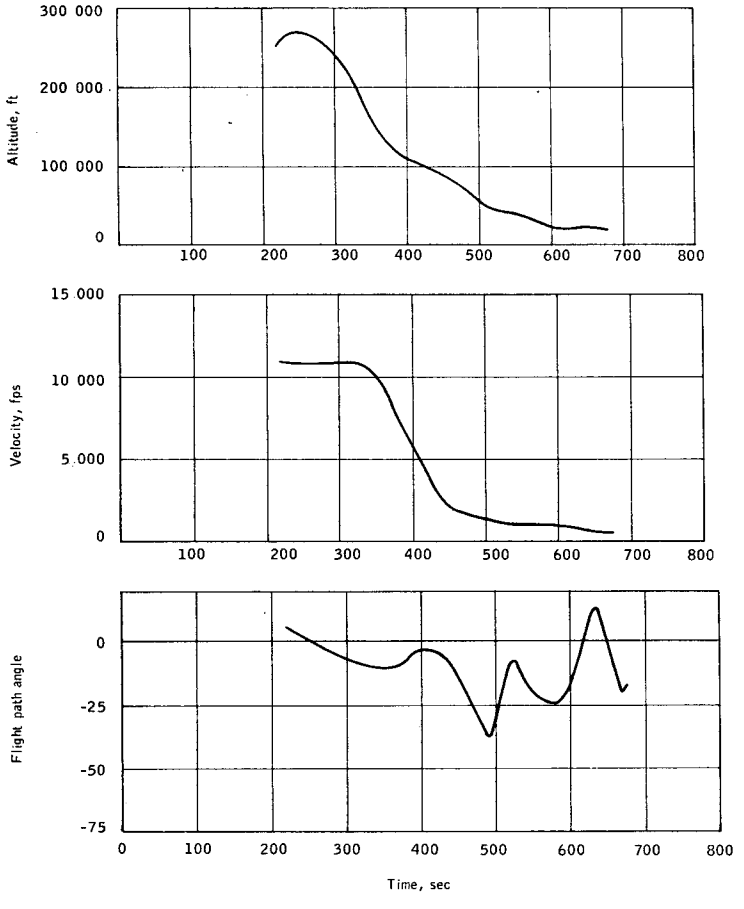

Figure B6a. B-9U Entry Trajectory

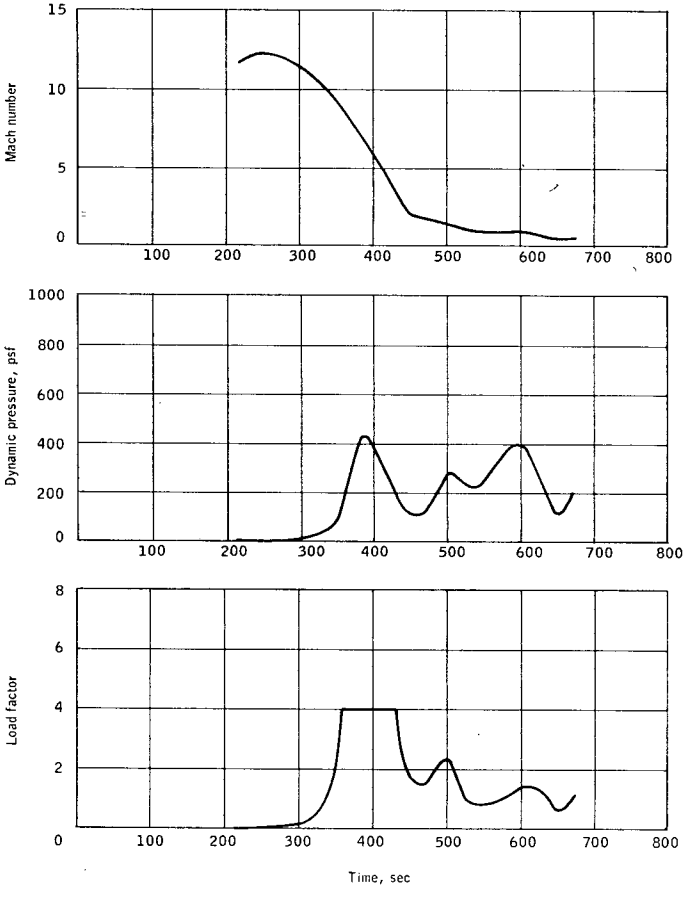

Figure B6b. B-9U Entry Trajectory (Continued)

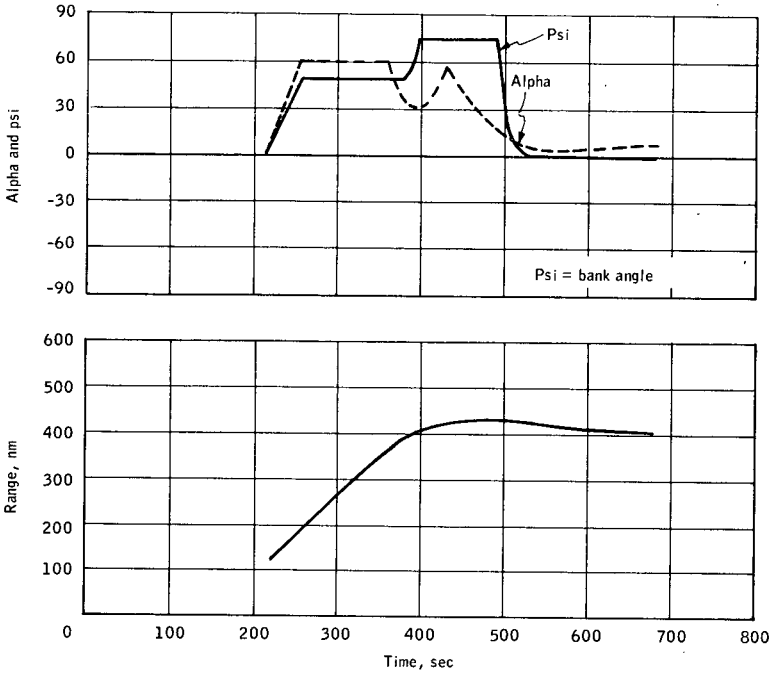

Figure B6c. B-9U Entry Trajectory (Continued)

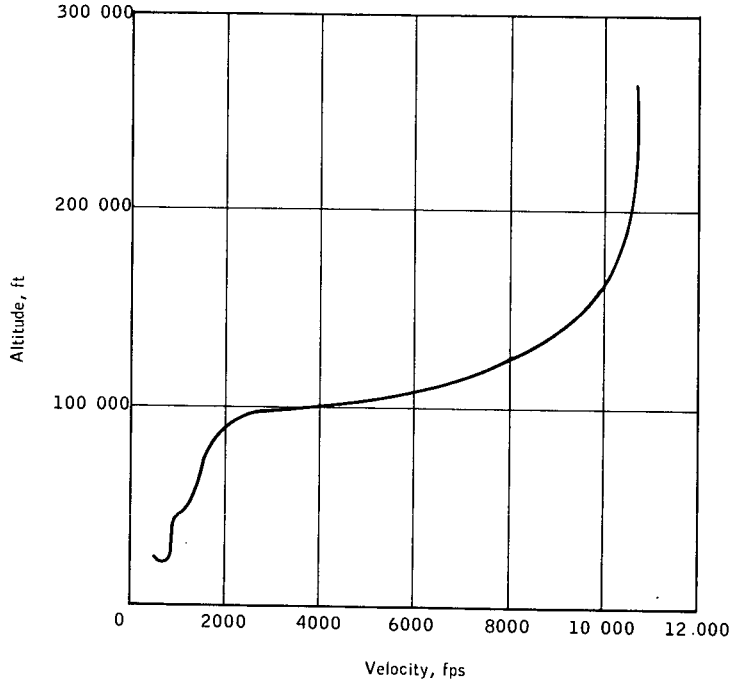

Figure B6d. B-9U Entry Trajectory (Continued)

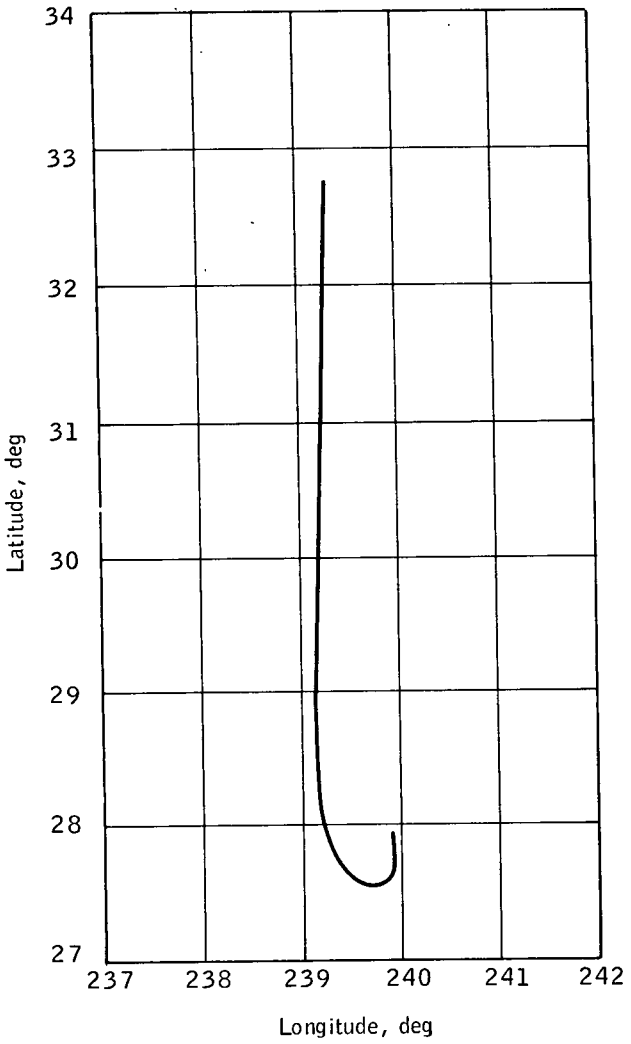

Figure B6e. B-9U Entry Trajectory (Continued)

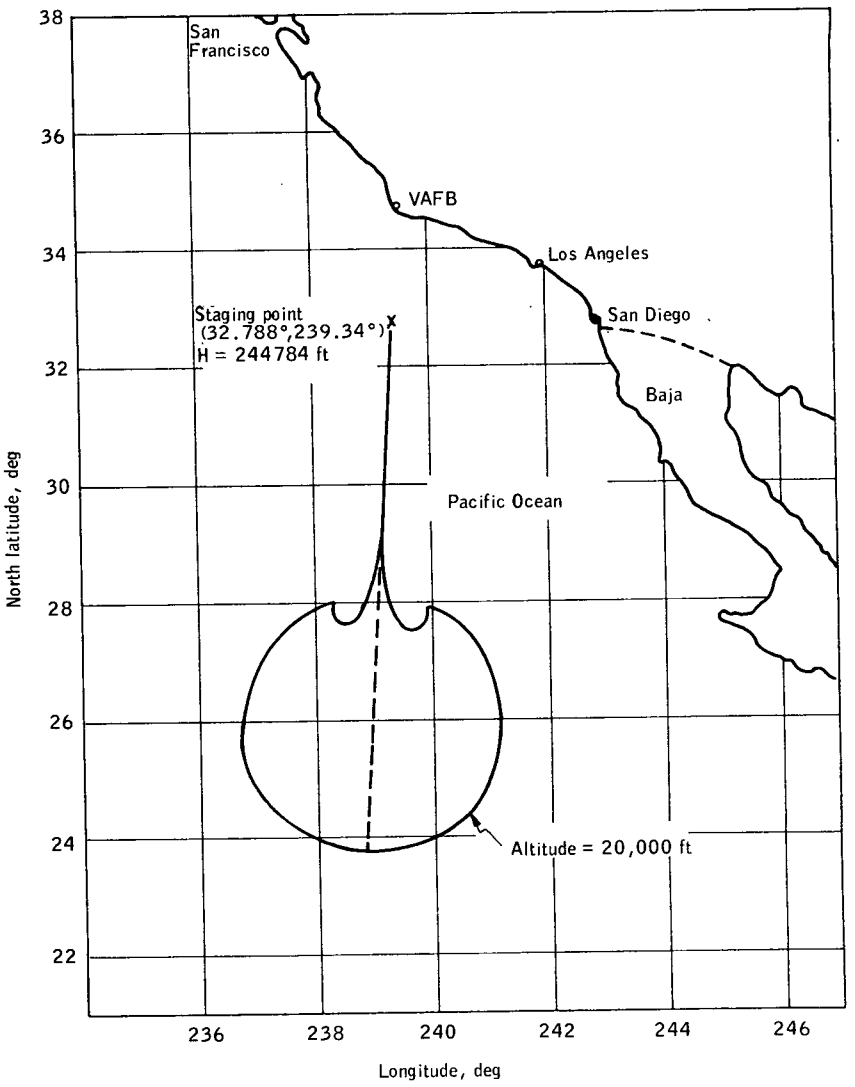

Figure B6f. B-9U Booster Entry Footprint

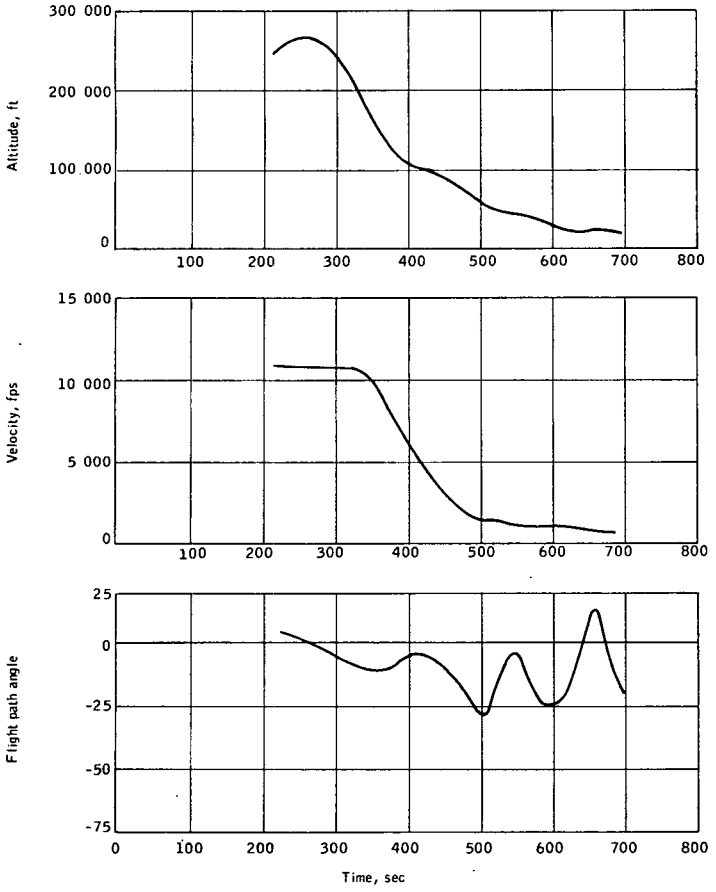

Figure B6g. Alternates B-9U Entry Trajectory Plots

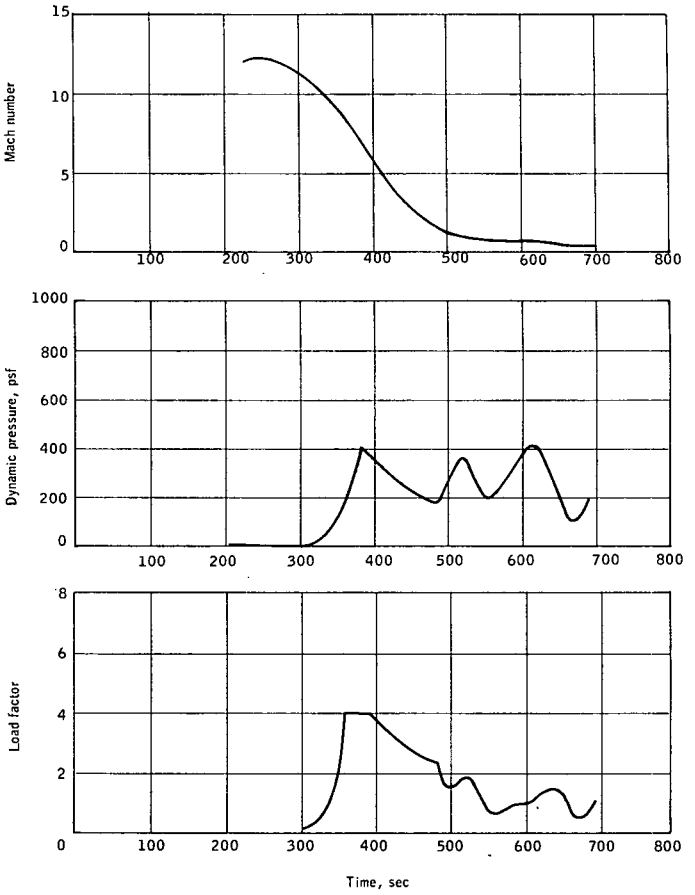

Figure B6h. Alternate B-9U Entry Trajectory Plots (Continued)

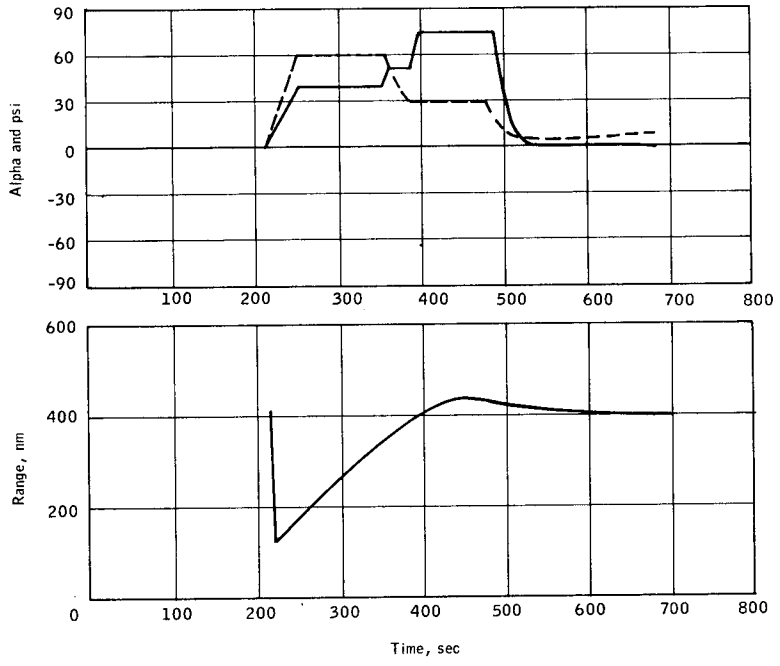

Figure B6i. Alternate B-9U Entry Trajectory Plots (Continued)

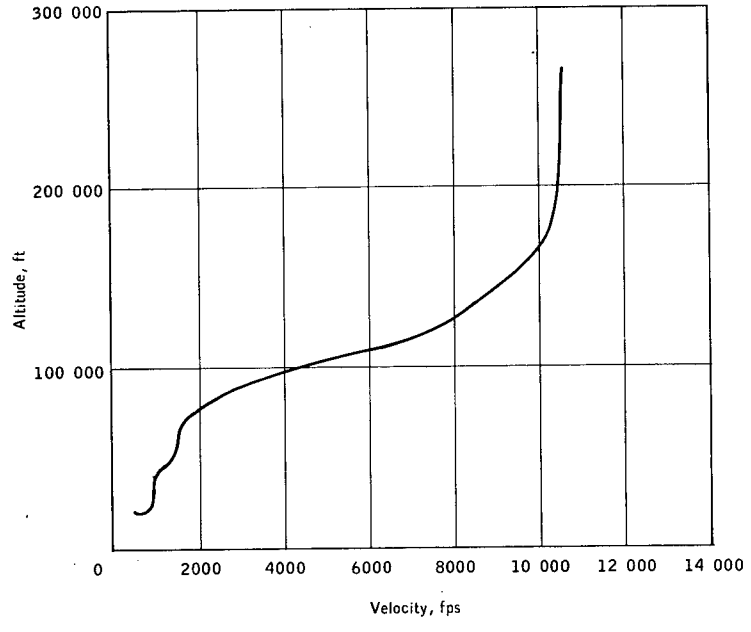

Figure B6j. Alternate B-9U Entry Trajectory Plots (Continued)

APPENDIX C

DENSITY ALTITUDE FROM INERTIAL SYSTEM MEASUREMENTS

This appendix describes some additional inertial system computations that provide the mechanization for deriving density altitude from inertial system measurements. A pencil and paper simulation of this mechanization is provided to show that measurement of altitude to ±2500 ft is achievable with rather crude representation of the delta wing orbiter's aerodynamic characteristics. Accuracy error sensitivity analysis is also presented. Ref. 14 provides another analysis; the method was used in the X-20 primary guidance system developed by Honeywell.

INTRODUCTION

The divergent inertial system altitude loop resulting from positive feedback of altitude error into a gravity error is well known. Uncertainties in orbit altitude at time of deorbit ΔV, and uncertainties in de-orbit trajectory lead to a large altitude uncertainty when the vehicle reaches sensible atmosphere. This initial uncertainty, together with its subsequent divergence, can lead to wholly unacceptable entry guidance and navigation error at the intended landing site. Thus, there is need for an independent means to correct the altitude error.

Air data probes mounted on the entry vehicle are a possibility. Problems inherent in such an approach are:

1) High Mach numbers during entry make correlations between probe pressures (and temperatures) and free stream quite inaccurate.

2) The heating during entry requires special provisions for probe construction and installation.

3) The large angle-of-attack range requires multiple probes.

Radar altimetry is another possibility. The high power and antenna gimbaling needs from high altitudes (with wide angle-of-attack variations) and the effects of the plasma sheath surrounding the vehicle during entry make this alternative extremely unattractive.

Thus, the possibility of using inertial measurements of velocity (relative wind), angle of attack, and deceleration (force per unit mass) to derive density altitude is extremely attractive, since only computations are added to the inertial system. The means to do this and its probable performance are discussed in the remainder of this report.

INERTIAL SYSTEM MECHANIZATION FOR DENSITY ALTITUDE MEASUREMENT

The inertial system sensors and computations are part of the integrated autonomous GN&C avionics for the Shuttle orbiter. Normal inertial measurements are position, velocity, and attitude of vehicle relative to one or more space reference frames. The discussion here will concentrate on those measurements needed to provide density altitude. Among the needed measurements and computational approaches to derive these are:

1) Vehicle velocity vector relative to the atmosphere (relative wind) - The air mass rotates with the earth; winds are small relative to the size of entry velocity and can be neglected. Thus, the needed velocity vector is that relative to the earth-fixed frame.

2) Vehicle angle of attack - The angle between the relative velocity vector's projection on the pitch plane and the vehicle's X-axis is angle of attack. Various formulae are possible, depending on which fits best with normal inertial computations.

3) Total vehicle deceleration - The inertial system accelerometers measure the total force per unit mass acting on the vehicle. Usually these accelerometers are of the integrating type requiring differentiation of their incremental velocity outputs to determine acceleration. An averaging time constant of at least 2 seconds should be allowable in smoothing this differentiation.

   For the delta wing orbiter analyzed, this deceleration vector is very near the negative -Z axis of the vehicle. Since only the magnitude of the "g-level" due to atmospheric forces; specific mechanization used should be coordinated with the aerodynamic parameter fitting process.

AERODYNAMIC CHARACTERISTICS

The aerodynamic data needed to determine density of the air currently being encountered are vehicle mass and the total force coefficient versus angle of attack. The total force coefficient is also a weak function of Mach number (relative velocity) at the higher velocities of concern here; the Mach dependence does not have to be included for the ±2500-ft precision and the delta wing vehicle considered here.

A rather crude (but adequate) fit of the C_F versus α data of ref. 15 for the delta wing orbiter analyzed is given by:

$$C_F = \frac{\alpha - 3°}{63°} \qquad 10° \leq \alpha \leq 25°$$

$$\frac{\alpha - 15°}{30°} \qquad 25° \leq \alpha \leq 60°$$

If significant variations in vehicle mass are possible from one mission to another some means of estimating and inserting vehicle mass into the GN&C system will be necessary. Since a percentage error in mass yields the same percentage error in derived air density and a 10 percent error in density represents 2000 ft only a crude estimate is needed.

DENSITY COMPUTATION

The derived air density equation is obtained from the total aerodynamic force formula:

$$F = C_F A q = C_F A \rho \frac{V^2}{2}$$

and is given by:

$$\rho = 2 g \left(\frac{M}{A}\right) \frac{(F/M)}{C_F V^2}$$

where

ρ = air density (pounds/ft^3).

F/M = the specific force per unit mass (in g's).

C_F = the total force coefficient (dimensionless) relative to a reference Area, A, and point mass dynamic pressure q.

M = vehicle mass (in pounds).

V = magnitude of relative wind (ft/sec).

g = 32 ft/sec^2.

DENSITY ALTITUDE COMPUTATION

Standard day geometric altitude versus density as given in ref. 16 can be represented as polynomial fits over needed ranges. Seasonal and weather variations of actual atmosphere from standard day make measurement to better than ±2500 ft of questionable value. Computer program scaling must be done carefully to accommodate a 10^4 dynamic range of density.

STARTING THE DENSITY MEASUREMENT PROCESS

Detecting decelerations of the order of 0.02 g can be used to start the density measurement process.

HOW FEASIBLE IS THIS INDIRECT METHOD TO DERIVE DENSITY ALTITUDE?

First from a mechanization point of view, the computations outlined above can easily be added into the GN&C system.

Second, to demonstrate workability, this system was simulated pencil and paperwise over the baseline trajectory. To some degree this only shows that the simulation was consistent; a second trajectory is necessary to show that it works over other parts of the entry corridor.

Finally, a cursory analysis of errors is presented. No difficulties were found; thus this approach is deemed feasible and adequate for controlling inertial system altitude divergence.

WORKABILITY DEMONSTRATION

Table C1 presents this demonstration. The values of time, altitude, velocity, g-level, and angle of attack were taken from ref. 17. The total force coefficient, C_F, was computed from the equations given above which were derived from data of ref. 15. Density was computed as:

$$\rho = 2043 \frac{(\text{g-level})}{C_F V^2} \ (\text{lb/ft}^3)$$

Geometric altitude was looked up in ref. 16. Geopotential altitude would have given smaller errors in most cases; it is not clear which altitude is used in ref. 17.

Table C1 shows ±2500-ft accuracy potential inherent in method.

CURSORY ERROR ANALYSIS

Over the 80K to 300K altitude range, the air density gradient is between 4 and 6 percent per thousand feet. Thus, a 5 percent/K ft sensitivity is used for error sensitivity purposes.

TABLE C1. FEASIBILITY OF DENSITY ALTITUDE FROM INS MEASUREMENTS

	H (1000 ft)	Time (sec)	V (Kfps)	g-level (g's)	α (deg)	Computed C_F	Computed ρ (lb/ft^3)	Computed geometric altitude (1000 ft)	Error (1000 ft)
	70								
	80								
End of →	90	2600	3	1.0	13	0.159	1.428-3	93.8	3.8
trajectory	100	2520	3.8	1.08	13	0.159	0.961-3	102.8	2.3
data	110	2450	4.7	1.0	13	0.159	0.582-3	112.6	2.6
	120	2340	6.0	1.085	13	0.159	0.387-3	121.5	1.5
	130	2190	7.7	1.07	13	0.159	0.232-3	132	2.0
	140	2120	8.5	0.91	13.4	0.165	0.156-3	141	1.0
	150	2020	9.6	0.92	16.8	0.219	0.931-4	154.3	4.3
	160	1940	10.4	0.86	18.2	0.241	0.674-4	162.7	2.7
	170	1830	11.5	0.825	20	0.27	0.472-4	172.1	2.1
	180	1710	12.7	0.81	22	0.302	0.340-4	181.25	1.25
	190	1620	13.8	0.78	24.5	0.342	0.245-4	190.2	0.2
	200	1515	15.0	0.744	28	0.433	0.156-4	202.2	2.2
	210	1410	16.3	0.71	29	0.467	0.117-4	210.2	0.2
	220	1260	17.8	0.603	30	0.5	0.778-5	220.7	0.7
	230	1025	20.2	0.51	30	0.5	0.510-5	231.2	1.2
	240	810	21.8	0.38	30	0.5	0.327-5	241.7	1.7
	250	600	23.15	0.29	30	0.5	0.221-5	250.5	0.5
	260	375	24.5	0.20	30	0.5	0.136-5	260.7	0.7
	270	225	25	0.27	53.5	1.275	0.692-6	273.1	3.1
	280	200	25.1	0.18	53.5	1.275	0.458-6	280.3	0.3
	290	180	25.2	0.12	53.5	1.275	0.303-6	287.6	-2.4
	300	165	25.2	0.06	53.5	1.275	0.151-6	299.7	-0.3
	310	145	25.2	0.03	53.5	1.275	0.757-7	311.7	1.7
	320	125	25.2	0.01	53.5	1.275	0.252-7	331.9	11.9
	360	60	25.2	0	53.5	1.275	---	---	
	400	0	25.2	0	53.5	1.275	---	---	

The logarithmic differential form of the density computation equation is:

$$\frac{d\rho}{\rho} = \frac{d(M/A)}{(M/A)} + \frac{d(F/\mathbf{M})}{(F/M)} - \frac{d\,C_F}{C_F} - 2\,\frac{dV}{V}$$

(1) (2) (3) (4)

(1) Errors in Mass and Reference Area

Knowledge of vehicle mass may require keeping track of fuel used and variations in payload. An error 5000 pounds causes a 500-ft altitude error.

(2) Errors in Specific Force Measurement

The IMU accelerometers have small error relative to 1 percent; the differentiation technique and associated time constant for smoothing can be designed to provide a 1 percent acceleration magnitude error. Thus, this error should result in less than 200-ft altitude error. More error could be allowed for this source to enable -Z axis force measurement.

(3) Errors in Force Coefficient

The correlation of wind tunnel data to actual flight vehicle and the fitting of C_F versus α should be possible within ±10 percent causing a 2K-ft altitude uncertainty. At lower altitudes, with the slower velocities, C_F becomes a stronger function of Mach number. If necessary, C_F can be made a function of Mach. The angle-of-attack error due to velocity error is negligible; however, at lower speeds atmospheric winds become a significant fraction of vehicle velocity determined inertially. This means of computing density altitude should be discontinued when velocity becomes less than, for example, 2000 fps. Revising to use C_L, the lift coefficient, may result in less uncertainty basic aerodynamics than C_F.

(4) Error in Velocity Measurement

During the initial portion of entry velocity is large and error due to initial conditions, measurement, and divergence is small. After engaging the divergence correction loop based on density altitude measurements the growth of velocity error is curbed and perhaps corrected somewhat by the slaving of the altitude loop. A 1 percent bound on velocity error should be easily achievable until winds become a significant fraction of vehicle velocity. Less than 400 ft should be possible due to this source, down to approximately 80K ft. Thereafter the drag-determined density altitude should be terminated in favor of conventional aircraft air data measurement methods or radar altimetry.

A ±2500-ft density altitude measurement from encounter of sensible atmosphere to end of entry should be possible using this bootstrapping method within the inertial system.

APPENDIX D
HEMISPHERE SURFACE PRESSURE DISTRIBUTION

INTRODUCTION

A formula describing the pressure distribution on a sphere is basic to an air data sensor for Space Shuttle. The concept is to use a fixed hemisphere and by measuring pressures at known locations calculate the air data parameters with a computer. Conventional formulae for spheres are well established for certain speed ranges, but are not applicable for speeds from reentry to aircraft landing of the Space Shuttle.

In general, the hemisphere pressure distribution is identical with that of a sphere. Flow separation near the equator of the sphere is avoided by the presence of the cylinder filling in the wake. Hence, changes in pressure distribution with Reynolds number, common for spheres, is avoided. Whether the after body is a cylinder or a small angle cone does not alter the pressure distribution except near the point of tangency. At high angles of attack of the hemisphere cylinder, the downwind side of the hemisphere can be expected to have flow separation similar to a sphere.

FLOW DESCRIPTION

As the speed increases, the character of the flow about a hemisphere changes. At low subsonic flight speeds, the surface speed remains subsonic over the whole body and increases from zero at the stagnation point to a maximum at the equator. Theories are available to compare with data. At the critical flight speed (about $M = 0.57$) the Mach number at the equator has increased to sonic and local shocks will form near the surface. The pressure discontinuity across the shocks will affect the pressure distribution and/or also by causing a flow separation downstream of the shock. The local shocks can be asymmetrical about the stagnation point, due to bumps or flat spots on the surface, and thus change the expected pressure distribution. Local surface shocks and their problems will be present until the flight speed has increased to about $M = 1.5$ where a stable bow wave is established. The speed range from just above critical Mach number to about $M = 1.5$ is called transonic and is where both experiment and theory are difficult. At high speeds (i.e., supersonic and hypersonic) the surface flow is stable, and one can expect better fit between formulae and experiment.

LOW-SPEED FORMULA

At low subsonic speeds potential theory leads to the formula

$$C_P = 1 - \left(\frac{3}{2}\right)^2 \sin^2 E \qquad \text{(D1)}$$

Potential flow does not include compressibility or viscous effects and thus best matches reality on the forward hemisphere at low subsonic speeds ($M < 0.3$). This relation is well verified by experiment and is discussed in standard textbooks, ref. 18. When using a cylindrical or cone after body, such as the aircraft fuselage, flow separation at large E is delayed. This is an advantage because it increases the useable angle-of-attack range of the sensor and makes it less sensitive to Reynolds number effects.

HIGH-SPEED FORMULA

At high supersonic speeds $M > 3$ there are several formulae available. The conventional one in the literature, ref. 19, is called Modified Newtonian, which for a sphere is

$$C_P / C_{P_o} = \cos^2 E \qquad \text{(D2)}$$

The Modified Newtonian relation is generally accepted as the standard for comparing with experimental data and new improved theories in the hypersonic speed range. It also is used as the starting point for developing improved empirical fits of experimental data.

Bertram, ref. 20, derives an empirical relation, based on Newtonian, to fit experimental data for the pressure distribution on a hemisphere at supersonic and hypersonic speeds. The equation is

$$\frac{P}{P_t} = \cos^2 E + 0.07 \sin^8 E \qquad \text{(D3)}$$

The fit is best at speeds above $M = 2.8$. Similarity of Bertram's relation, Equation (D3), with modified Newtonian can be seen by rewriting the Newtonian relation, Equation (D2), in pressure ratio form and comparing it with Equation (D3). Equation (D2) rewritten is

$$\frac{P}{P_t} = \cos^2 E + \frac{P_\infty}{P_t} \sin^2 E \qquad \text{(D2a)}$$

When the atmospheric pressure, P_∞, is small compared to the surface stagnation pressure, P_t, which is true at hypersonic speeds and/or for small values of E, the Newtonian relation becomes

$$\frac{P}{P_t} \approx \cos^2 E \qquad \text{(D4)}$$

For example, at M = 4 and M = 10 the ratio P_∞/P_t = 0.047 and 0.0077, respectively. This shows that Bertram's equation is basically Modified Newtonian with a second term to improve the fit at large values of E.

Another empirical relation for hemisphere pressure distribution derived from Modified Newtonian according to Romeo, ref. 21, is

$$\frac{P}{P_t} = \cos^n E \tag{D5}$$

Here "n" is a function of Mach number determined from experimental data shown in Figure D1. Reference 20 derived the expression for use at hypersonic speeds where n is essentially constant at n = 2.24 and suggested possible applicability at lower speeds. In order to investigate this, we have written an empirical relation through the data of ref. 21, which is shown plotted in Figure D1.

$$n = 2.24\left(1 - e^{-\frac{M}{2.1}}\right) \tag{D6}$$

The Romeo expression, Equation (D5), shows an improvement over the Newtonian relation at moderate values of E, but of course Equation (D5) has the disadvantage of always going to zero absolute pressure at E = 90 deg, which is unrealistic. Reference 21 says that the Romeo expression is acceptable for a speed range from hypersonic down to as low as M = 0.5.

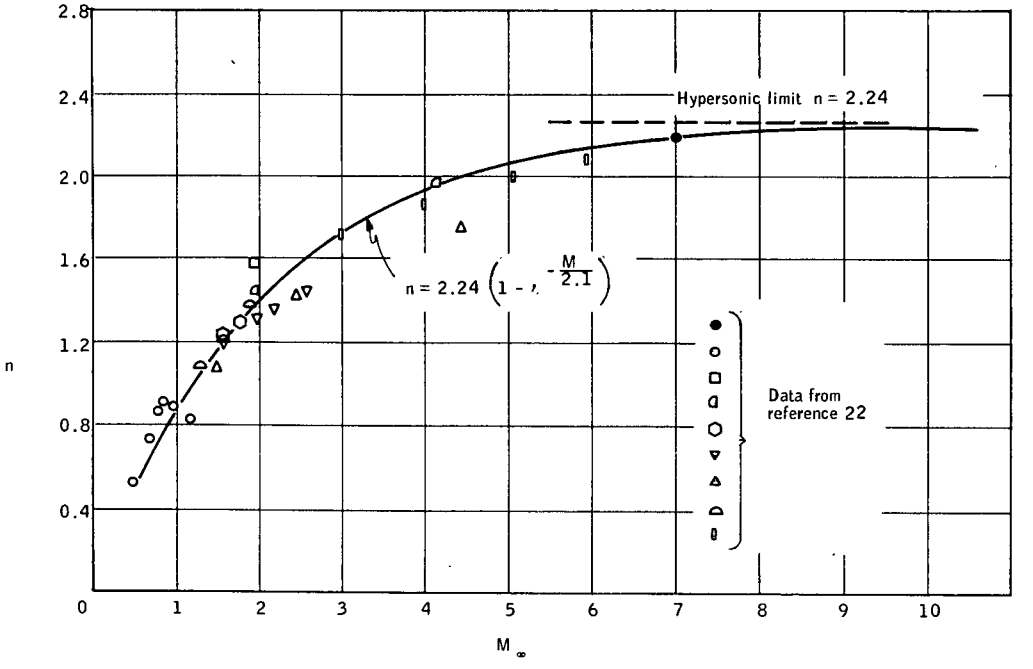

Figure D1. Exponent "n" versus Mach No. for Hemisphere Pressure Distribution Formula II

To measure angle of attack using the Romeo formula, ref. 21 suggests using the ratio of measured absolute pressures of taps located on the $\beta = 0$ great circle. The equation to be implemented is

$$\frac{\log (P_1/P_2)}{\log (P_3/P_4)} = \frac{\log \left[\frac{\cos \alpha_{t_1}}{\cos \alpha_{t_2}} \left(\frac{1 + \tan \alpha \tan \alpha_{t_1}}{1 + \tan \alpha \tan \alpha_{t_2}}\right)\right]}{\log \left[\frac{\cos \alpha_{t_3}}{\cos \alpha_{t_4}} \left(\frac{1 + \tan \alpha \tan \alpha_{t_3}}{1 + \tan \alpha \tan \alpha_{t_4}}\right)\right]} \tag{D7}$$

The ratio of pressure eliminates P_t and the ratio of logs eliminates "n" and thus, Mach number from the relation. The subscripts indicate that four taps are needed, but in practice one tap could be common to both ratios so that only three are needed. Romeo suggests a further simplification by locating the common tap at the point where $\alpha = 0$, and $\beta = 0$. Then

$$\frac{\log (P_1/P_2)}{\log (P_3/P_2)} = \frac{\log \left[\cos \alpha_{t_1} \left(1 + \tan \alpha \tan \alpha_{t_1}\right)\right]}{\log \left[\cos \alpha_{t_3} \left(1 + \tan \alpha \tan \alpha_{t_3}\right)\right]} \tag{D7a}$$

COMBINED RELATION

A combination of the potential flow relation for low speeds with the Modified Newtonian relation is proposed here. Examination of the Potential flow, Equation (D1), and Newtonian, Equation (D2), leads to the expression of form similar to both.

$$C_P = C_{P_o} - B \sin^2 E \tag{D8}$$

where B is a function only of Mach number.

Equation (D8) is attractive because it leads to a simple method for measuring angle of attack, α, and sideslip, β, with a fixed sphere that is independent of altitude and speed. This is done by first sensing the pressure difference of a pair of taps on the sphere. Using Equation (D8) the pressure difference is

$$P_1 - P_2 = qB (\sin^2 E_2 - \sin^2 E_1) \tag{D9}$$

The product qB is a function of both pressure and Mach number (altitude and speed) which is eliminated by ratioing the first pressure difference with the pressure difference of a second pair of taps. One tap of the second pair could

be common with one of the first pairs which means that only three taps are necessary. The result ratio is

$$\frac{P_1 - P_2}{P_3 - P_4} = \frac{\cos^2 E_1 - \cos^2 E_2}{\cos^2 E_3 - \cos^2 E_4} \tag{D10}$$

Angle of attack, α, and sideslip, β, are measured in sequence and hence β is not independent of α. The general relation of α, β and the angle E (angle between the stagnation point and the tap) is

$$\cos E = \sin \beta_t \sin \beta + \cos (\alpha - \alpha_t) \cos \beta_t \cos \beta \tag{D11}$$

where the subscript "t" refers to the angular location of the tap which are known. In order to measure α independent of sideslip, β, taps can be located so $\beta_t = 0$ for each tap. Then

$$\cos E = \cos (\alpha - \alpha_t) \cos \beta \tag{D11a}$$

and substituting (D11a) into (D10) the expression is

$$\frac{P_1 - P_2}{P_3 - P_4} = \frac{\cos^2 \left(\alpha - \alpha_{t_1}\right) - \cos^2 \left(\alpha - \alpha_{t_2}\right)}{\cos^2 \left(\alpha - \alpha_{t_3}\right) - \cos^2 \left(\alpha - \alpha_{t_4}\right)} \tag{D12}$$

Equation (D12) does not contain β, hence the angle of attack can be solved for by the measurement of two pressure differences, independent of sideslip as well as altitude and speed. Knowing α, the sideslip can be determined by measuring one or more additional pressure difference.

These advantages are possible if Equation (D8) is valid. To show this, one must first choose expression for "B" with Mach number and then at specific Mach numbers compare the pressure distribution of Equation (D8) with experimental data. Of course, in use the actual values of B are not needed except to calculate the pressure at some point on the surface. Examples of this would be the stagnation pressure or the pressure at a point known to be the same as the atmospheric pressure.

Three formulae for "B" are chosen, one for each speed range -- subsonic, transonic and super-hypersonic. Reasoning for the resulting equation is described below.

- At low subsonic speeds C_{P_o} approaches one, so according to potential flow theory, B approaches 9/4.

- At subsonic speeds up to the critical Mach number (M = 0. 57) "B" would be expected to increase proportional to $(1 - M^2)^{-1/2}$ according to the Prandtl-Glauert rule which is the conventional compressible flow correction, ref. 5. The critical Mach number is sphere velocity where the surface velocity first becomes sonic at 90 deg from the stagnation point, i. e., E = 90 deg. The expression for speeds below the critical Mach number is

$$B = \frac{9}{4} \frac{1}{\sqrt{1 - M^2}} \qquad \text{(D13)}$$

- At intermediate speeds between critical (M = 0. 57) and speeds where modified Newtonian can be used, B would decrease according to an empirical fit through experimental data. The curve used here is a parabola fit between "B" at the critical Mach number (M = 0. 57) predicted by the Prandtl-Glauert rule and "B" predicted by the Modified Newtonian relation at M - 1. 8 as shown in Figure D2. Extending the Newtonian approximation, which is normally considered applicable for M > 4. 0, down to M = 1. 8 would at first appear to be a daring extrapolation. However, the data on Figure D2 show it is a reasonable match point and the resulting predicted surface

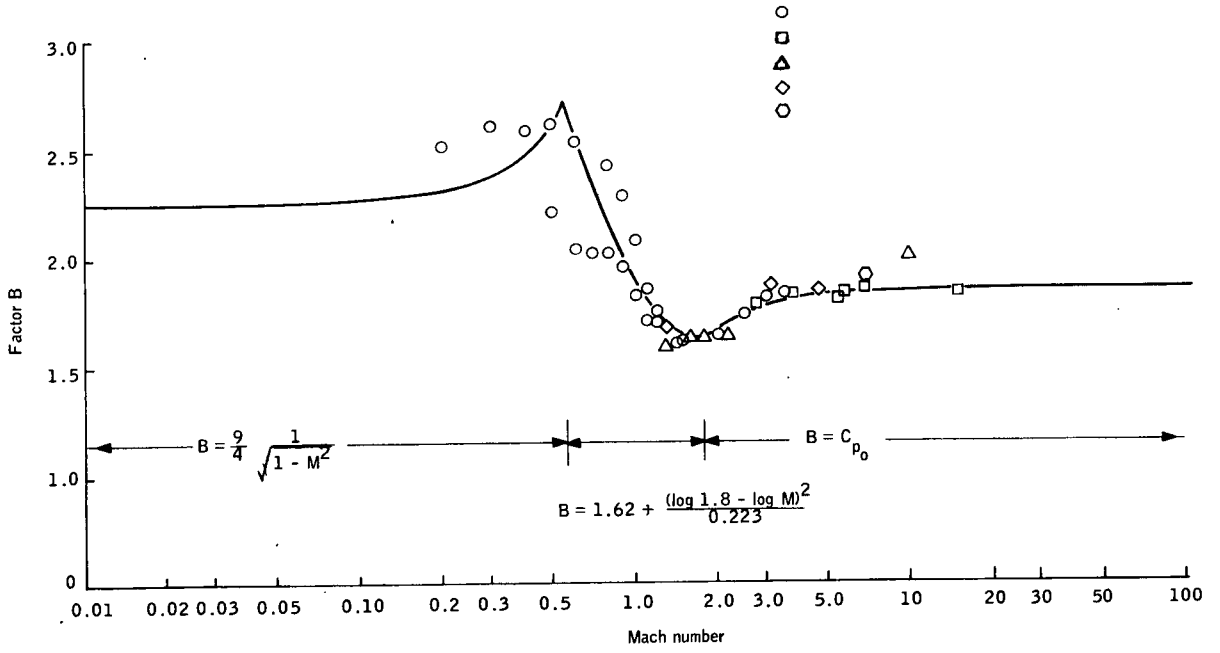

Figure D2. Pressure Coefficient Factor "B" versus Mach No. for Hemisphere Pressure Distribution Formula I

pressure distribution in the extrapolated speed range agree reasonably well with experiment as is shown in Figures D14 to D24. The parabola fit on the semi-log plot of Figure D2 results in the expression

$$B = 1.62 + \frac{(\log 1.8 - \log M)^2}{0.223} \qquad \text{(D14)}$$

This expression does not provide a tight fit with available data at speeds between M = 0.57 and M = 1.0. Additional data are needed in this high subsonic, transonic speed range. With such data, an improved expression for "B" in this region can easily be formulated. However, Equation (D14) is still a reasonable fit with the surface pressure data in this speed range, Figures D6 to D9.

- At supersonic and hypersonic speeds where the Modified Newtonian approximation is applicable, the constant B becomes the pressure coefficient of the surface pressure at the stagnation point, C_{P_o}. At these speeds, the total pressure decrease through bow wave must be included. Using the Rayleigh pitot formula in the derivation, the expression for B is

$$B = \frac{10}{7M^2}\left[\left(\frac{6M^2}{5}\right)^{\frac{7}{2}}\left(\frac{6}{7M^2 - 1}\right)^{\frac{5}{2}} - 1\right] \qquad \text{(D15)}$$

COMPARISON OF FORMULA

There are two candidate formulae for the sphere pressure distribution that can be used for the shuttle α and β sensor, Equation (D8) and Equation (D5). For purpose of comparison, they will be labeled Formula I and II, respectively.

$$\text{Formula I} \quad C_P = C_{P_o} - B\sin^2 E \qquad \text{(D8)}$$

$$\text{Formula II} \quad \frac{P}{P_t} = \cos^n E \qquad \text{(D5)}$$

Each is a function of Mach number. In Formula I it is the factor B and in Formula II it is the exponent "n". Each formula can be written in either pressure coefficient or pressure ratio form. Thus

$$\text{Formula I} \quad \frac{P}{P_t} = 1 - \frac{q}{P_t} B \sin^2 E \tag{D8a}$$

$$\text{Formula II} \quad C_P = \frac{P_t}{q} \cos^n E - \frac{P_\infty}{P_t} \tag{D5a}$$

where q/P_t, P_∞/P_t are well known functions of Mach number.

A first comparison is that Formula I can be implemented with pressure difference gages for a result that is independent of M while Formula II cannot. This can be seen below

$$\text{Formula I} \quad \frac{P_1 - P_2}{P_3 - P_4} = \frac{\cos^2 E_1 - \cos^2 E_2}{\cos^2 E_3 - \cos^2 E_4} \tag{D16}$$

$$\text{Formula II} \quad \frac{P_1 - P_2}{P_3 - P_4} = \frac{\cos^n E_1 - \cos^n E_2}{\cos^n E_3 - \cos^n E_4} \tag{D17}$$

The reverse is true when considering the use of absolute pressure gages. Formula I cannot be made independent of Mach number while Formula II can, as shown below.

$$\text{Formula I} \quad \frac{P_1}{P_2} = \frac{1 - K \sin^2 E_1}{1 - K \sin^2 E_2} \tag{D18}$$

where

$K = \frac{qB}{P_t}$ a function of Mach number

$$\text{Formula II} \quad \frac{\log (P_1/P_2)}{\log (P_3/P_4)} = \frac{\log (\cos E_1 - \cos E_2)}{\log (\cos E_3 - \cos E_4)} \tag{D19}$$

COMPARISON WITH EXPERIMENTAL PRESSURE DISTRIBUTION

Experimental pressure distribution data are taken from ref. 20, 21, and 22 which are themselves collections of pressure data taken from many sources and ref. 23. For the comparison all data and formulae use non-dimensional pressure ratio form with the surface stagnation pressure, P_t, as the

reference. Below M = 1, P_t is the same as the total pressure, and above M = 1 it is the total (stagnation) pressure behind a normal shock.

Plots of surface pressure versus angle from the stagnation point as predicted by Formula I and Formula II are compared with experimental data in Figures D3 through D31, in the order of increasing Mach number from 0.2 to 15.

A general observation of the pressure distributions illustrated in the figures is that from the stagnation point to about E = 15 deg, both Formulae I, II and the experimental data are in tight agreement. The range of angle E of most interest for angle-of-attack sensing is from E = 30 to 60 deg because the best sensitivity is about E = 45 deg. If the angle-of-attack sensor is to operate over a large range, as in the case of some Space Shuttle trajectories, then formula accuracy at E = 70 or 80 deg should also be considered.

SUBSONIC SPEEDS M = 0 TO 0.6

At low subsonic speeds Formula I is best in that it is the proven potential flow relation which agrees with experimental data up to about E = 60 deg for laminar flow and past 90 deg for turbulent flow. Data points are not shown in Figures D3 and D4, but confirmation can be found in textbooks. At these low speeds, Formula II is inadequate because it has an E error of about 30 deg for pressure taps about 45 deg from the stagnation point, at M = 0.2, Figure D3. At M = 0.4 and 0.5, Formula I and II are about E = 5 deg apart and experimental data do not favor either formula.

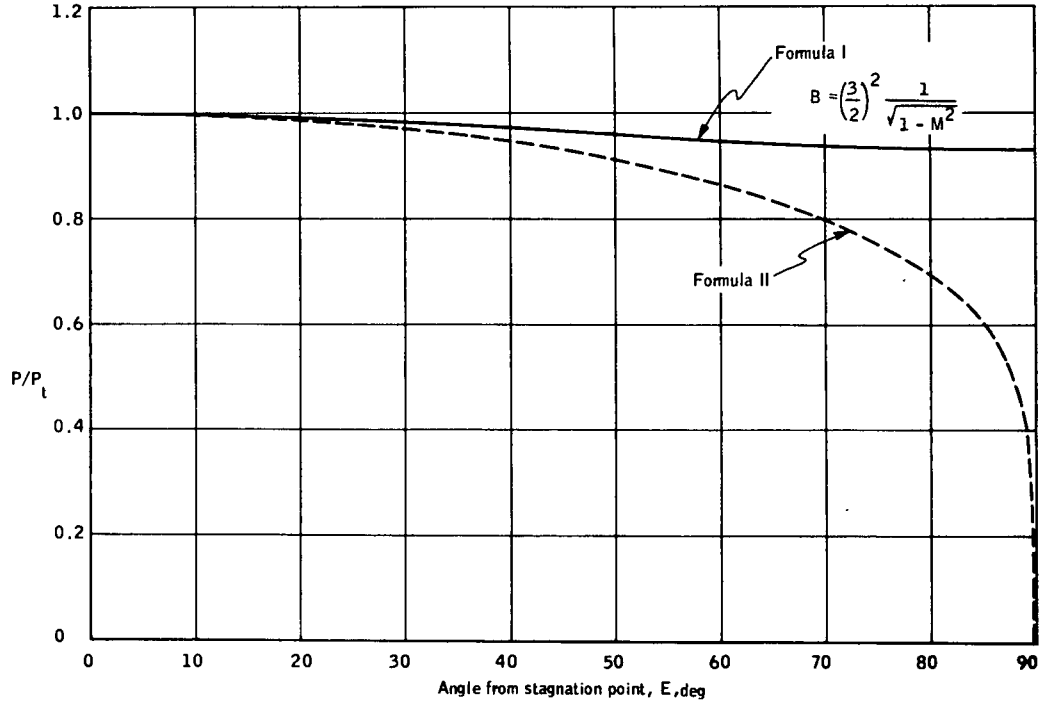

Figure D3. Comparison of Formula I and II at M = 0.2

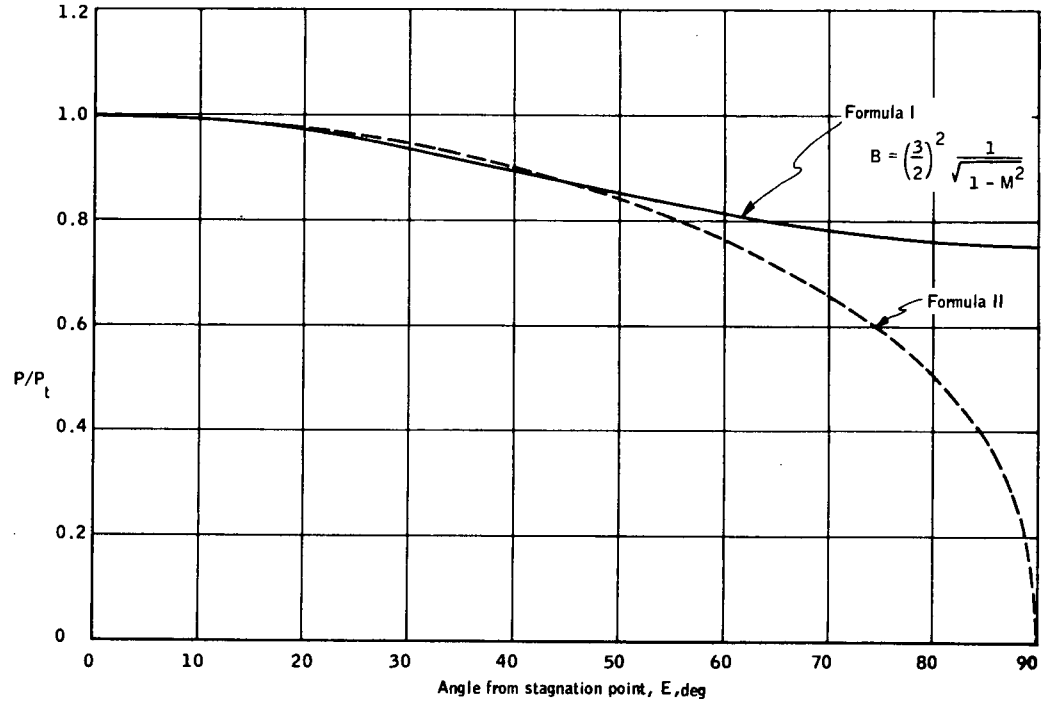

Figure D4. Comparison of Formula I and Formula II at M = 0.4

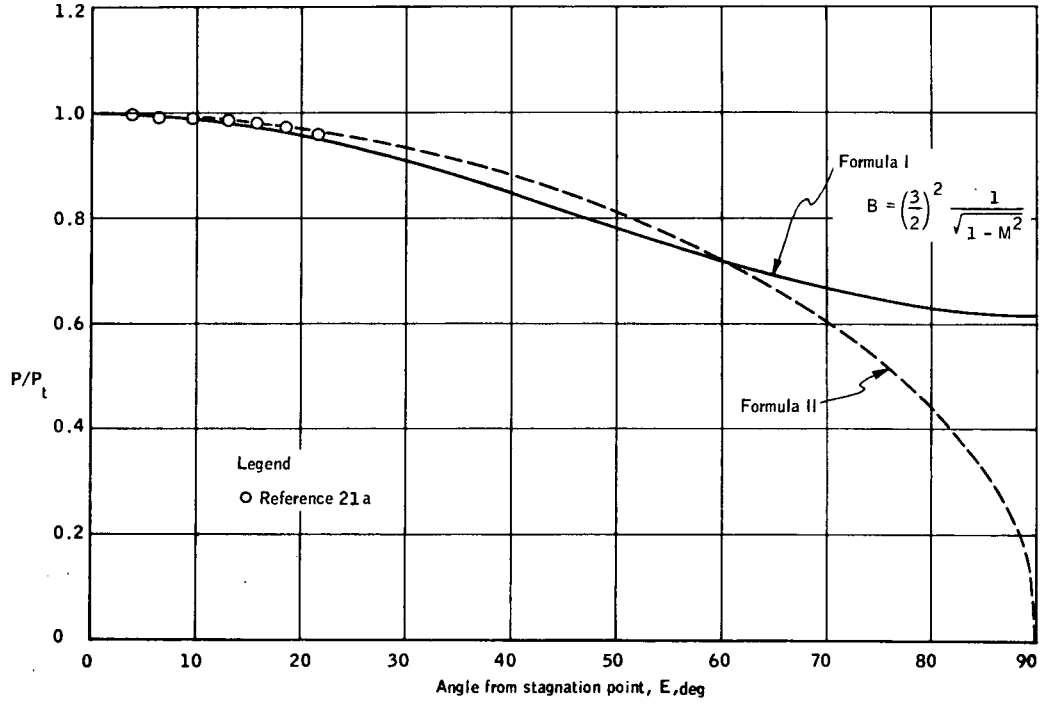

Figure D5. Comparison of Formula I and II and Experimental Data at M = 0.5

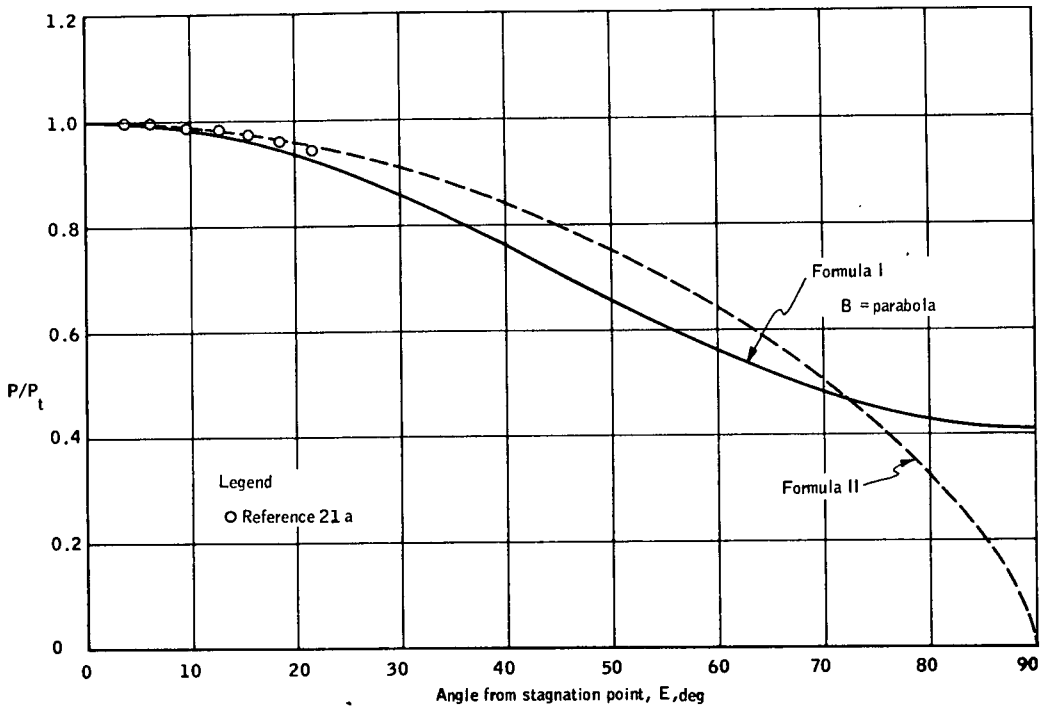

Figure D6. Comparison of Formula I and II and Experimental Data at M = 0.7

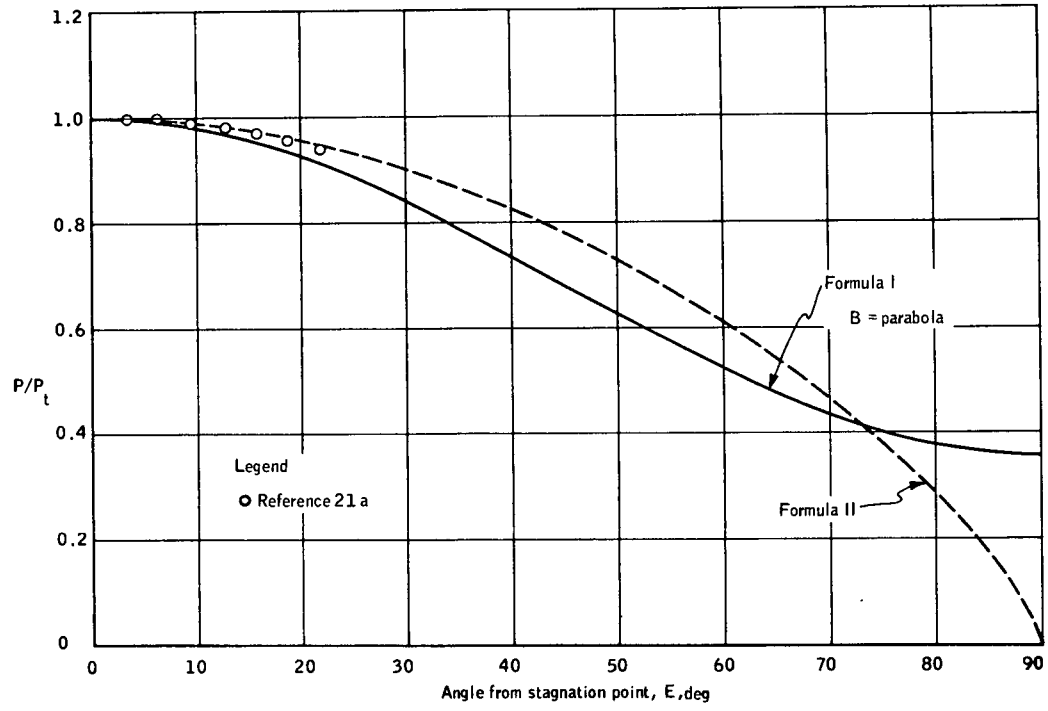

Figure D7. Comparison of Formula I and II and Experimental Data at M = 0.8

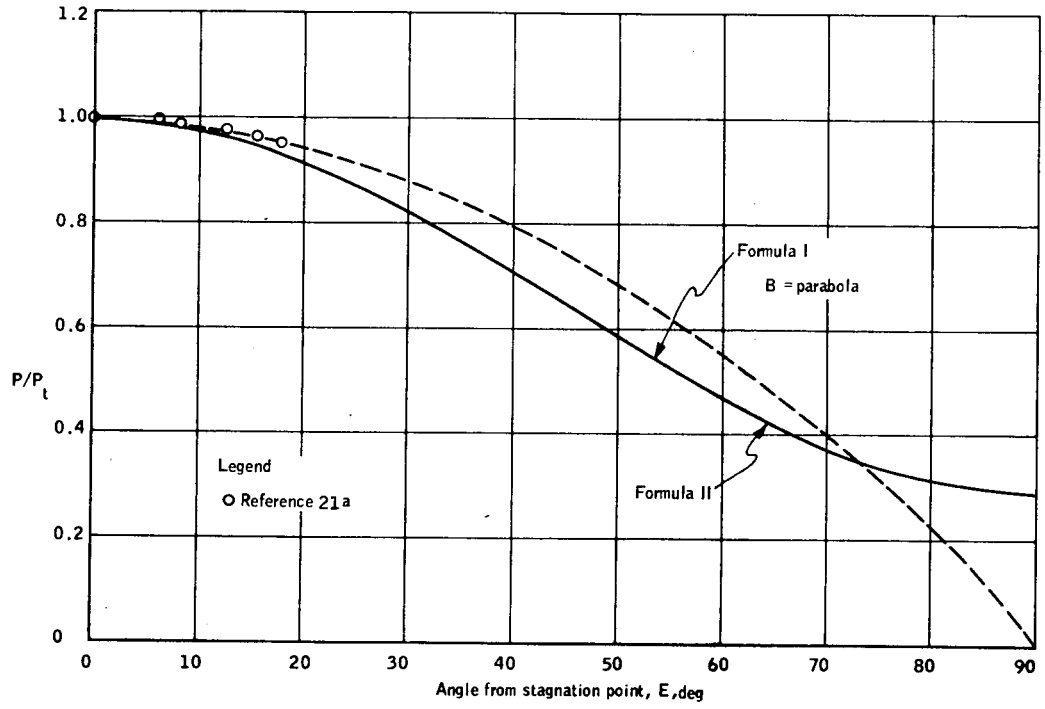

Figure D8. Comparison of Formula I and II Experimental Data at M = 0.9

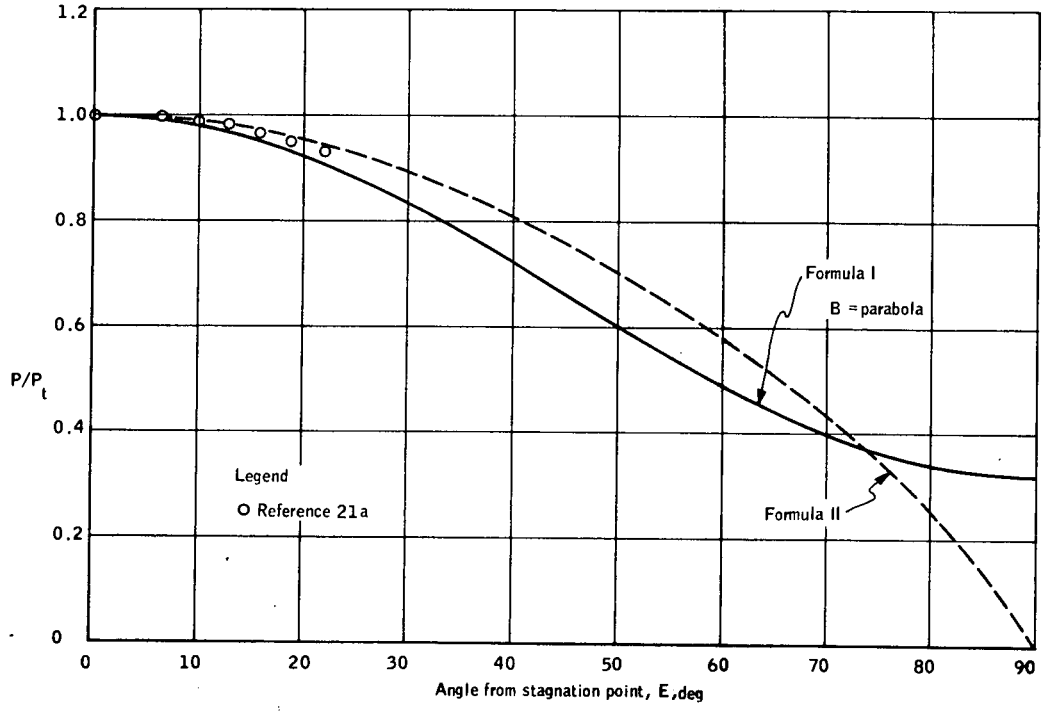

Figure D9. Comparison of Formula I and II and Experimental Data at M = 1.0

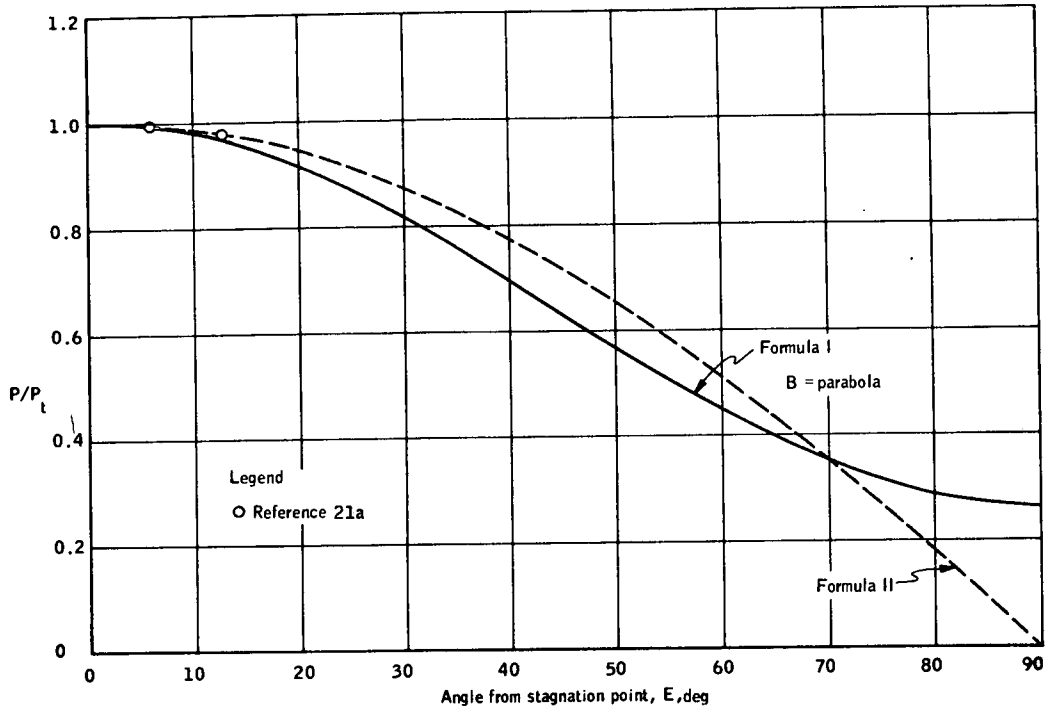

Figure D10. Comparison of Formula I and II and Experimental Data at M = 1.2

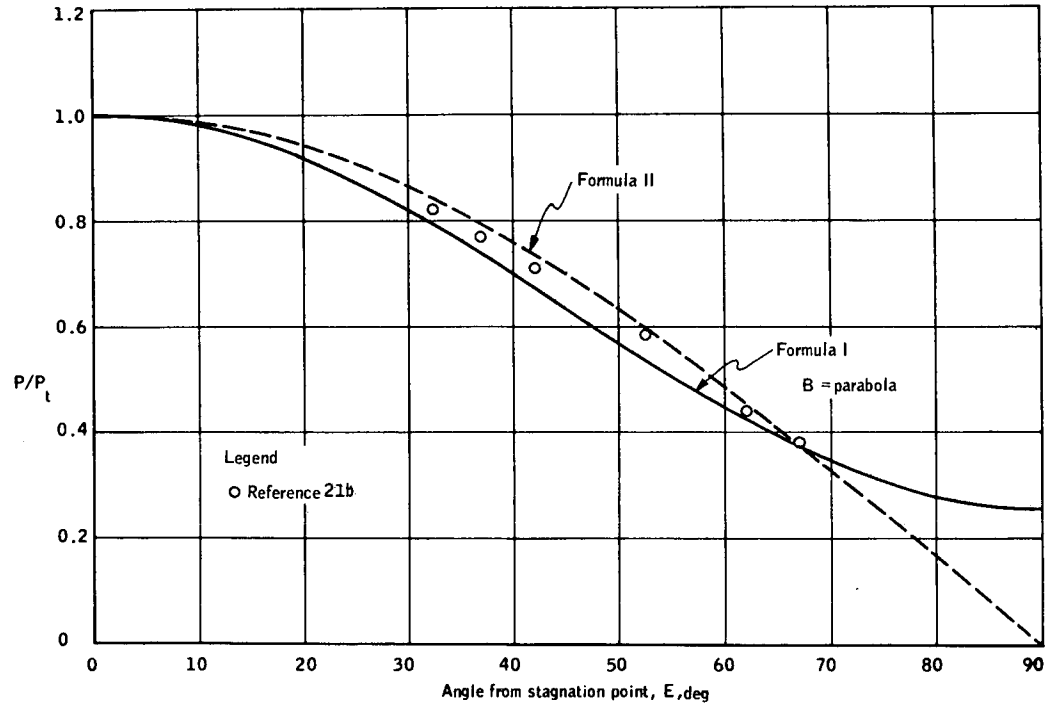

Figure D11. Comparison of Formula I and II and Experimental Data at M = 1.3

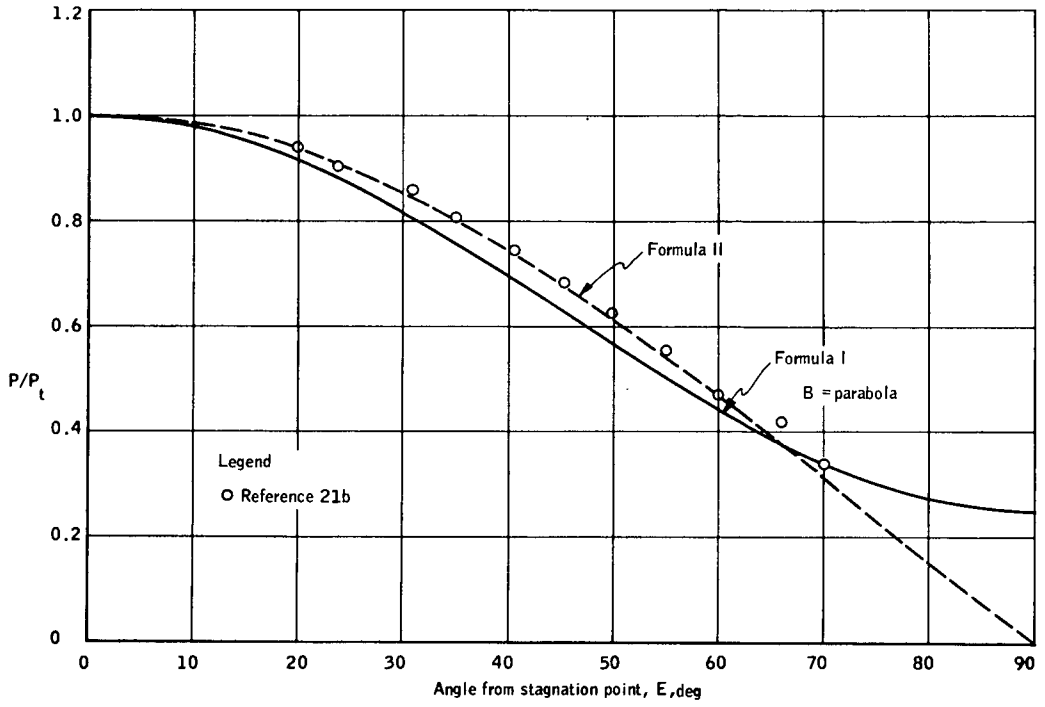

Figure D12. Comparison of Formula I and II and Experimental Data at M = 1.5

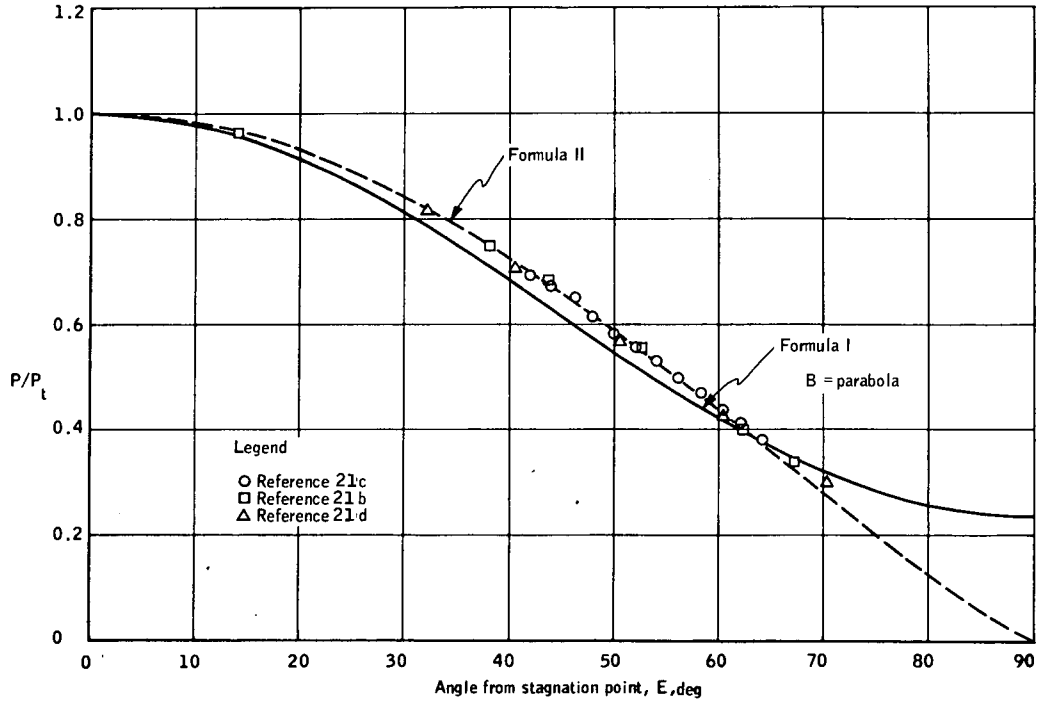

Figure D13. Comparison of Formula I and II and Experimental Data at M = 1.6

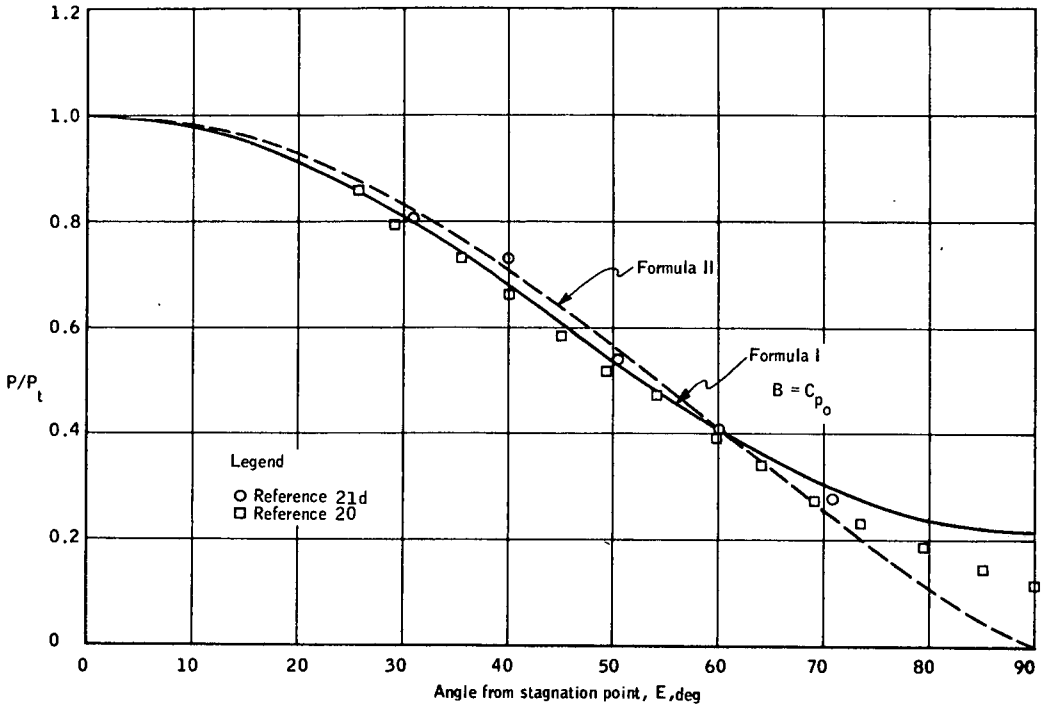

Figure D14. Comparison of Formula I and II and Experimental Data at M = 1.8

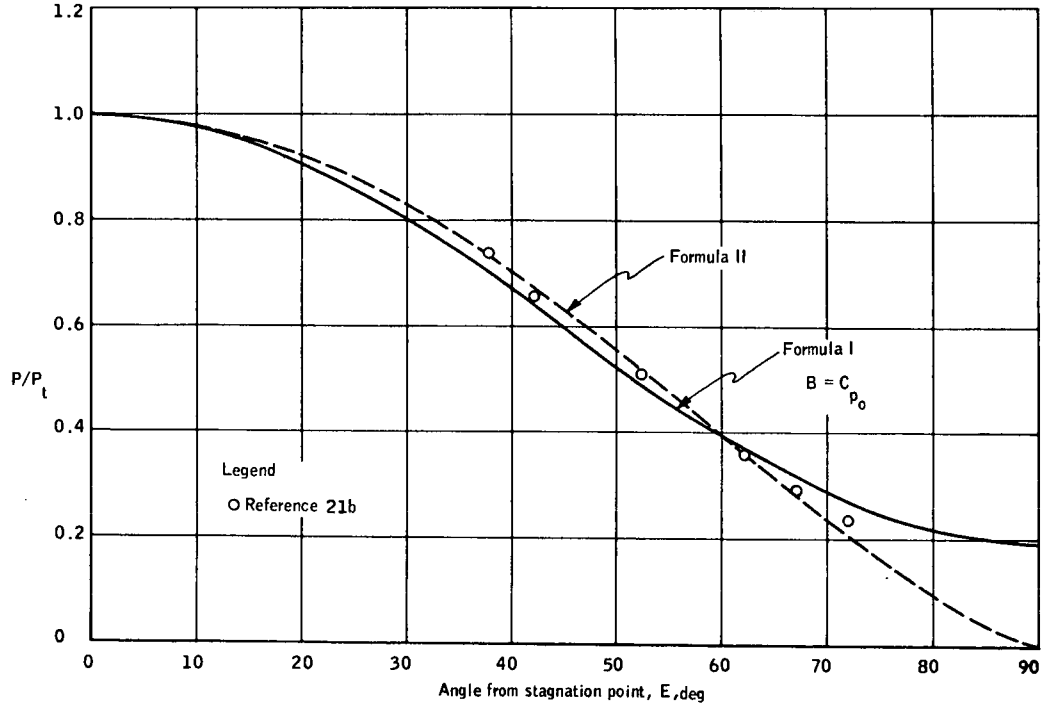

Figure D15. Comparison of Formula I and II and Experimental Data at M = 1.9

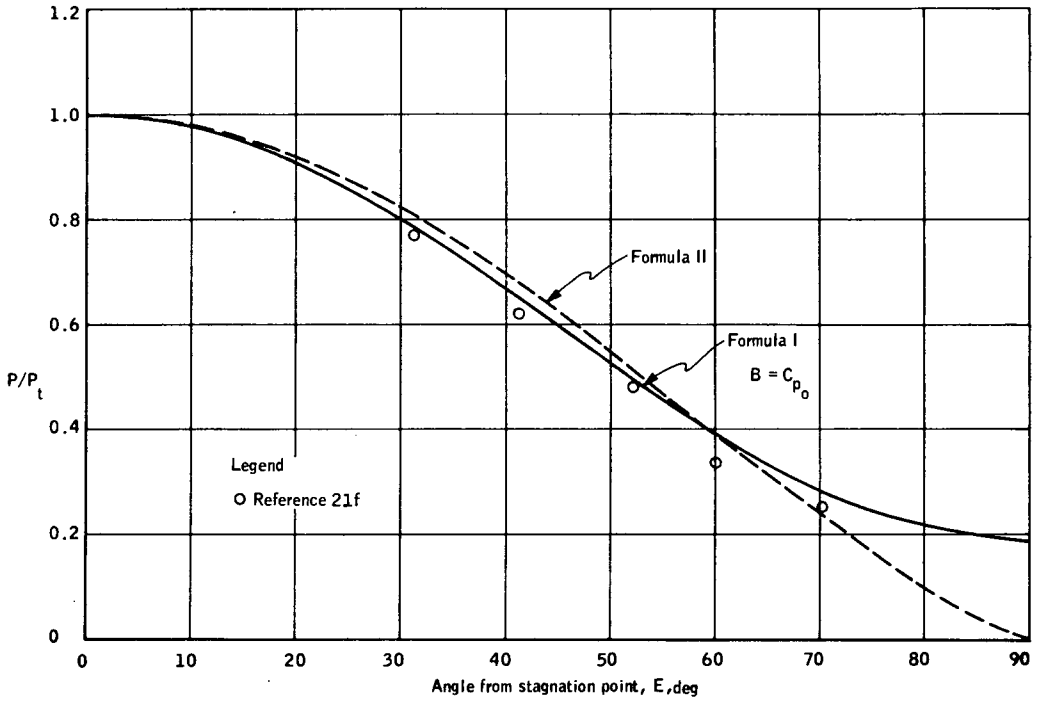

Figure D16. Comparison of Formula I and II and Experimental Data at M = 1.97

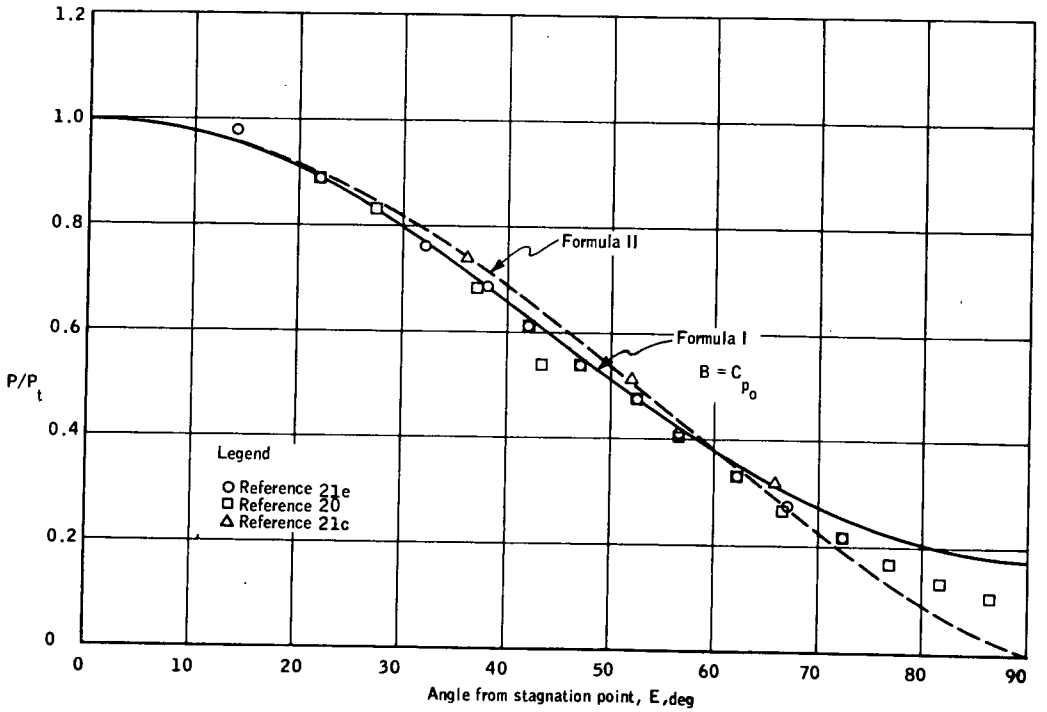

Figure D17. Comparison of Formula I and II and Experimental Data at M = 2.0

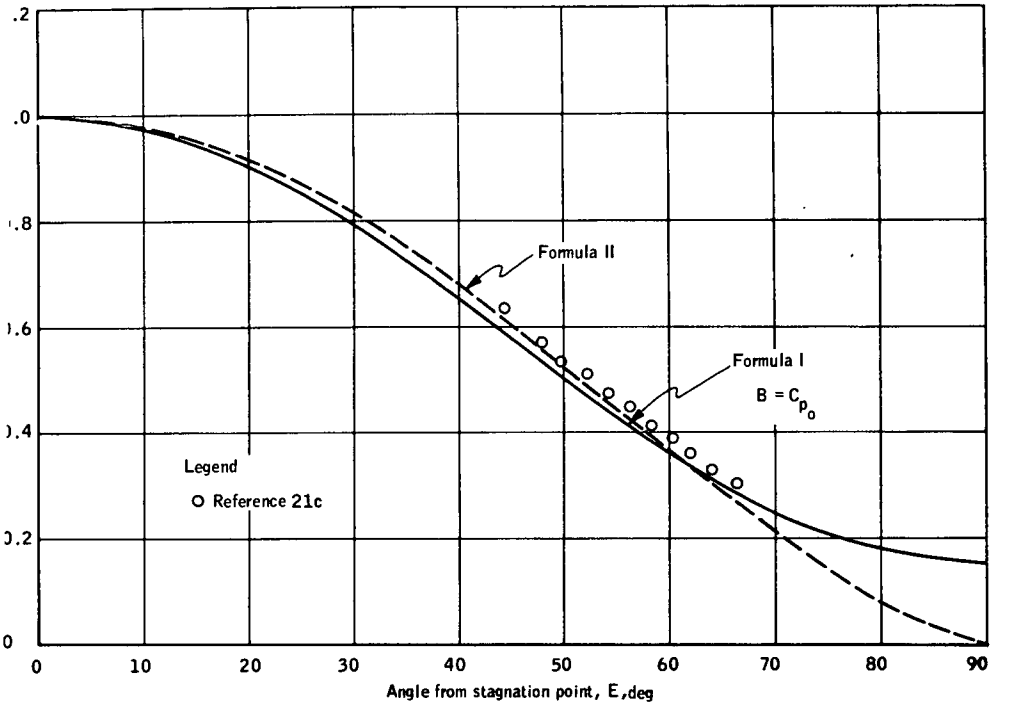

Figure D18. Comparison of Formula I and II and Experimental Data at M = 2.2

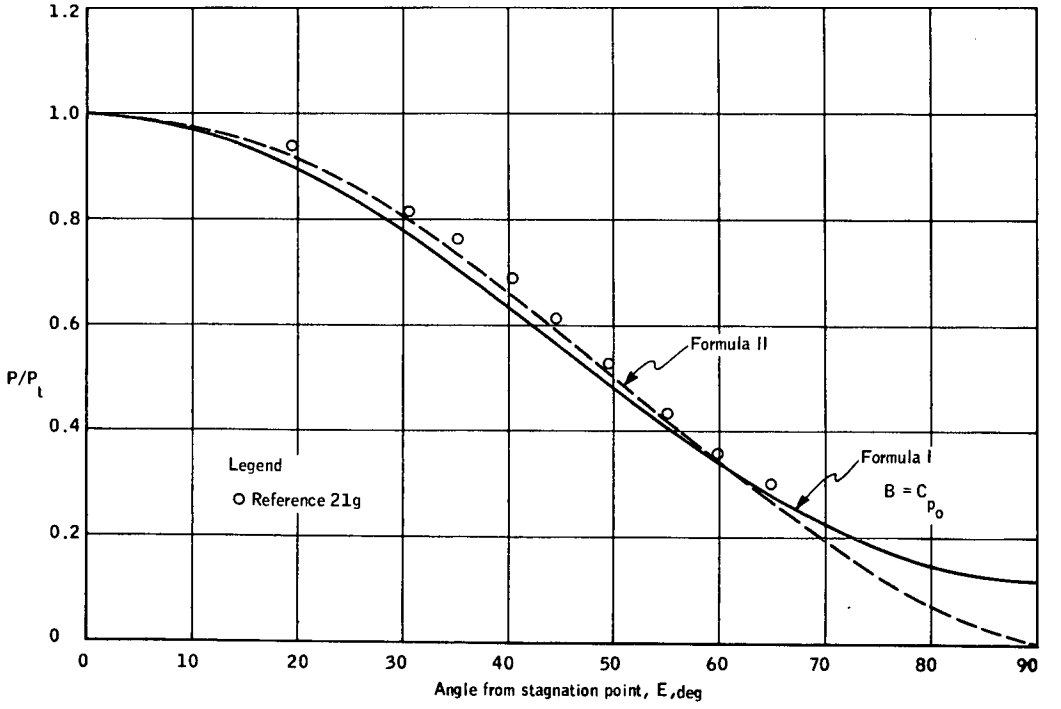

Figure D19. Comparison of Formula I and II and Experimental Data at M = 2.47

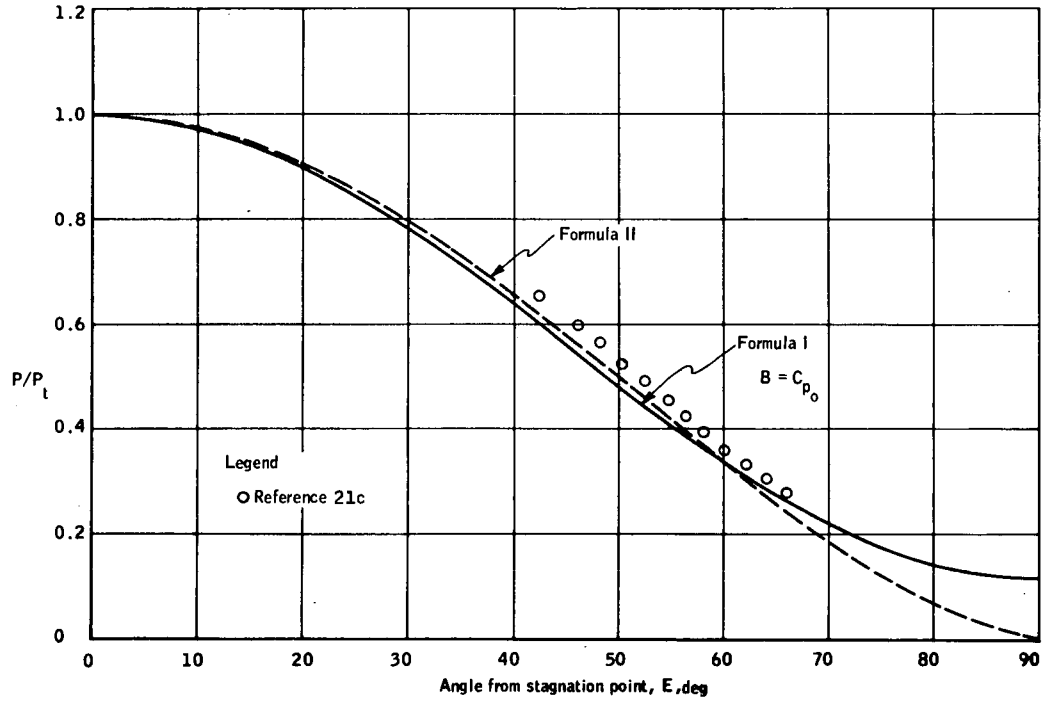

Figure D20. Comparison of Formula I and II and Experimental Data at M = 2.6

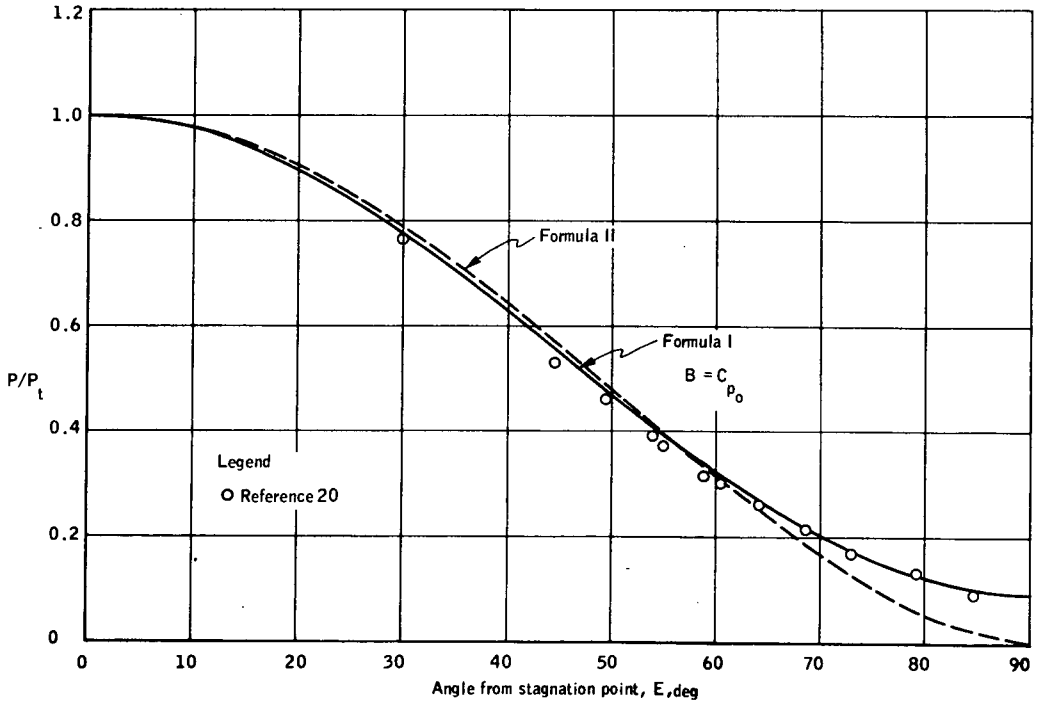

Figure D21. Comparison of Formula I and II and Experimental Data at M = 2.8

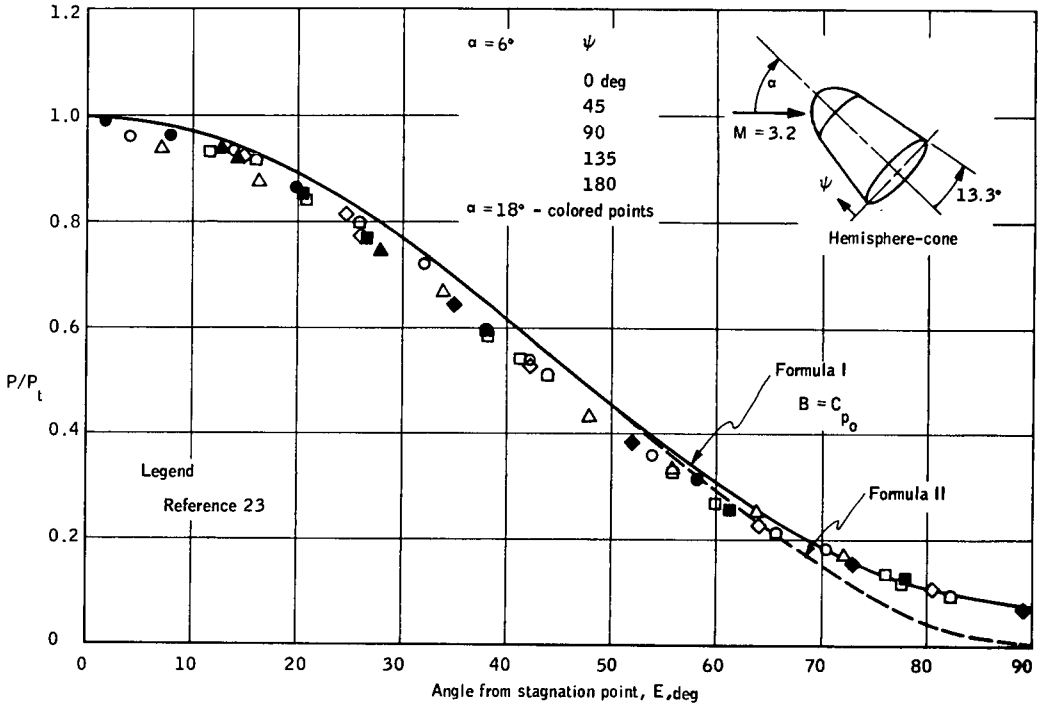

Figure D22. Comparison of Formula I and II and Experimental Data at M = 3.2

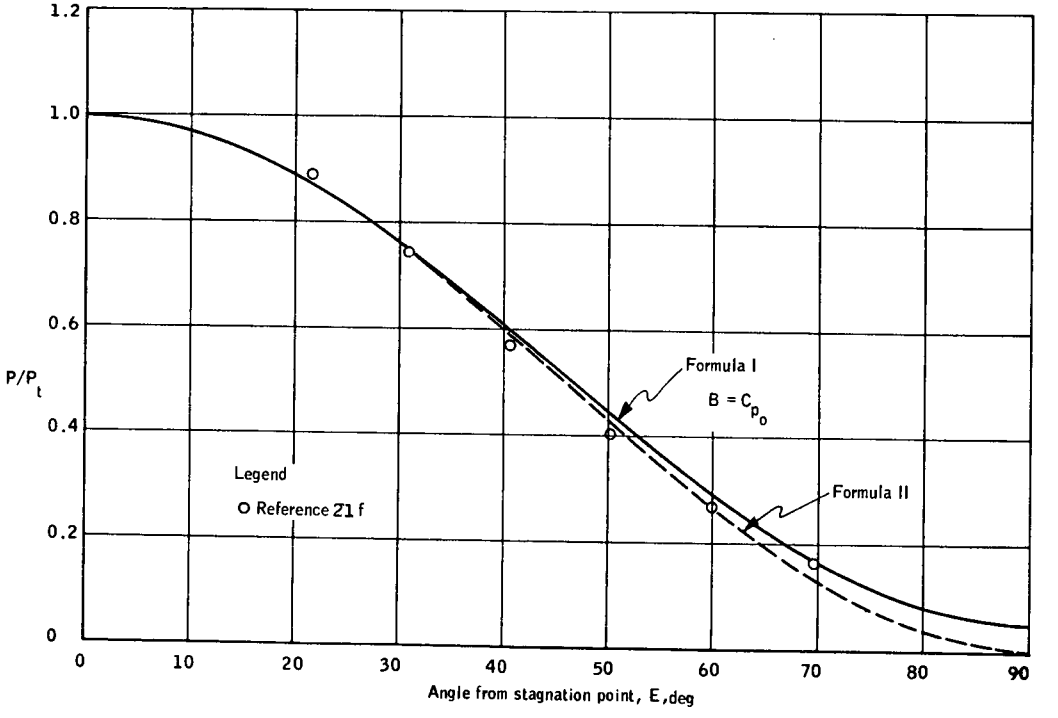

Figure D23. Comparison of Formula I and II and Experimental Data at M = 3.8

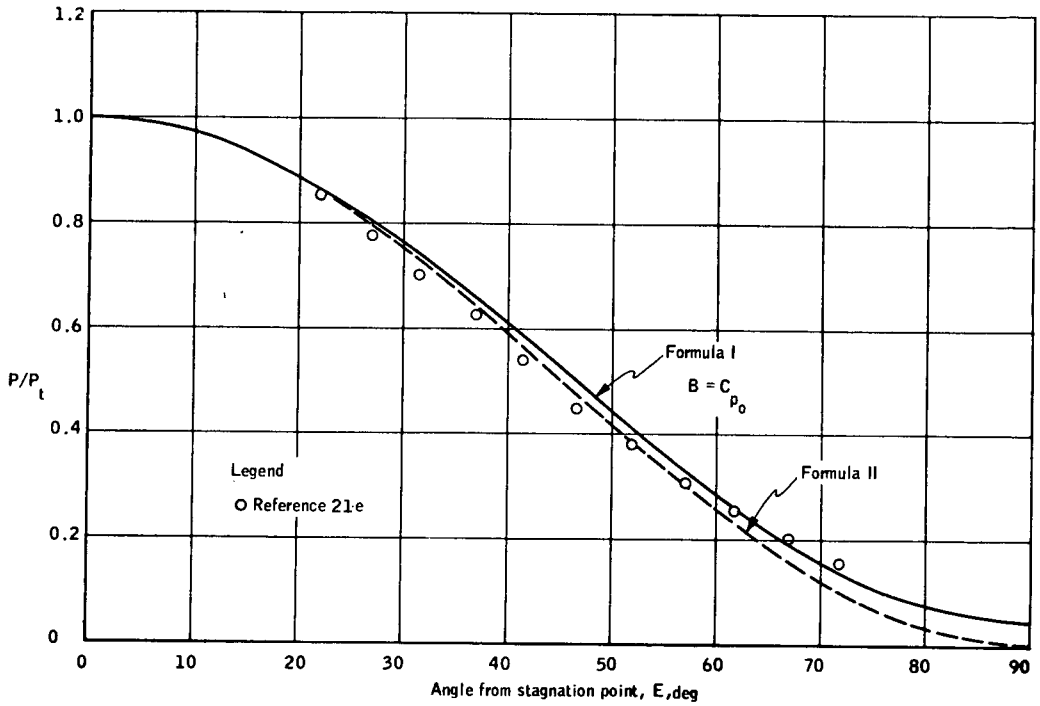

Figure D24. Comparison of Formula I and II and Experimental Data at M = 4.15

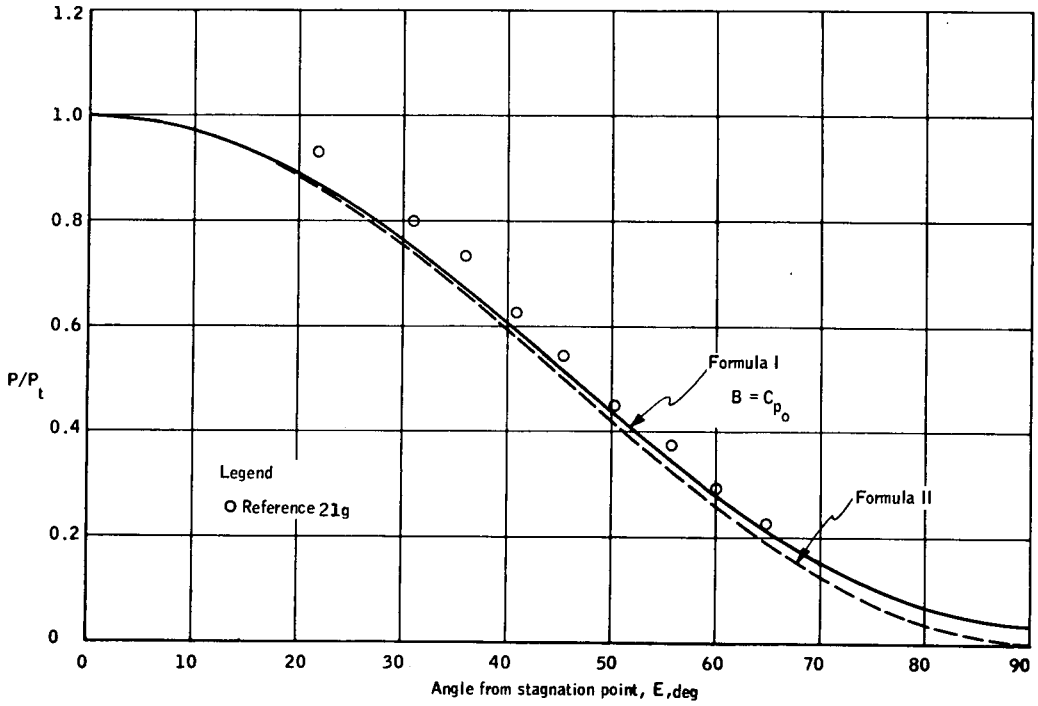

Figure D25. Comparison of Formula I and II and Experimental Data at M = 4.45

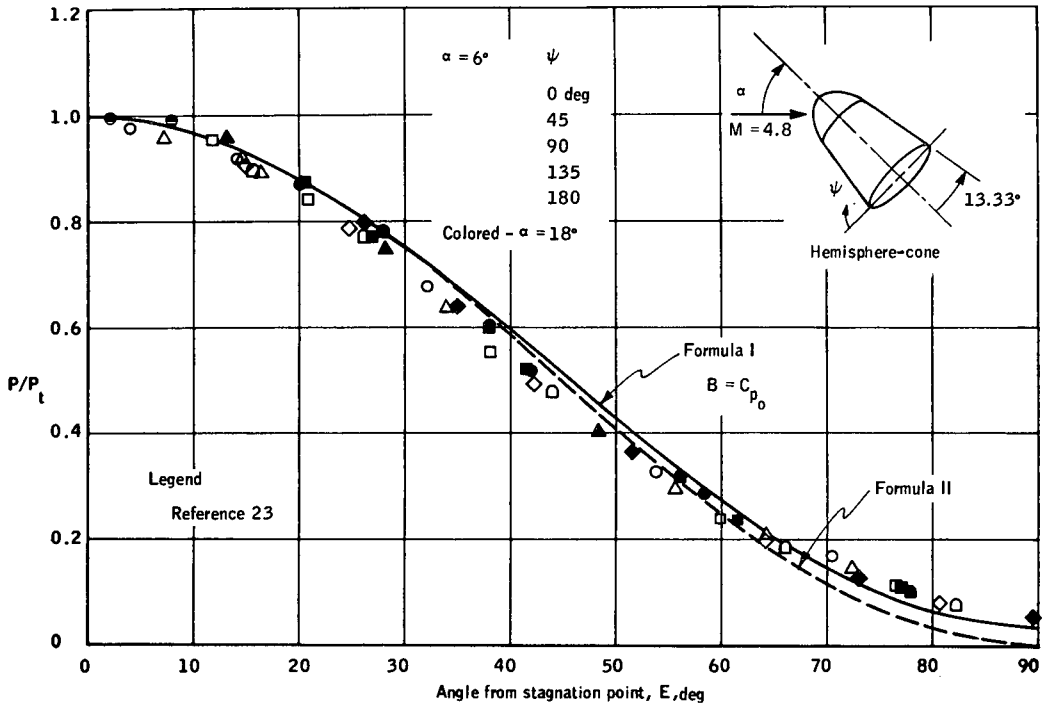

Figure D26. Comparison of Formula I and II and Experimental Data at M = 4.8

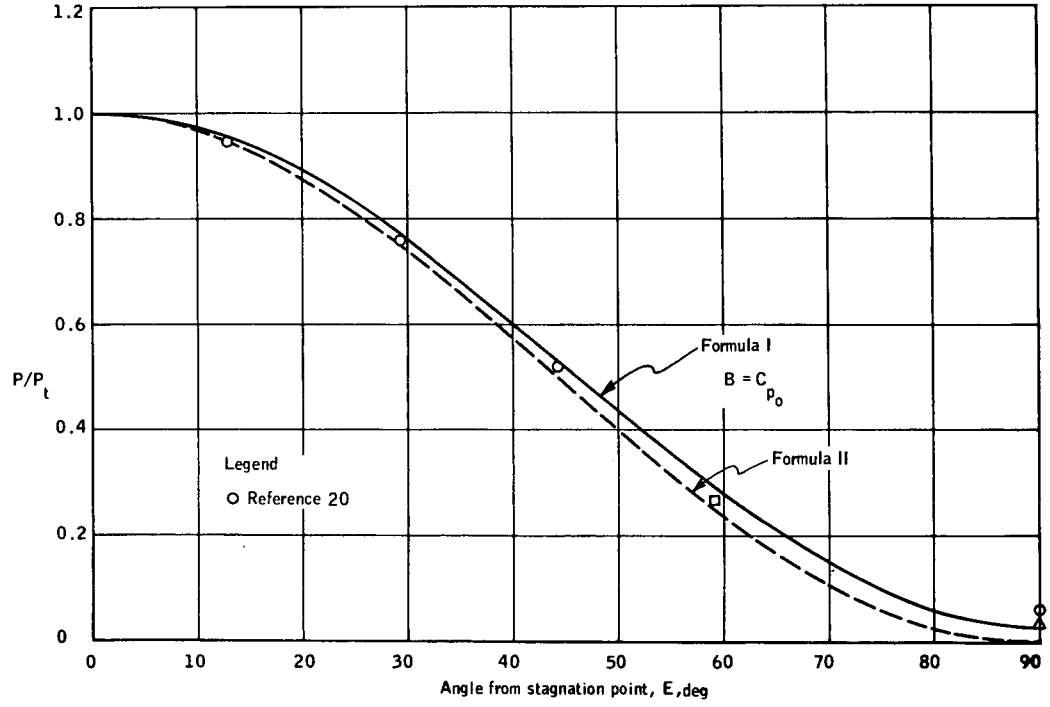

Figure D27. Comparison of Formula I and II and Experimental Data at M = 5.7

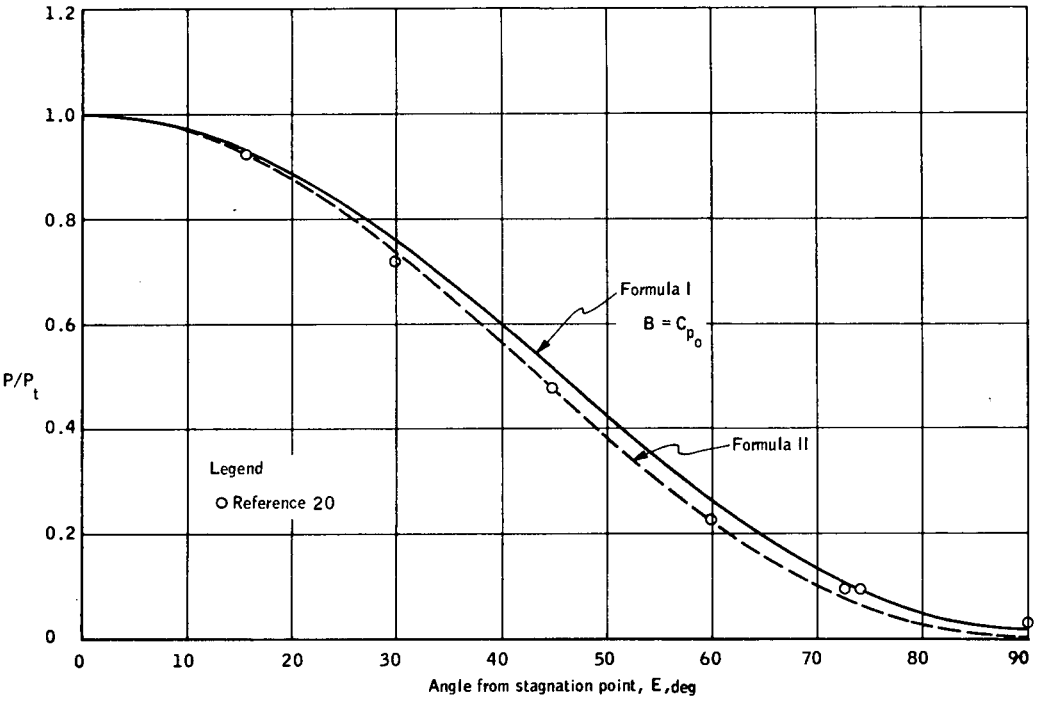

Figure D28. Comparison of Formula I and II and Experimental Data at M = 6.8

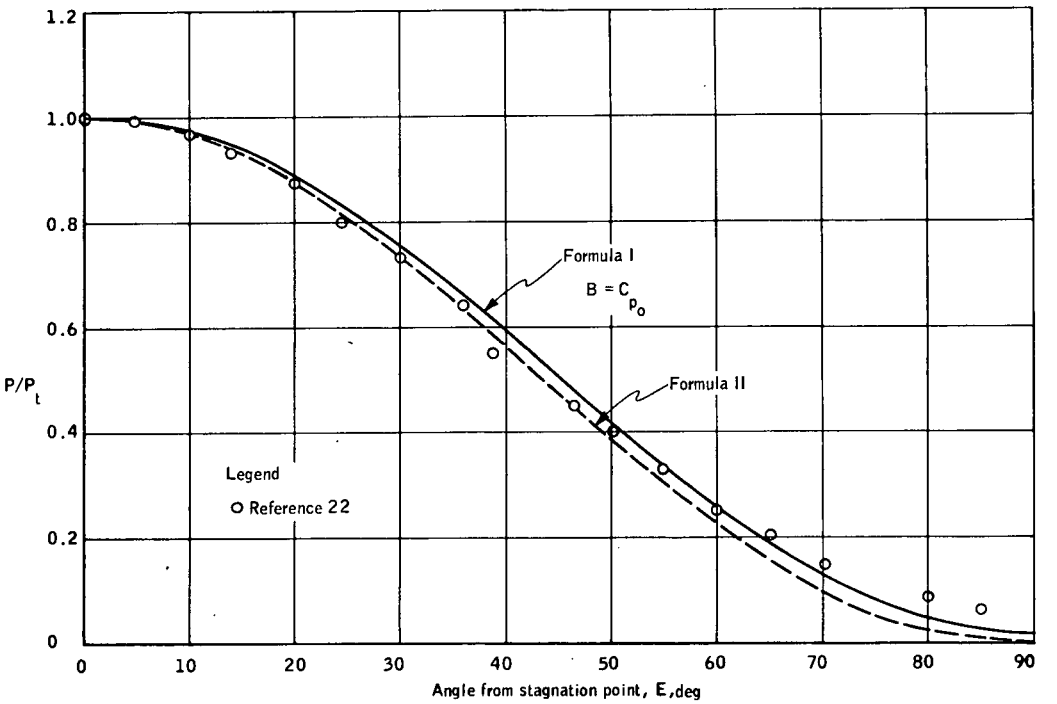

Figure D29. Comparison of Formula I and II and Experimental Data at M = 7.0

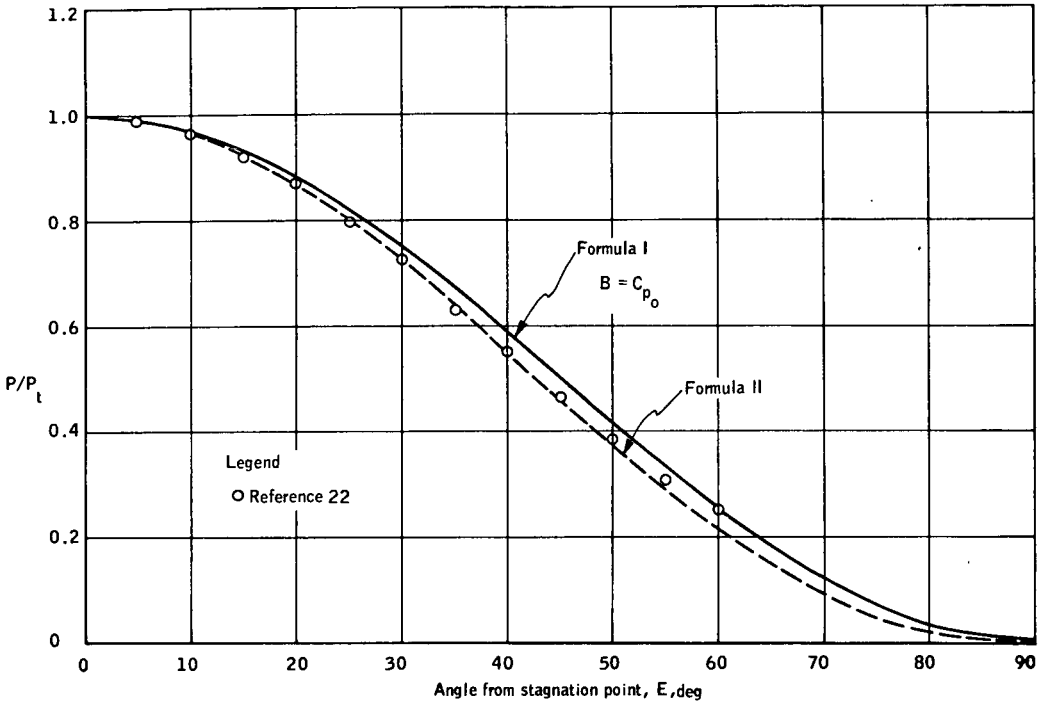

Figure D30. Comparison of Formula I and II and Experimental Data at M = 10.0

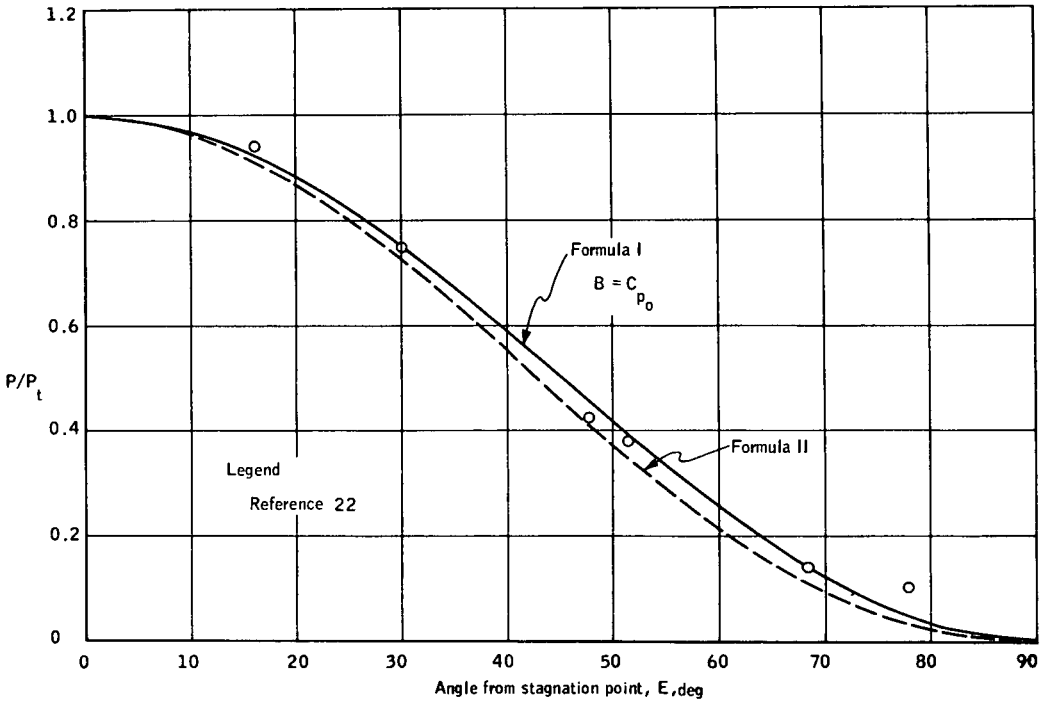

Figure D31. Comparison of Formula I and II and Experimental Data at M = 15.6

TRANSONIC SPEEDS (M = 0.6 TO 1.8)

At speeds between M = 0.6 and M = 1.2 the experimental data do not cover a sufficiently large range of E to make good comparison with either formula. Between M = 1.3 and M = 1.8 experimental data agree equally well with the experimental data and all are within a degree of each other.

SUPERSONIC SPEEDS (M = 1.8 TO 4.0)

Formula I and II agree with each other and the experimental data within about a degree up to E = 60 deg at larger E Formula I agrees with the data better. This is best seen in Figure D22.

HYPERSONIC SPEEDS M > 4.0

Formula II agrees best with the data, within less than a degree of E, while Formula I agrees within a degree of E. E less than E = 60 deg. At larger E Formula I is better (see Figures D24, D25, D26, D28, and D29).

SUMMARY OF COMPARISON

- Pressure measurements required for measuring angle of attack

  Formula I 2 different pressures

  Formula II 4 absolute pressures

- Accuracy of Formulation

  About the same for M > 2.0

  Formula I best for E > 50 deg

- Formula I is better for the Space Shuttle because

  a) It covers the entire speed range, i.e., low subsonic through hypersonic.

  b) It is more accurate at large E.

  c) It requires fewer transducers.

FORMULATION ERROR

Formulation error is the angle of attack and sideslip error due to the assumption that the sphere pressure distribution formula (i. e., Formulae I or II) agrees perfectly with actual surface pressures at a particular E and Mach number. Presently, the best data for the Shuttle nose surface pressures is the measured pressures on hemisphere cylinders and cones in Figures D3 through D31 and the best pressure distribution formulation is Formula I. The formulation error applicable to the Shuttle is found by choosing a set of pressure tap locations on the spherical nose of the shuttle and then for specified trajectory points determine the angle of attack and sideslip that would be computed using Formula I. This error would not include any other sources such as transducer errors. Specifically, the formulation error is found by:

1) Choosing a set of pressure tap locations (i. e., α_{t_1}, β_{t_1}; α_{t_2}, β_{t_2}, etc.).

2) At a specified trajectory point of velocity, altitude, α, β.

3) Calculate Mach number using standard atmosphere and V from No. 2.

4) Calculate angle E for each tap using α and β from step 2 in Equation (D11).

5) Determine pressure at each tap using M and E in Figures D3 through D31.

6) Calculate angle of attack using Equation (D20) using pressures from step 5.

7) Calculate α error as calculated α (step 6) minus actual α (step 2).

The angle of attack is measured by pressure taps all located on the $\beta = 0$ great circle (i. e., $\beta_{t_1} = 0$, $\beta_{t_2} = 0$, etc.). Then the equation for calculating the angle of attack from two pressure difference measurements ΔP_N and ΔP_D, is

$$\tan 2\alpha = \frac{K_1 \Delta P_N - K_2 \Delta P_D}{K_3 \Delta P_N - K_4 \Delta P_D} \qquad \text{(D20)}$$

The constants are based on the geometry of the tap locations.

$$K_1 = \frac{\sin \Delta\alpha N}{\sin \Delta\alpha D} \sin 2\bar{\alpha} D$$

$$K_2 = \sin 2\bar{\alpha} N$$

$$K_3 = \frac{\sin \Delta\alpha N}{\sin \Delta\alpha D} \cos 2\bar{\alpha} D$$

$$K_4 = \cos 2\bar{\alpha} D$$

where

α = angle difference of two taps; e. g., $\alpha_{t_1} - \alpha_{t_2}$

$\bar{\alpha}$ = average angle of two taps (i. e., location of midpoint of a pair of taps) e. g.: $\frac{\alpha_{t_1} + \alpha_{t_2}}{2}$

ORBITER ENTRY - FORMULATION ERROR

Three units of pressure taps are chosen for redundancy. Location of the taps all on the $\beta = 0$ great circle, is (Table D1):

TABLE D1. - TAP LOCATION

Unit	α_{t_1} (deg)	α_{t_2} (deg)	α_{t_3} (deg)	α_{t_4} (deg)
I	60	15	45	-15
II	60	15	30	-45
III	45	-15	30	-45

Orbiter entry formulation error is presented in Table D2.

TABLE D2.- FORMULATION ERROR

Trajectory				Formulation error, deg		
Altitude (1000 feet)	M	α (deg)	β (deg)	Unit I α error	Unit II α error	Unit III α error
205	15.6	35	0	1.6	-0.6	4.0
190	10.0	35	0	1.6	-0.2	4.0
135	7.0	15	0	0.0	0.5	0.0
130	5.7	15	0	0.0	0.5	0.0
125	4.2	15	0	0.0	-0.6	0.0
100	2.8	10	0	3.6	-0.4	-0.1
95	2.5	10	0	-0.4	1.2	0.5
90	2.0	10	0	-0.7	0.6	0.0
85	1.5	10	0	-0.1	1.3	1.6
5	0.4	10	0	0.0	0.0	0.0

BOOSTER ENTRY - FORMULATION ERROR

The booster nose is expected to be blunt and can be approximated by a sphere cone that has a half angle of about 40 to 50 deg. Hence, the angle-of-attack sensing taps would be located on the $\beta = 0$ great circle and two possible configurations of three taps each are:

	α_{t_1}, deg	α_{t_2}, deg	α_{t_3}, deg
Configuration I	37.5	15	-7.5
Configuration II	60	30	0.0

The pressure differences are $\Delta P_N = P_1 - P_2$ and $\Delta P_D = P_1 P_3$.

Booster entry formulation error is presented in Table D3.

TABLE D3. BOOSTER ENTRY FORMULATION ERROR

Trajectory				Formulation error, deg	
Altitude (1000 feet)	M	α (deg)	β (deg)	Configuration I α error	Configuration II α error
180	10.0	60	0	3.0	1.7
120	7.0	30	0	-0.2	0.0
105	5.7	33	0	1.2	-0.4
101	4.8	36	0	0.2	-0.1
100	4.2	43	0	1.2	-0.2
100	3.2	55	0	5.0	1.1
98	2.8	52	0	2.6	1.0
80	2.0	37	0	-2.5	0.5
70	1.5	20	0	0.6	-1.0
20	0.4	8	0	0.0	0.0

SUMMARY OF FORMULATION ERROR

These calculations show:

- The α formulation error is ± 1 or 2 deg, which is within the uncertainties resulting from the experimental data, providing the best tap configuration is used.
- The α error goes to zero when the stagnation point is midway between either port pair, i.e., when either $\Delta P_N = 0$ or $\Delta P_D = 0$.
- The symmetric location of β sensing parts also has the property of zero formulation error.
- The largest α errors occur at a combination of large α and α_t where a port is more than 70 deg from the stagnation point.

- Tap locations should be chosen or scheduled according to the expected α to keep the distance from the stagnation point less than a maximum of 65 or 70 deg.

- If β is not zero, the effect is to increase the distance of the α sensing ports from the stagnation point according to:

$$\cos E = \cos \beta \cos (\alpha - \theta)$$

- Because only small β are considered $\cos \beta \approx 1$ and the effect of sideslip on α error is small.

SYMBOLS

C_P pressure coefficient at a point on the sphere surface $\left(C_P = \frac{P - P_\infty}{q}\right)$

C_{P_o} pressure coefficient at the stagnation point

E angular distance from stagnation point to a point (pressure tap)

M Mach number

P surface pressure at a point on the sphere

P_t stagnation pressure on the sphere

P_∞ ambient static pressure (atmospheric pressure)

q dynamic pressure $\left(q = \frac{\rho}{2} V^2\right)$

α vehicle angle of attack

β vehicle angle of sideslip

α_t & β_t are the ordered pair of angular coordinates locating a pressure tap from the $\alpha = 0$, $\beta = 0$ point on the sphere. Similarly, α and β are the ordered pair of angular coordinates locating the stagnation point on the sphere.

B

REFERENCES

1. Technical Requirements Document, Space Shuttle Avionics System (Preliminary Issue), MSC-02432, Manned Spacecraft Center, 14 May 1970.

2. A Conceptual Design of the Space Shuttle Integrated Avionics System, NASA TM X-53987 by Electronics and Control Division (Fred E. Digesu, editor), Marshall Space Flight Center, 3 February 1970.

3. Stillwell, Wendell H.: X-15 Research Results, NASA SP-60, 1965.

4. Stephan, Jr., Dr. Samuel C.: Study and Experimental Research into Flight Instrumentation for Vehicle Operation in the Fringe or Outside of the Atmosphere. (Vol. I and II) ASDTR61-142, November 1961.

5. Bailey, Ronald G.: High Total Temperature Sensing Probe for the X-15 Hypersonic Aircraft, Report No. 12080-FR1, September 1968.

6. Proceedings of ASSET/Advanced Lifting Re-entry Technology Symposium, AFFDL-TR-66-22, December 1965.

7. Dobrzanski, Janusz Stalony: Re-entry Guidance and Control Using Temperature Rate Flight Control System. Journal of Spacecraft and Rockets, Vol. 3, No. 10, Northrup Norair, October 1969.

8. Johannes, Robert P.: Re-entry Energy Management, AFFDL-TR-65-61, June 1965.

9. Dommasch, Daniel O. and Landeman, Charles W.: Requirements for Air Data Sensors on Lifting Re-entry and Glide Return Systems, FDL-TDR-64-37, October 1964.

10. Pasach, L.: Supersonic Aerodynamic Heat Transfer and Pressure Distributions on a Sphere Cone Model at High Angles of Yaw. NOL TR 62-35, June 1962.

11. Stephan: Study and Experimental Research into Flight Instrumentation for Vehicle Operation in the Fringe or Outside of the Atmosphere. ASD Tech. Report 61-142, November 1961.

12. Livingston, Sadie P. and Gracey, William: Tables of Airspeed, Altitude, and Mach number based on Latest International Values for Atmospheric Properties and Physical Constants (NASA TN D-822), Langley Research Center, August 1961.

13. U.S. Standard Atmosphere 1962, United States Committee on Extension to the Standard Atmosphere (COESA), December 1962.

14. Drag Measurement as a Method for Reducing Altitude Continuation Errors During SSV Entry. MIT Memo 23A STS No. 10-71, 25 January 1971.

15. Lift and Drag Curves for Delta Wing Orbiter, Part of the Data Base received from NAR by the Honeywell Phase B Shuttle Project, 24 April 1970.

16. 1962 U.S. Standard Atmosphere.

17. Witte, N.F.: Baseline Entry Trajectory for 134C Wing Orbiter. NAR Report, 29 July 1970.

18. Schlichting: Boundary Layer Theory, McGraw-Hill Book Co., 1955.

19. Cox and Crabtree: Elements of Hypersonic Aerodynamics. The English Universities Press Ltd., 1965.

20. Stephan: Study and Experimental Research into Flight Instrumentation for Vehicle Operation in the Fringe or Outside of the Atmosphere. ASD Tech. Report 61-142, November 1961.

21. Romeo, D.J.: Analytical Study of Air Data Equations for a Hemispherical Pressure Probe through the Hypersonic Mach Number Range. AFFDL-TR-67-128, September 1967.

    a. Anderson, N.Y., "Final Report Transonic Flight Line Computer," Cal Report IH-933-P-2, October 1956.

    b. Beecham and Collins, ARC CP414 02/54.

    c. Roberts, WRE TN HSA TN 43 11/59.

    d. Hunt, Unpublished MOA Report.

    e. Beckwith and Gallagher, NASA TN 4125, 12/57.

    f. Perkins and Jorgensen, NACA TIB 3466, 11/52.

    g. Unpublished RAE Data.

22. Ryder, M.O. Jr., and Romeo, D.J.: Experimental Investigation of Hypersonic Air Data Attitude Equations for a Hemispherical Pressure Probe. AFFDL-TR-69-77, September 1969.

23. Pasiuk, L.: Supersonic Aerodynamic Heat Transfer and Pressure Distributions on a Sphere Cone Model at High Angles of Yaw, NOL TR 62-35, June 1962.

BIBLIOGRAPHY

Ames Research Staff: Equations, Tables and Charts for Compressible Flow. NASA Report 1135.

Herman, R., Moynihan, F., and Olson, D.: Wind Tunnel Investigation of a Spike-Bluff Body Combination for a Monorail Rocket Sled, M = 2.0 to M = 5.0. AF Office of Scientific Research, Technical Report AFOSR/DRA-62-18.

Kriegsman, B.A. and Gustafson, D.E.: SSV Navigation and Guidance Studies, 9 July 1970.

Kuethe and Schetzer, Foundations of Aerodynamics. John Wiley and Sons, Inc., 1950.

Sowada, D.J., Moynihan, F.A., Bailey, R., and Hafner, A.: Air Data Sensing for Space Shuttle. Proceedings of Space Shuttle Integrated Electronics Technology Conference, May 1971, NASA MSFC, Houston, Texas.

Stone, Irving: Gentry of Re-entry. Air Force Magazine, December 1970.

Wolowitz, C.H., and Gossett, T.D.: Operation and Performance Characteristics of the X-15 Spherical Hypersonic Flow-Direction Sensor, NASA TN D-3070. Flight Research Center, NASA, November 1965.

Unpublished Wind Tunnel Data for a Hemisphere Cylinder Angle-of-Attack Sensor, NASA FRC, 1970.